ISOTOPIC AND TEXTURAL EVIDENCE FOR DIAGENETIC FLUID MIXING IN THE SOUTH BRAE OILFIELD, NORTH SEA

A thesis submitted for the degree of
Doctor Of Philosophy

by Órla Marie Mc Laughlin
B.A. Trinity College Dublin

Department of Geology & Applied Geology
University of Glasgow

August 1992

Thesis Declaration

The material presented in this thesis is the result of research carried out between October 1988 and August 1992 in the Department of Geology and Applied Geology, University of Glasgow, under the supervision of Dr. Stuart Haszeldine.

This thesis is based on my own independent research and any published or unpublished material used by me has been given full acknowledgement in the text.

Órla Mc Laughlin

August, 1992

We certify that Órla Mc Laughlin has undertaken the bulk of the work involved in this thesis. Specifically: background geology, sample preparation, examinations and analyses, and interpretation. We have assisted with advice and help of a general, technical, conceptual nature, as would be expected in the course of normal Ph.D. supervision and advice. Órla Mc Laughlin has written the thesis and papers within it herself, and is responsible for its content.

R.S. Haszeldine

A.E. Fallick

G. Rogers

A.J. Boyce

ACKNOWLEDGEMENTS

I would like to start by thanking Marathon (U.K.) for providing the funding of this project and for allowing me access to their data and core of the South Brae Oilfield. I would like to thank Colin Turner, Roger Connell, John Crane and Jim Hardy for all of their assistance during the course of this research.

Many thanks go to my brave and long suffering supervisor Stuart Haszeldine, for giving me the opportunity to work on such an exciting project and for his helpful supervision throughout the four years. I am also greatly indebted to Tony Fallick and Graeme Rogers for their advice, guidance and encouragement. Also many thanks to the staff of the SURRC Isotope Geology Unit for their assistance, particularly Terry, Adrian, Gawen (for years of chauffeuring), Paul, Alison, Julie, Elisbeth, Margaret, Tricia, Anne and the Three Amigos.

I would like to thank Peter Hill and John Millar in Edinburgh University, for kindly allowing me use of their microprobe and CL facilities.

I am also greatly indebted to the academic and technical staff in the Glasgow Geology Department for all their assistance, George Bowes, Mike Russell, Alan Hall, Brian Bell, Colin Braithwaite, Peter Pigg, Dougie, Murdo, John and Robert. Special thanks to Peter Ainsworth for teaching me the joys of mineral separation, and piloting the SEM. For sterling work on the photography side, special thanks to Douglas Maclean. A big thanks to the "Diaboredom/Dukes Gang" Calum, Morgan, Gordie, Brint of Brent, P.C., Clark, Magic, Maggie, Rachael, Rona, Gary, Mark and Gian for their friendship (& pint buying ability!) and support through these harrowing years. Mil Stricivic is also thanked for being a non-geologist and the best friend I could ever have.

I would especially like to thank my Mother and Father for all the understanding, support and love they have shown me over the years. Finally, thanks to Chris for putting up with the slight transatlantic problem we had earlier, and for doing the right thing.

ABSTRACT

Reservoirs of the South Brae Oilfield comprise a 1540m sequence of Upper Jurassic submarine fan sandstones and conglomerates. The diagenetic history of the reservoir between 3684 and 4204m was studied using petrographic, geochemical, fluid inclusion thermometry and isotope techniques in core samples from 5 wells. This enabled interpretation of the processes involved in the supply of ions for authigenic mineral growth and allowed the paragenetic sequence and associated porefluid movements to be related to the burial and tectonic history.

The earliest diagenetic phase was calcite cementation, which formed concretionary bodies 0.8-4m diameter during shallow burial. These concretions were precipitated from a meteoric fluid ($\delta^{18}O$=-7‰SMOW), which flushed through the reservoir during shallow burial, displacing the depositional marine porefluid and causing aggressive dissolution of detrital shell debris, plagioclase (supplying Ca) and K-feldspar. Oxygen isotope values record precipitation at temperatures between 15° and 70°C at depths of 0.3 to 2.3 km. $\delta^{13}C$ and $^{87}Sr/^{86}Sr$ ratios record increasing thermal decarboxylation and silicate dissolution. No significant diagenetic clays are present, so Al has been lost to the system.

This was followed by quartz cementation. Oxygen isotope and fluid inclusion data suggest that the greatest volume of quartz was precipitated at temperatures between 70° and 110°C (2.3 to 3.7km), from a layered porewater. Our model suggests that warm, isotopically modified, compaction-driven, basinal waters ($\delta^{18}O$=+4‰) overlay cooler meteoric derived waters ($\delta^{18}O$=-4‰). Cementation occurred from 55 to 20Ma and may be related to periods of overpressure release. Silica was supplied locally by pressure solution and possibly from mudrocks.

A late dissolution event has enhanced porosity by up to 8%, due to dissolution of diagenetic calcite and K-feldspar, particularly in the upper reservoir zones. This secondary porosity formation was probably due to the movement of basinal fluids, compacted from the interdigitating Kimmeridge Clay and drained out of the basin laterally through the reservoir. Subsequently, minor amounts of illite, kaolinite, calcite, dolomite and pyrite have further reduced the porosity of South Brae to 3-19%. The oilwater contact has no poroperm effect. From 2Ma, the reservoir sealed and became overpressured by 900psi halting fluid movement through the oilfield, and permitting final hydrocarbon accumulation to occur.

CONTENTS

1.0. INTRODUCTION

The interstitial water-sediment complex is a site of intense chemical, physical and biological reactions, which can lead both to the formation of new and altered mineral phases and to changes in the composition of the waters themselves. These changes may be grouped together under the term *diagenesis* , which has been defined by Berner (1980) as 'the sum total of processes that bring about changes in a sedimentary rock subsequent to its deposition in water'.

Interstitial waters are aqueous solutions that occupy the porespaces between particles in rocks and sediments. For most marine sediments the interstitial fluids originated as sea water trapped during deposition from the overlying water column. The origins of the present day porefluids can be inferred from their isotopic compositions. Stable and radiogenic isotopic analysis of reservoir diagenetic minerals and formation waters allows us to interpret the isotopic composition of the ancient porefluids from which the minerals were precipitated.

This is possible for oxygen isotopes because at equilibrium, both temperature and porewater composition control the $\delta^{18}O$ of a precipitating mineral. If the precipitation temperature is known one can then calculate the pore water composition and vice versa (Bigeleisen & Mayer 1947). The $\delta^{13}C$ analyses from diagenetic cements may be interpreted to diagnose the source of the CO_2 in the porefluids from which the cements precipitate, and the variation in $\delta^{13}C$ values reflects a variation in the source or process of carbon supply. Measurement of strontium isotopes of cements is also a helpful tool when attempting to interpret ancient porefluids, $^{87}Sr/^{86}Sr$ records the strontium

isotopic composition of the cement and therefore also records the $^{87}Sr/^{86}Sr$ sources.

The study of diagenesis includes the physical and chemical processes which affect sediments upon burial. Blatt (1979) defines the range of conditions for diagenesis as between 0-200°C, 1-2000kg/cm^2, with water compositions from fresh to hypersaline. This is equivalent to burial depths of 0 to 6km in the North Sea. The important physical processes are dependent on depth of burial with the associated increases in temperature and effective stress on grains - this leads to varying amounts of compaction and pressure solution. As increasing temperature overcomes kinetic barriers, and mineral stability fields change, so chemical processes may cause dissolution or recrystallization of unstable detrital grains and control the precipitation of new authigenic minerals into existing porosity. Both processes modify the sediment's original texture and have a marked effect on the porosity and permeability. Prior to compaction and early cementation the intergranular volume of the sandstone is close to 40% (McBride 1989, Bjørlykke et al. 1989), physical and chemical processes can reduce the intergranular volume to 0%. Diagenetic processes in sandstones are mainly a function of the primary composition of the sandstone, its texture and depositional environment, the porewater composition and the temperature the sediments have been subjected to due to burial.

In recent years the petroleum industry and the academic community have taken a heightened interest in diagenetic processes, with increased oil prices and expense of offshore drilling there is the incentive to evaluate the quality of existing and potential reservoir rocks. Only upon understanding the diagenetic processes can we then construct models that are capable of

describing and predicting porosity and permeability distribution for reservoirs.

1.1. AIMS OF THE PROJECT

The aim of this project was to determine the paragenetic sequence and volume of diagenetic minerals, and to discover their relationship to the final porosity and permeability of the South Brae oilfield reservoir rocks. From this an hypothesis could be formed for the processes involved in the supply of ions for diagenetic mineral growth and the causes of any porefluid movements or exchanges within the field. Finally, the origins of the paleofluids and their successive movements could be integrated with the burial history of the field and the associated diagenetic and tectonic events.

1.2. APPROACH

A multidisciplinary approach was applied to this study of diagenesis in South Brae - thin section studies, employing optical microscopy and Scanning Electron Microscopy (SEM) formed the basis for understanding and quantifying the textural relationships between authigenic and detrital minerals. This was supplemented by the use of a Technosyn cold cathode luminescence microscope (CL) which helped clarify the growth history of the calcite cements. X-Ray Diffraction (XRD) aided in identification of minerals and was particularly useful in checking purity of mineral separates prepared for isotopic analyses. Microthermometric studies of fluid inclusions trapped within quartz overgrowths (in the Brae sandstones) provided data on the temperature of formation and the chemical composition of the porefluids. The (SEM) was also used with the CL facility to quantitatively assess the abundance of diagenetic quartz. Stable and radiogenic isotope analyses of

detrital and authigenic minerals were carried out (D/H, $^{18}O/^{16}O$, $^{13}C/^{12}C$, $^{34}S/^{32}S$, Rb-Sr).

1.3. GEOGRAPHICAL LOCATION & GEOLOGICAL SETTING

The Brae Oilfield is located in the U.K. sector of the North Sea, 240 km east of the Orkney Islands (Fig.1.1.). The initial discovery of the Brae Oilfield in Upper Jurassic sandstones was made in April 1975 when the 16/7-1 well was drilled by the Pan Ocean group. Additional discoveries were made over the following years, with the South Brae field being discovered when well 16/7a-8 was drilled in July 1977. The South Brae field covers an area of approximately 24.3km^2 and has a maximum oil column of 500 metres. The source rocks (Kimmeridge Clay Formation) are currently at 110-120°C (at 3,900m beneath the sea bed) and are actively generating and expelling petroleum fluids, chiefly crude oil, into adjacent sandstones due to capillary pressure differences. Sands were tested at pore pressures of 50-51MPa and there is a mild overpressure (Fig.1.2.) relative to the hydrostatic gradient of about 10MPa (Mackenzie et al. 1987). Reservoir bottom hole temperatures range from 113° to 127°C.

Where the Brae field is located, the Viking Graben is narrow and its structural style differs from that further north as the area is cut by numerous SW - NE trending cross faults of probable Caledonide origin. These normal cross faults dip down to the east steeply and become younger in general to the west (Harms et al.1981). The South Brae trap was formed by a combination of stratigraphic discontinuities, faulting and folding. The main trapping mechanism is a major fault zone which is located at the western edge of the

detrital and authigenic minerals were carried out (D/H, $^{18}O/^{16}O$, $^{13}C/^{12}C$, $^{34}S/^{32}S$, Rb-Sr).

1.3. GEOGRAPHICAL LOCATION & GEOLOGICAL SETTING

The Brae Oilfield is located in the U.K. sector of the North Sea, 240 km east of the Orkney Islands (Fig.1.1.). The initial discovery of the Brae Oilfield in Upper Jurassic sandstones was made in April 1975 when the 16/7-1 well was drilled by the Pan Ocean group. Additional discoveries were made over the following years, with the South Brae field being discovered when well 16/7a-8 was drilled in July 1977. The South Brae field covers an area of approximately 24.3km^2 and has a maximum oil column of 500 metres. The source rocks (Kimmeridge Clay Formation) are currently at 110-120°C (at 3,900m beneath the sea bed) and are actively generating and expelling petroleum fluids, chiefly crude oil, into adjacent sandstones due to capillary pressure differences. Sands were tested at pore pressures of 50-51MPa and there is a mild overpressure (Fig.1.2.) relative to the hydrostatic gradient of about 10MPa (Mackenzie et al. 1987). Reservoir bottom hole temperatures range from 113° to 127°C.

Where the Brae field is located, the Viking Graben is narrow and its structural style differs from that further north as the area is cut by numerous SW - NE trending cross faults of probable Caledonide origin. These normal cross faults dip down to the east steeply and become younger in general to the west (Harms et al.1981). The South Brae trap was formed by a combination of stratigraphic discontinuities, faulting and folding. The main trapping mechanism is a major fault zone which is located at the western edge of the

Viking Graben, where Brae Formation reservoir rocks are juxtaposed against impermeable Devonian sandstones providing a classic example of hanging-wall fault closure trap (Roberts 1992). To the east the field is in part bounded by an original oil-water contact at 13488 ft T.V.D.S.S. (4180m) and in part by reservoir pinchout. The Kimmeridge Clay Formation provides an excellent vertical seal (Fig.1.3.).

The South Brae Oilfield consists of overlapping submarine fan deposits that form a sediment apron along the western margin of the Viking Graben. The reservoir sequence is the Upper Jurassic Brae Formation (dated as Kimmeridgian-Volgian) which comprises conglomerates, sandstones and mudstones, it is about 1540 metres thick at the graben margin (Turner et al. 1987). These coarse clastic deposits are overlain and partly-sealed by the Kimmeridge Clay Formation. The Kimmeridge Clay has a thickness over the field area of 55-70 metres (Harms et al.1981). Towards the axis of the graben, the conglomerates and sandstones pass laterally and distally to sandy siltstone - shale intercalations and finally beds of Kimmeridge Clay Formation shale. Beneath this is a thick sequence of mid Jurassic - Permian sediments resting on "basement" Devonian (Fig.1.3.), the reservoir sequence is downfaulted against rocks of probable Devonian age on the Fladen Ground Spur. The Devonian quartzites have very low porosity and permeability as a result of compaction and diagenetic alteration. To the east of the Viking Graben is the Vestland Arch, a narrow fault-bounded ridge, with a thin Jurassic cover separating the Viking Graben from the Stord Basin. Since deposition the sequence has been continuously buried at average regional rates of 30-40 m./Ma.(Fig.1.4.) (Mackenzie et al. 1987).

1.4. BASIN FORMATION

The Viking Graben was probably initiated in the latest Carboniferous or early Permian, developing as a N - S trending fracture system, and was periodically active until the Paleocene. The origin of the graben was initially due to differential movement between Laurasia and Gondwana, which caused limited crustal attenuation and subsidence: the rift resulted from the localisation of more intense crustal stretching during the Triassic (Glennie 1984).

West - east extension during early and middle Jurassic times together with the doming of the Forties volcanic centre led to extensive deltaic and shallow marine deposits within the graben until the Callovian. During the late Jurassic significant downfaulting and subsidence occurred in the narrow South Viking Graben. The Fladen Ground Spur and the Vestland Arch hinterland supplied clastic sediments to the basin. The late Jurassic fill is entirely submarine, being deposited by a range of sediment gravity flows (Turner et al. 1987). Continued subsidence of the Graben was accompanied by a global highstand in sea level during the early Kimmeridgian which led to the deposition of the Kimmeridge Clay Formation. This was followed by a lowstand during the Valanginian which greatly reduced sediment supply to the Viking Graben (Glennie 1984).

Some minor faulting-controlled subsidence occurred during the Cretaceous; however, the Graben continued to subside due to thermally induced sag. During the Paleocene some uplift of the Graben flanks occurred, with continued coarse clastic deposition and subsidence. During the late Paleocene regional tectonism was terminated; this was accompanied by widespread transgressions, which resulted in flooding of the uplifted flanks.

1.5. REASONS FOR CHOOSING SOUTH BRAE

The South Brae field lies close to major faults at the margin of the Viking Graben (see Fig.1.1). These could have acted as flow pathways for diagenetic fluids. It was therefore an ideal place to examine if any diagenetic fluid flow has occurred via a fault system, or whether the fluids have been introduced by other means. This reservoir could have experienced the interaction of four possible fluid types - depositional marine interstitial porefluid; meteoric water introduced via a fault system or, water carried with the sediment from the nearby paleoshore; deep waters ascending via faults; or basinal decompactional waters (Fig.1.5.).

This reservoir has extremely good core coverage with more than 38 fully or partly cored wells and the background sedimentological understanding of the geology is at an advanced stage. The excellent core coverage of South Brae gives us a wonderful opportunity to attempt 3-dimensional mapping of diagenetic facies which can then be used to provide information on 'plumbing systems' or regional fluid migration pathways. As many of the wells used here are deviated, sample depths are recorded in core depth (M.D.) in feet. Table 1.1 shows M.D. and T.V.D. in feet and metres for the samples thin sectioned. Samples for analysis were taken in the oil and water zones, the oil water contact was at the depth of 13,488 ft T.V.D.(4180m) throughout the field.

1.6. SEDIMENTOLOGY

The sedimentology, petrology and reservoir structure of the South Brae field

has been described by Harms et al.(1981), Stow et al.(1982) and recently by Turner et al.(1987). With the continuing development of the oilfield modified depositional models for the South Brae Formation have evolved - these models are based on continuing information from exploration and appraisal drilling.

The initial paper on South Brae by Harms et al.(1981) examined the five released boreholes (16/7a-8,10,11,12,13) and interpreted the depositional setting as coalescing fan deltas spilled into the basin from adjacent uplands, with the reservoir sequence (ie. conglomerates and sandstones) deposited subaerially by shallow streams on the fan surfaces. In contrast Stow et al.(1982) suggested a submarine fan origin for South Brae, with the fans being shallow, small basin type and fault-controlled, most closely analogous to the Jurassic fans of East Greenland described by Surlyk (1978). Stow et al. suggested that deposition took place through sediment gravity flow processes. Turner at al.(1987) recognized that the reservoir sequence was deposited as a unique type of submarine fan. They noted that commonly cited submarine fan models are not readily applicable to South Brae as it represents the proximal portion of a tectonically influenced submarine fan system, with major avenues of sediment transport possibly controlled by syn-depositional faults. At present, the favoured hypothesis for the location of the major sediment entry points is structural control caused by the intersection of the N-S and ENE-WSW trending faults. The Stow et al. and Harms models limit the reservoir facies to a distance of 5km from the basin margin. The model of Turner et al.(1987) however, allows prediction of a larger reservoir; they recognise that the reservoir facies extends up to 15km into the basin. Stoker and Brown (1987) depict this model in Figure 1.6.

The conglomeratic sediment source was the Devonian sediment subaerially exposed on the Fladen Ground Spur (Turner et al. 1987). The South Brae conglomerates are made up of subangular to subrounded pebble to boulder size clasts, which are quartzose/feldspathic, fine-grained and well-lithified. Some show oil staining. Stow et al.(1982) attributed their angularity and maximum size of 1-5m to the short distance they had travelled - they postulated that the clasts had been eroded from a nearby upland of substantial relief. Well-rounded quartz pebbles are also very common in the conglomerate facies. They range from granule to pebble size, and were derived from a pre-existing Devonian conglomerate that was available for erosion and entrainment within the drainage systems of the Fladen Ground Spur. Analysis of the relationships of structure, clastic distribution and petrographic variation carried out by Marathon indicate that the sedimentary entry point for the main area of the South Brae field lies to the West of well 16/7a-A3, and the channels of the fan are mapped radiating eastwards from this area (C.Turner, Marathon *pers. comm.* 1990). Figures 1.7a & 1.7b show generalized facies maps for the lower Brae Formation and the upper Brae Formation. In the lower Brae Formation (Fig.1.7a.) the reservoir is defined by two apron-shaped conglomeratic complexes. A small northern lobe and the main southern lobe merge to form a restricted sandstone fan eastward. In Figure 1.7b. the upper Brae Formation is seen to be made up of channelized conglomerates, separated by shaly islands. The sandstone is much more widespread to the east in more distal fan positions.

Based on detailed core logging the South Brae lithologies have been subdivided by Marathon into six descriptive major lithofacies. These facies are consistent with deposition from various types of submarine gravity flows or by hemipelagic settling (Turner et al. 1987).

Facies 1. Sand Matrix Conglomerate

Facies 2. Mud Matrix Breccia

Facies 3. Medium to thick bedded Sandstone

Facies 4. Alternating thin bedded Sandstone with interlaminated Sandstone - Mudstone

Facies 5. Interlaminated Sandstone - Mudstone

Facies 6. Laminated Mudstone

Turner et al.(1987) showed that a considerable degree of vertical facies organization exists to give repeated vertical sequences, which suggests that the depositional processes of these facies are closely linked. These sequences display strong upward-fining tendencies, whilst the bases are commonly sharply defined, the fining upwards transitions are generally gradational and occur through interbedding (Fig.1.8.). Such sequences throughout the Brae Formation tend to be stacked vertically and give the overall reservoir sequence a well developed layering into coarse-grained packages (Facies 1 & 3) and finer grained packages (Facies 4, 5 & 6). Within this large scale layering, the coarse-grained packages often occur as channel-like bodies separated by finer-grained interchannel areas (Turner et al.1987).

A combination of lithostratigraphic, structural, biostratigraphic and reservoir pressure correlation techniques has been utilised by Marathon to delineate seven reservoir layers across the field (C. Turner, Marathon *pers. comm.* 1990) (Layers 1&2; Layer 3; Layer 5a; Layer 5b; Layer 5c; Layer 6; and Layer 7). The majority of the layers are separated vertically from those above or below by finer rock units (either beds of shale or sandstone). These fine-grained rock units restrict vertical reservoir communication over large areas of the field. Layer 7 is the deepest reservoir subdivision, the base of which is ill defined

(Fig.1.8.). In 1989 the existing reservoir correlations were reviewed and a new reservoir correlation nomenclature was generated to incorporate the shaly (non-reservoir) layers as well as additional intra-layer subdivisions. Four reservoir zones have been designated A, B, C and D. Zone A is equivalent to the upper Brae Formation that mainly corresponds to the previous Layer 1 & 2 and Layer 3. Zone B the middle Brae Formation correlates with previous layers 5a, 5b & 5c. Zones C/D make up the lower Brae Formation and correspond to Layers 6 & 7 or older. Each of these major zones have been subdivided into layers (eg.Aa, Ab, Ac and Ad), and sublayers (eg. Aa1, Aa2, Aa3) see Figure 1.8. This refined lithology distribution should facilitate more accurate modelling of fluid flow in the reservoir.

1.7. RESERVOIR FLUIDS

Formation water analysis revealed that water composition varies with depth. With increasing depth there is an increase in all the dissolved solids; these include sodium, calcium, magnesium, barium and strontium (see Table 1.2). Bicarbonate decreases with depth from 3,620 to 1,620 p.p.m. The $^{87}Sr/^{86}Sr$ ratios are distinctly different for the different stratigraphic layers, there is an increase of measured $^{87}Sr/^{86}Sr$ as we go down the layers within the field. In Layer 1 & 2 for well A8 the $^{87}Sr/^{86}Sr$ is 0.72470±3, in Layer 3 for well A5 the ratio is 0.72641±4. The pH of South Brae formation brine has been estimated by Marathon to be between 4.5 and 4.8 (J. Hardy, Marathon *pers. comm.* 1991). Formation water analysis is very important as its variation within a field indicates the extent of reservoir connectivity (Coleman et al.1990). The API Gravity for the South Brae oil ranges from 33° to 37° API, CO_2 contents range from 32% to 35%, and low concentrations of H_2S exist (85 p.p.m.) (Scottish Petroleum Annual 1988-89; Roberts 1992).

1.8. MINERALOGY

Petrographic examination was performed for over seventy thin section samples from the South Brae wells 16/7a - A3, 16/7a - A6, 16/7a - A11, 16/7a - A27 & 16/7b - A19 (Fig.1.9.) at true vertical depths ranging from 12,080-13,689 ft (3,685-4,170m). Prior to sectioning samples were impregnated with blue epoxy resin to highlight porosity. Each sample was petrographically examined and point counted (500 counts) for grain size and composition (Table 1.1.). The results showed the primary controls on mineralogical composition are provenance and depositional facies, rather than any variation due to stratigraphic position within the reservoir system.

The sandstones are composed predominantly of various amounts of quartz, and lesser amounts of feldspar, micaceous minerals, metamorphic and sedimentary rock fragments, bitumen and opaques. Diagenetic minerals include authigenic quartz, pyrite, calcite cement and authigenic clays. These sandstones fall under the classification of a quartz arenite (Fig.1.10. from Table 1.3).

Detrital single grains of quartz (48-88%) are the most common constituent in these samples, with trace amounts of polycrystalline and stretched or recrystallized metamorphic quartz grains (0.5-2%). The polycrystalline quartz is more common in the coarser sandstone than the finer-grained sandstone. Subangular to subrounded quartz grain shapes dominate. Floating contacts are common in the calcite-cemented horizons, with long and point contacts abundant in the sandier lithologies and concave/convex and sutured contacts more common in the siltier samples.

Chert occurs as detrital grains displaying the characteristic microcrystalline texture. The metamorphic rock fragments consist of schists and phyllites. The sedimentary rock fragment suite consists of claystones, siltstones, sandstones and carbonates. The fossil fragments observed include sponge spicules, echinoderms, bivalves and various shell fragments.

The clast composition is dominated by subangular fine-grained feldspathic sandstones which make up 60-95% of the clasts. The maximum sizes are mostly 20-40cm although other workers have observed boulders up to 150cm (Stow et al.1982). Quartz pebbles are also quite common and range in size from 2-7cm, they are usually very well-rounded.

The detrital micaceous minerals predominantly consist of muscovite with trace amounts of chlorite and biotite. Some of these detrital micas have been altered to kaolinite, and others show variable amounts of fraying and expansion.

Well 16/7a-A6 is particularly feldspathic with approximately 9.0 to 10.0% evident in some of the quartz-cemented sandstones. Minor amounts of detrital feldspar (usually <5%) occur in the sandstones of wells A3,A11,A19 & A27, most of which have been affected by dissolution. Within the calcite-cemented concretions the feldspar content ranges from 1-3%. The majority of the feldspar grains have been dissolved during early diagenesis and have been replaced by the early calcite cement. Some replacement of feldspar by late carbonate was observed and small feldspar inclusions still exist within the later calcite cement. The K-feldspar content is greater than that of plagioclase. The plagioclase grains look fresh and unaltered whereas the K-feldspar grains

appear leached and replaced by calcite. This would suggest that the amount of dissolution appears to be controlled by the composition of the feldspar ie. the K-feldspar is more unstable. In some cases all the feldspar has been totally dissolved leaving large equigranular secondary pores, and a consequent enhancement of the porosity. An approximate estimate of the original feldspar content before any early dissolution would be close to 10%.

The opaques in these samples include pyrite, carbonaceous material, wood fragments, zircon and rutile. The pyrite occurs as two forms, in small framboids and as larger cubes. The smaller framboids are an early diagenetic feature and are associated with carbonaceous wispy layers in the finer-grained sandstones. The cubic pyrite is a late diagenetic mineral and occurs in the dissolution pores.

1.9. DIAGENESIS

The diagenetic sequence observed by the study of 70 thin sections of South Brae reservoir rocks appears similar for all sandstones and the matrix of the conglomerates. The paragenetic sequence also appears similar above and below the oil water contact when examined in thin section. Not all the diagenetic events occurred everywhere in South Brae and it is extremely unlikely that these events happened at precisely the same time throughout the whole of the reservoir. Certain lithologies have undergone diagenetic changes that have not affected all of the reservoir and therefore there may be a slight overlap of the various diagenetic events in the paragenetic sequence (Fig.1.11.). Carbonate diagenesis is discussed in detail in Chapter 2, silica in Chapter 3 and dissolution porosity in Chapter 4.

The general sequence of events leading to the preservation, enhancement and destruction of porosity in the South Brae samples following deposition is as follows: early formation of calcite cements with partial dissolution of detrital quartz and feldspar grains (some of which is contemporaneous with compaction), formation of trace amounts of authigenic framboidal pyrite, chlorite and illite, authigenic quartz overgrowth formation, dissolution of carbonate cement and detrital feldspar and mica, further calcite and minor dolomite cementation, formation of authigenic clays (illite and kaolinite) and cubic pyrite, and finally hydrocarbon emplacement (Fig.1.11).

Compaction continued throughout the burial history of the sediment, except during the early Cretaceous (Fig.1.5.). Mechanical compaction led to the destruction of porosity by rearranging the configuration of the component detrital grains. Clay clasts were deformed to form a pseudomatrix, mica flakes were squeezed (Fig.1.12.), frayed and sheared and in some places pebbles and detrital grains were fractured. Compaction also released some silica through pressure dissolution shown by interpenetrating detrital quartz grains (Fig.1.13.). Many of the effects of compaction were locally halted by early calcite and quartz cementation events.

Shortly after deposition of the sediments, carbonate cements of either concretionary or pervasive nature were the first to precipitate. Carbonate cemented concretions range from 0.8 to 4m thick (Fig.1.14.), whereas pervasive (non-concretionary) cements are usually only a few cm thick. They do not appear to correlate from well to well. The presence of 30-40% calcite cement within these concretions and the fact that the detrital grains have a very open texture and appear to float within the cement (Fig.1.15.) indicates that these cements developed prior to any significant compaction of the rocks

(Table 1.3). In samples where the original calcite cement is preserved, porosity is reduced to zero.

Two types of calcite cement occur; - firstly an early cement which is found in concretions and some thin bedding parallel horizons. These developed both before any other diagenetic minerals formed and prior to significant compaction - detrital grains have a very open texture. Concurrent with this early calcite cementation event, feldspars were being dissolved within the cemented areas and calcite was being precipitated in their place (Fig.1.16.). Secondly some later calcite cementation postdates a much later feldspar dissolution event (Fig.1.17.). The calcite cements are discussed in more detail in Chapter 2. Dolomite cement which is not a common feature, is of late origin and usually seen in dissolution pores in the form of small rhombs (Fig.1.18.). Some siderite rhombs were found, but they are extremely rare.

Authigenic clay occurs in small amounts in a number of the samples; it usually coats detrital grains or can be found in small dissolution pores where it seems to be very locally derived from the dissolution of the feldspar. Illite, or occasionally chlorite, are found as authigenic coatings, but they are not very common (<1%). The pore-filling clays take the form of wispy illite or vermiform kaolinite (1-2%). No authigenic clay coatings were seen within the concretions. Some authigenic pyrite was seen as framboids within the concretions and as tiny inclusions within quartz overgrowths and therefore predates quartz overgrowth formation, but is contemporaneous with calcite cementation.

Authigenic quartz overgrowth formation was the next major diagenetic event. Where the early carbonate cements are absent, authigenic quartz

cements are the main lithifying agents. Quartz cementation was polyphase (Fig.1.19.) - at least 2 zones were noted in some samples examined with CL - and occurred over significant periods of time (see Chapter 3). Some small overgrowths were found protruding into secondary pores (Fig.1.20.). The quartz cements constitute from 1-10% of the overall sandstone. The overgrowths have reduced the primary porosity but probably have prevented further compaction. It is difficult in most cases to distinguish the overgrowths from the detrital cores, as there are few or no dustrims and in most instances a total lack of delineating features. With the aid of CL on the SEM the percentage of quartz overgrowth was quantified more accurately, as the overgrowth and the detrital core display different luminescence intensities; the core luminesces brightly whereas the authigenic overgrowth does not (Fig.1.21.). Diagenetic quartz occurs as grain-rimming cements, as small euhedral overgrowths surrounding the original detrital grain or occasionally, as long prismatic overgrowths.

The next major diagenetic event, was dissolution of early pervasive calcite cement and mica, feldspar, calcareous fossil fragments and carbonate clasts. Some of the concretionary calcite cement was also dissolved, but it was restricted to the outer limits of the concretions (Fig.1.22.). It is difficult to quantify how much cement was lost, but thin section petrography shows that up to 5cm at the rim of a 1m concretion has increased secondary porosity. The feldspar dissolution is most abundant in the sandy coarse-grained lithologies where compaction has been halted mechanically to a certain extent by authigenic quartz growth (Fig.1.23.). This has maintained pathways for the migration of fluids which are capable of dissolving feldspar, or at a later stage precipitating authigenic clays. This accords with the suggestion of Harris (1989) that the low flux of formation water through the finer-grained

sandstone should result in less dissolution of feldspar grains as the permeability is lower than that of a coarse-grained sandstone.

This secondary porosity was not greatly affected by subsequent diagenetic processes. Small quantities of pore-filling kaolinite and illite (Fig.1.24.) were precipitated, and some late-stage cubic pyrite (Fig.1.25.) and minor amounts of quartz, calcite (Fig.1.26.) and dolomite rhombs have been observed.

Hydrocarbons then entered the reservoir system. The oil-water contact (O.W.C.) seems to have little effect on the vertical secondary quartz distribution and the secondary porosity. Due to the lack of oil bearing fluid inclusions in the quartz overgrowths it is certain that secondary quartz cementation has ceased prior to oil infiltration.

1.10. ISOTOPIC ANALYSES

1.10.1. Stable Isotopes Principles & Applications.

With the use of several isotope systems in this thesis, it may be beneficial to expand on some important aspects of their principles and applications. The variations measured by mass spectrometers may be reported as absolute ratios such as $^{18}O/^{16}O$, but they are more often reported in terms of a factor δ in per mil (‰) or parts per thousand, where

$$\delta = \left(\frac{R\ sample}{R\ standard} - 1 \right) .10^3$$

and R is the ratio of the two selected isotopes in a sample or standard, so R= D/H, $^{13}C/^{12}C$, $^{18}O/^{16}O$ and $^{34}S/^{32}S$.

For oxygen the standards commonly used are either Standard Mean Ocean

Water, SMOW as defined by Craig (1961), or PDB, the carbonate from a Cretaceous belemnite first used as a standard by Urey et al. (1951). Likewise D/H variations are referred to SMOW and $^{13}C/^{12}C$ variations to PDB. Troilite (FeS) from the Canyon Diablo meteorite is the standard used for $^{34}S/^{32}S$. Positive or negative δ values indicate enrichment or depletion of the heavier isotope in the sample relative to the standard.

The isotopic variations are due to mass differences between the isotopes that lead to small differences in the vibrational frequencies of the atoms in a molecule or crystal. As a result, the thermal properties of the isotope vary and may lead to fractionation in the distribution of the isotopes between two phases (Mason & Moore 1982). For the distribution of ^{18}O and ^{16}O, for example, an isotope fractionation factor α between two phases M and W may be calculated as

$$\alpha = \frac{R_M}{R_W} = \frac{(^{18}O/^{16}O)\text{phase M}}{(^{18}O/^{16}O)\text{phase W}}$$

Fluid and mineral oxygen isotope values and temperature can be related by

$$1000\ln\alpha_{\text{Mineral - } H_2O} = A.\,10^6.\,T^{-2} - B$$

Where α is the oxygen isotope equilibrium fractionation factor between M and W, T is temperature in °K and A and B are numerical constants. The temperature dependence of α at equilibrium forms the basis of oxygen isotope geothermometry (Bigeleisen & Mayer 1947, Urey 1947)

1.10.2. Carbon and Oxygen analyses

Samples were systematically selected from centre to edge of the carbonate concretions, and also from early non-concretionary and late cemented sandstones and veins. Each sample was thin sectioned and the petrography

examined with optical microscopy and CL. The samples were disaggregated by a jaw crusher (approximately 500g) and the clays removed by settling. The samples were placed in 6% vol. hydrogen peroxide in order to remove any organics present. After being dried they were then sieved into various size fractions. The 250-500μm fraction was selected for stable isotope analysis as thin section examination showed it to be a representative size fraction for the grains of carbonate forming the cements. Tetrabromoethane was used to separate the carbonate grains from the framework silicate grains. XRD analysis was carried out on the samples to check purity. The separates were oxygen plasma ashed for two hours in a Polaron Bio-Rad Asher in order to destroy any organic matter. Some of the separates contained small amounts (<5%) of quartz but this was not extracted in isotope analyses.

Carbon and oxygen extractions for calcite were performed using the method outlined by Mc Crea (1950). Samples weighing 25 to 35 mg. were reacted with 5ml. 100% phosphoric acid for three hours in a water bath kept at the constant temperature of 25°C. The evolved carbon dioxide gas was dried, purified and analysed on a VG SIRA 10 Mass Spectrometer. Carbon isotope values for the carbonates are shown in δ notation as parts per thousand relative to PDB (Pee Dee Belemnite), and the oxygen isotope analyses are quoted relative to SMOW (Standard Mean Ocean Water). A phosphoric acid fractionation factor of 1.01025 (Friedman & O'Neil, 1977) was used to correct the raw values for the $\delta^{18}O$ compositions of the samples

$$\alpha \text{ (fractionation factor)} = \frac{(^{18}O/^{16}O)CO_2}{(^{18}O/^{16}O) \text{ carbonate}}$$

Replicate analysis of inter-laboratory standard MBL1 produced an average $\delta^{18}O$ value of 28.74‰(SMOW) and a $\delta^{13}C$ value of 1.98‰(PDB) with a precision of $\delta^{18}O \pm 0.2$‰(SMOW) and $\delta^{13}C \pm 0.1$‰(PDB).

Oxygen isotope analysis requires approximately 10mg of quartz sample, this was loaded into nickel reaction vessels, which were then outgassed at high vacuum at 250°C for one hour. The oxygen was liberated from the samples by oxidation reaction with ClF_3 (Borthwick & Harmon 1982) at 650°C. The oxygen was purified and reduced to CO_2 using a vacuum extraction line similar to that described by Clayton & Mayeda, (1963). The CO_2 gas was analysed on a VG-SIRA 10 mass spectrometer and $\delta^{18}O$ compositions of the quartz are quoted relative to SMOW (Standard Mean Ocean Water). The oxygen yield for each sample was calculated by comparing the initial weight of the sample with the number of micromoles of gas produced. The replicate analysis of inter-laboratory standard NBS#28 produced an average $\delta^{18}O$ value of 9.9‰±0.31 (SMOW).

1.10.3. Strontium analyses

The same samples prepared for oxygen and carbon isotope analyses were analysed for their strontium and rubidium abundance and strontium isotopic composition. All sample dissolution and purification was performed in PFA teflon screw-top beakers (Savillex). Samples of calcite were initially weighed, and then ultrasonically washed in reverse osmosis (RO) ultrapure water to remove any labile Sr. After centrifuging and decanting the supernatant liquid, the dried residue from this washing was reweighed. The calcite was then dissolved overnight in cold 2.5M HCl. After centrifuging, any residue from this procedure (e.g. intergrown quartz or feldspar) was dried and weighed, and thus the weight of calcite dissolved in the HCl was calculated by difference. The samples were now spiked with ^{84}Sr and ^{87}Rb spikes. The solution was dried down and the residue taken up in 2 mls 2.5M HCl.

Micas and feldspars were dissolved using 10mls 40% HF and 1ml 14M HNO_3 on a hotplate overnight at 150°C. The beakers were removed, cooled, and then the solution dried down under lamps. The residue was then dissolved in 3 mls 14M HNO_3 overnight on a hotplate, and dried down as before. The residue was now dissolved in 8 mls 6M HCl on a hotplate. After cooling the sample was spiked with ^{84}Sr and ^{87}Rb spikes. This solution was dried down and the final residue taken up in 2 mls 2.5M HCl.

Formation waters were weighed and then centrifuged to remove any particulate matter. The residue from this process was weighed and the weight of water to be analysed calculated by difference. Waters were then spiked for Rb and Sr as above. The sample was then dried down and taken up in 2 mls 2.5M HCl.

The strontium and rubidium were separated by conventional cation-exchange chromatography, and their concentrations were determined by isotope dilution. Rubidium and strontium analyses were performed on a Micromass MM30 and on a VG - Isomass 54E thermal ionization mass spectrometer respectively. Strontium isotopic ratios were corrected for mass fractionation during mass spectrometry by normalizing the $^{87}Sr/^{86}Sr$ ratios to a value of 0.1194. The NBS 987 Sr standard gave an $^{87}Sr/^{86}Sr$ value of 0.71028±2 (2σ) during the course of this study. All data are reported relative to NBS 987 = 0.71022. Measured $^{87}Sr/^{86}Sr$ values have to be corrected for the radioactive decay of ^{87}Rb to ^{87}Sr, between formation of the mineral and the present day; $^{87}Sr = {}^{87}Rb(e^{\lambda t}-1)$. To calculate the initial $^{87}Sr/^{86}Sr$ ratio of the mineral at the time of precipitation,

$(^{87}Sr/^{86}Sr)$ radiogenic = $(^{87}Rb/^{86}Sr)$ measured $(e^{\lambda t}-1)$

$(^{87}Sr/^{86}Sr)$ measured = $(^{87}Sr/^{86}Sr)$ initial + $(^{87}Rb/^{86}Sr)$ measured $(e^{\lambda t}-1)$

$(^{87}Sr/^{86}Sr)$ measured - $(^{87}Rb/^{86}Sr)$ measured $(e^{\lambda t}-1)$ = $(^{87}Sr/^{86}Sr)$ initial

$\lambda = 1.42 \times 10^{-1}.a^{-1}$ t = age of formation (140Ma)

1.10.4. Sulphur Analyses

Six pyrite samples were analysed for $\delta^{34}S$. The pyrite (~5mg) was reacted with excess Cu_2O at 1070°C (after Robinson & Kusakabe 1975) so producing SO_2. The prepared gas was analysed on a SIRA 2 Mass Spectrometer. standard correction factors were applied to the raw $\delta^{34}S$ ratios (Craig 1957). The analyses show a narrow range of values from +7.5 to -1.6‰ relative to CDT (Table 1.4.). One early framboidal pyrite sample gave a value of -1.6‰, late stage cubic pyrite values ranged from 0.7 to 1.8‰, and samples which contained both forms of pyrite (and a lot of bitumen material) ranged from 7.5 to 6.7‰. These values are recorded for the sake of completeness. Further interpretation of such a small database is not warranted.

1.11. DIAGENETIC POREFLUIDS

Fluids and their dissolved solutes are inextricably linked to the burial diagenesis of sediments. Studies of formation water chemistry in conjunction with a study of the authigenic cements in a reservoir, can potentially constrain the source of elements involved in cementation, and the volumes of waters and acids necessary for dissolution of detrital and authigenic minerals. Therefore a porewater may have a very complex chemistry - as it reflects the original depositional water which may be altered by water-rock interaction and has possibly mixed with externally-derived fluids. It is possible to combine isotopic analysis (which can potentially indicate the origin of the porefluid ie. marine, meteoric etc.) with chemical data (dissolved solid analyses, salinity measurements using fluid inclusion

microthermometry) to help us understand the origin and the evolution of the porefluid through time. Several terms are used within the next few chapters pertaining to the waters found in sedimentary basins:

1.11.1. Meteoric Water

Meteoric water is derived ultimately from atmospheric precipitation. Because of the solvent power of water the runoff from the land is never pure H_2O but always contains dissolved solids, therefore the composition of the water can be very varied. The world average salinity is 1.0g/l (Clarke 1924). Fresh water and glacial ice and snow are enriched in ^{16}O and H and have negative $\delta^{18}O$ and δD values. The enrichment in the lighter isotope increases with decreasing air temperature and therefore varies seasonally as well as being strongly latitude dependent. The $\delta^{18}O$ values of meteoric waters range from about 0 to -60‰ SMOW whereas δD varies from about +10 to less than -360‰ SMOW (Faure 1986). The range of $\delta^{13}C$ values available within the meteoric diagenetic environment is also enormous, ranging from -20‰ (PDB) characteristic of soil gas CO_2 to +20‰ (PDB) associated with organic fermentation processes (Irwin et al. 1977).

Chemical weathering of rocks releases strontium into solution in lakes, rivers and groundwater. The isotopic composition of the Sr varies and depends ultimately on the relative solubilities of the minerals, the age and Rb/Sr ratio of the rock being weathered (Faure 1986). Weathering of the terrigenous clastics derived from the Caledonides during the Upper Jurassic (140Ma) are likely to give rise to solutions having low Sr concentrations and high $^{87}Sr/^{86}Sr$ ratios. We can potentially distinguish these detrital values from a possible marine contribution, as they will have lower $^{87}Sr/^{86}Sr$ ratios and higher Sr concentrations .

1.11.2. Marine Water

Marine water in the open ocean the salinity (dissolved solids) averages 35‰ with a regional range between 32-37‰ (Mason & Moore 1982). The relative proportions of the major ions are practically constant, and the $\delta^{18}O$ and δD values of seawater are close to zero and vary only within narrow limits. The $\delta^{18}O$ value of +0.5‰SMOW varies slightly with changes in salinity (a decrease of 0.11‰ per 1‰ decrease in salinity; Craig & Gordan 1965). The isotopic composition of the seawater is positively correlated with its salinity. The $\delta^{13}C$ value of seawater is normally 0‰PDB but it may vary considerably due to changes in ocean structure and its productivity (Kroopnick et al. 1977).

The $^{87}Sr/^{86}Sr$ of modern oceans is 0.70906±0.00033 and appears to be constant worldwide. The $^{87}Sr/^{86}Sr$ ratio of seawater is controlled by the mixing of three isotopic varieties of strontium 1) young volcanic rocks 2) old sialic rocks of the continental crust and 3) marine carbonate rocks of Phanerozoic age (Faure et al.1965). Peterman et al. (1970) postulated that the $^{87}Sr/^{86}Sr$ ratio of seawater is an indicator of the type of rocks exposed to weathering at a particular time. Analyzing Sr extracted from marine limestones and dolomites of known ages geologists discovered that the $^{87}Sr/^{86}Sr$ ratio of the oceans had varied systematically during Phanerozoic time. The $^{87}Sr/^{86}Sr$ seawater curve for Phanerozoic time (after Burke et al. 1982) can be found in Figure 1.27.

1.11.3. Connate Water

Connate water is found in deeply buried sedimentary rocks; this was originally the porewater trapped during accumulation of the sedimentary pile. Such waters - oilfield brines, interstitial pore-waters have remained in contact with most lithologies at elevated temperatures for millions of years

and tend to be highly saline (Gill 1989). If the fluid has undergone chemical modification and/or physical migration it is no longer a connate fluid. In theory connate fluids of different ages could be used to reconstruct the geochemical history of seawater (Hanor 1987).

The isotopic composition of Sr in interstitial waters of marine sediments also deviate from that of seawater due to the release of Sr from minerals during diagenesis after deposition (Clauer et al. 1975).

1.11.4. Formation Water

Formation water is the aqueous fluid, generally a brine, found today in a sedimentary formation with no specific implication concerning its age or origin. Formation waters are an important part of the hydrologic cycle because they are the medium within which crude oil and natural gas are found (Hitchon & Friedman 1969). The δD and $\delta^{18}O$ of oilfield brines and connate waters were expected to converge to the isotopic composition of seawater (Fig.1.28.). However they intersect the line representing the meteoric line. The hypothesis advanced by Clayton et al. (1966), is that the evolution is a progressive isotope exchange between the water and the mineral constituents of the rocks. Ultimately the $\delta^{13}C$, $\delta^{18}O$ and δD values are extremely variable.

Subsurface brines contain Sr whose isotopic composition depends on the kinds of rocks that they have interacted with. Chadhuri (1978) and Steuber et al. (1984) found the $^{87}Sr/^{86}Sr$ ratios of oilfield brines were different from those of seawater at the time of deposition of the host rocks, they noted that the Sr was derived from the rocks with which the brines had interacted.

1.12. REVIEW OF EARLIER STUDIES

In the last two decades, clastic diagenesis of North Sea reservoirs has been extensively studied. It is of great practical importance to understand the diagenetic reactions which control in part the quality and quantity of porosity and permeability in reservoir rocks. Quartz and calcite form the bulk of diagenetically-produced pore filling in the South Brae sandstones. Here, the possible sources for these cements are reviewed and the various mechanisms for developing secondary porosity are considered.

1.12.1. Sources of $CaCO_3$

Shallow marine sandstones very often contain calcite-cemented intervals or concretions. This diagenetic phenomenon has been documented by Hamilton et al. (1987), Saigal & Bjrlykke (1987), Brint (1989) and Bjorkum & Walderhaug (1990) for the North Sea. Similar intervals have been reported by Davies (1967), Kantorowicz et al. (1987) and Bryant et al.(1988) for onshore England and Boles & Ramseyer (1987) have looked at concretions in the United States. In all cases these concretions have severely reduced reservoir quality from the early stages of diagenesis.

Many papers have discussed the possible sources of calcite cement. Irwin et al. (1977) and Curtis & Coleman (1986) showed, using the stable isotopes of carbon and oxygen, that carbonate has been produced by the decomposition of organic matter with characteristic $\delta^{13}C$ signatures for the depth-related biogenic and thermal processes. An influx of CO_2 cannot lead to calcite precipitation unless some source of Ca^{2+} is present as shown by Saigal & Bjørlykke (1987). Dissolution of carbonate fossils is commonly observed in shallow marine sandstones (Hudson & Andrews, 1987) and in some cases the

isotopic composition of the calcite cement indicates that biogenic carbonate has been its dominant source (Bjørkum & Walderhaug, 1990). With the influx of organically-derived CO_2 the $\delta^{13}C$ of the calcite cements will be drastically altered reverting to low $\delta^{13}C$. Ca^{2+} may also be derived from plagioclase (Boles & Ramseyer 1987), but in many sandstones there is little evidence of plagioclase dissolution (Saigal & Bjørlykke 1987, Walderhaug et al. 1989). Where carbonate cementation occurs at the seafloor, Ca^{2+} may be supplied from the seawater (Bathurst 1975). This type of early cementation gives rise to 'hardgrounds' which are texturally and isotopically distinct from calcite cemented intervals (Marshall & Ashton 1980).

Many calcite-cemented fossiliferous concretions have precipitated from meteoric waters; this is the case in South Brae and also for concretions described by Hamilton et al.(1987) and Saigal & Bjørlykke (1987). Since carbonate fossils are usually the only significant source of calcium, it is most likely that the critical degree of supersaturation necessary for nucleation of the new cement will be first achieved within the fossil-rich layer. This fluid is supersaturated with respect to aragonite and high Mg calcite and cementation is commonly associated with corrosion of silicate minerals; this was noticed in the South Brae samples and also by Saigal & Bjørlykke (1987). Wilkinson (1991) has suggested that pre-existing carbonate can act as a template for easier nucleation. The majority of this cementation seems to occur between 0.25 - 2km at relatively low temperatures of 10°-60°C.

1.12.2. Sources of SiO_2

Quartz cement as syntaxial overgrowths is one of the most abundant cements in sandstones; it is the major destroyer of porosity and the main control of reservoir quality (Glasmann et al.1989). Most quartz cement grows after

sandstones have been buried 1 to 2km and are subjected to temperatures greater than 50°C (McBride 1989). Using the present geothermal gradient the depth of cementation can be calculated indirectly from fluid inclusion temperatures (eg. Haszeldine et al.1984, Walderhaug 1990) and oxygen isotopic composition of quartz overgrowths (eg. Land & Dutton 1978, Brint et al.1991).

Several different sources of silica have been proposed as the source of quartz cement in sandstones. Many authors have cited intergranular pressure solution as an important source of silica, especially in sands that have undergone significant burial and contain stylolite seams (Blanche & Whitaker 1978, Ehrenberg 1990). Few of these studies have been quantitative, and in many cases quartz cementation took place before pressure solution began (eg. Houseknecht 1988). Large volumes of silica could possibly be generated during diagenesis of clay minerals in shales, but it is uncertain if the silica ever leaves this site. A model proposed by Haszeldine et al.(1984) had silica supplied by temperature-dominated illitization of smectitic clays in deep sandstones which was then transported upwards by convecting porefluids. Bjørlykke et al.(1989) similarly suggested that thermal convection may be a mechanism that can significantly modify silica distribution in thick sandbodies as it allows dissolution and precipitation of silica from the same volume of porewater. However this mechanism is probably only important where relatively steep sloping isotherms exist ie. adjacent to igneous and hydrothermal intrusions and saltdomes. It is highly unlikely for thermal convection to take place in a natural sedimentary sequence (sand/shale) as the conditions for Rayleigh convection are rarely met (Bjorlykke et al.1989). Kantorowicz (1985) reported early quartz cement to be dominant in the fluvial facies of the Ravenscar Group. He favoured a meteoric source where silica was derived from silicate mineral dissolution in the zone of weathering. Isotopic evidence presented by

Fisher & Land (1986) and Dutton & Land (1988), Dutton & Diggs (1990) for fluvial-deltaic sediments indicate that quartz cement can be precipitated by formation waters with a strong meteoric component- this occurs as the gravity-driven water flow cools during upward migration. Quartz cementation in the Travis Peak Formation, East Texas occurred at depths of 1-1.5km.

1.12.3 Secondary Porosity

The development of secondary porosity is a potential method of improving the quality of a hydrocarbon reservoir (Schmidt & MacDonald 1979). It has a widespread presence in many of the North Sea reservoirs - and it is hypothesized to occur at all stages of diagenesis depending on local conditions.

In the Middle Jurassic Brent sandstones shallow dissolution porosity was created following the dissolution of feldspar and early calcite cement (Blanche & Whitaker 1978, Hancock & Taylor 1978, Sommer 1978 and Blackbourn 1984). Secondary porosity in many North Sea reservoirs is formed at relatively shallow burial and is associated with meteoric water throughflow (Bjørlykke et al.1989). Meteoric water containing CO_2 is known to dissolve feldspars during shallow burial in sandstone aquifers (Schmidt & MacDonald, 1979). However studies by Bjørlykke (1984) and Lundegard et al.(1984) showed that organic matter generally contains insufficient oxygen to generate enough CO_2 in deep burial to explain the observed amounts of secondary porosity in U.S.A. Gulf Coast or North Sea basins. Secondary porosity may also be generated by mixing corrosion (Plummer 1975); this is most likely to occur at sites where meteoric water mixes with seawater or basinal brines, and may be relatively common in deltas. It arises when two solutions of different

compositions which are both in equilibrium with a given mineral are mixed - the result is a solution either under or oversaturated with respect to the mineral in question. Cementation may occur due to oversaturation, while leaching may result due to undersaturation.

Favoured mechanisms for developing late diagenetic secondary porosity at depth out of reach of meteoric waters are either: - 1) By utilizing acidic porewaters generated in the zone of abiotic decarboxylation reactions (Curtis 1978), or 2) By the effects of porewater enriched in organic acids derived from the maturation of kerogens (Surdam & Cressey 1985), or 3) By hydrothermal solutions of deep-seated origins rising along deep-seated faults (Riches et al.1986) or 4) By slow equilibrium dissolution of thermodynamically unstable feldspar (Giles & de Boer 1989) or 5) By episodic release of formation waters such as the release of large volumes of porefluids during seismic pumping (Sibson et al.1975, Burley 1986)

1.13. THESIS FORMAT

This thesis comprises 3 papers, Chapters 2 to 4, which investigate various aspects of the diagenetic history of the South Brae Oilfield. It also contains a summary of the conclusions which are presented in Chapter 5.

The first paper, Chapter 2, examines the origin and formation of early concretionary calcite bodies and late calcite cements using petrographic, geochemical and isotopic techniques. In Chapter 3 the origins of quartz cement, timing of cementation, controls on cement distribution and the

hydrologic conditions which transport the silica to the site of cementation are examined in detail. Chapter 4 investigates the origin of secondary porosity and attempts to integrate the geometrical areal extent of the porosity zone with the 'plumbing' of the reservoir.

1.14. ACKNOWLEDGEMENTS

Marathon Oil (U.K.) Ltd. provided the funding for this project and allowed access to their data and core of the South Brae Oilfield. This research was carried out at the Department of Geology and Applied Geology, University of Glasgow, and the Isotopes Geology Unit, Scottish Universities Research and Reactor Centre (SURRC). The authors would like to thank Douglas Maclean (Glasgow University) for his help with the production of photomicrographs.

1.15. REFERENCES CITED

Bathurst, R.G.C. (1975) Carbonate sediments and their diagenesis. Elsevier, Amsterdam, 2nd ed. 658pp.

Berner, R.A. (1980) Early Diagenesis: a Theoretical Approach. Princeton, NJ: Princeton University Press.

Bigeleisen, J. & Mayer, M.G. (1947) Calculation of equilibrium constants for isotopic exchange reactions. Journal of Chemical Physics, 15. pp.261-267.

Bjørlykke, K. (1984) Formation of secondary porosity: How important is it? In McDonald, D.A and Surdam, R.C. (eds). Clastic Diagenesis: Association of American Petroleum Geologists, Memoir 37. pp.277-286.

Bjørlykke, K., Ramm, M. & Saigal, G.C. (1989) Sandstone diagenesis and porosity modification during basin evolution. Geologische Rundschau, v.78/1. pp.243-268.

Bjørkum, P.A. & Walderhaug, O. (1990) Geometrical arrangement of calcite cementation within shallow marine sandstones. Earth Science Reviews, v.29. pp.145-161.

Blackbourn, G.A. (1984) Diagenetic history and reservoir quality of a Brent sand sequence. Clay Mineralogy, v.19. pp.377-389.

Blanche, J.R. & Whitaker, J.H.McD. (1978) Diagenesis of part of the Brent sand

Formation (Middle Jurassic) of the northern North Sea basin. Geological Society of London, v.135. pp.73-82.

Blatt, H. (1979) Diagenetic processes in sandstones. Society of Economic Paleontologists and Mineralogists Special Publication, No.26, pp.141-157.

Boles,J.R. & K. Ramseyer. (1987) Diagenetic carbonate in Miocene Sandstone Reservoir, San Joaquin Basin, California. American Association of Petroleum Geologists, v.71. pp.1475-1487.

Borthwick, J. & Harmon, R.S. (1982) A note regarding ClF_3 as an alternative to BrF_5 for oxygen isotope analysis: Geochimica et Cosmichima Acta, v.46. pp.1665-1668.

Brint, J.F. (1989) The formation and origin of carbonate cemented zones in the Brent Sandstones of the Dunlin Field, Northern North Sea. Unpublished Ph.D. thesis, University of Strathclyde.

Brint, J.F., Hamilton, P.J., Haszeldine, R.S., Fallick, A.E. & Brown, S. (1991) Oxygen isotopic analysis of diagenetic quartz overgrowths from the Brent sandstones: A comparison of two preparation methods. Journal of Sedimentary Petrology, v.6. pp.527-533.

Bryant, T.D. Kantorowicz, J.D. & Love, C.F. (1988) The origin and recognition of laterally continuous carbonate cemented horizons in the Upper Lias Sands of southern England. Marine and Petroleum Geology, v.5. pp.108-133.

Buhrig, C. (1989) Geopressured Jurassic reservoirs in the Viking Graben:

modelling and geological significance. Marine and Petroleum Geology, v.6. pp.31-48.

Burke, W.H., Denison, R.E., Hetherington, E.A., Koepnick, R.B., Nelson, H.F. & Otto, J.B. (1982) Variation of seawater $^{87}Sr/^{86}Sr$ throughout Phanerozoic time. Geology, v.10, pp.516-519.

Burley, S.D. (1986) The development and destruction of porosity within Upper Jurassic reservoir sandstones of the Piper and Tartan fields, Outer Moray Firth, North Sea. Clay Minerals, v.21. pp.649-694.

Chaudhuri, S. (1978) Strontium isotopic composition of several oilfield brines from Kansas and Colarado. Geochimica et Cosmochimica Acta, v.42. pp.329-331.

Clarke, F.W. (1924) The data of geochemistry (fifth ed.) 841 pp. U.S. Geological Survey Bulletin, 770.

Clauer, N., Hoffert, M., Grimaud, D. & Millot, G. (1975) Composition isotopique du strontium d'eaux interstitielles extraits de sediments recents: Un argument en faveur de l'homogeneisation isotopique des mineraux argileux. Geochimica et Cosmochimica Acta, v.39. pp.1579-1582.

Clayton, R.N. & Mayeda, T.K. (1963) The use of bromine pentafluoride in the extraction of oxygen from oxides and silicates for isotope analysis. Geochimica et Cosmochimica Acta, v.27. pp.43-52.

Clayton, R.N., Friedman, I., Graf, D.L., Mayeda, T.K., Meents, W.F. & Schimp, N.F. (1966) The origin of saline formation waters. 1. Isotopic composition. Journal of Geophysical Research, 71. pp.3869-3882.

Coleman, M.L., Jones, M.R.O. & Cox, M.A. (1990) Analysis of formation water sampled from core. North Sea Oil and Gas Reservoirs II.The Norwegian Institute of Technology, (Graham & Trotman). pp.165-171.

Craig, H. (1957) Isotopic standards for carbon and oxygen and correction factors for mass-spectrometric analysis of carbondioxide: Geochimica et Cosmochimica Acta, v. 12. pp.133-149.

Craig, H. & Gordan, L.I. (1965) Deuterium and oxygen-18 variations in the ocean and the marine atmosphere. In Stable Isotopes in Oceanographic Studies and Paleotemperatures (ed. E. Tongiorgi), pp.9-130. Consiglio Nazionale delle Richerche, Laboratorio di Geologia Nucleare, Pisa.

Curtis, C.D. (1978) Possible links between sandstone diagenesis and depth related geochemical reactions occurring in enclosing mudstone. Journal of the Geological Society of London, v.135. pp.107-117.

Curtis, C.D. & Coleman, M.L. (1986) Controls on the precipitation of early diagenetic calcite, dolomite and siderite concretions in complex depositional sequences, in D.L.Gautier (Ed), Roles of Organic Matter in Sediment Diagenesis. Society of Economic Paleontologists and Mineralogists Special Publication, v.38. pp.22-35.

Davies, D.K. (1967) Origin of friable sandstone - calcareous sandstone rhythms

in the Upper Lias of England. Journal of Sedimentary Petrology, v.37. pp.1179-1188.

Dutton, S.P. & Land, L.S. (1988) Diagenetic history of a well cemented quartz arenite, Lower Cretaceous Travis Peak Formation, East Texas. Geological Society of America Bulletin, v.100. pp.1271-1282.

Dutton, S.P. & Diggs, T.N. (1990) History of quartz cementation in the Lower Cretaceous Travis Peak Formation, East Texas. Journal of Sedimentary Petrology, v.60. pp.191-202.

Ehrenberg, S.N. (1990) Relationship between diagenesis and reservoir quality in sandstones of the Garn Formation, Haltenbanken area, Mid-Norwegian continental shelf. American Association of Petroleum Geologists Bulletin, v.74, pp.1538-1558.

Faure, G., Hurley, P.M. & Powell, J.L. (1965) The isotopic composition of strontium in surface water from the North Atlantic Ocean. Geochimica et Cosmichimica Acta, v.29. pp.209-220.

Faure, G. (1986) Principles of Isotope Geology, (2nd ed.) John Wiley & Sons, Canada, pp.183-196.

Fisher, R.S. & Land, L.S. (1986) Diagenetic history of Eocene Wilcox sandstones, south-central Texas. Geochimica et Cosmichimica Acta, v.50. pp.551-561.

Friedman, I. & O'Neil, J.R. (1977) Compilation of stable isotope fractionation

factors of geochemical interest. In: Data of Geochemistry, sixth edition, M. Fleischer (ed). United States Geological Survey Professional Paper, 440-kk, 12pp.

Giles, M.R. & de Boer, R.B. (1989) Secondary porosity: Creation of enhanced porosities in the subsurface from the dissolution of carbonate cements as a result of cooling formation water. Marine and Petroleum Geology, v.6. pp.261-269.

Gill, R. (1989) Chemical Fundamentals of Geology. (1st ed.) Unwin Hyman Ltd. London, pp.78-203.

Glasmann, J.R., Lundegard, P.D., Clark, R.A., Penny, B.K. & Collins, I.D. (1989) Geochemical evidence for the history of diagenesis and fluid migration: Brent sandstone, Heather Field, North Sea. Clay Minerals, v.24. pp.255-284.

Glennie, K.W. (1984) Structural framework and pre-Permian history of the North Sea area, In Glennie, K.W. (Ed.) Introduction to the Petroleum Geology of the North Sea, Blackwell, Oxford, pp.25-60.

Hamilton,P.J., Fallick,A.E., Macintyre,R.M. & S.Elliott. (1987) Isotopic tracing of the provenance and diagenesis of Lower Brent Group Sands, North Sea.In Brooks, J., and Glennie, K. (Eds) Petroleum Geology of North West Europe, Graham & Trotman, London, pp.939-949.

Hancock, N.J. & Taylor, A.M. (1978) Clay mineral diagenesis and oil migration in the Middle Jurassic Brent Sand Formation. Journal of the Geological of London, v.135. pp.69-72.

Hanor, J.S. (1987) Origin and migration of subsurface sedimentary brines. Short Course no. 21. Society of Economic Paleontologists and Mineralogists.

Harms, J.C., Tackenberg, P., Pickles, E. & Pollock, R.E. (1981) The Brae oilfield area, In Illing, L.V. & Hobson, G.D. (Eds) Petroleum Geology of the Continental Shelf of North-west Europe. Heyden, London, pp.352-357.

Harris, J.P. & Fowler, R.M. (1987) Enhanced prospectivity of the Mid-Late Jurassic sediments of the South Viking Graben, Northern North Sea. In Brooks, J., and Glennie, K. (Eds) Petroleum Geology of North West Europe, Graham & Trotman, London, pp.879-898.

Harris, N.B. (1989) Diagenetic quartz arenite and destruction of secondary porosity: an example from the Middle Jurassic Brent sandstones of North West Europe. Geology, v.17. pp.361-364.

Haszeldine, R.S., Samson, I.M. & Cornford, C. (1984) Quartz diagenesis and convective fluid movement; Beatrice Oilfield, U.K. North Sea. Clay Mineralogy. v.19, pp.391-402.

Hitchon, B. & Friedman, I. (1969) Geochemistry and origin of formation waters in the Western Canada sedimentary basin - 1. Stable isotopes of hydrogen and oxygen. Geochimica et Cosmochimica Acta, v.33. pp.1323-1349.

Houseknecht, D.W. (1988) Intergranular pressure solution in four quartzose sandstones. Journal of Sedimentary Petrology, v.58. pp.228-246.

Hudson, J.D. & Andrews, J.E., (1987) The diagenesis of the Great Estuarine Group, Middle Jurassic, Inner Hebrides, Scotland. In J.D. Marshall (Ed.) Diagenesis of Sedimentary Sequences. Blackwell, Oxford, pp.259-276.

Irwin, H., Curtis, C.D. & Coleman, M. (1977) Isotopic evidence for source of diagenetic carbonates formed during burial of organic-rich sediments. Nature, v.269. pp.209-213.

Kantorowicz, J.D. (1985) The petrology and diagenesis of Middle Jurassic sediments, Ravenscar Group, Yorkshire, Sedimentology, v.32. pp.833-853.

Kantorowicz, J.D., Bryant, T.D. & Dawans, J.M. (1987) Controls on the geometry and distribution of carbonate cements in Jurassic sandstones: Bridport Sands, southern England and the Viking Group, Troll Field, Norway. In J.D. Marshall (Ed.) Diagenesis of Sedimentary Sequences. Blackwell, Oxford, pp.103-118.

Kroopnick, P.M., Margolis, S.V. & Wong, C.S. (1977) $\delta^{13}C$ variations in marine carbonate sediments as indicators of the CO_2 balance between the atmosphere and the oceans. In The Fate of Fossil Fuel CO_2 in the Oceans (eds. N.R. Anderson & A. Malahoff) pp.295-321. New York: Plenum Press.

Land, L.S. & Dutton, S.P. (1978) Cementation of a Pennsylvanian deltaic sandstone: isotopic data. Journal of Sedimentary Petrology, v.48. pp.1167-1176.

Lundegard, P.D., Land, L.S. & Galloway, W.E. (1984) Problem of secondary porosity: Frio Formation (Oligocene), Texas Gulf Coast. Geology, v.12. pp.399-402.

Mackenzie, A.S., Price, I., Leythaeuser, D., Muller, P., Radke, M. & Schaefer, R.G. (1987) The expulsion of petroleum from Kimmeridge clay source rocks in the area of the Brae Oilfield. U.K. In Brooks, J. & Glennie, K. (Eds) Petroleum Geology of North West Europe, Graham & Trotman, London, pp.865-877.

Marshall, J.D. & Ashton, M. (1980) Isotopic and trace element evidence for submarine lithification of hardgrounds in the Jurassic of eastern England. Sedimentology, v.27. pp.271-289.

Mason, B. & Moore, C.B. (1982) Principles of Geochemistry. (4th ed.) James Wiley & Sons, Inc. Canada. pp.233-250.

McBride, E.F. (1963) A classification of common sandstones. Journal of Sedimentary Petrology, v.33. pp.664-669.

McBride, E.F. (1989) Quartz cement in sandstones : A review. Earth Science Reviews, v.26, pp.69-112.

McCrea, J.M. (1950) . On the isotope chemistry of carbonates and a paleotemperature scale, Journal of Chemical Physics, v.18, pp.849-857.

Peterman, Z.E., Hedge, C.E. & Tourtelot, H.A. (1970) Isotopic composition of strontium in seawater throughout Phanerazoic time. Geochimica et Cosmochimica Acta, v.34. pp.105-120.

Plummer, L.N. (1975) Mixing of sea water with calcium carbonate ground water. Geological Society of America, Memoir 142. pp.219-236.

Riches, P., Traub-Sobott, I., Zimmerle, W. & Zinkernagel, U. (1986) Diagenetic peculiarities of the potential Lower Jurassic reservoir sandstones: Troms I area of Northern Norway and their tectonic significance. Clay Minerals, v.21. pp.565-584.

Roberts, M.J. (1991) The South Brae Field, Block 16/7a, UK North Sea. Geological Society Memoirs No. 14. From Abbotts, I.L. (ed) United Kingdom Oil and Gas Fields. Geology Society of London Press. pp.55-62.

Robinson, B.W. & Kusakabe, M. (19750 Quantative preparation of sulphur dioxide, for sulphur-34/sulphur-32 analysis, from sulphides by combustion with cuprous oxide: Analytical Chemistry, v.47. pp.1179-1181.

Saigal,G.C. & Bjørlykke, K. (1987) Carbonate cements in clastic reservoir rocks from offshore Norway - relationships between isotopic composition textural development and burial depth. From Marshall, J.D. (ed) Diagenesis of Sedimentary Sequences. Geological Society Special Publication, no.36. pp.313-324.

Schmidt, V. & MacDonald, D.A. (1979) The role of secondary porosity in the course of sandstone diagenesis. In: Scholle, P.A. and Schuger, P.R. (eds): Aspects of diagenesis. Society of Economic Paleontologists and Mineralogists. Special publication, 26. pp.175-207.

Scottish Petroleum Annual 1988-89. Ed. Ted Strachan. Aberdeen Petroleum Publishers Ltd, Waverley Press. pp.38.

Sibson, R.H., Moore, McM. & Rankin, A.H. (1975) Seismic pumping, a

hydrothermal fluid transport mechanism. Journal of the Geological Society of London, v.31. pp.653-659.

Sommer, F. (1978) Diagenesis of Jurassic sandstones in the Viking Graben. Journal of the Geological Society of London, v.135, pp.63-67.

Steuber, A.M., Pushkar, P. & Hetherington, E.A. (1984) A strontium isotopic study of Smackover brines and associated solids, southern Arkansas. Geochimica et Cosmichimica Acta, v.48. pp.1637-1649.

Stoker, S., & Brown, S. (1987) Coarse clastic sediments of the Brae field and adjacent areas, North Sea: a core workshop. British Geological Survey. Hydrocarbons Research Programme.

Stow, D.A.V., Bishop, C.D. & Mills, S.J. (1982) Sedimentology of the Brae oilfield, North Sea. Fan models and controls. Journal of Petroleum Geology, v.5, No.2, pp.129-148.

Surdam, R.C. & Cressey, L.J. (1985) Organic - inorganic reactions during progressive burial: key to porosity and permeability enhancement and preservation. Philosophical Transactions of the Royal Society of London, A315. pp.135-156.

Surlyk, F. (1978) Jurassic basin evolution of East Greenland. Nature, v.274. pp.130-133.

Turner, C.C., Cohen, J.M., Connell, E.R. & Cooper, D.M. (1987) A depositional model for the South Brae Oilfield, In Brooks, J., and Glennie, K. (Eds)

Petroleum Geology of North West Europe, Graham & Trotman, London, pp.853-864.

Urey, H.C. (1947) The thermodynamic properties of isotopic substances. Journal of the Chemical Society. pp.562-581.

Urey, H.C., Lowenstam, H.A., Epstein, S. & McKinney, C.R. (1951) Measurement of paleotemperatures and temperatures of the Upper Cretaceous of England, Denmark and the Southeastern United States. Bulletin of the Geological Society of America, v.62. pp.399

Walderhaug, O. (1990) A fluid inclusion study of quartz-cemented sandstones from offshore Mid-Norway - possible evidence for continued quartz cementation during oil emplacement. Journal of Sedimentary Petrology, v.60. pp.203-210.

Walderhaug, O., Bjørkum, P. A. & Bolas, H.M.N. (1989) Correlation of calcite cemented layers in shallow marine sandstone of Fensfjørd Formation in the Brage Field. Correlation in Hydrocarbon Exploration. Norwegian Petroleum Society. (Graham & Trotman) pp.367-375.

Wilkinson, M. (1991) The concretions of the Bearreraig Sandstone Formation: geometry and geochemistry. Sedimentology, v.38. pp.899-912.

Ziegler, P.A. (1978) North-Western Europe: tectonics and basin development. Geologie Mijnbouw, v.57. pp.589-626.

1.16. TABLES

TABLE 1.1. List of samples selected from the Brae Formation in the South Brae Oilfield, North Sea, U.K. Zone A is equivalent to the Brae Formation, Zone B the middle Brae Formation and Zone C makes up the lower Brae Formation.

MD (ft)	TVD (ft)	TVD (m)	LITHOLOGY	ZONE
16/7a-A3				
13387'	12080'	3684.4	sandstone (<10% silty laminae)	Aa1
13418'5"	12111'5"	3694	sandstone (<10% silty laminae)	Aa2-4
13740'	12433'2"	3792.1	sandstone (<10% silty laminae)	Ad
14055'5"	12746'	3887.5	sandstone (<10% silty laminae)	Bc1-4
14382'5"	13072'5"	3987.1	siltstone (20-50% sdst laminae or ripple lenses)	Bd
14396'2"	13086'2"	3991.2	sandstone (<10% silty laminae)	Ca1-4
14755'1"	13444'1"	4100.5	sandstone (<10% silty laminae)	Cc1-3
16/7a-A6				
14944'2"	12995'2"	3963.5	sandy sandstone conglomerate (sdst clast only)	Ac2-6
14945'6"	12996'6"	3963.8	sandy sandstone conglomerate (sdst clast only)	Ac2-6
14946'7"	12997'7"	3464.3	sandstone (<10% silty laminae)	Ac2-6
14948'5"	12999'5"	3964.8	sandstone (<10% silty laminae)	Ac2-6
14988'	13037'	3976.3	sandstone (<10% silty laminae)	Ad
15197'	13243'	4039.1	shale	Ba1-4
15369'	13412'	4090.6	sandstone (<10% silty laminae)	Bc1-4
15372'	13415'	4091.6	sandstone (<10% silty laminae)	Bc1-4
15376'	13419'	4092.8	sandstone (<10% silty laminae)	Bc1-4
15379'8"	13422'8"	4093.9	sandstone (<10% silty laminae)	Bc1-4
15419'3"	13462'3"	4106	siltstone (<20% sdst laminae or ripple lenses)	Ca1-4

TABLE 1.1. continued.

MD (ft)	TVD (ft)	TVD (m)	LITHOLOGY	ZONE
<u>16/7a-A11</u>				
14875'6"	12712'6"	3877.3	sandstone (<10% silty laminae)	Aa1
14895'	12750'	3888.8	sandstone (<10% silty laminae)	Aa1
14935'	12790'	3901	sandstone (<10% silty laminae)	Aa2-4
14958'	12813'	3908	sandstone (<10% silty laminae)	Aa2-4
14973'	12828'	3912.5	sandstone (<10% silty laminae)	Ab
15293'3"	13145'3"	4009.3	silty sdst (50-80% sdst laminae or ripple lenses)	Ba1-4
15312'6"	13164'6"	4015.2	sandstone (<10% silty laminae)	Ba1-4
15338'3"	13190'3"	4023	silty sdst (50-80% sdst laminae or ripple lenses)	Ba1-4
15382'	13233'	4036.1	sandy sdst conglomerate (sdst clasts only)	Ba1-4
15387'	13238'	4037.6	sandstone (<10% silty laminae)	Ba1-4
15570'	13422'	4093.7	siltstone (<20% sdst laminae or ripple lenses)	Bc1-4
15780'5"	13629'5"	4157	sandstone (<10% silty laminae)	Cc1-3
15783'	13632'	4157.8	sandstone (<10% silty laminae)	Cc1-3
15829'9"	13678'9"	4172.1	sandstone (<10% silty laminae)	Cc1-3
15845'	13694'	4176.7	calcite cemented conglomerate	Cc1-3
15853'4"	13702'4"	4179.2	calcite cemented conglomerate	Cc1-3
15854'5"	13703'5"	4179.6	calcite cemented conglomerate	Cc1-3
15858'9"	13707'9"	4180.9	calcite cemented conglomerate	Cc1-3
15870'	13719'	4184.3	sandy qz conglomerate (qz & sdst clasts)	Cc1-3
15871'	13720'	4184.7	sandy qz conglomerate (qz & sdst clasts)	Cc1-3
15888'4"	13737'4"	4189.9	calcite cemented conglomerate	Cc1-3
15927'	13776'	4201.7	calcite cemented conglomerate	Cc1-3

TABLE 1.1. continued.

MD (ft)	TVD (ft)	TVD (m)	LITHOLOGY	ZONE
<u>16/7a-A11</u>				
15929'	13778'	4202.3	calcite cemented conglomerate	Cc1-3
15929'6"	13778'6"	4202.5	sandstone (<10% silty laminae)	Cc1-3
15936'4"	13791'4"	4204.5	sandstone (<10% silty laminae)	Cd
<u>16/7b-A19</u>				
19270'	13355'	4073.3	sandstone (<10% silty laminae)	Aa1
19326'	13404'	4088.2	sandstone (<10% silty laminae)	Aa2-4
19332'	13410'	4090.1	sandstone (<10% silty laminae)	Aa2-4
19337'	13415'	4091.6	sandstone (<10% silty laminae)	Aa2-4
19380'3"	13460'3"	4105.4	sandstone (<10% silty laminae)	Aa2-4
19432'	13501'	4117.8	sandstone (<10% silty laminae)	Aa2-4
19432'5"	13501'5"	4117.9	sandy qz conglomerate (qz & sdst clasts)	Aa2-4
19433'	13502'	4118.1	sandy qz conglomerate (qz & sdst clasts)	Aa2-4
19433'8"	13502'8"	4118.4	sandy qz conglomerate (qz & sdst clasts)	Aa2-4
19435'	13504'	4118.7	sandy qz conglomerate (qz & sdst clasts)	Aa2-4
19435'1"	13504'1"	4118.8	sandy qz conglomerate (qz & sdst clasts)	Aa2-4
19437'8"	13506'	4119.3	sandy qz conglomerate (qz & sdst clasts)	Aa2-4
19441'	13570'	4120.6	sandstone (<10% silty laminae)	Aa2-4
19567'	13630'	4157.2	sandy sdst conglomerate (sdst clast only)	Aa2-4
19605'	13660'	4166.3	sandstone (<10% silty laminae)	Aa2-4
19626'6"	13672'6"	4170.1	sandy sdst conglomerate (sdst clast only)	Aa2-4
19641'6"	13688'6"	4168.9	sandy slst.(50-80% sdst laminae or ripple lenses)	Aa2-4

TABLE 1.1. continued.

MD (ft)	TVD (ft) ZONE	TVD (m)		LITHOLOGY
<u>16/7a-A27</u>				
16389'	12891'	3931.7	shale	Kimmeridge Clay
16402'	12904'	3935.7	shale	Kimmeridge Clay
16481'	12978'	3958.4	sandstone (<10% silty laminae)	Kimmeridge Clay
16483'	12980'	3958.9	sandstone (<10% silty laminae)	Kimmeridge Clay
16488'	12986'	3960.4	sandstone (<10% silty laminae)	Kimmeridge Clay
16490'	12987'	3961	sandstone (<10% silty laminae)	Kimmeridge Clay
16496'	12993'	3962.9	sandstone (<10% silty laminae)	Kimmeridge Clay
16520'	13016'	3969.9	sandstone (<10% silty laminae)	Aa1
16525'	13026'	3972.9	sandstone (<10% silty laminae)	Aa1
16564'	13061'	3983.6	sandstone (<10% silty laminae)	Aa1
16619'	13114'	3999.8	sandstone (<10% silty laminae)	Aa1
16746'	13240'	4038	sandstone (<10% silty laminae)	Ac1
16929'6"	13413'6"	4091.1	shale	Ad
17043'	13526'	4125.4	calcite cemented sandstone	Ba1-4
17048'	13531'	4126.8	calcite cemented sandstone	Ba1-4
17051'	13534'	4127.9	calcite cemented sandstone	Ba1-4
17052'	13535'	4128.2	calcite cemented sandstone	Ba1-4
17053'	13536'	4128.5	calcite cemented sandstone	Ba1-4
17057'4"	13540'4"	4129.8	shale	Ba1-4
17058'	13541'	4130	calcite cemented sandstone	Ba1-4
17072'4"	13554'4"	4134.1	sandstone (<10% silty laminae)	Ba1-4

Table 1.2. Composition of formation water samples, total dissolved solid analyses (ppm) were carried out by Marathon Oil, U.K . Isotopic analyses were carried out by the author.

Well	16/7a - A5	16/7a - A5	16/7a - A8	16/7a - A8	16/7a - A27	16/7a - A27	16/7a - A31	16/7a - A31
Zone	Aa_{1-4}	Ac_{1-6}	Aa_{1-4}	Ba_{1-4}	Aa_{1-4}	Bc_{1-4}	Ba_{1-4}	Cc_{1-3}
Sodium	17300	26180	22650	29210	23700	35220	27800	28600
Potassium	675	860	900	1240	920	1490	930	990
Calcium	345	230	210	350	345	705	385	350
Magnesium	69	37	43	68	33	77	46	49
Barium	290	670	550	780	490	1610	1170	1330
Strontium	12	20	26	67	19	145	91	95
Chloride	29500	39720	34790	46800	36730	58680	48270	46830
Sulphate	12	11	30	10	17	14	110	300
Bicarbonate	2980	3360	3270	3090	3620	1620	2980	3120

Table 1.2. continued

Well Zone	16/7a - A5 Aa_{1-4}	16/7a - A5 Ac_{1-6}	16/7a - A8 Aa_{1-4}	16/7a - A8 Ba_{1-4}	16/7a - A27 Aa_{1-4}	16/7a - A27 Bc_{1-4}	16/7a - A31 Ba_{1-4}	16/7a - A31 Cc_{1-3}
δ D (SMOW)	-11‰	-24‰	-	-	-	-	-20‰	-22‰
$^{87}Sr/^{86}Sr$	0.72456±4	0.72641±4	0.72470±3	-	-	-	-	0.71770±5
Rubidium	3.37	5.34	5.0	-	-	-	-	5.49
Strontium	12.2	16.4	31	-	-	-	-	84.3
$\delta^{18}O$ (SMOW)	-0.22‰	+0.76‰	-	-	-	-	-0.58‰	+0.58‰

Table 1.3. Point count data for South Brae Sandstones.

Well	16/7a-A3					16/7a-A6	
T.V.D. (ft)	12080'	12111'5"	12433'2"	13072'5"	13444'1"	12995'2"	12996'6"
Detrital							
Quartz	64.6	63.2	58			63.6	50.4
Feldspar	5.6	3.8	5.8			4.6	7.6
Rock Fragments	7.0	5.2	12.6			4.4	4.0
Pebbles	-	-	-			-	-
Clay Matrix	-	-	-			5.4	9.0
Mica	0.4	0.6	0.4			0.6	1.8
Authigenic							
Quartz	2.2	5.0	4.0			0.6	-
Calcite	0.2	1.0	0.8			5.6	22.4
Dolomite							
Clay	6.6	8.0	5.8			-	-
Pyrite	1.8	2.4	1.6			2.4	0.2
Shells	-	-	-			obs.	obs.
Porosity	11.6	9.2	11.0			12.8	4.6

Table 1.3. continued

Well	16/7a-A6							
T.V.D. (ft)	12997'7"	13037'	13243'	13412'	13415'	13419'	13422'8"	13462'3"
Detrital								
Quartz	57.2	57.4	75.0	49.0	46.8	50.9	62.6	65.6
Feldspar	4.6	10.6	7.0	3.0	3.2	4.6	3.6	5.0
Rock Fragments	7.4	0.2	2.0	10.0	5.4	5.8	9.0	2.0
Pebbles	-	-	-	-	-	-	-	-
Clay Matrix	7.0	24.2	7.0	-	-	-	-	-
Mica	1.0	3.4	1.4	0.4	-	0.2	0.2	3.0
Authigenic								
Quartz	-	0.6	1.4	-	-	-	-	2.6
Calcite	21.4	0.2	1.6	37.4	44.4	38.6	23.8	18.0
Dolomite								
Clay	-	-	-	-	-	-	-	-
Pyrite	0.8	3.8	1.6	0.2	0.2	0.8	0.8	1.8
Shells						obs.		obs.
Porosity	0.6	-	3.0	-	-	-	-	2.0

Table 1.3. continued.

Well 16/7a-A11 T.V.D. (ft)	12712'6"	12750'	12790'	12813'	12828'	13145'3"	13164'6"	13190'3"
Detrital								
Quartz	57.0	74.0	85.0	61.6	71.2	60.0	59.4	68.0
Feldspar	4.2	3.0	2.0	5.0	0.2	6.0	5.4	4.8
Rock Fragments	-	-	0.6	4.2	4.0	1.0	4.6	4.6
Pebbles	-	-	-	-	-	-	-	-
Clay Matrix	2.2	1.6	0.4	5.8	4.2	10.0	6.0	6.6
Mica	1.2	-	-	0.1	0.1	8.0	1.0	1.8
Authigenic								
Quartz	-	5.0	4.0	5.8	0.2	2.0	10.8	5.6
Calcite	34.0	-	-	-	0.2	3.0	-	0.1
Dolomite	-	-	-	-	-	-	-	-
Clay	-	1.2	0.8	0.1	-	-	2.0	0.1
Pyrite	1.4	2.2	1.2	0.2	-	2.0	1.8	1.8
Shells								
Porosity	-	13.0	6.0	17.2	19.0	18.0	9.0	6.6

Table 1.3. continued.

Well	16/7a-A11							
T.V.D. (ft)	13233'	13238'	13629'5"	13632'	13678'9"	13694'	13702'4"	13703'5"
Detrital								
Quartz	65.8	65.6	74.8	63.6	73.4	55.2	55.0	49.8
Feldspar	4.8	3.8	1.8	6.4	1.8	5.0	3.4	7.0
Rock Fragments	1.0	3.6	3.8	3.4	-	4.8	3.6	4.6
Pebbles	-	-	-	-	-	-	-	-
Clay Matrix	11.6	8.8	4.6	9.2	2.4	1.6	2.0	2.8
Mica	2.8	1.6	1.8	1.4	1.0	1.2	1.0	1.2
Authigenic								
Quartz	3.8	10.2	2.8	1.8	4.2	-	-	-
Calcite	-	-	-	5.6	-	28.2	34.2	32.0
Dolomite	-	-	-	-	-	-	-	-
Clay	2.8	0.8	3.8	0.8	2.6	-	-	-
Pyrite	0.8	-	-	0.8	-	4.0	0.8	2.6
Shells	-	-	-	-	-	obs.	obs.	obs.
Porosity	6.6	5.6	6.6	7.0	14.6	-	-	-

Table 1.3. continued.

Well	16/7a-A11							
T.V.D. (ft)	13707'9"	13719'	13720'	13737'4"	13776'	13778'	13778'6"	13791'4"
Detrital								
Quartz	57.0	52.0	48.4	56.0	46.4	50.8	48.6	69.0
Feldspar	8.0	2.0	4.4	5.0	4.4	5.4	4.6	5.8
Rock Fragments	4.4	8.0	9.0	-	10.0	1.6	8.6	5.0
Pebbles	-	-	-	-	-	-	-	-
Clay Matrix	0.8	-	0.2	32.0	1.0	-	-	7.7
Mica	0.3	1.4	1.2	4.0	-	0.2	0.2	2.2
Authigenic								
Quartz	-	0.8	-	-	-	-	-	7.0
Calcite	29.5	33.0	36.8	-	38.2	41.4	35.8	-
Dolomite	-	-	-	-	-	-	-	-
Clay	-	1.8	-	-	-	-	-	2.0
Pyrite	-	1.0	-	-	-	0.6	2.2	1.3
Shells	obs.	obs.	obs.	-	obs.	obs.	obs.	
Porosity	-	-	-	3.0	-	-	-	-

Table 1.3. continued.

Well	16/7b-A19							
T.V.D. (ft)	13355'	13410'	13415'	13460'3"	13501'	13504'	13506'8"	13570'
Detrital								
Quartz	65.4	65.8	65.6	74.0	57.4	64.0	67.0	76.5
Feldspar	3.8	1.6	2.0	2.6	3.0	5.0	3.0	1.0
Rock Fragments	0.4	2.6	1.6	4.4	4.0	-	3.0	2.8
Pebbles	-	-	-	-	obs.	-	-	-
Clay Matrix	1.2	-	1.4	1.8	-	-	2.0	2.0
Mica	0.6	1.6	-	-	1.2	-	-	-
Authigenic								
Quartz	3.6	5.0	5.6	3.4	-	-	-	2.0
Calcite	-	0.8	-	0.2	32.4	30.0	18.5	-
Dolomite	-	-	-	-	-	-	-	-
Clay	-	5.0	3.0	0.8	-	-	-	1.0
Pyrite	0.6	0.6	1.4	0.6	2.0	-	-	1.6
Shells	-	-	-	-	obs.	obs.	obs.	-
Porosity	19.0	17.0	19.4	12.2	-	-	6.5	13.0

Table 1.3. continued.

Well	16/7b-A19				16/7a-A27		
T.V.D. (ft)	13630'	13660'	13672'6"	13688'6"	12978'	12987'	13016'
Detrital							
Quartz	74.6	66.8	56.0	64.0	65.8	64.6	57.0
Feldspar	4.0	2.2	9.4	4.0	4.4	2.6	0.4
Rock Fragments	1.6	4.2	7.0	2.0	3.6	6.0	28.6
Pebbles	-	-	-	-	-	-	-
Clay Matrix	2.0	4.2	-	7.0	-	2.0	-
Mica	-	-	1.0	1.2	2.4	0.6	0.2
Authigenic							
Quartz	2.0	4.0	2.6	-	3.0	5.2	1.2
Calcite	-	-	6.0	19.0	1.2	0.2	1.0
Dolomite	-	-	-	obs.	-	-	-
Clay	0.6	2.4	3.0	0.8	5.0	2.4	2.6
Pyrite	0.4	2.0	2.0	0.8	1.8	0.6	0.6
Shells	-	-	-	-	-	-	-
Porosity	14.8	14.2	13.0	1.2	12.8	15.8	5.4

Table 1.3. continued.

Well	16/7a-A27							
T.V.D. (ft)	13061'	13413'6"	13526'	13531'	13535'	13536'	13538'	13554'4"
Detrital								
Quartz	71.4	61.2	66.6	43.0	36.6	36.4	27.2	57.6
Feldspar	2.6	2.8	2.8	2.0	4.2	6.0	3.6	2.2
Rock Fragments	7.6	8.8	-	-	-	-	-	18.6
Pebbles	-	-	5.2	23.6	27.0	18.0	41.0	-
Clay Matrix	0.8	3.0	1.0	-	2.0	0.2	0.2	2.0
Mica	-	0.4	0.6	-	-	-	-	0.2
Authigenic								
Quartz	1.8	1.8	1.2	-	-	-	-	2.2
Calcite	-	-	21.8	31.0	28.8	37.4	26.0	-
Dolomite	-	-	-	-	-	-	-	-
Clay	3.4	3.6	-	-	1.2	-	-	4.2
Pyrite	-	1.8	0.6	0.4	1.4	0.8	1.4	0.4
Shells	-	-	-	-	-	-	-	-
Porosity	12.4	16.6	0.2	-	-	-	-	12.6

Table 1.4.
List of samples from the South Brae Oilfield which were analysed for $\delta^{34}S$.

Well	Depth (T.V.D.)	$\delta^{34}S$	Pyrite Type
16/7b-A19	13688'6"	7.47	Early Framboids & Late cubes in micas
16/7b-A19	13672'6"	1.43	Late cubic
16/7b-A19	13660'	1.81	Late cubic
16/7b-A19	13630'	6.71	Early & Late Mix
16/7b-A19	13504'1"	-1.64	Early Framboidal
16/7a-A3	12111'5"	0.74	Late Euhedral

1.17. FIGURE CAPTIONS & FIGURES

Figure 1.1 Location of Brae relative to major tectonic elements. The shaded areas contain thick Jurassic deposits (after Ziegler, 1978).

Figure 1.2 Plot of formation overpressures versus aquifer depth (UK sector) after Buhrig, 1989. South Brae is moderately overpressured relative to the hydrostatic gradient.

Figure 1.3 Schematic cross section showing approximate position of the wells sampled in the South Brae area (see Fig.1.9. for location of drillholes).

Figure 1.4 Burial curve for the Brae Formation (Oxfordian) in the South Brae field. The reconstructed burial curve is based on well 16/7a-8 and uses present day rock thicknesses.

Figure 1.5 Conceptual hypothesis indicating four fluid influences on South Brae, from deposition through diagenesis.

Figure 1.6 Schematic depositional model, Unit 2 (late Oxfordian to late Volgian age), South Viking Graben (after Stoker & Brown, 1987)

Figure 1.7a Generalized facies map of (Cc) Lower Brae Formation reservoir defined by two apron shaped conglomeratic complexes (after internal Marathon report).

Figure 1.7b Generalized facies map of (Ac) Upper Brae Formation reservoir, made up of channelized conglomerates which are separated by shaly islands (after internal Marathon report).

Figure 1.8 Brae Formation type section well 16/7a-8, a composite fining upwards 'mega sequence' 500m thick apex upward triangles define the seven reservoir layers (after Harris & Fowler, 1987). The 1989 Marathon new reservoir

correlations (zones A to D) have also been included, where they relate to the old Layer nomenclature.

Figure 1.9 South Brae area top structure map showing location of wells studied, location of the major faults and the approximate line of section in Figure 1.4.

Figure 1.10 Framework - grain compositions from South Brae, wells 16/7a- A3, A6, A11, A27 & 16/7b - A19. Classification after Mc Bride, 1963. Point count data in Table 1.3.

Figure 1.11 Paragenetic sequence showing timing of major diagenetic events in the South Brae oilfield. Diagenesis above and below the O.W.C. appears to be identical.

Figure 1.12 Crossed polars photomicrograph of mica flakes squeezed, frayed and sheared due to compaction in 16/7b-A19, 13410' (T.V.D.).

Figure 1.13 Crossed polars photomicrograph of interpenetrating quartz grains showing a pressure solution texture 16/7a-A27, 13413'6" (T.V.D.).

Figure 1.14 South Brae core photograph showing a conglomerate with a coarse grained sandy matrix, calcite cemented to the right and quartz cemented to the left 16/7a-A27, 13535' (T.V.D.). Scale bar is 2cm.

Figure 1.15 Crossed polars photomicrograph of detrital quartz grains exhibiting a floating grain texture in a calcite cemented concretion. Some of the quartz grains are etched around the edges 16/7a-A6, 14945'6" (T.V.D.).

Figure 1.16 Cathodoluminescence photomicrograph showing concurrent feldspar dissolution and early calcite cementation 16/7a-A11, 13776' (T.V.D.). Note that certain feldspar grains have not been effected by this dissolution

event and are extremely well preserved. This is due to compositional differences.

Figure 1.17 Cathodoluminescence photomicrograph showing late stage dissolution of feldspar (quartz overgrowths protrude into the pores) followed by later calcite cementation 16/7a-A6, 15419'3" (T.V.D.).

Figure 1.18 Cathodoluminescence photomicrograph of a late stage dolomite rhomb luminescing scarlet 16/7b-A19, 13506' (T.V.D.).

Figure 1.19 Scanning Electron Microscope cathodoluminescence photomicrograph of polyphase quartz cementation, showing at least two distinct zones 16/7a-A11, 13791'4" (T.V.D.).

Figure 1.20 Quartz overgrowth protruding into a large secondary pore which contains remnants of the original grain (possibly feldspar) 16/7a-A3, 12433'2" (T.V.D.). The black porefilling material is bitumen.

Figure 1.21 Scanning Electron Microscope cathodoluminescence photomicrograph of detrital (luminescent) and authigenic (non-luminescent) quartz 16/7a-A27, 12978' (T.V.D.).

Figure 1.22 Plane polarized light photomicrograph showing dissolution of concretionary cement resulting in oversized pores 16/7b-A19, 13501' (T.V.D.).

Figure 1.23 Late stage intense feldspar dissolution 16/7a-A3, 12080' (T.V.D.). The black porefilling material is bitumen.

Figure 1.24 Late stage hairy illite infilling large secondary pores and overgrowing the secondary quartz 16/7b-A19, 13415' (T.V.D.).

Figure 1.25 Late stage cubic pyrite found in primary and secondary porespace 16/7a-A3, 12112' (T.V.D.).

Figure 1.26 Crossed polars photomicrograph of late stage calcite cement which has cemented in the quartz overgrowths 16/7b-A19, 13460' (T.V.D.).

Figure 1.27 Variation of the $^{87}Sr/^{86}Sr$ ratio of marine carbonates in Phanerozoic time (after Faure 1986). Adapted from data by Burke et al. (1982).

Figure 1.28 Relationships between δD and $\delta^{18}O$ in brines from the Gulf Coast, Illinois, Michigan and Alberta collected from oil wells in sedimentary rocks of marine origin. The lines that were fitted to experimental data points bear no relationship to the isotopic composition of seawater but intersect the trajectory for meteoric water at compositions close to present day precipitation in these areas (after Clayton et al.1966 and Faure, 1986).

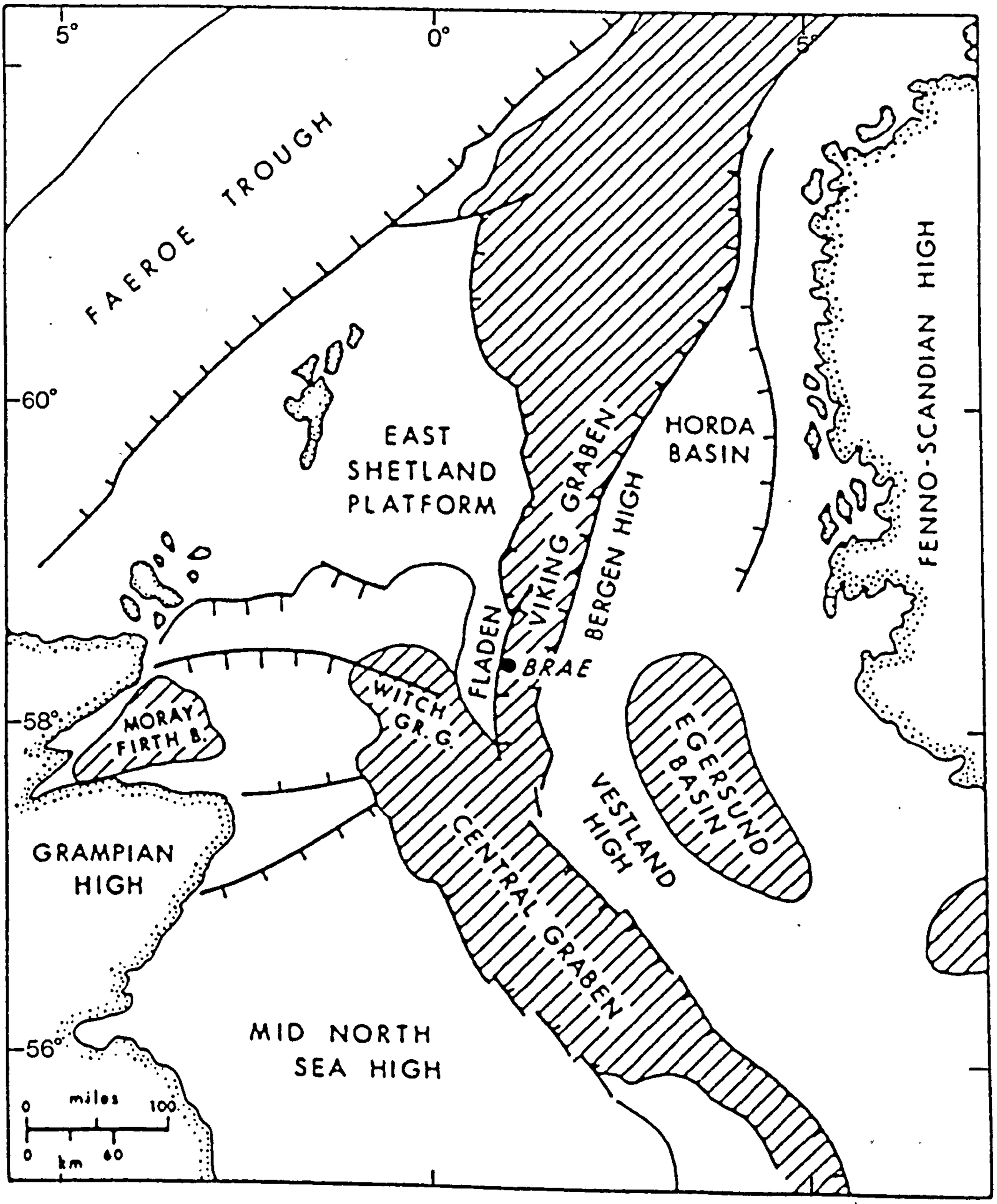
5°
0°
5°
FAEROE TROUGH
60°
EAST SHETLAND PLATFORM
HORDA BASIN
FENNO-SCANDIAN HIGH
VIKING GRABEN
BERGEN HIGH
FLADEN
BRAE
WITCH GR.
MORAY FIRTH B.
58°
EGERSUND BASIN
VESTLAND HIGH
CENTRAL GRABEN
GRAMPIAN HIGH
MID NORTH SEA HIGH
56°
0 miles 100
0 km 60

Figure 1.1.

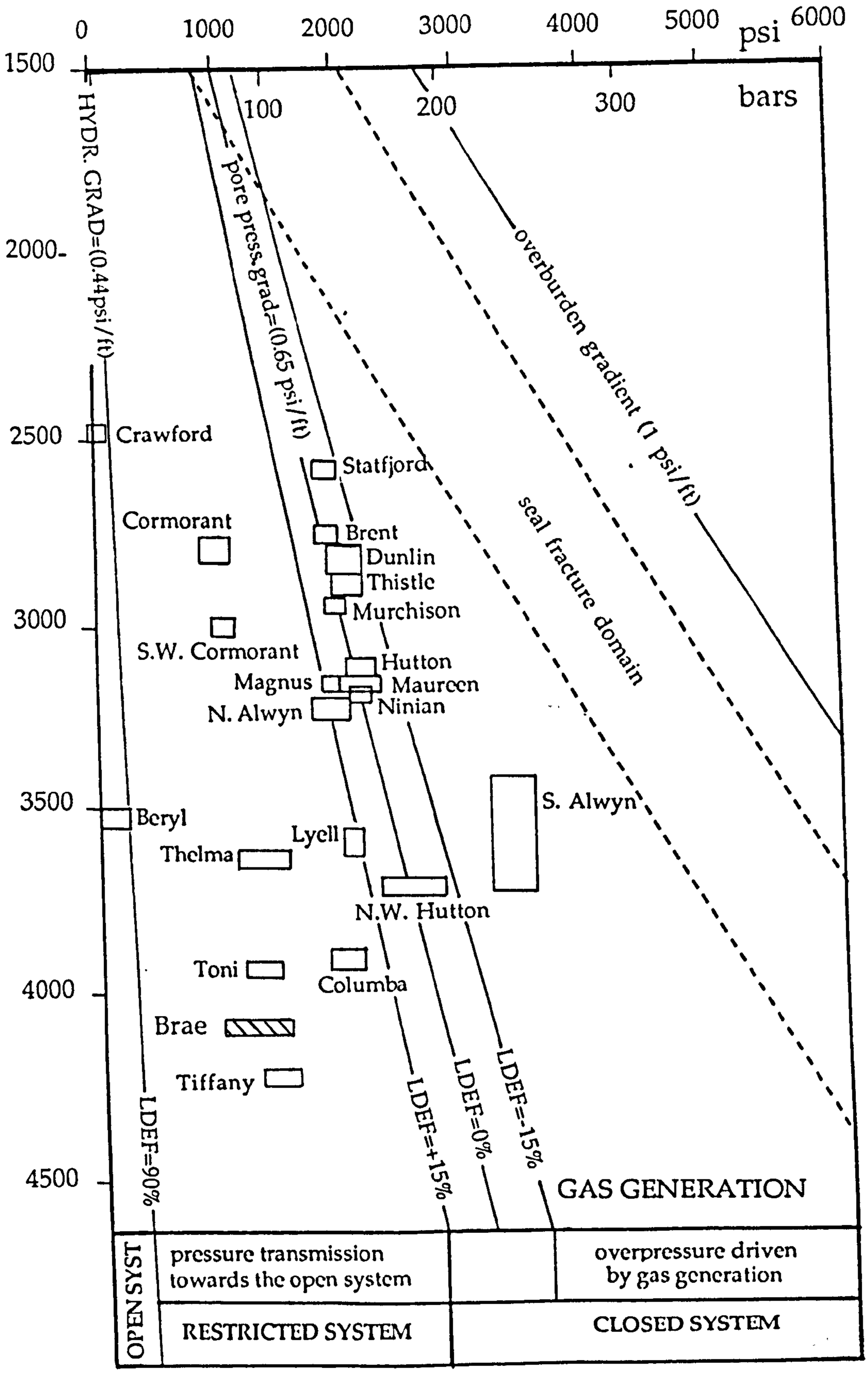
Formation Overpressure
0
1000
2000
3000
4000
5000
psi
6000
1500
bars
100
200
300
HYDR. GRAD=(0.44psi/ft)
pore press. grad=(0.65 psi/ft)
overburden gradient (1 psi/ft)
seal fracture domain
2000
2500
3000
3500
4000
4500
Aquifer Depth (mSL)
Crawford
Statfjord
Cormorant
Brent
Dunlin
Thistle
Murchison
S.W. Cormorant
Hutton
Magnus
Maureen
Ninian
N. Alwyn
S. Alwyn
Beryl
Lyell
Thelma
N.W. Hutton
Toni
Columba
Brae
Tiffany
LDEF=90%
LDEF=+15%
LDEF=0%
LDEF=-15%
GAS GENERATION
OPEN SYST
pressure transmission
towards the open system
overpressure driven
by gas generation
RESTRICTED SYSTEM
CLOSED SYSTEM

Figure 1.2.

South Brae

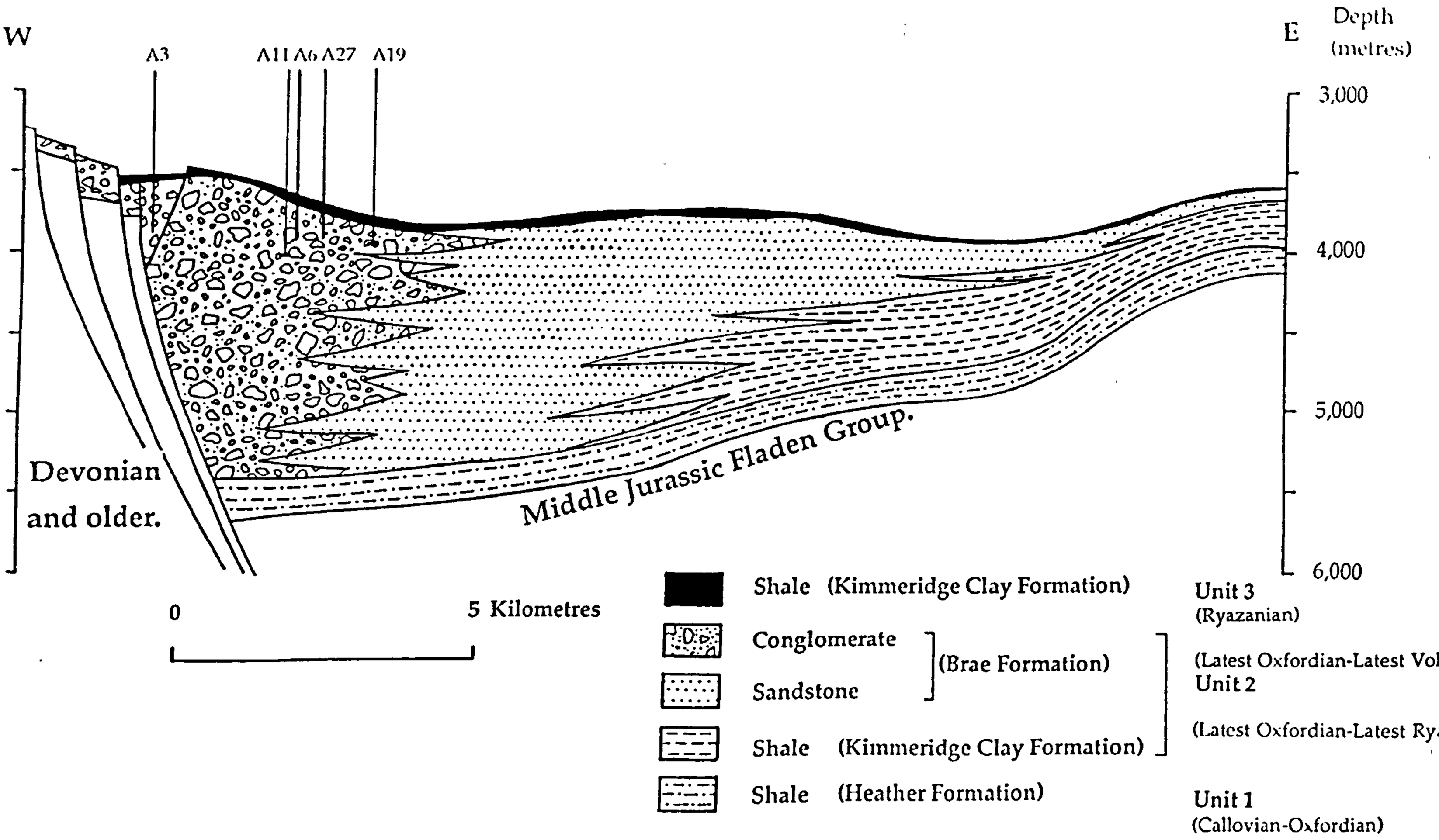

Figure 1.3.

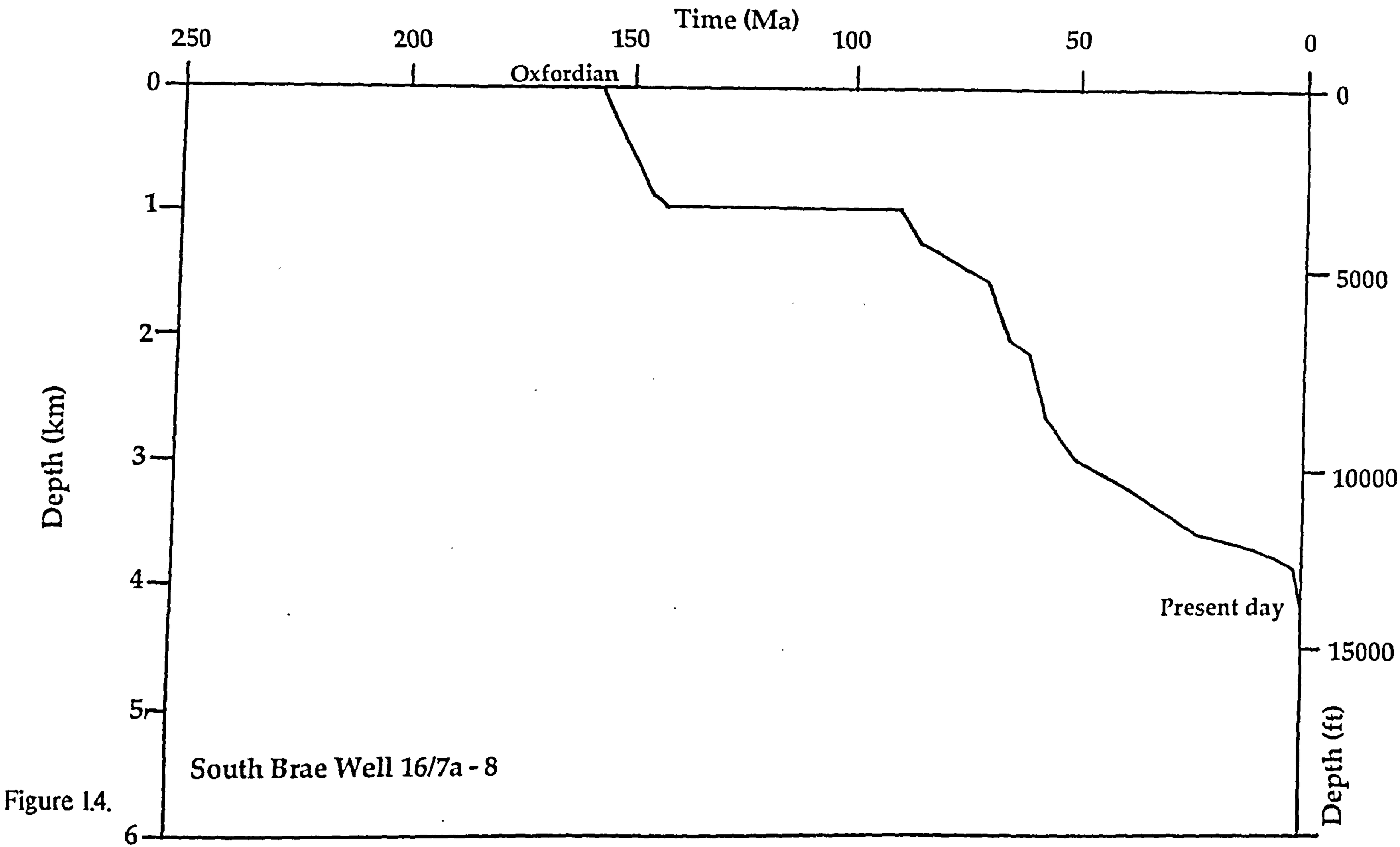
Time (Ma)
250
200
150
100
50
0
Oxfordian
0
1
2
3
4
5
6
Depth (km)
0
5000
10000
15000
Depth (ft)
Present day
South Brae Well 16/7a - 8

Figure 1.4.

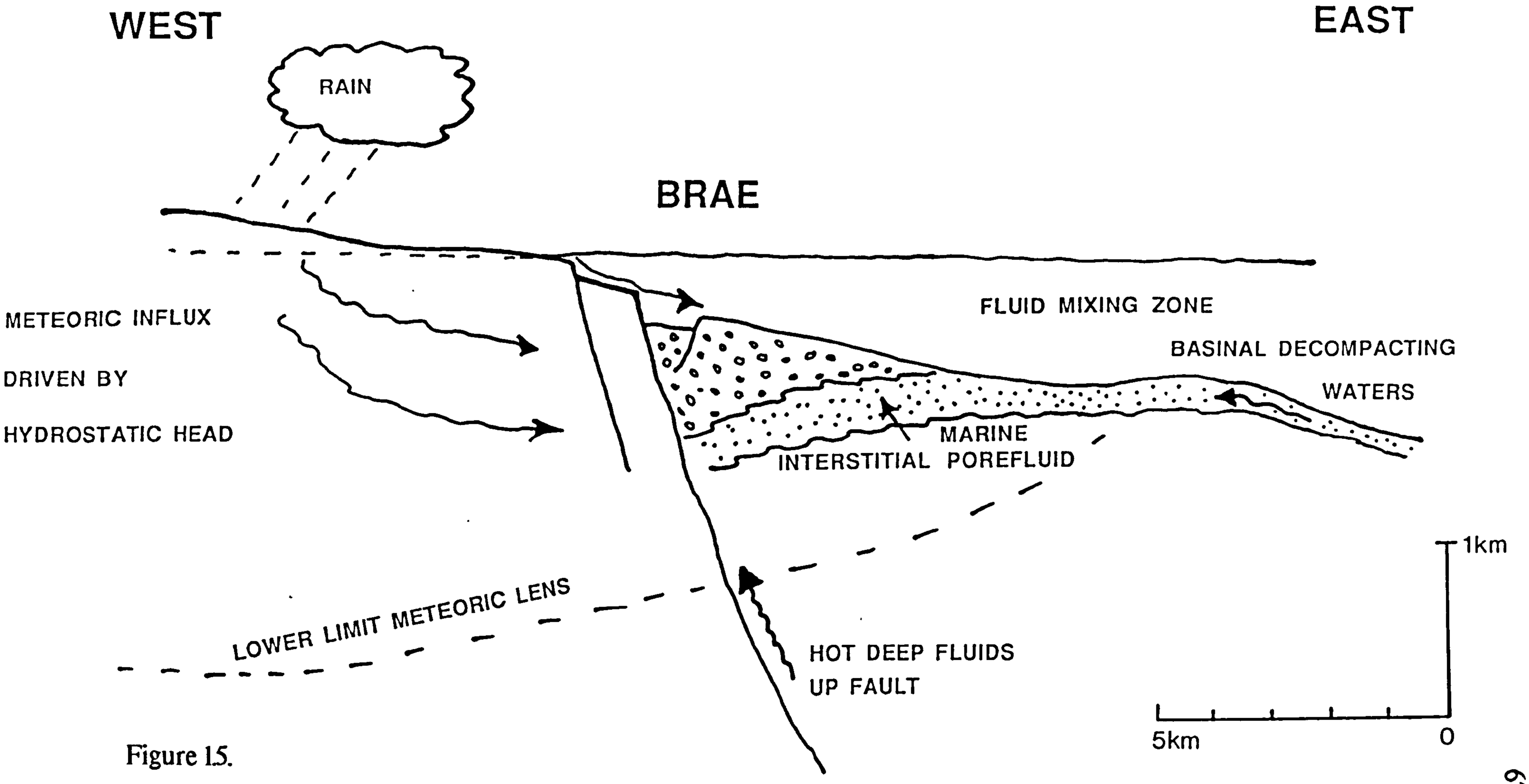
WEST
EAST
RAIN
BRAE
METEORIC INFLUX
DRIVEN BY
HYDROSTATIC HEAD
FLUID MIXING ZONE
BASINAL DECOMPACTING
WATERS
MARINE
INTERSTITIAL POREFLUID
LOWER LIMIT METEORIC LENS
HOT DEEP FLUIDS
UP FAULT
1km
5km
0

Figure 1.5.

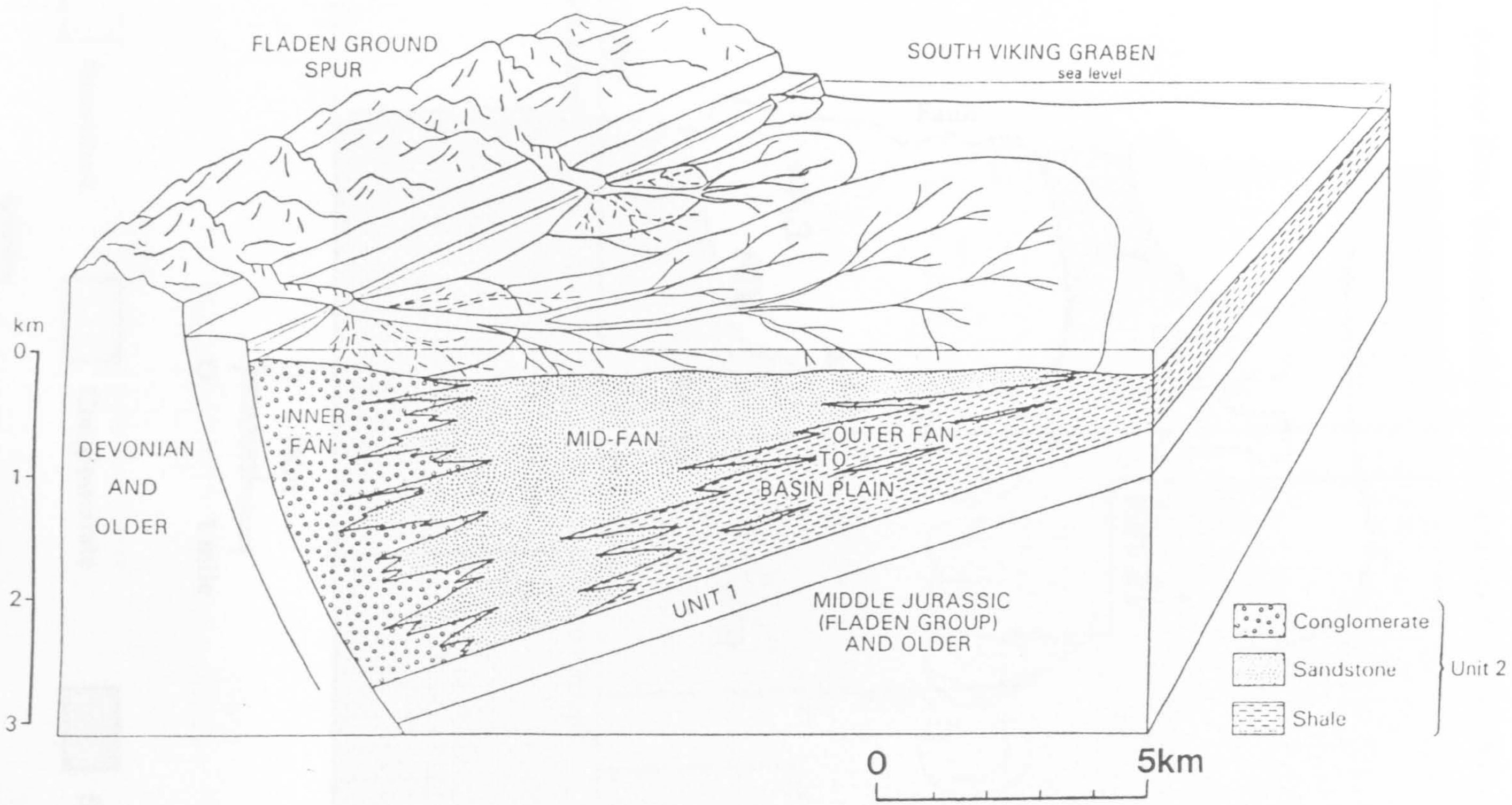
FLADEN GROUND
SPUR
SOUTH VIKING GRABEN
sea level
km
0
1
2
3
INNER
FAN
MID-FAN
OUTER FAN
TO
BASIN PLAIN
DEVONIAN
AND
OLDER
UNIT 1
MIDDLE JURASSIC
(FLADEN GROUP)
AND OLDER
Conglomerate
Sandstone
Shale
Unit 2
0
5km

Figure 1.6.

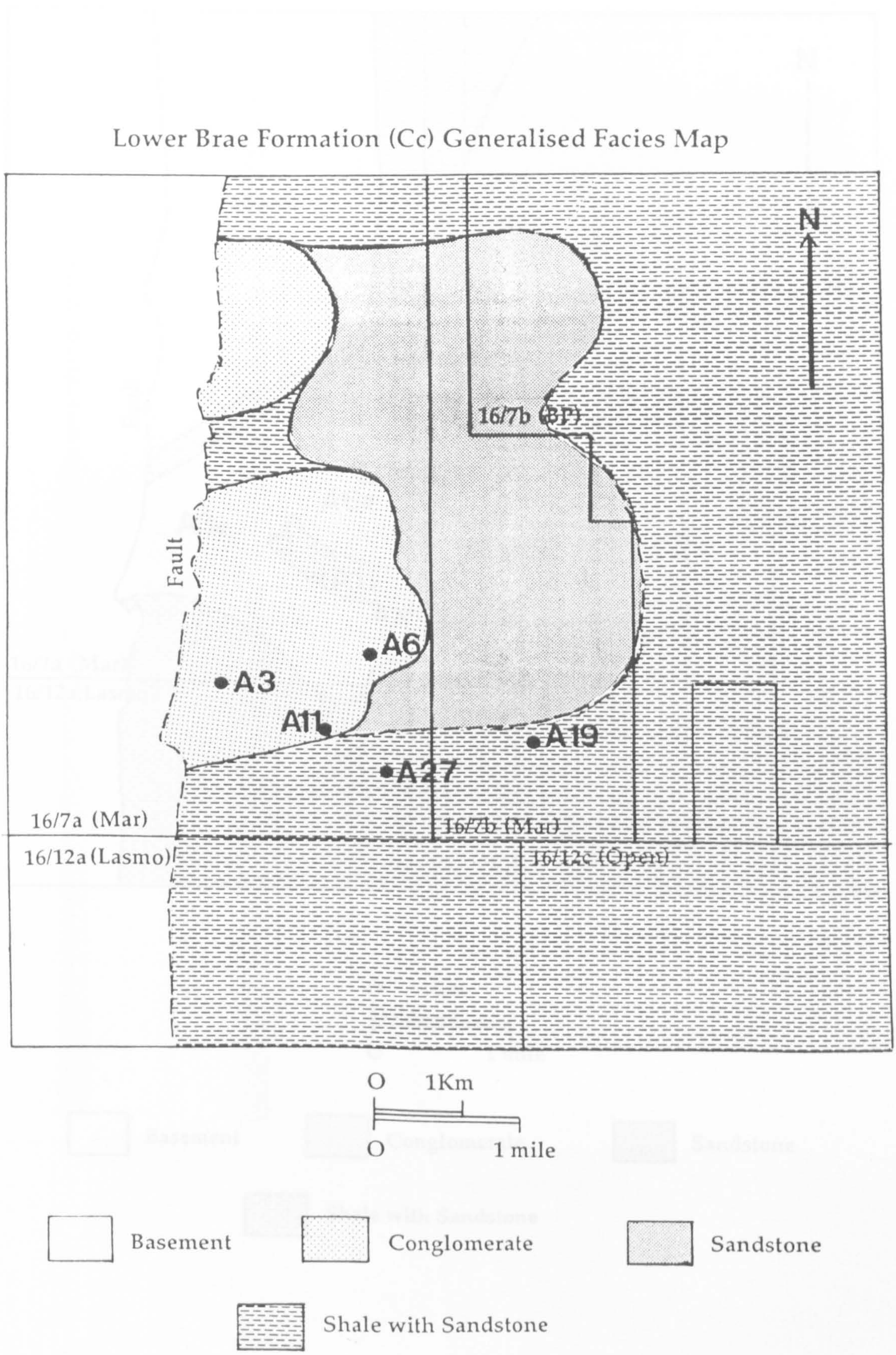
Lower Brae Formation (Cc) Generalised Facies Map
N
16/7b (BP)
Fault
A6
A3
A11
A19
A27
16/7a (Mar)
16/12a (Lasmo)
16/7b (Mar)
16/12c (Open)
O 1Km
O 1 mile
Basement
Conglomerate
Sandstone
Shale with Sandstone

Figure 1.7a.

Upper Brae Formation (Ac) Generalised Facies Map

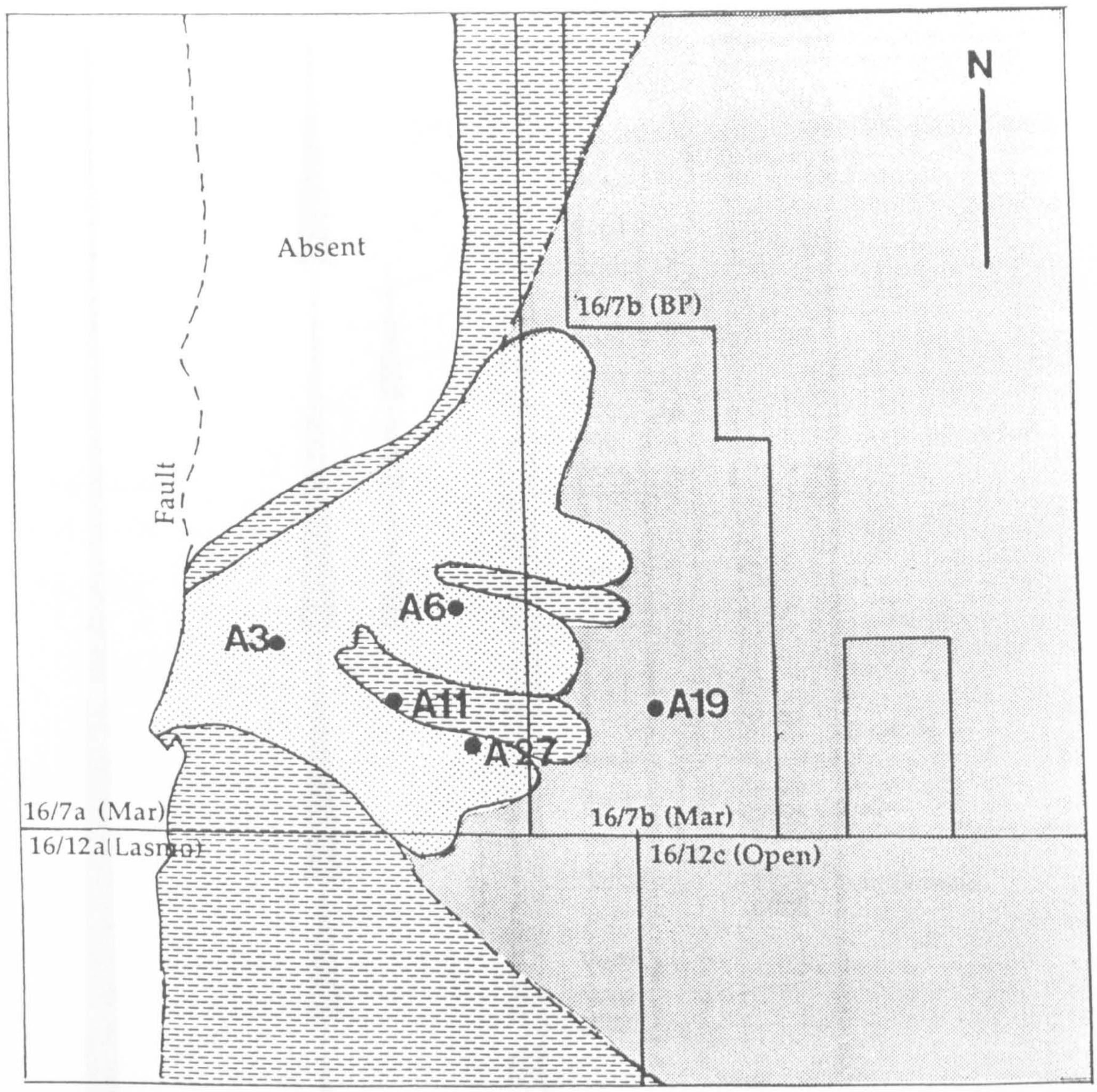

Figure 1.7b.

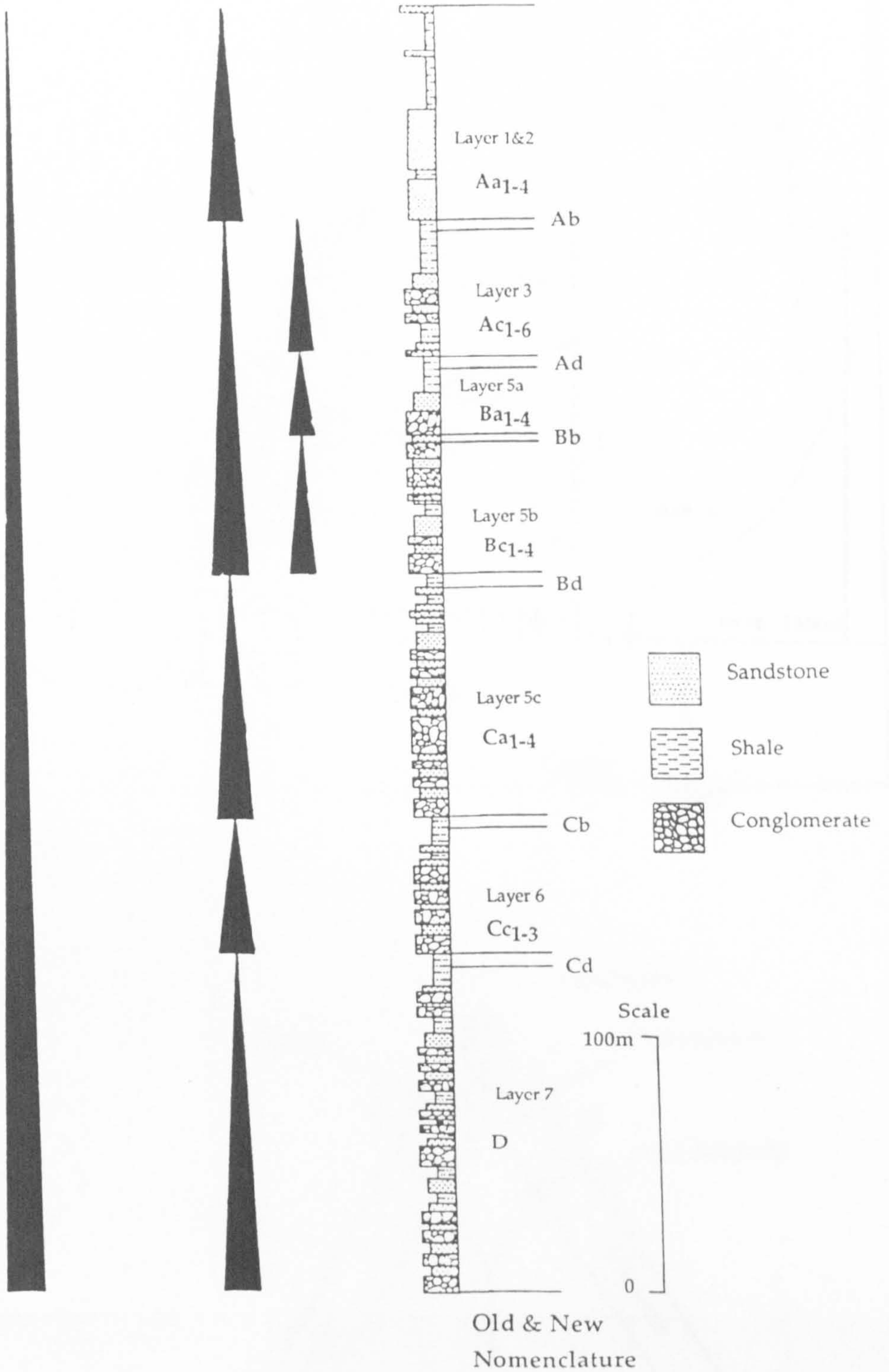
Layer 1&2
Aa1-4
Ab
Layer 3
Ac1-6
Ad
Layer 5a
Ba1-4
Bb
Layer 5b
Bc1-4
Bd
Layer 5c
Ca1-4
Cb
Layer 6
Cc1-3
Cd
Layer 7
D
Sandstone
Shale
Conglomerate
Scale
100m
0
Old & New
Nomenclature

Figure 1.8.

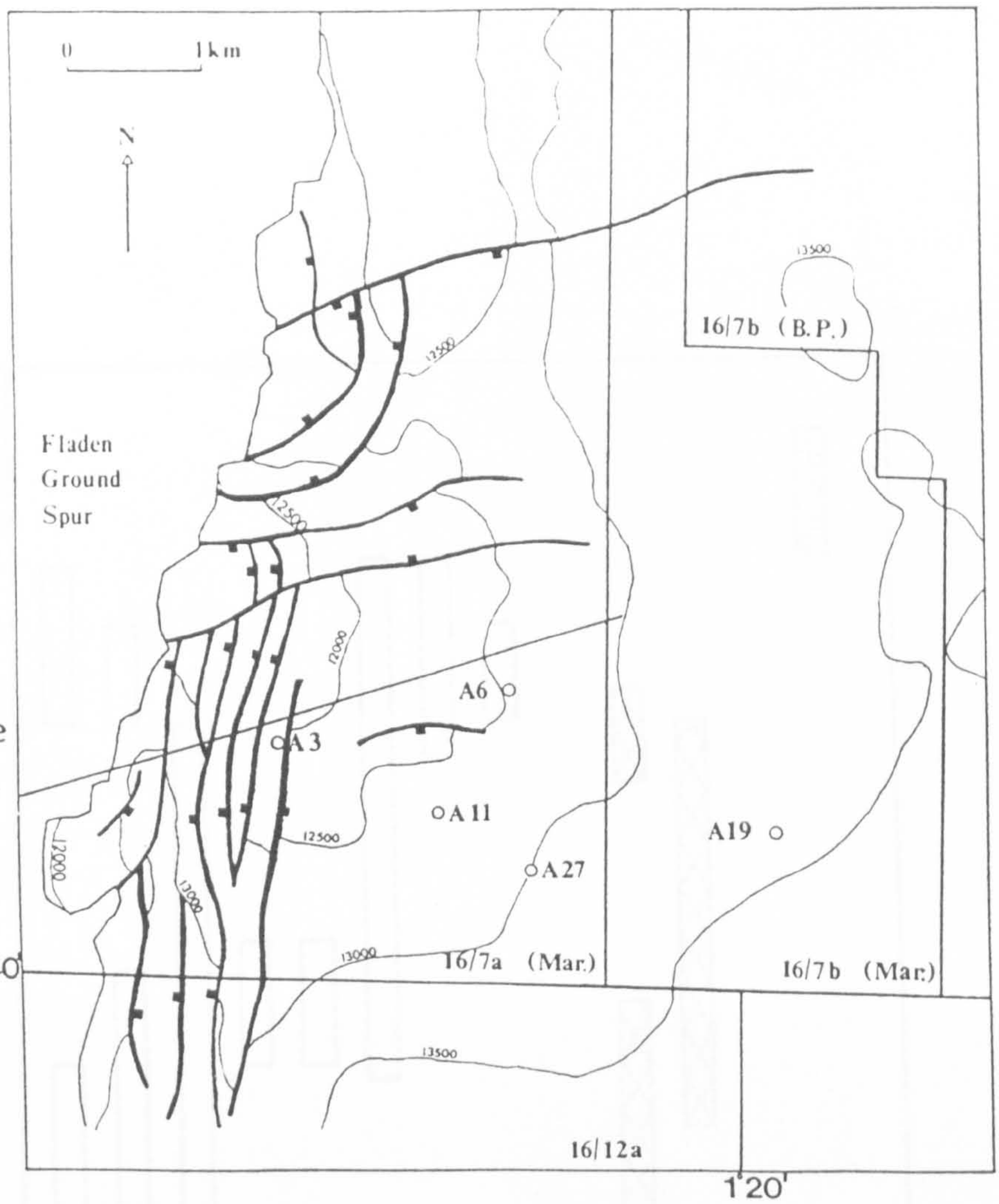

(Approx. line of section in Fig. 1.4.)

Figure 1.9.

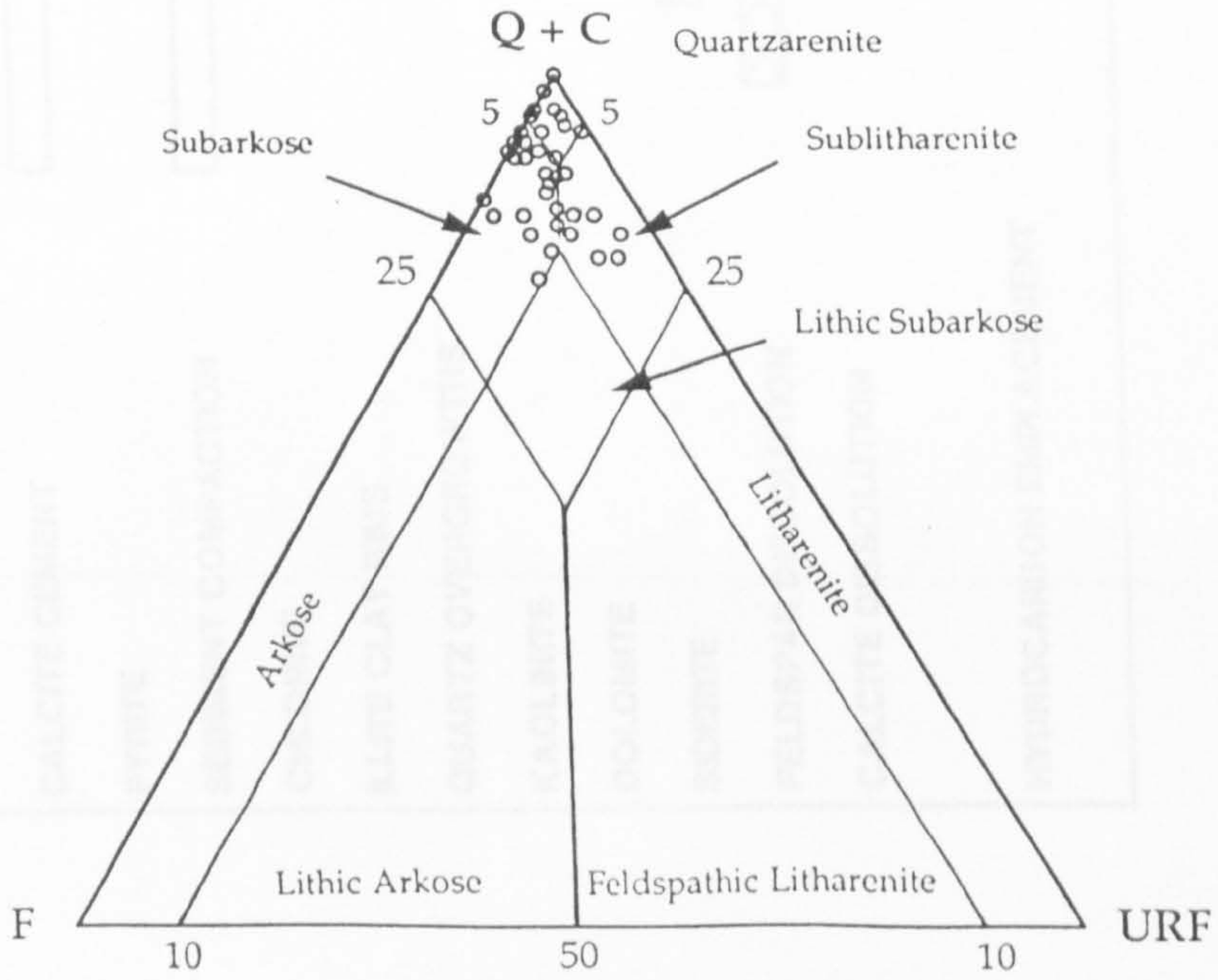

Figure 1.10.

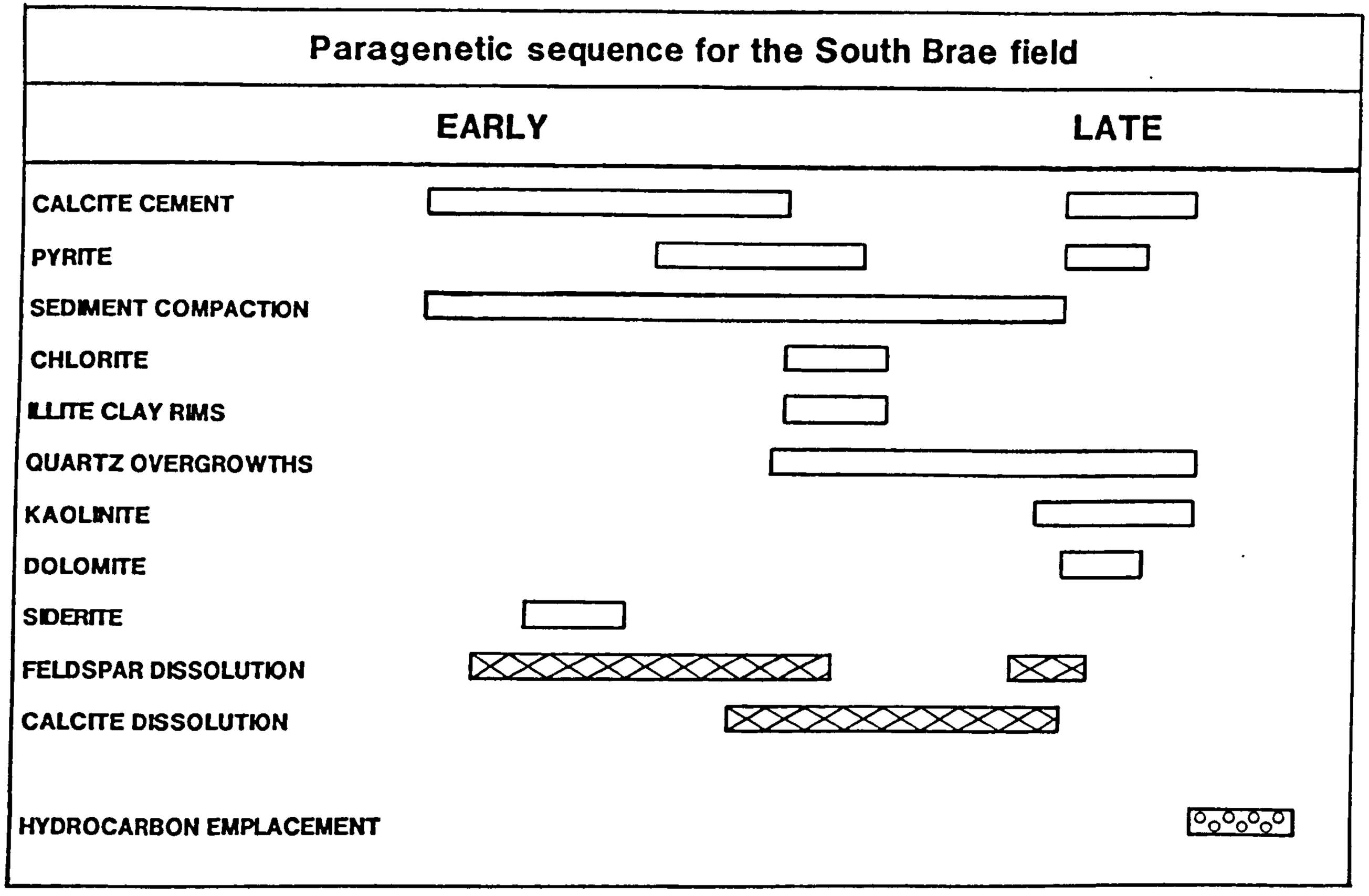
Paragenetic sequence for the South Brae field
EARLY
LATE
CALCITE CEMENT
PYRITE
SEDIMENT COMPACTION
CHLORITE
ILLITE CLAY RIMS
QUARTZ OVERGROWTHS
KAOLINITE
DOLOMITE
SIDERITE
FELDSPAR DISSOLUTION
CALCITE DISSOLUTION
HYDROCARBON EMPLACEMENT

Figure 1.11.

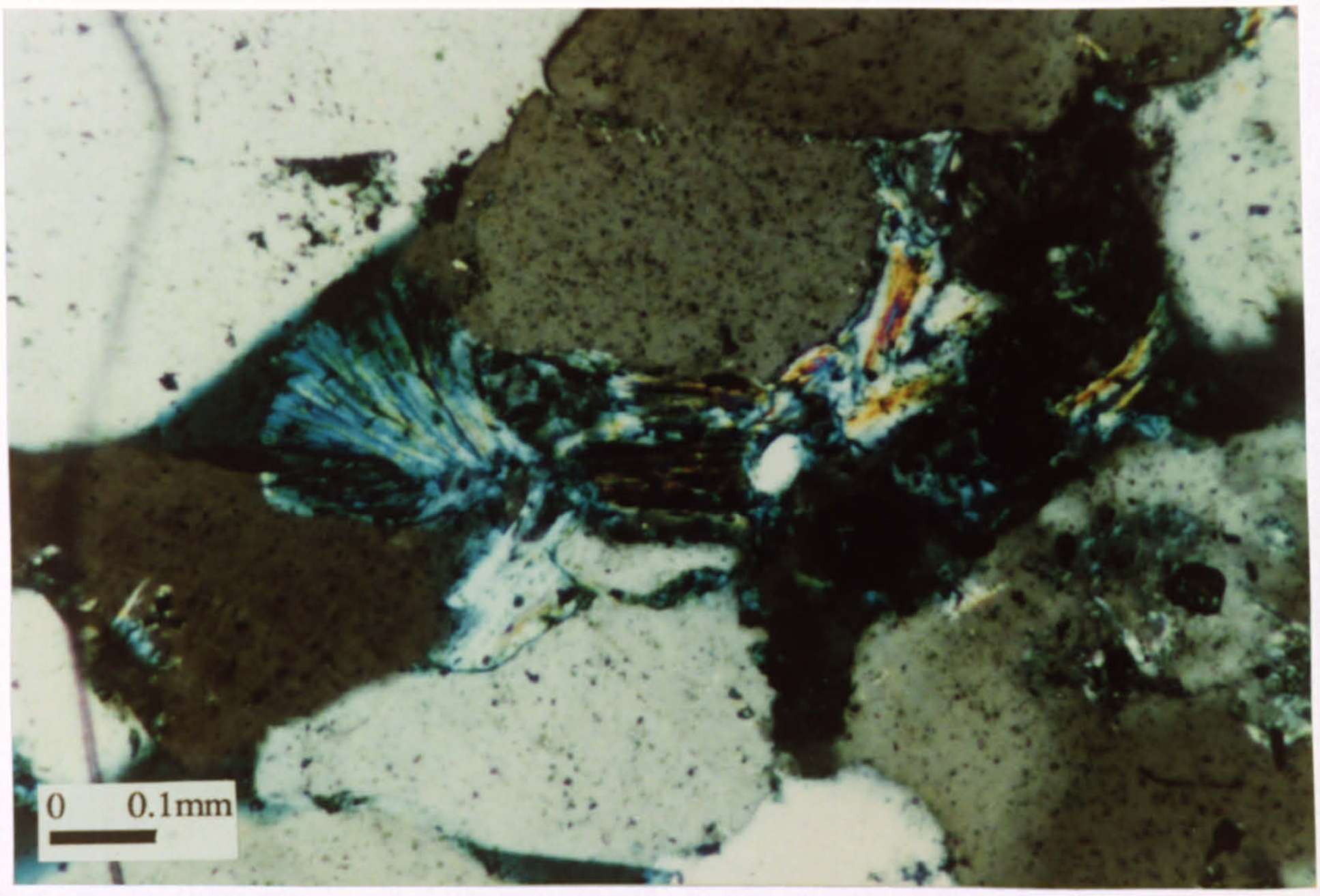

Figure 1.12.

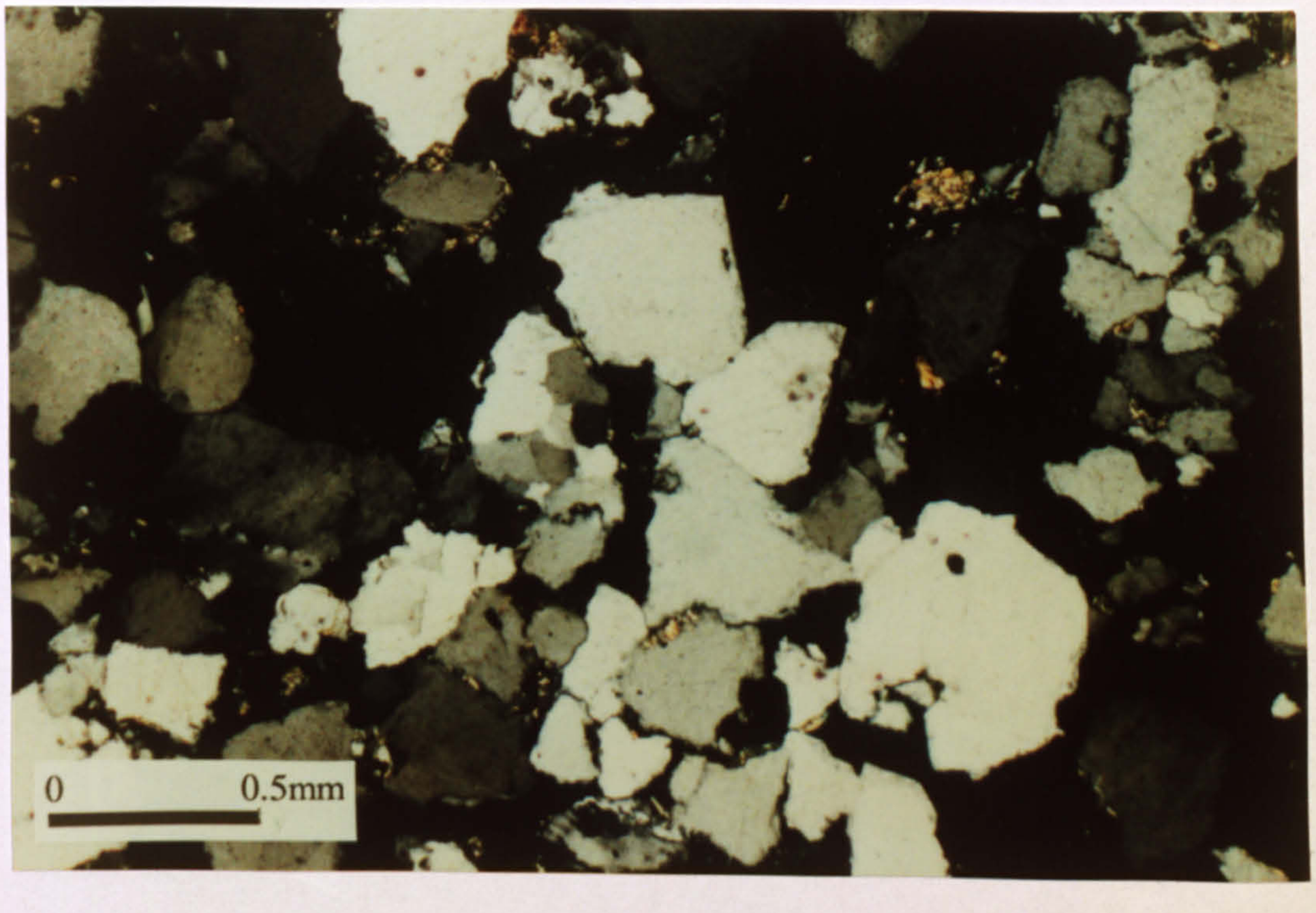

Figure 1.13.

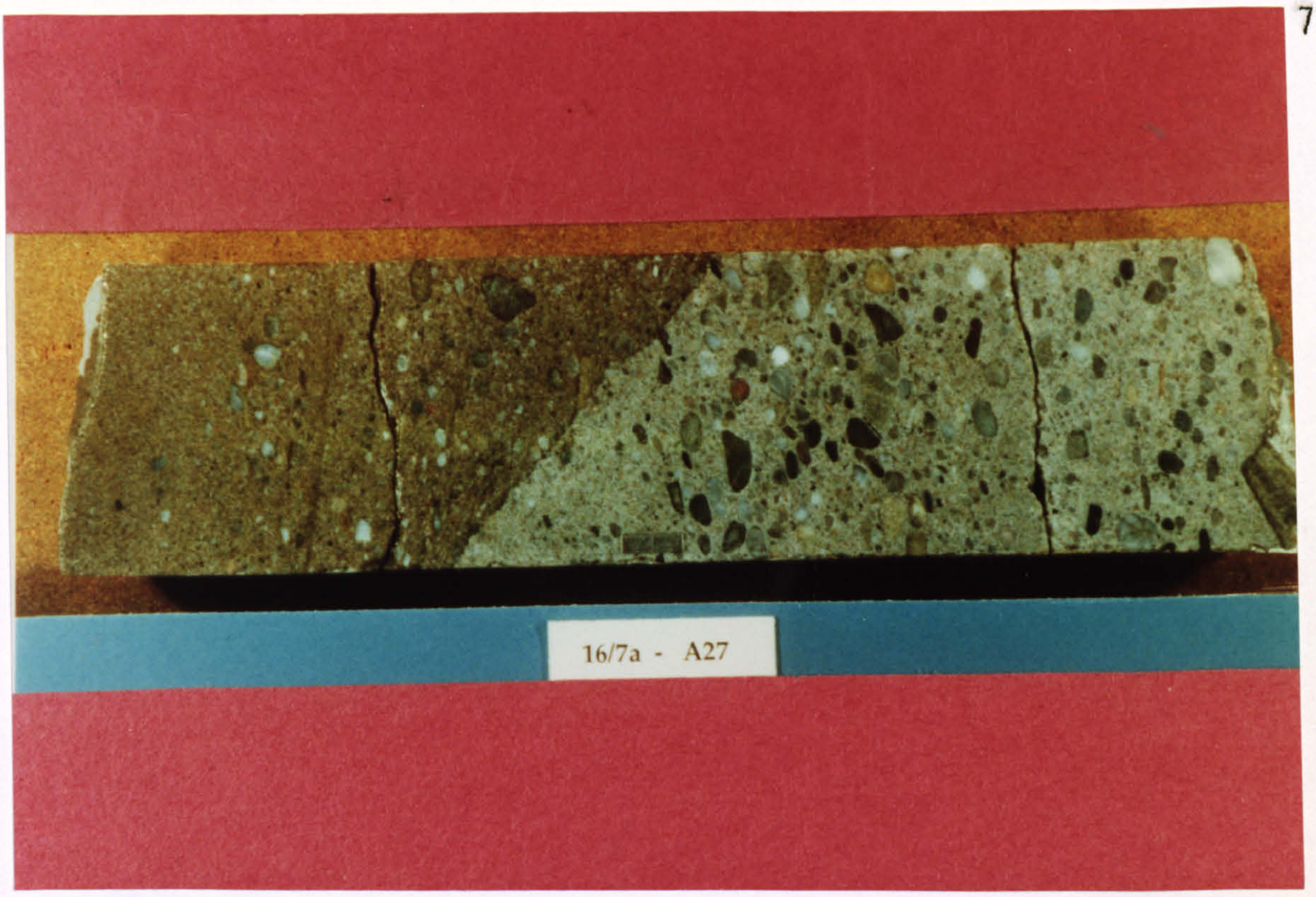

Figure 1.14.

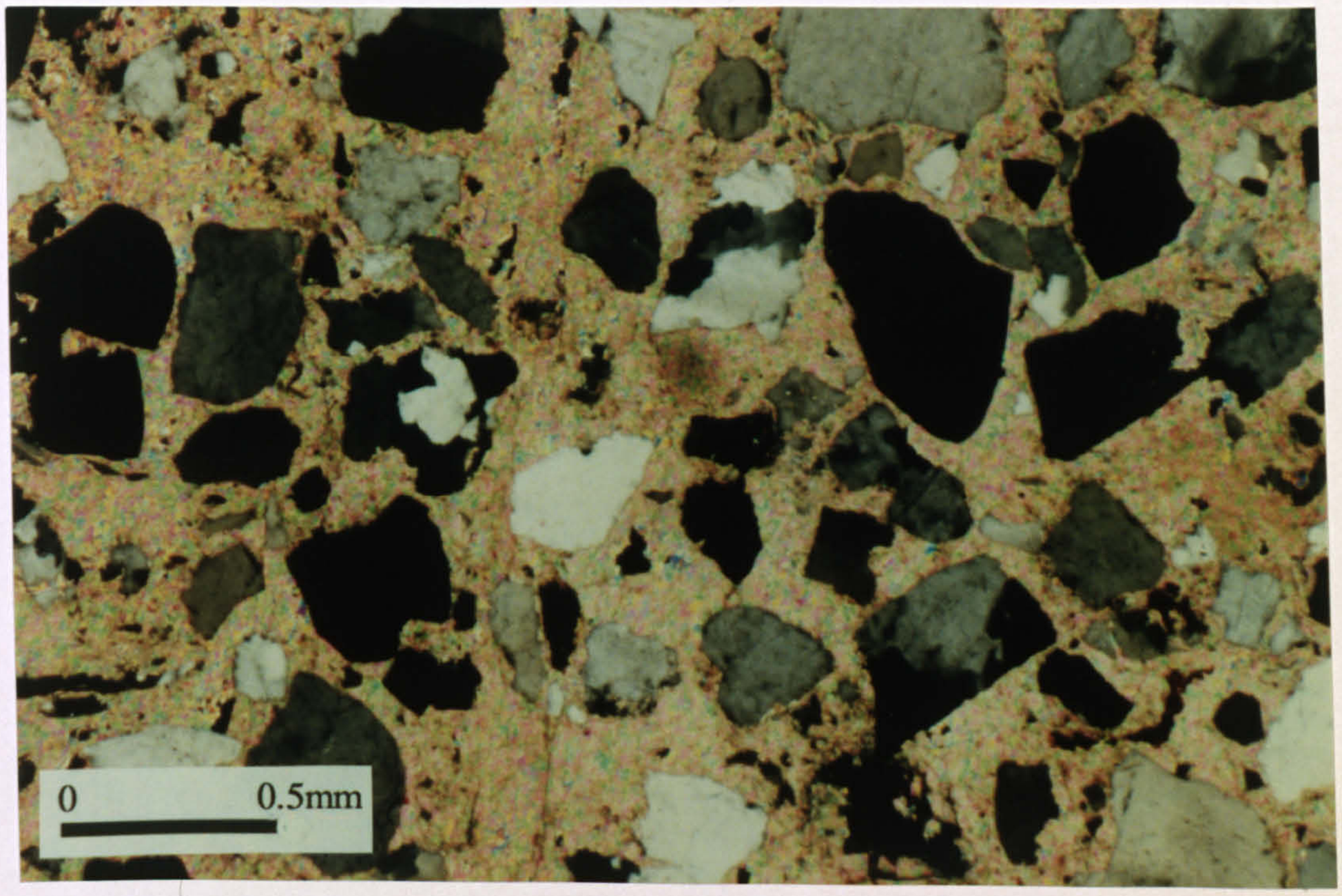

Figure 1.15.

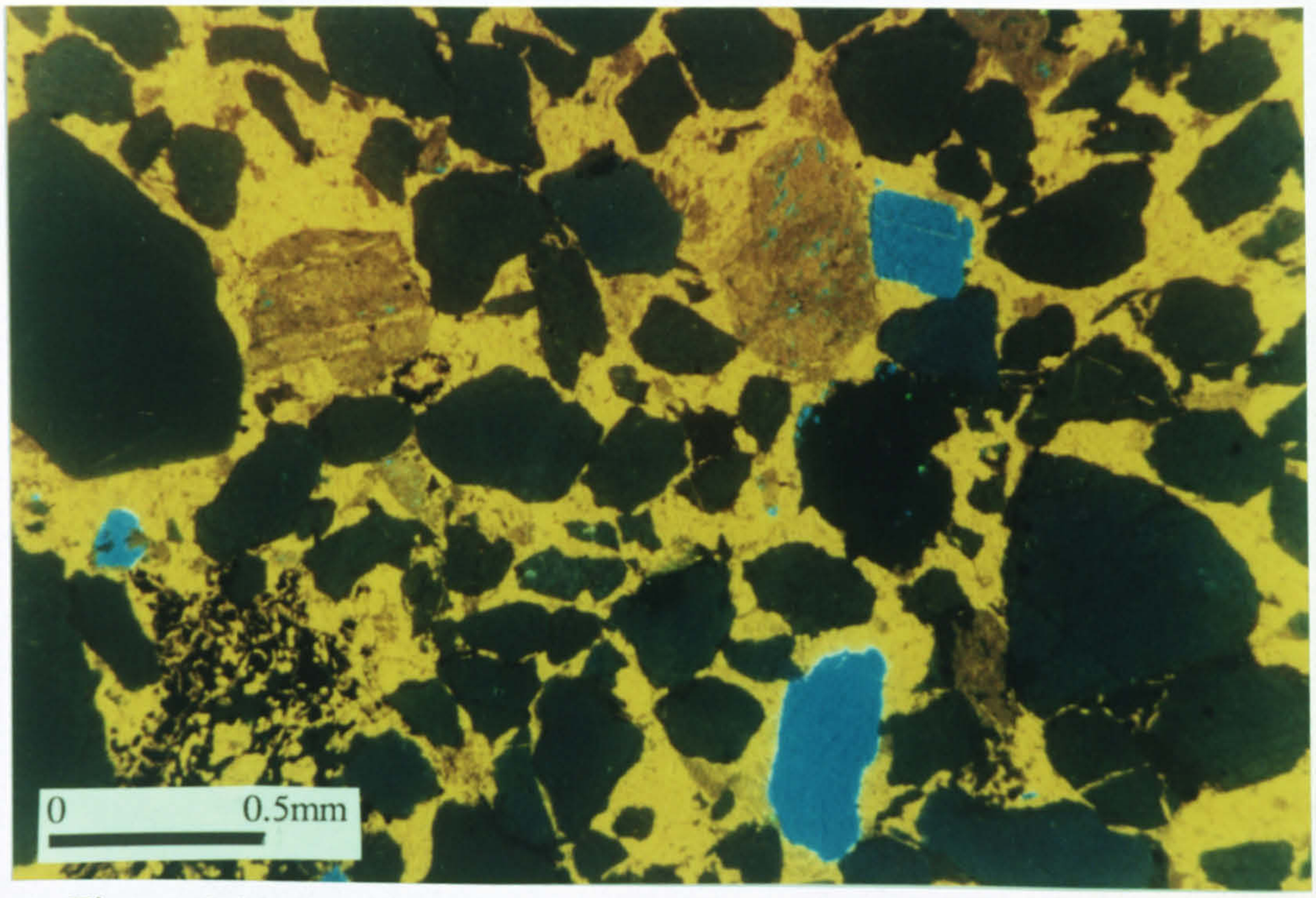

Figure 1.16.

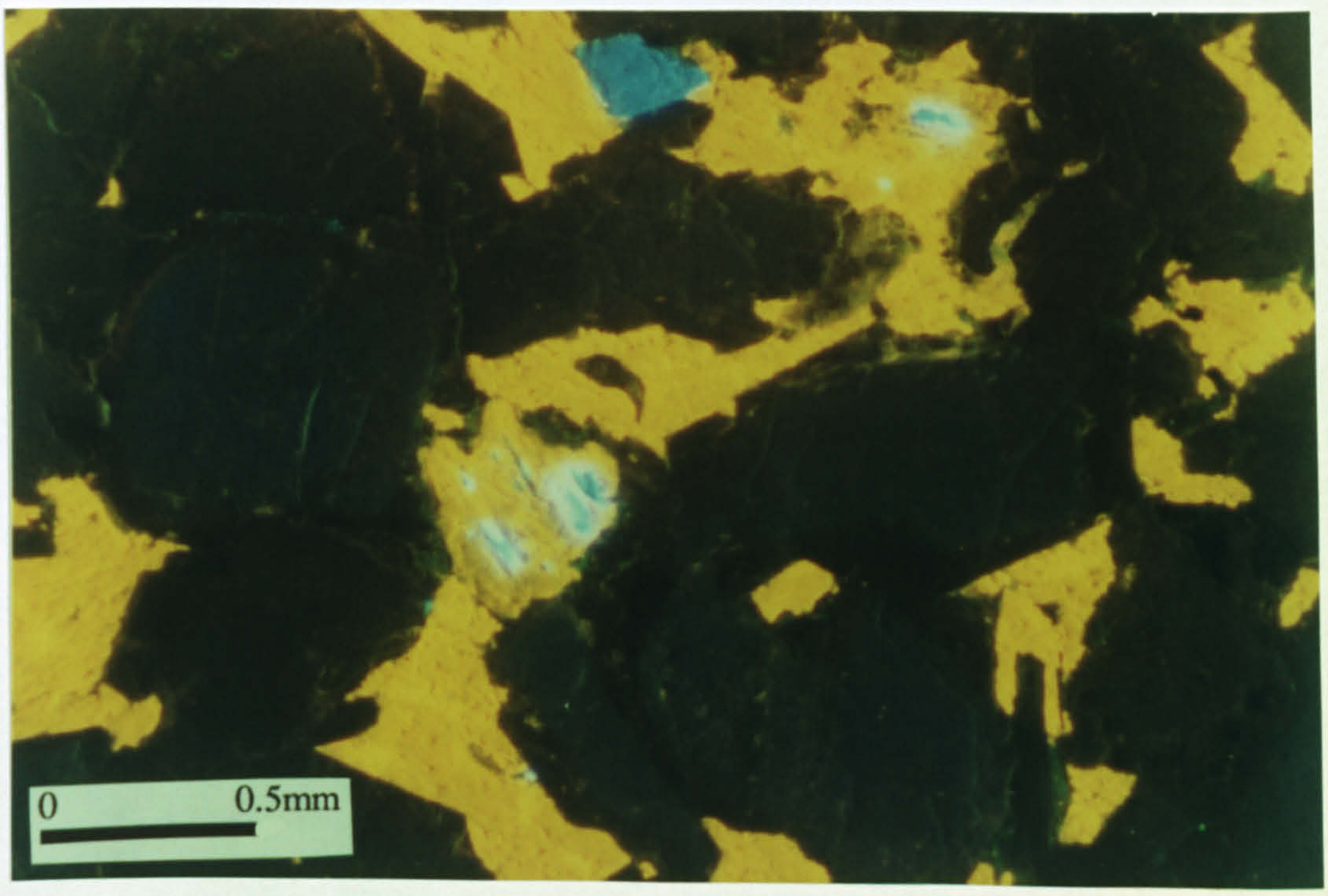

Figure 1.17.

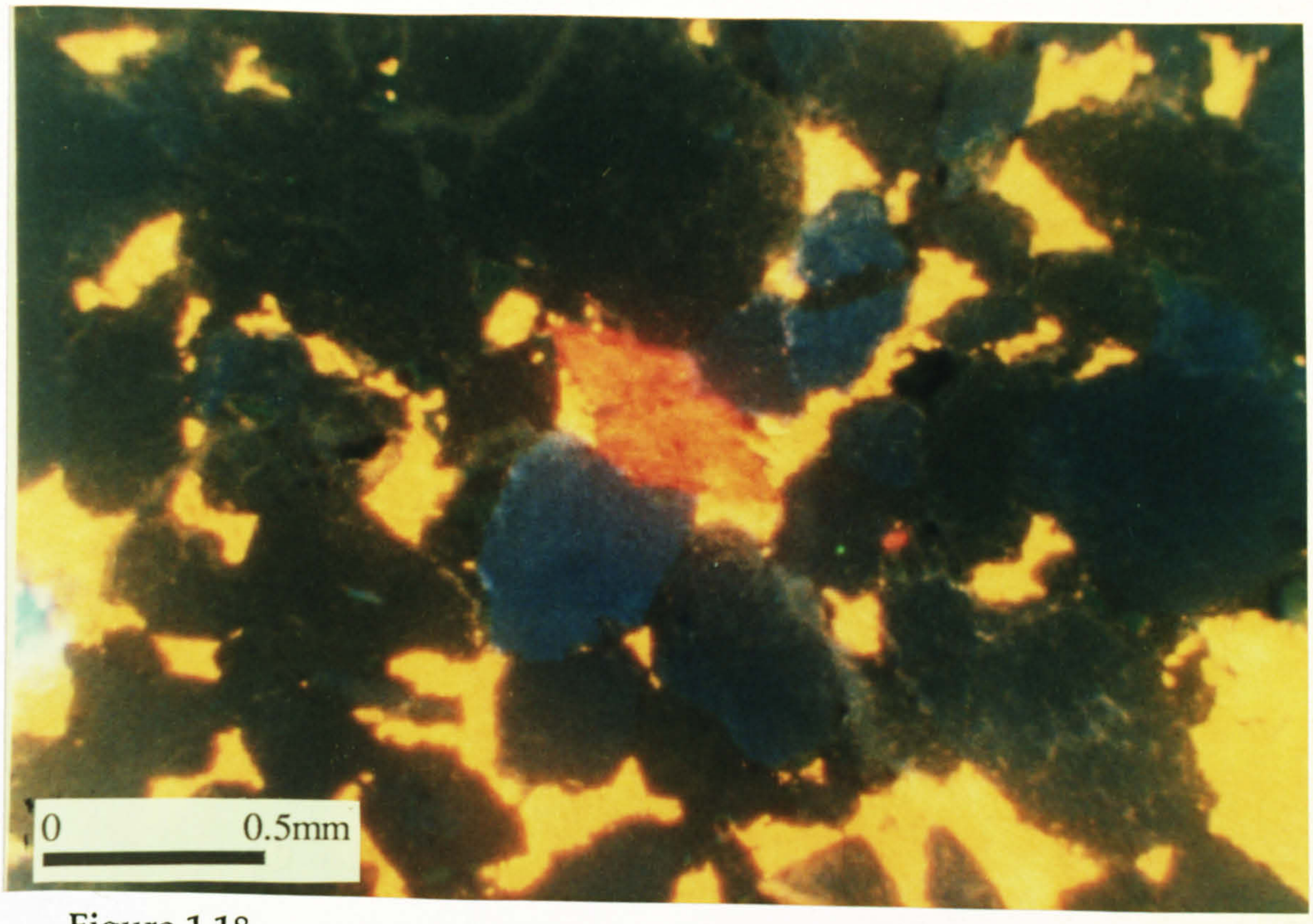

Figure 1.18.

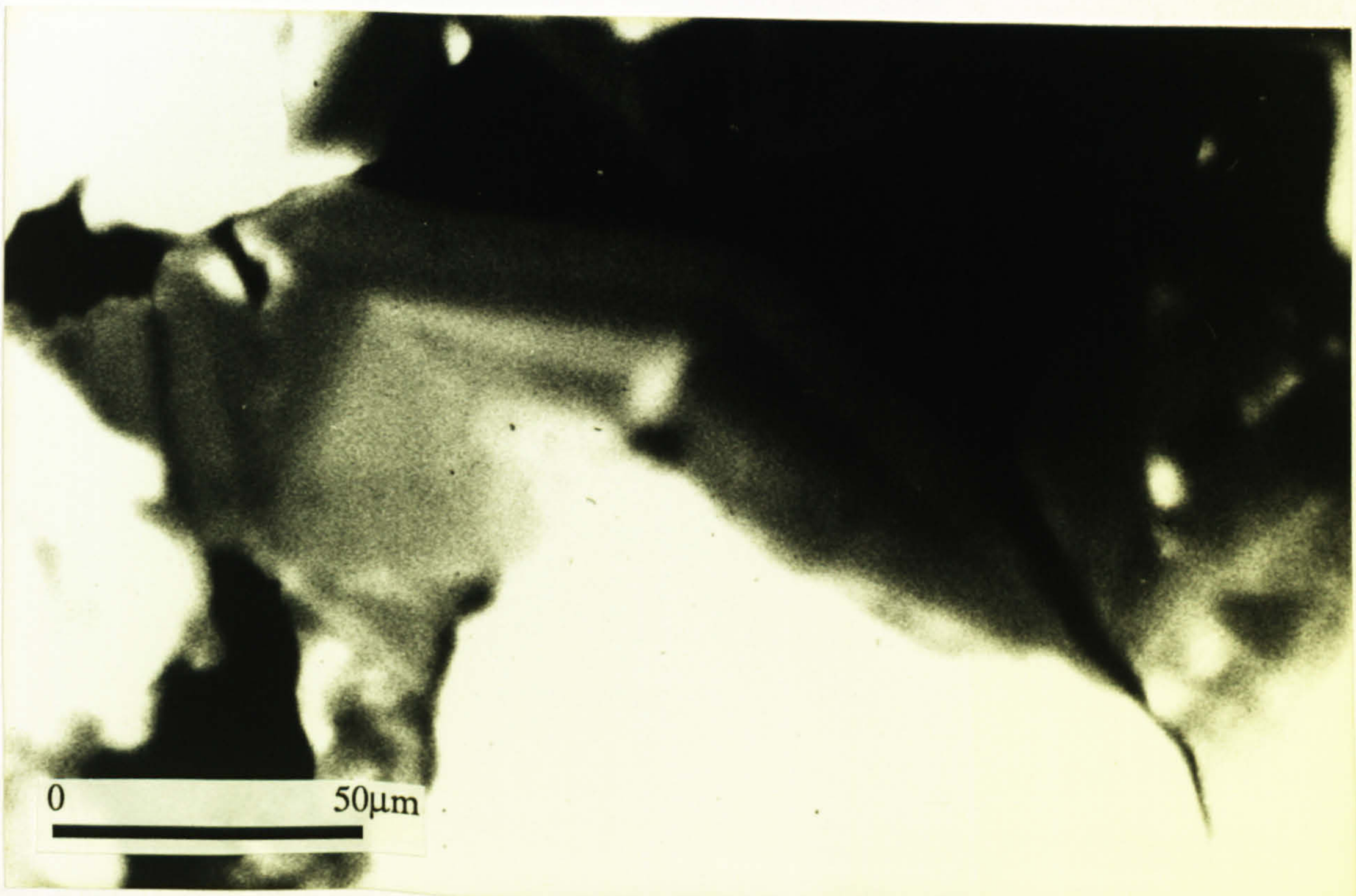

Figure 1.19.

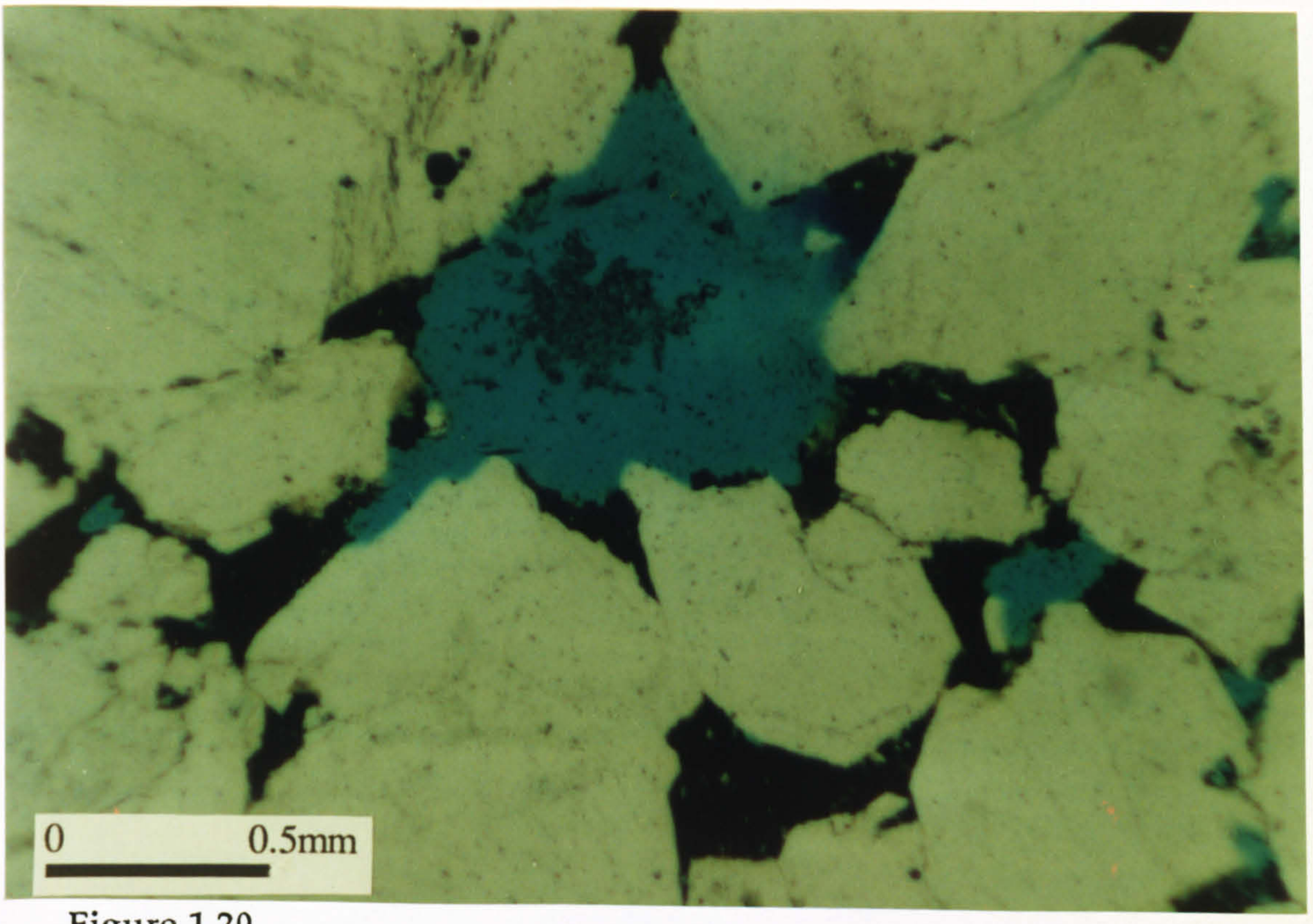

Figure 1.20.

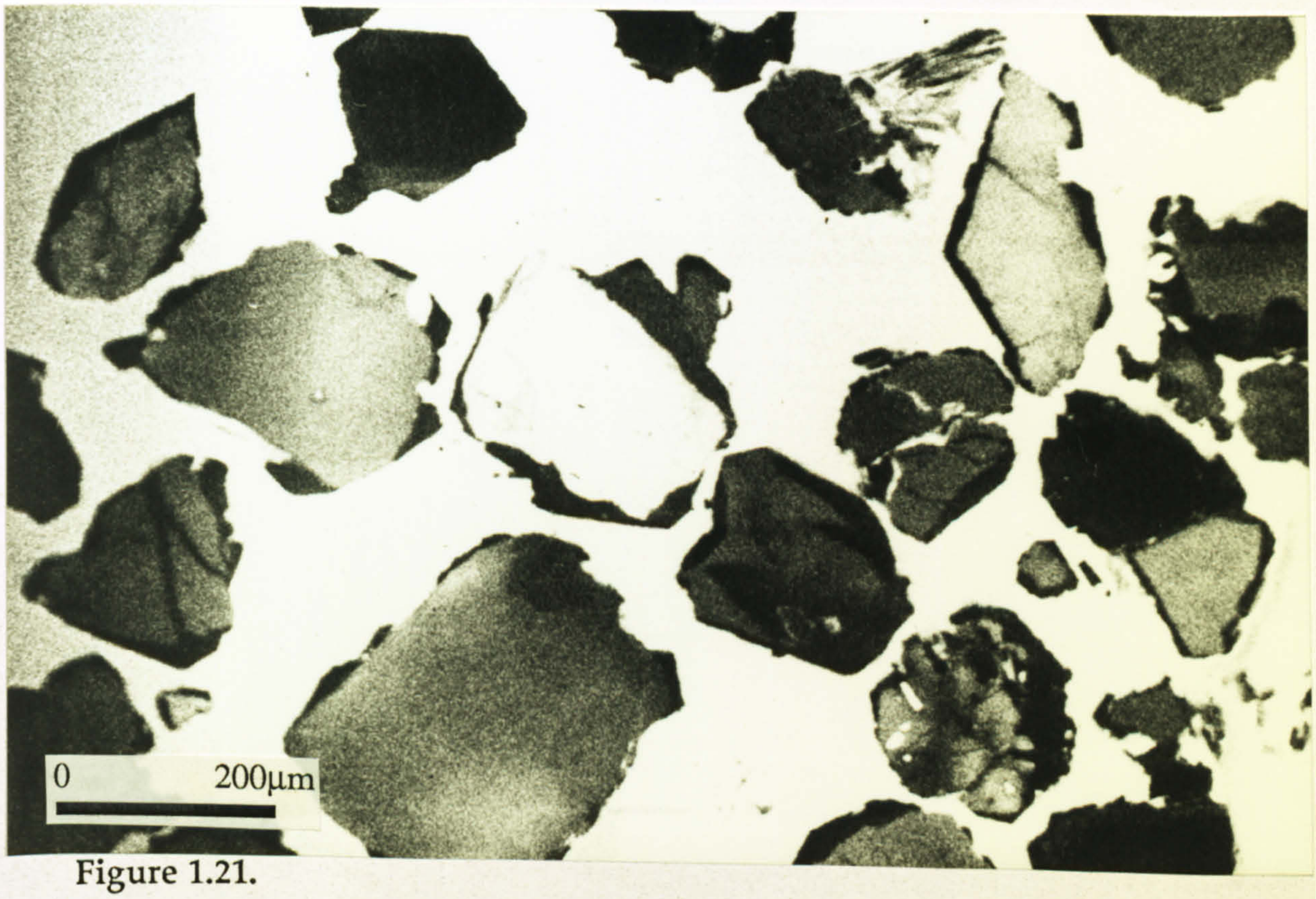

Figure 1.21.

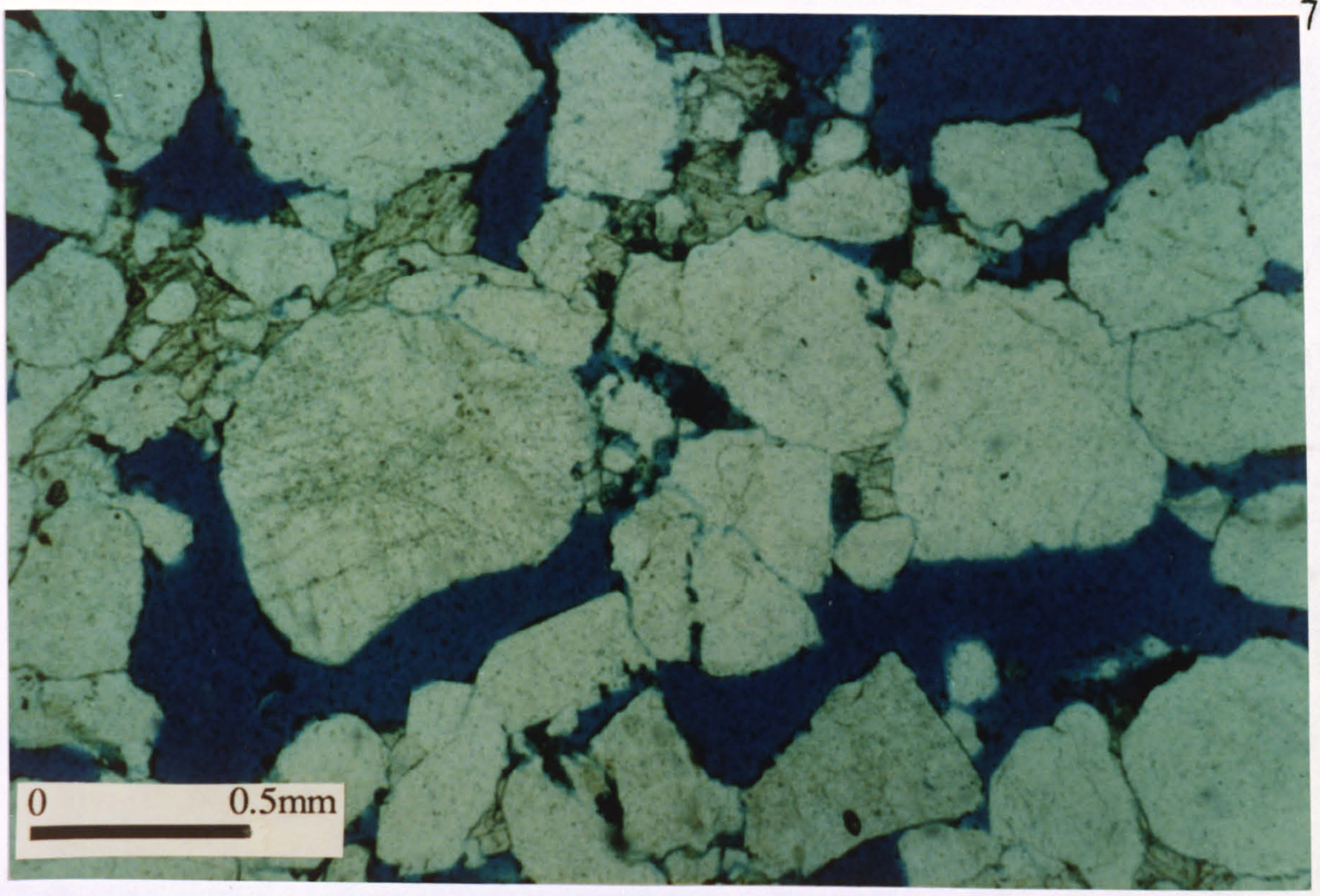

Figure 1.22.

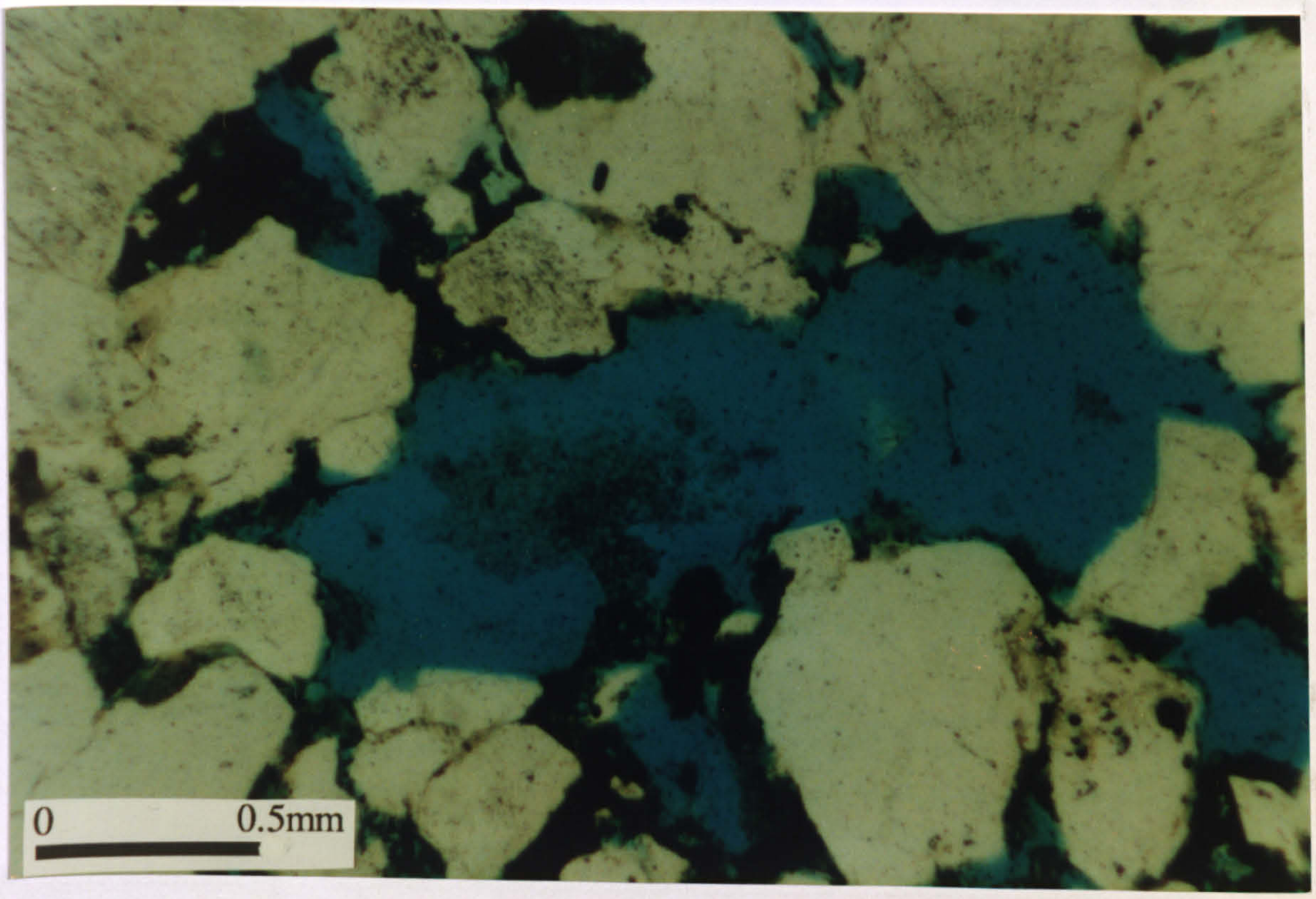

Figure 1.23.

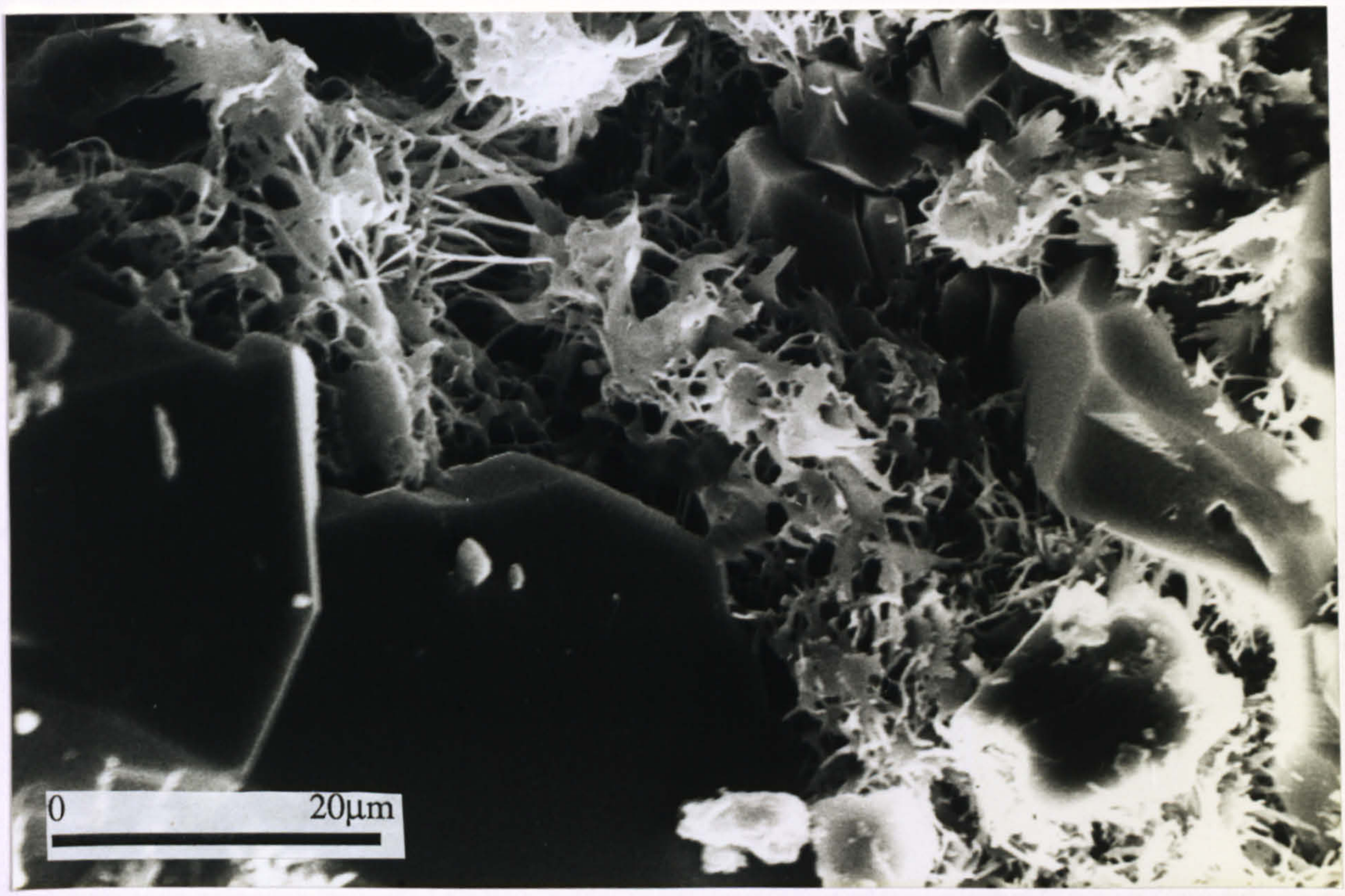

Figure 1.24.

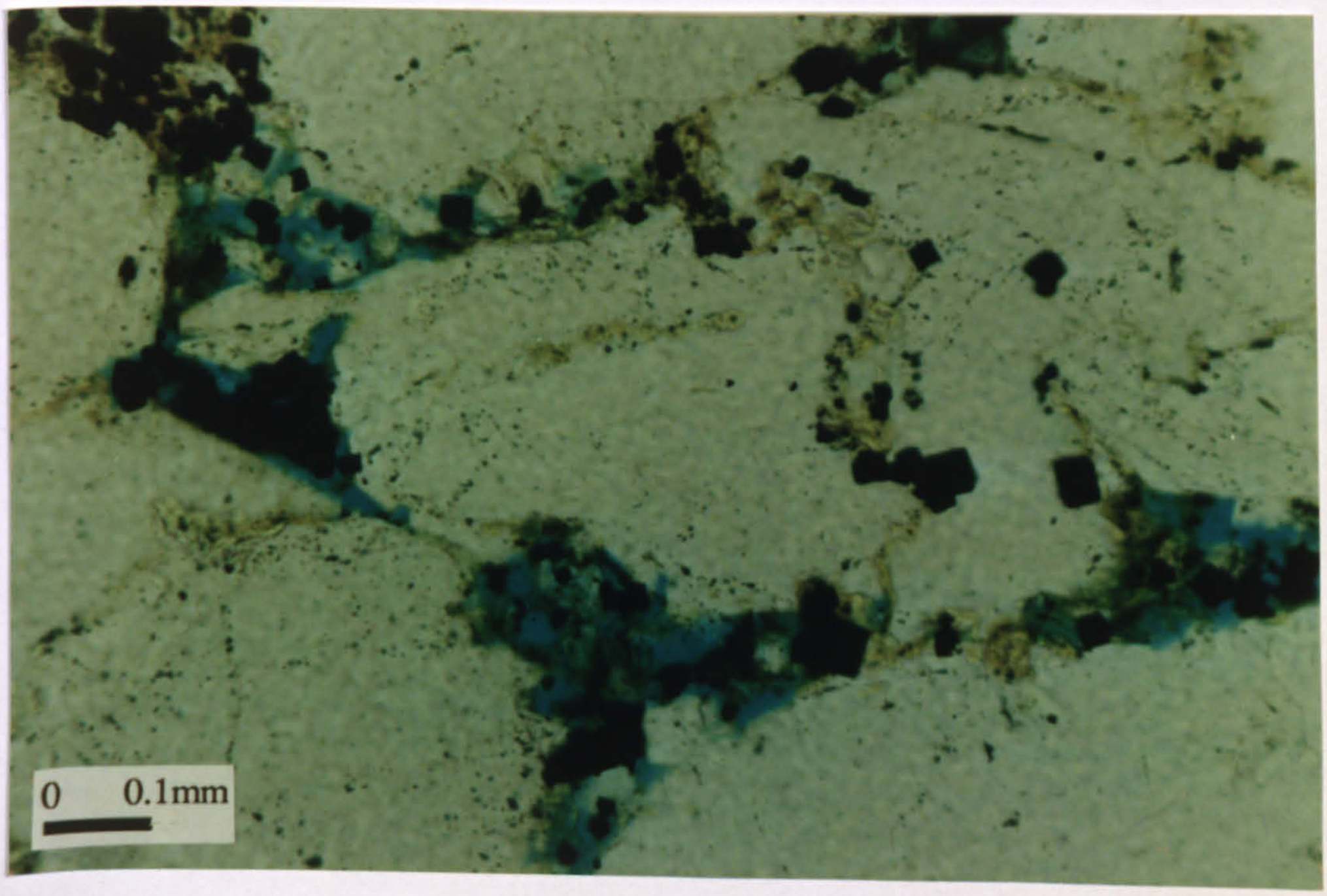

Figure 1.25.

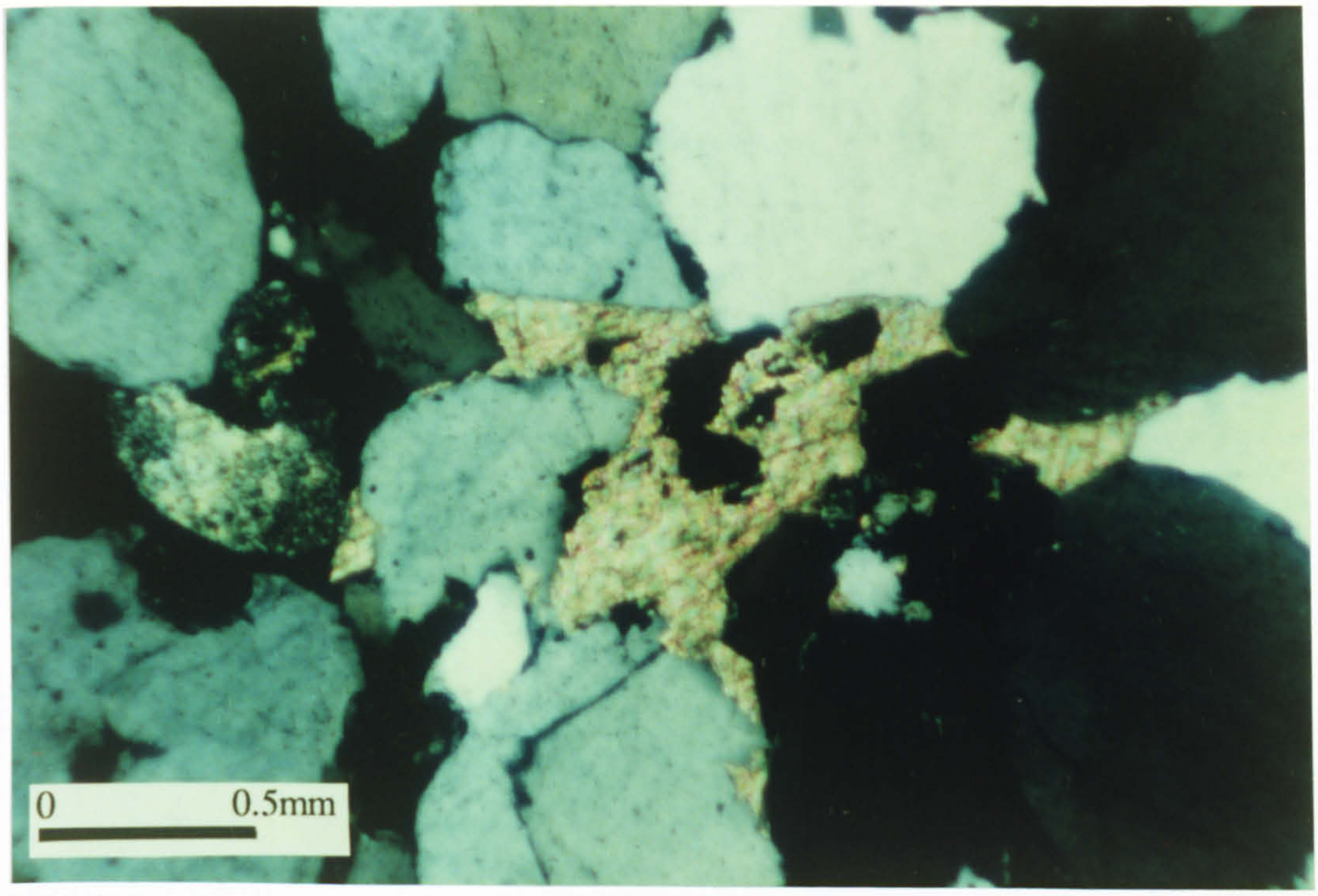

Figure 1.26.

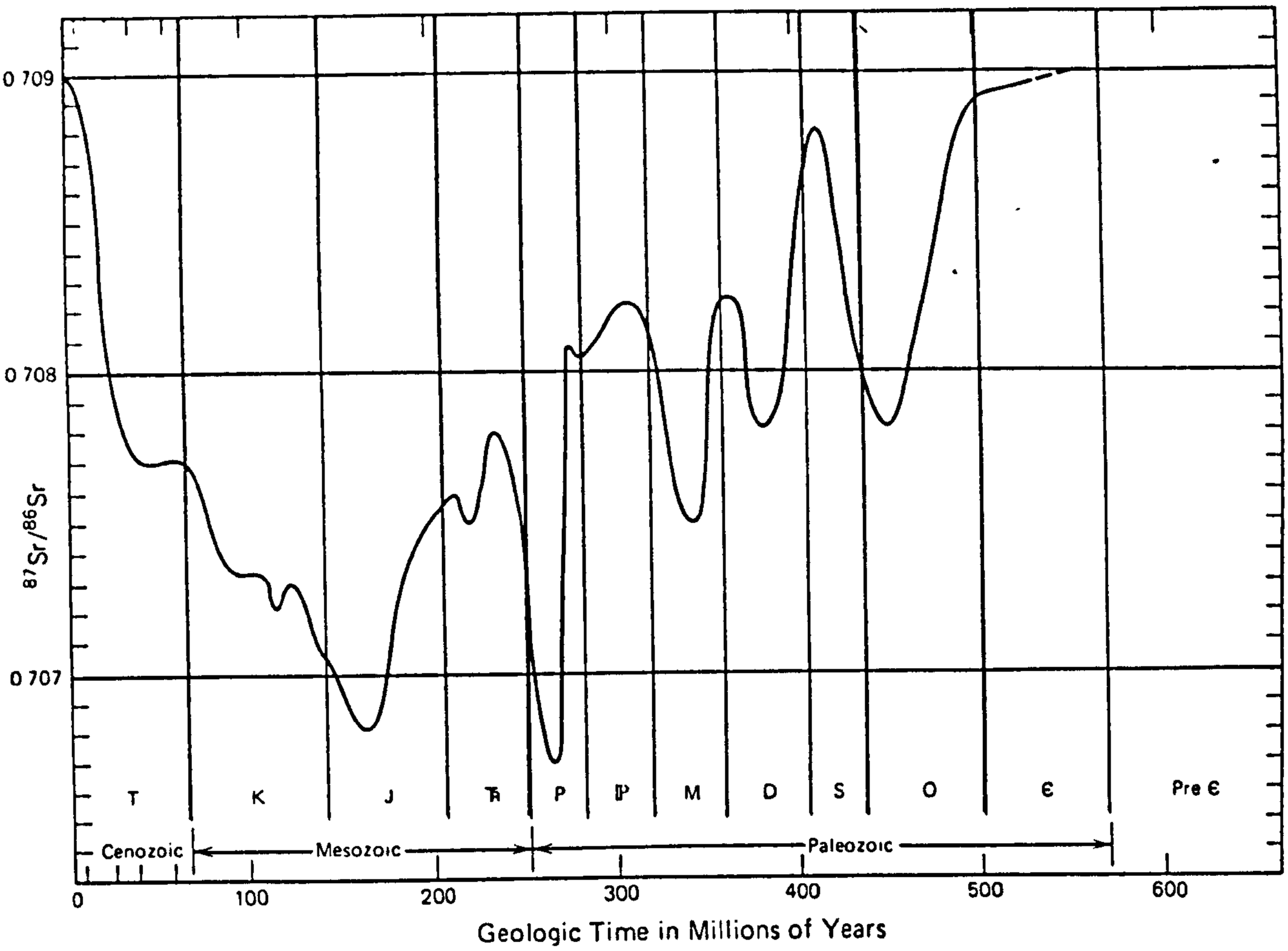

Figure 1.27.

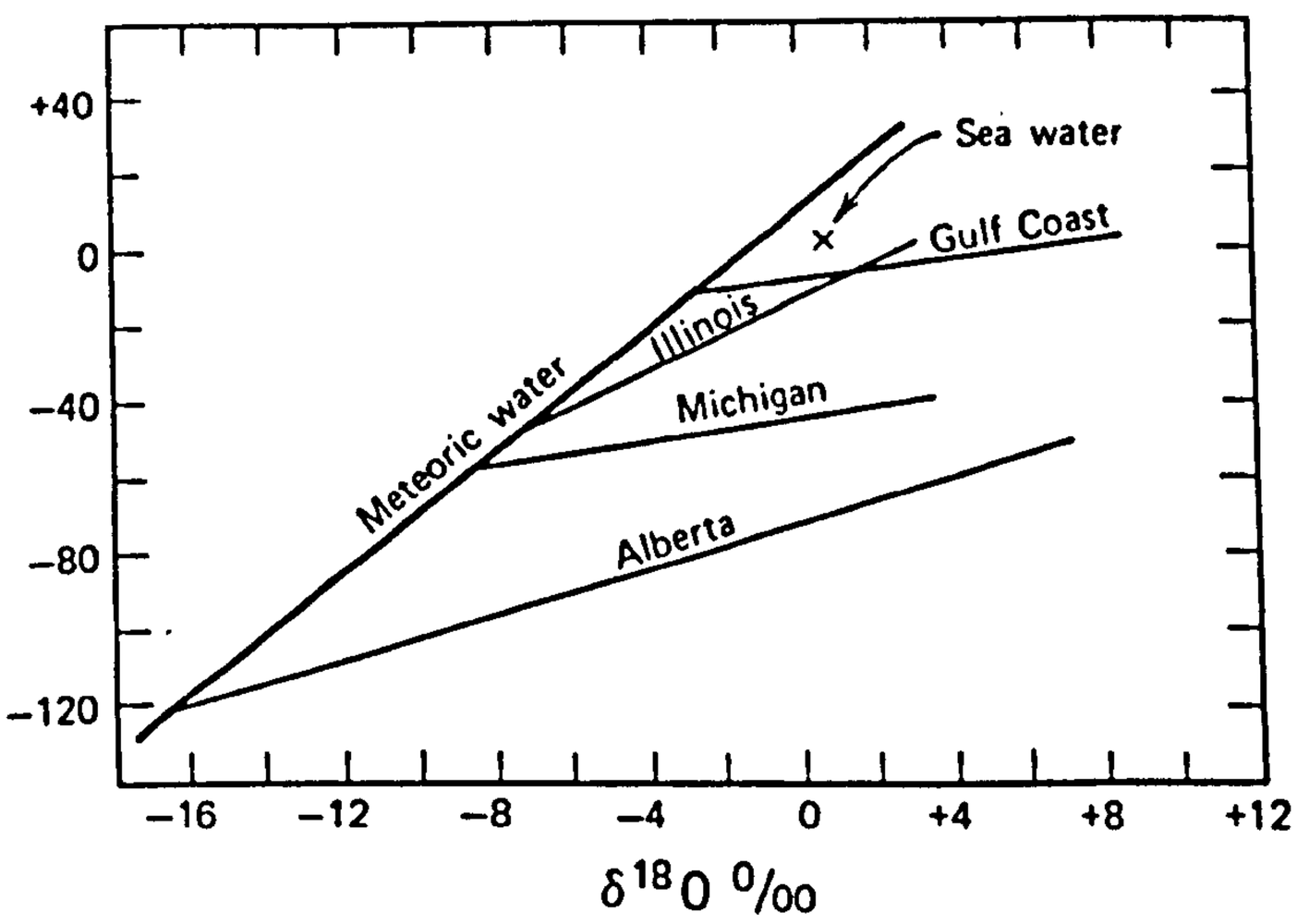

Figure 1.28.

CARBONATE CEMENTS IN SOUTH BRAE OILFIELD, NORTH SEA. ORIGIN, DISTRIBUTION AND ISOTOPIC COMPOSITION

Orla M. Mc Laughlin, R. Stuart Haszeldine
Department of Geology and Applied Geology, University of Glasgow,
Glasgow G12 8QQ, Scotland

Anthony E. Fallick, Graeme Rogers
Isotope Geology Unit, Scottish Universities Research and Reactor Centre,
East Kiulbride, Glasgow G75 0QU, Scotland

2.1 ABSTRACT

The reservoir sandstones and conglomerates of the South Brae Formation are locally cemented by calcite cement which formed from shallow down to medium burial (0.3-2.3km) The calcite cemented bodies are up to 4 metres thick and are interpreted as concretions. Corroded feldspars within concretion centres indicate that a period of time and waterflow elapsed between deposition and the initiation of concretion growth. Feldspar dissolution during diagenesis has changed the bulk rock percentage remnant feldspar from 10 to 2%. The earliest-formed core of the concretions are ferroan rich (0.6 to 3.5wt%$FeCO_3$) and the calcium and carbon is sourced by shell dissolution ($\delta^{13}C$ of cements from +3.66 to -1.75‰). The concretion margins are non-ferroan with lower $\delta^{13}C$ values -5.65 to -11.66‰. These are indicative of a mixture of CO_2 sources, including shell dissolution and decarboxylation of surrounding organic mudrocks. $\delta^{18}O$ values (24.26 to 14.5‰ SMOW) are interpreted as indicating that the concretions were precipitated from evolving meteoric waters at temperatures between 15° and 75°C. $^{87}Sr/^{86}Sr$ ratios recorded by concretion cements become increasingly radiogenic with time; this is correlated with the increased amount of high ^{87}Sr feldspar dissolved within the concretion bodies. The Brae reservoir sediments were deposited in a submarine fan environment (Turner et al. 1987), therefore the original porewaters must have been replaced by meteoric waters before the onset of concretion growth. Because concretion growth occurred over a prolonged period, the $\delta^{18}O$ of the meteoric fluid precipitating the calcite cements would have become modified. This is partially due to the increasing interaction with basinal fluids associated with increasing burial, and the decarboxylation of the surrounding mudrocks.

2.2 INTRODUCTION

The South Brae oilfield lies 240km. east of the Orkney Islands in the U.K. sector of the North Sea. The field is located on the western edge of the Viking Graben and separated from the Fladen Ground Spur to its west by the N-S Viking Graben fault (Fig.2.1.). The 500 metre thick Brae Formation reservoir consists of fining up cycles of sands and conglomerates deposited as nearshore submarine fans in the Upper Jurassic. They overlie a thick sequence of Permian-mid Jurassic sediments which rest on "basement" Devonian (Fig.2.2.). The reservoir unit is overlain and partly sealed by the Kimmeridge Clay Formation which, together with mudstones within the South Brae Formation, has been proven as the regional and local source rocks for the South Brae oil accumulation (Reitsema 1983, Cornford 1984, MacKenzie et al. 1987). The sedimentology of this area has been previously described by Harms et al.(1981), Stow et al.(1982) and Turner at al.(1987).

There are three major controls on the porosity and permeability in the South Brae reservoir:- diagenesis, facies distribution and fault location.

1.) Several diagenetic processes have operated to modify the original mineralogy and texture of the reservoir rocks, these have resulted in reduction or enhancement of porosity and permeability (see Sect.1.8). The diagenetic sequence (Fig.2.3.) can be simplified to:- compaction of the sediment followed closely by early calcite cementation, and then a widespread long-term authigenic quartz phase. A dissolution event followed and small amounts of clay minerals (principally illite and kaolinite), and some later calcite partly infilled these dissolution pores at a later stage. This dissolution event leads to major enhancement in secondary porosity, particularly in the top reservoir layers (see Chapter 4).

2.) Facies type and distribution controls porosity and to a lesser extent permeability. The highest porosity (24.2%) and permeability values (961mD) are found in the sandy matrix conglomerates and massive sandstones, except where early calcite cementation has occurred. The finer-grained sandstones have medium porosities but the permeabilities are lower due to the existence of mudstone laminae. In general both parameters show an overall decline with depth. As sorting becomes poorer and the section becomes more conglomeratic towards the base there is a decline in permeability. The vertical porosity distribution shows considerable variability, but each figure has a distinct decline of porosity with depth (Fig.2.4.).

3.) Faulted sections within the field have low porosities (Stow et al.1982) due to calcite and quartz cementation along steeply dipping fracture fills (16/7a-A12, A13 & A14). Wells adjacent to the Graben margin have slightly enhanced porosity and permeability particularly in the top reservoir layers, 16/7a-A1 & A3 (see Chapter 4).

2.3 EFFECTS ON RESERVOIR POROSITY

The South Brae reservoir formation contains calcite cemented layers with thicknesses of up to a few metres. These sandstones and conglomerates have severely reduced reservoir quality from the earliest stages of diagenesis. Within such layers practically all the porosity is filled by calcite cement (up to 45% whole rock), and permeability is insignificant. Zones which have the pore space totally filled with calcite cement are interpreted as concretions. They have curved edges (Fig.2.5.) in the core (which could suggest a concretionary shape) and they do not continue laterally to the adjacent wells. Concretions form impermeable baffles to vertical fluid flow within the Brae Formation during hydrocarbon production (Kantorowicz et al. 1987). Because the calcite is not uniformly distributed within the

sandstones but concentrated in certain zones, it is important that we endeavour to understand the processes controlling formation of these concretions and attempt to predict their geometry and how laterally continuous these units may be. Concretions often show changes in cement composition from the centre (presumably early) outwards. Complex precipitation histories can be revealed by detailed petrographic and isotopic investigations. Similar tightly calcite-cemented horizons from shallow marine sandstones have been described by Bjorkum & Walderhaug (1990), Bryant et al. (1988), Haszeldine et al. (1992), Hudson and Andrews (1987), Kantorowicz et al.(1987), Mc Bride (1988), Schwarzkopf (1990) and Wilkinson (1991) and for deeper marine sandstones by Boles and Rameseyer (1987).

2.4 ANALYTICAL METHODS

2.4.1 Carbonate petrography methods

Thirty five thin sections from four wells (16/7a-A6, A11, A27 & 16/7b-A19) (Fig.2.2.) were examined using a standard polarizing microscope. These included sections from six concretions sampled from edge to centre, sections across fractures and sections of early non-concretionary calcite and late calcite cements. Prior to sectioning samples were impregnated with blue epoxy resin to highlight porosity. Each sample was petrographically examined and point counted (500 counts) for grain size and composition (Table 1.1.). Thin sections were examined using a Technosyn cold cathode luminescence microscope. Textural relationships were examined in detail using a CAMBRIDGE STEREO SCAN 360 Scanning Electron Microscope equipped with a LINK Energy Dispersive Analysis of X-rays System (EDS). Bulk mineralogies were analysed using a Philips X-Ray Diffractometer and trace elements were analysed at Edinburgh University by Wavelength

Dispersive Analysis on a Microscan Mark V, Cambridge Instruments electron microprobe.

2.4.2 Carbonate petrography

Two phases of calcite cement occur in the South Brae samples, an early cement which is mostly seen in concretions and a late calcite cement which postdates dissolution (Fig. 2.6a, b & c) A later stage dolomite can also be found filling secondary pores.

Early Cements.

In reservoir units most of the calcite is of a concretionary nature; it appears to be limited to either the more massive sandstones or the conglomerates with sand matrix (Fig.2.5.). The concretions we have examined range in size from 0.8m to 4m thick. Early non-concretionary calcite cementation is restricted to thin sandstones in dominantly shaly sections and is usually only a few cm thick (Fig.2.7.). This cement is presently not volumetrically significant. Its original distribution was probably much greater as shown by the widespread remnants of this cement. In these areas quartz overgrowth development has been inhibited resulting in good secondary porosity. This calcite was seen to replace feldspar to a limited extent.

The calcite cement in the concretions is poikilotopic, and the average crystal size is 0.25 to 2mm (Fig.2.8.). The porefluid which precipitated the cement in all the concretions was aggressive in places, with the edges of the framework grains showing the effect of dissolution. As the concretions grew, feldspar and shells were being dissolved and replaced by calcite (Fig.2.9.); in some areas total replacement occurred - but commonly small leached grains of feldspar remained. The sediment within these concretions underwent no further diagenetic changes. Not all shells have suffered dissolution as a few intact fossil fragments were found, but the

majority have been replaced. A later dissolution event has preferentially removed the top margins of the concretions, increasing effective porosity (Fig.2.10.). Elsewhere porosity is totally occluded and there is no oil staining.

Point counts of thin sections show calcite cement contents of 19 to 45%; this represents the sandstone porosity during calcite growth (known as Minus Cement Porosity - MCP), showing that these concretions started to form prior to substantial sediment compaction. The point counted calcite cement is slightly over estimated as it also includes the dissolved feldspar pores infilled by calcite, only by point counting with a CL can this extra porosity be calculated. Other evidence for early cementation is the lack of framework grain to grain contacts. This floating texture can be accomplished by replacement of grains; but, in these concretions most of the quartz grains are only slightly etched and are similar in size to framework grains in adjacent sandstones. Many of these concretions have grown over a geologically significant time span, as their margins display more evidence of framework grain compaction than their cores (Fig.2.11.). Decreasing carbonate contents from the centre to the exterior of the concretions (45-19%) reflect decreasing pore space volume during concretion growth (similar to concretions described by Oertel and Curtis 1972). Occasional small fractures crosscut the concretionary cements and the detrital quartz grains; these are infilled with calcite cement (Fig.2.12.).

Late cements.

The late calcite was seen to infill obvious dissolution pores and to cement small patches of sandstone and conglomerate after quartz overgrowths had formed. The majority of the late calcite cement was precipitated in former feldspar sites (Fig.2.13.), although in most cases small fragments of feldspar remained. Some of this late calcite was probably created by local

reprecipitation of the early calcite cement and was found at the extremities of the large early concretion in 16/7b - A19. Calcite was also seen to fill fractures which in one instance cross cuts a concretion indicating a possible later origin. Dolomite rhombs were found sporadically infilling late dissolution pores (Fig.2.14.).

2.4.3 Cathodoluminescence petrography

Cathodoluminescence observations show that some cemented concretions and pore fillings are uniform in their CL characteristics, implying that they formed under conditions which remained constant over a period of time. In other instances, however, the CL observations provide evidence of the presence of cements of varying luminescence intensity, indicating that the carbonate cements have formed under varying conditions (Marshall, 1988). The CL technique was also useful in identifying the fossils within cemented concretions which had undergone complete recrystallization, or replaced fossils which could be recognized with CL but were not visible in plane polarized light. Bioclasts were also distinguishable from the silicate matrix. CL was very useful in determining the sequence of events and the relationship of fracturing to the events.

Early cements.

Six concretions were examined, five of which showed systematic spatial CL variation of the cement ie. from the centre to the edge. The centres of the concretions have a dull-luminescing orange cement (Fig.2.15.). This dull cement (Early I) when microprobed showed a greater wt% of Fe than the brightly luminescent marginal cement (Early II). Corresponding to this enhancement in Fe (a quencher of luminescence) 0.09/0.34 to 0.6/3.17wt% we also found a decrease in wt% Mn (an activator of luminescence). The centres of the concretions have suffered little compaction, so the detrital grains float in the poikilotopic cement. The detrital quartz grains are

etched slightly . Some of the feldspar and mica grains still remain fresh, but where they have been leached, a brighter orange cement has been precipitated (Fig.2.16.). There is a higher percentage of shell material in the concretion core (most of which has been replaced). Wood and plant tissue are commonly found throughout the concretions (Fig.2.17.).

The edges of the concretions have a brightly luminescent orange cement (Early II). More compaction is evident, with increased amounts of grain to grain contacts and some fracturing of the detrital grains (Fig.2.18.). Detrital feldspar grains have suffered more dissolution and alteration, and in some places have almost been completely replaced. The extreme edges of the concretions have usually suffered a late dissolution event and have many large secondary pores. There appears to be a gradational change from non luminescent to luminescent cement, although thin section sampling bias does not portray this too clearly.

Late cements.

Later carbonate cements are not very common and are usually only found in fractures at concretion margins, or in association with dissolved/remnant feldspar grains. In one fracture we found a zoned cement lining the fracture, but it was not totally intact as large pieces had been broken off; the cement infilling the rest of the fracture was orange and brightly luminescent. We also found some late-stage dolomite (Fig.2.14.) (which luminesces bright red and usually forms rhombs) and occasional bioclasts (Fig.2.19.).

2.5 DEPTH OF FORMATION

There are some crude constraints on estimating the depth of cementation events, which help later in distinguishing the correct $\delta^{18}O$ SMOW value

for the cementing porewater. The concretion centres exhibit diagenetically early calcite cementation, and there is no evidence of early quartz cementation or authigenic clay development. Evidence for the length of time involved in the growth of these concretions is directly related to the amount of cement present throughout the concretions. Lippmann (1955) and Raiswell (1971) suggested that carbonate cement passively infills the porespaces of the host sediment, therefore the volume percentage cement provides a direct estimate of the host sediment porosity (and in effect the degree of compaction) at the time of concretionary growth. Point counts of thin sections show calcite cement contents of 20-45% which represents a geologically significant growth time span (Fig.2.11.).

Consequently an estimate of porosity loss by the time cementation had occurred also constrains the depth of calcite precipitation assuming that compaction is related directly to the depth of burial. The Minus Cement Porosity (=1/solidity) where, S (solidity) is the volume of solid grains as a percent of total volume of sediment, was measured by point counting for each concretionary sample (±1% accuracy; it is the complement of porosity. The depths of calcite precipitation were then calculated using empirically-derived compaction curves (Baldwin & Butler, 1985). By applying a geothermal gradient of 30°C/km (suitable for this reservoir), approximate temperatures of cementation were then calculated (Fig.2.20.). For sandstones, Baldwin and Butler used the following equation to calculate burial depth

$$\text{Burial depth (kms)} = 3.7 \ln (0.49/(1-S))$$

The data are projected onto an empirically derived compaction curve. The compaction curve provides us with the burial depths of our samples, and from this information we can calculate the temperatures at which these cements were precipitated (using a geothermal gradient of 30°C/km). We have calculated a possible range from 11° to 108°C, at depths from 0.3 to

3.6km (Table 2.1.). Table 2.1. is a combination of early and late calcite cements, with the early cements growing to depths of approximately 2.3km. Our estimates of host sediment porosity clearly demonstrate that concretion growth occurred over a long geological time span. Estimating the precise duration of concretionary growth is more problematic, but presently it seems that porosity estimations are the most useful measure of the timing of concretionary growth.

2.6 CARBON & OXYGEN STABLE ISOTOPES

The $\delta^{18}O$ value produced from analysis may be related to the temperature of cement formation and the $\delta^{18}O$ of the porewater from which the cement precipitated via the experimentally determined fractionation equation (Bigelsein & Mayer 1947, Urey 1947), provided the mineral precipitated in isotopic equilibrium with the fluid. It may also be a function of the extent to which isotopic equilibrium was maintained during mineral authigenesis and the extent and nature of isotopic exchange between the mineral and fluids following crystallisation (Longstaffe 1983).

The $\delta^{13}C$ results from the cements may be interpreted to diagnose the source of the CO_2 in the porefluids from which the cements precipitated (Irwin, 1980). Variation in $\delta^{13}C$ values of diagenetic carbonates reflects a variation in the source or process of carbon supply rather than temperature fractionation effects.

Organic matter is modified by several depth related processes; CO_2 is a common product of each process (Irwin et al. 1977). These processes each have a characteristic carbon isotope signature (Fig.2.21.). With increasing burial depth these are,

1. aerobic oxidation ($\delta^{13}C$ = -25‰)
2. sulphate reduction ($\delta^{13}C$ = -25‰)
3. bacterial fermentation ($\delta^{13}C$ = +15‰)
4. thermal abiotic processes ($\delta^{13}C$ = -10 to -25‰)

Dissolved primary marine carbonate ($\delta^{13}C$ = 0‰) is another isotopic signature which can be an influencing factor. Intermediate isotopic signatures would imply a mixture from various sources.

2.6.1 Carbon Isotope Results

The $\delta^{13}C$ for the carbonate cements in South Brae ranges from +3.66 to -11.66‰PDB (see Table 2.2.) There is no systematic variation with depth within the wells. Similarly the $\delta^{13}C$ sources have remained constant throughout the burial of the reservoir as early and late cements show the same range of $\delta^{13}C$ values.

These concretions have similar $\delta^{13}C$ and $\delta^{18}O$ values to other North Sea concretions, notably those analysed by Brint (1989) from Tarbert and Ness in the mid-Jurassic Brent Sandstones. The early concretionary calcites display a wide range of values, with a spatial trend of more depleted $\delta^{13}C$ values towards the margins (Fig.2.22.); such a trend has also been noted in the Moeraki septarian concretions described by Thyne and Boles (1980).

The concretion cores have the highest $\delta^{13}C$ values of +3.7, -0.8, -1.7 and -1.8‰PDB. These values are not indicative of any one source of carbon but suggest a mixture of carbon sources. The lower values (-0.8, -1.7 & -1.8‰PDB) are akin to Jurassic marine carbonate ($\delta^{13}C$=+0.48‰PDB), measured by Veizer et al. (1980). These values suggest the main bicarbonate source is the dissolution of Jurassic marine shells with the more enriched value (+3.7‰PDB in well 16/7a-A6) due to the addition of CO_2 from bacterial fermentation of organic matter (+15‰PDB). Although

these values may be obtained by mixtures of sulphate reduction and fermentation, the calculated growth depths place concretion formation within or below the fermentation zone and the presence of recrystallized shell material and the strontium isotope data favour the former interpretation.

The depleted values for the concretion margins, and later cements -5.7 to -11.7‰PDB are attributed to a mixture of bicarbonate from dissolution and reprecipitation of shell material (0‰) and low $\delta^{13}C$ carbon from decarboxylation of organic carbon from surrounding mudrocks (-25‰PDB). Assuming this, the intermediate calcite values have a contribution from organic derived bicarbonate of between 22.2 and 46.6%

We initially assumed that Jurassic marine shells grew contemporaneously with sedimentation and should have a $\delta^{13}C$ ~+0.5‰PDB as reported by Veizer et al.(1980). Two shells were measured and we found this not to be the case; they had $\delta^{13}C$ values of -6.6 and -11.0‰PDB. From these values and by imaging the shells with CL we found that they have been recrystallized (Fig.2.23.). The majority of the shells in the reservoir have been recrystallized apparently contemporaneously with early calcite cementation. The light $\delta^{13}C$ carbon signature is due to the input of CO_2 which is produced from organic matter by thermal maturation. Analysis of concretions associated with organic rich shales (eg. Kimmeridge Clay Formation) shows that organically derived CO_2 is readily absorbed into diagenetic carbonates (Irwin et al .1977, Smith, 1978; Reitsema, 1980).

As previously mentioned $\delta^{13}C$ values for later carbonate cements and vein infills are also depleted (-8.5 to -10.6‰PDB), suggesting there has been little change in the carbon sources over a significant period of time.

Calculated growth depths 0.5 to 2.5km (Fig.2.20.) put concretion formation within zone III (the bacterial fermentation zone) and zone IV (the zone of decarboxylation). The $\delta^{13}C$ values of the South Brae calcite cements are a combination of bicarbonate from dissolved shells and CO_2 characteristic of the zone in question.

In zone III the bicarbonate produced is isotopically heavy (+15‰PDB). The process involves the fermentative degradation of organic matter and is dependent on the availability of suitable organic substrates.The reduction of iron compounds continues in zone III so that iron-rich carbonates are precipitated (Curtis 1978). Therefore the concretion cores in South Brae (wells A6 & A11) are slightly enhanced in Fe, particularly the concretion core in A6 (which also has the heaviest $\delta^{13}C$). These cements are similar to those found in the Brent reservoir rocks by Samways cited in Giles et al. (1992). Their early cements (mixed ferroan calcite and siderite) exhibit a wide variation in $\delta^{13}C$, up to 20‰ PDB, which they interpreted as a dominance of methanogenic bicarbonate.

The remaining $\delta^{13}C$ values are due to a mixture of CO_2 from decarboxylation of organic matter in nearby source rocks or mudrocks at the increased temperature of zone IV, and dissolved shell material. The isotopic composition reverts to the low $\delta^{13}C$ values approaching those of the organic substrate (-25‰PDB). In this zone acetate is generated from kerogen which is found within the source rocks; the acetic acid migrates with the expressed porewaters and has the ability to leach carbonates and silicates. Only small concentrations of acetic acids are found in waters below 80°C. This porefluid does not have far to travel as the mudrocks and shales in the South Brae reservoir interdigitate with the sandstones. These porefluids may also be responsible for the leaching of the shells, feldspar and detrital quartz grains.

2.6.2 Oxygen Isotope Results

The $\delta^{18}O$ values range from +14.9 to +24.3‰SMOW. There are three distinct populations of $\delta^{18}O$ recognisable, which suggest either changing temperature and/or changing porewater (Fig.2.24.). It seems that as diagenesis proceeds, the isotopic composition of the enclosed porewater changes, usually towards lower $\delta^{18}O$ values. This change is possibly due to the strongly dependent fractionation of oxygen isotopes between cement and fluid (Moore 1989).

The highest $\delta^{18}O$ values range from +24.3 to +19.7 ‰SMOW, and make up the early concretionary and non-concretionary calcites. The lowest $\delta^{18}O$ values range from +14.9 to +15.9‰SMOW and they are late calcite cements (post secondary porosity). There is also a third intermediate group of values ranging from +17.4 to +18.7‰SMOW; this group is a physical mixture of early (I and II) and late cements, which show dull and bright orange luminescence in CL and occur at the margins of the concretions.

If calcite $\delta^{18}O$ values are plotted versus temperature and $\delta^{18}O$ porewater the temperature range for calcite formation can be extrapolated for marine ($\delta^{18}O$ = -1.2‰ SMOW Shackleton & Kennett, 1975) and meteoric waters of -7.0‰SMOW (Hamilton et al.1987, Hudson & Andrews, 1987). (Fig.2.25a&b.) For precipitation from Upper Jurassic meteoric waters for which δw=-7.0‰SMOW, calculated temperatures for the early cements are 14° to 36°C and temperatures from 40-47°C for the mixed cements. For Jurassic marine porewater with δw=-1.2‰SMOW the corresponding temperature are 42° to 70°C for early cements and 78-88°C for mixed cements (Fig.2.25a.) Comparison of the calculated isotopic temperatures with the present day geothermal gradient of 30°C/km for the South Brae reservoir helps to distinguish the porewater present at the time of calcite

formation. From our empirical curve (Fig.2.20.) we calculate that the concretions were precipitated at temperatures ranging from 11° to 70°C (early I & II cements); this temperature range is most compatible with precipitation from a meteoric water ($\delta^{18}O$=-7‰SMOW). We must assume that part of the change in $\delta^{18}O$ is due to increasing temperatures of precipitation as our concretions become buried increasingly deeper, and also due to the addition of basinal fluids . In Chapter 3 we discuss the porefluids which precipitate the authigenic quartz, these fluids are a mixture of basinal and meteoric water. The later calcite cements (post quartz cementation) are precipitated from an evolved meteoric fluid similar to that which has precipitated the overgrowths. They have grown at temperatures >75°C (-7‰ SMOW) or probably at higher temperatures if the fluid is more evolved.

2.7 STRONTIUM ISOTOPES

The isotopic composition of strontium in solution depends on the $^{87}Sr/^{86}Sr$ ratios of the rocks that interact with water on the earth's surface. As the water is transported to the oceans and enclosed basins mixing of the strontium is achieved rendering the solution isotopically homogeneous. The strontium then re-enters the rock cycle through calcite precipitation, thus preserving a record of the changing isotope composition of strontium throughout Proterozoic and Phanerozoic time (Faure 1986).

The lack of biogenic and kinetic fractionation of the $^{87}Sr/^{86}Sr$ ratio means that this parameter records the strontium isotopic composition of the porefluid which has precipitated the carbonate cement; it therefore also records the $^{87}Sr/^{86}Sr$ sources (Veizer 1983)

Consequently the concentration and isotopic composition of strontium in the carbonate cements in South Brae should provide us with a record of the porewater from which they have precipitated. The $^{87}Sr/^{86}Sr$ ratios of marine carbonate minerals are assumed to be identical to those of seawater at the time of their deposition (Faure 1986). The isotopic composition of strontium in the oceans is homogenous with a $^{87}Sr/^{86}Sr$ ratio of 0.70910 at present, but seawater $^{87}Sr/^{86}Sr$ has varied through geological time (Burke et al. 1982). In the late Jurassic when the South Brae reservoir was being deposited seawater had a value of 0.7070 (Fig.2.26.). Any differences in the initial $^{87}Sr/^{86}Sr$ ratio may be due to a variety of source components, in addition to the depositional marine porewaters. These include meteoric porefluids, hot formation fluids at/or derived at depth, fossil carbonate shells and local reactive mica or feldspar mineral detritus (Hamilton et al.1987). We found that all the cements contain more radiogenic strontium than Upper Jurassic seawater.

2.7.1 Strontium Isotope Results

$^{87}Sr/^{86}Sr$ ratios and the strontium concentrations were measured on the concretionary and non-concretionary calcite cements (Table 2.3.). The data have been age-corrected to 140Ma, this is an approximate calculation for the commencement of calcite precipitation. The calcite strontium isotopes show a wide spread from 0.71024 to 0.72320 and establish two important conditions for interpretation. The calcites contain strontium variably more radiogenic than Upper Jurassic seawater (Fig.2.26.) which has a value of 0.7070 (Burke et al.1982), and there seems to be a systematic spatial distribution of radiogenic enrichment within the concretions (Fig.2.27.).

The strontium from the texturally earliest carbonate (ie. the centre of the concretions) is significantly less radiogenic than that of the carbonate at the concretion margins. The cores have isotopic ratios ranging from 0.71024 to

0.71186, the margins range from 0.71206 to 0.72044. Corresponding to the increasing radiogenic trend we find a decreasing concentration in strontium concentration (Fig.2.28.). The concretion cores have high strontium concentrations 594.6 to 192.9ppm whereas the margins have much lower values, 168.9 to 68.9ppm. The rubidium concentrations throughout the concretions were low ranging from 4.8 to 0.3ppm. Later cements were slightly more enriched in rubidium 12.42 to 5.4ppm (Table 2.3.).

Dissolution of diagenetically unmodified fossil shells would yield high strontium abundances to the porefluid precipitating the cores of the concretions and would release strontium of isotopic composition close to Upper Jurassic seawater (0.7070). The $(^{87}Sr/^{86}Sr)_{140}$ ratios for the shell debris measured (0.70719 and 0.70834) are higher than Upper Jurassic seawater. From CL we can see that their original mineralogy has been replaced and therefore they have undergone diagenetic reactions which have replaced some strontium. Further evidence from $\delta^{13}C$ values (-6.64 and -11.03‰PDB) indicate that they no longer have a marine $\delta^{13}C$ signature. The majority of the shells in the reservoir have been recrystallized apparently contemporaneously with early calcite cementation. The light $\delta^{13}C$ carbon signature is due to the input of CO_2 which is produced from organic matter by thermal maturation.

The concretion $(^{87}Sr/^{86}Sr)_{140}$ ratios are also higher than the Upper Jurassic seawater value this implies they too have incorporated some radiogenic component (silicate dissolved Sr) and that the values could be due to mixing marine strontium (0.7070) with silicate derived strontium (Fig.2.29.). However, we also note that the shell debris has itself been diagenetically altered. Consequently, because concretion growth and shell dissolution texturally occurred simultaneously, the concretion drained its

unradiogenic strontium from the shell dissolution. The margins were precipitated from a fluid much more enriched in radiogenic strontium, which indicates that a more significant proportion of the strontium must have come from the dissolution of silicates with high $(^{87}Sr/^{86}Sr)_{140}$ ratios.

Leaching and dissolution of detrital silicate minerals will result in $^{87}Sr/^{86}Sr$ ratios of 0.720 and higher (Faure 1986). Such a mechanism has been invoked to explain the Smackover brines (Steuber et al.1984) and cements in the Lincolnshire Limestone (Emery et al.1987). There are a few possible sources of radiogenic strontium in these sandstones. As mentioned before a large amount of feldspar dissolution has taken place and there is also some altered muscovite and clay fragments, all of which could have contributed to the radiogenic strontium budget. The silicate grains may be from the Scottish Caledonian orogen (Hamilton et al.1987). Frost and O'Nions (1985) suggest a bulk value of 0.722 for the Dalradian Supergroup of this orogen, whereas the average of Dempster (1985) Dalradian metasediment data gives an $(^{87}Sr/^{86}Sr)_{140} = 0.7388$. The average Caledonian K-feldspar of Haughton et al. (1990) has an $(^{87}Sr/^{86}Sr)_{140} = 0.7239$.

Some simple standard mass balance type modelling (with the Emery et al. (1987) type calculations) is useful in order to try to assess the relative proportions of a radiogenic component. For instance in order to change a seawater value of ~0.7070 to 0.710 we need to add ~20% of a component with an $(^{87}Sr/^{86}Sr)_{140}$ of 0.722 (Caledonian detritus) (assuming constant strontium concentrations in all components).

2.8 MINOR ELEMENT GEOCHEMISTRY OF CARBONATES

Minor element concentrations within the calcite cemented concretions were determined by wavelength dispersive analysis using a Microscan Mark V, Cambridge Instruments Microprobe. Analyses are taken for 40-sec counting periods at 20kv acceleration potential with a defocused electron beam (2-3µm diameter) and 30nA sample current. Ca, Fe, Mn, Mg, Sr and Si concentrations were analyzed (Table 2.4.).

Minor element trends across four of the concretions suggest that porewater iron decreased during precipitation (Fig.2.30.), while manganese levels increased (assuming centre to margin growth). Magnesium variations were not significant.

2.9 POREWATER INTERPRETATION

Textural evidence shows us that after initial deposition and some minor compaction calcite was the first diagenetic phase to occur. From our compaction curve we calculated that the (early I & II) cements should have precipitated between 11° and 70°C (applying a present day geothermal gradient of 30°C/km) and over a range of depths 0.3 to 2.3km - therefore it seems that early diagenetic calcite is most compatible with being precipitated from a meteoric fluid ($\delta^{18}O$ = -7‰SMOW). This meteoric fluid has replaced the original marine interstitial fluid at a very early stage, approximately before 360m burial (as this is the depth of the onset of calcite cement growth). This porewater $\delta^{18}O$ signature evolved through concretion growth (due to the leaching of feldspasr and quartz and the addition of basinal and marine porefluids), the temperature also increased due to increasing burial producing the changing $\delta^{18}O$ values measured.

In the late Jurassic the Fladen Ground Spur (Fig.2.1.) was a topographic high, meteoric water was driven by the head of the elevated ground water table. The water was recharged into the shallow marine Jurassic reservoir shortly after deposition. It is difficult to estimate the flow rates of the water and the total flux, the Brae reservoir formation was probably being constantly renewed by rain water similar to reservoirs described by Bjorlykke et al. (1989). Such gravity fed flow rates are probably several orders of magnitude higher than that of the compactional waters (Giles, 1987).

The porewater may have initially been undersaturated with respect to carbonate phases (ie. shell material) and so dissolution occurred as the fluid descended through the sediments. Groundwater relatively rapidly approaches equilibrium with respect to carbonate, but may have remained undersaturated with respect to silicate minerals for a long time. The groundwater often has a high CO_2 content from the soil horizon (Bjorylkke et al. 1989), so it has the potential to leach silicate minerals (ie. quartz and feldspar dissolution is observed early within the concretions). With increasing water/rock reactions and the dissolution of shell material the porefluids eventually become saturated with respect to carbonate resulting in the precipitation of calcite. Poikilotopic cements are the most common within the reservoir as these are probably the most stable habit of the low Mg calcite phase (Moore 1989). This type of cement is commonly associated with sequences deposited during periods of low sedimentation or a hiatus (Raiswell 1971).

Due to progressive burial, dewatering of the reservoir occurs. These fluids will be rich in organic carbon with a negative $\delta^{13}C$ due to a major contribution from the decarboxylation of Brae Formation shales and

muds. The mixture of meteoric water saturated with respect to carbonate and CO_2 charged waters with characteristically depleted $\delta^{13}C$ values could result in carbonate cements with intermediate values.

The initial development of these concretionary nodules is inferred to be associated with a pause in deposition which occurs between late Jurassic times and late Cretaceous. From the burial curve constructed for South Brae field (Fig.2.31.) there is a slow subsidence hiatus of 50 My. The formation of a concretionary horizon appears to require that a supersaturation maximum is maintained in the same position for long enough to allow growth within a stratigraphically confined interval (Canfield & Raiswell 1991). Raiswell (1987) showed that the rate of concretion growth within shales can be determined by the rate of surface reaction processes, but that concretion growth in sandstones may be dominated by two processes 1). solute transport 2). surface reaction. Either of these processes may dominate depending upon the specific geological conditions. Wilkinson & Dampier (1990) calculated for concretions in the Valtos Sandstone Formation, Scotland, a 1m diameter concretion will take up to 9Ma to form. We believe that 50My is an adequate time period for the growth of the South Brae concretions.

2.10 CONCRETION FORMATION & DISTRIBUTION

Concretion formation and distribution has been reported to be controlled by a number of geological factors,

1). Bjorkum and Walderhaug (1990) suggest that concretion distribution mirrors shell distribution. They hypothesize that at low degrees of supersaturation concretions grow upon detrital shells. This mechanism is driven by the different solubilities of high Mg calcite, low Mg calcite and aragonite. Therefore the porewaters only become supersaturated with

respect to calcite within the shell-rich horizons and nucleation points are confined to these layers. This type of concretion growth invokes very small input of porefluid and assumes diffusion-controlled growth. In systems where the fluid flow rates are high eg. South Brae, where the sediments have been exposed to meteoric water flow, diffusion mass transport may only dominate within a small distance from the nucleus. Bjorkum and Walderhaug (1990) postulate that the range of influence would be small eg. 1mm for a flow rate of 10m/yr; therefore only patchy calcite would develop. This does not seem to be the case for the Brae concretions, as they grow up to 4m in diameter.

2). Nielson (1961), Berner (1968) and Wilkinson & Dampier (1991) have put forward evidence for concretions preferably growing where porefluid flow is most rapid ie. in the most porous and permeable sands. It is documented that concretions form more rapidly in flowing fluids than in stationary ones. The South Brae concretions tend to occur in the coarsest grained sandstones or conglomerates with a coarse grained matrix which would have had highest initial porosity and permeability values. The only shells found in the South Brae sandstones exist within the concretions. It would therefore seem most likely that this shell material formed the nucleus for the concretions to develop on. In this setting the concretions could grow more rapidly, as there was lots of shelly material present and permeabilities were high allowing rapid throughflow of porefluids. The spatial distribution of the calcite concretions and cement is controlled by a late stage dissolution event. In the lower reservoir zones, calcite cement was ubiquitous (found in the channel and interchannel areas) but it seemed slightly more concentrated in close proximity to the western graben margin. In the shallower zones only small amounts of cement were found, these tended to occur on the edges of the fan (see Chapter 4 and Figures 4.25a&b.)

2.11 CONTROLS ON THE MINERALOGY OF THE CONCRETIONS

The Hamilton Group calcite concretions described by Dix & Mullins (1987) are organic rich and shale hosted. They are similar mineralogically to the South Brae concretions as they have a notable absence of both siderite and dolomite. The presence of pyrite during concretion growth indicates the interstitial waters were relatively rich in sulfate - this would inhibit dolomite precipitation (Baker & Kastner, 1981) and also create an unstable environment for siderite (Garrels & Christ, 1965 and Gautier, 1982). Because the interstitial marine porewaters were replaced by meteoric water, magnesium concentrations were low, inhibiting dolomite growth. The presence of organic matter in the interdigitating sediments did not promote dolomite formation even though early dolomite precipitation has been related to the presence of organic matter (Pisciotto & Mahoney, 1981 and Kelts & Mackenzie, 1982).

2.12 CONCLUSIONS

1. Calcite concretions commenced growth at shallow burial depths (0.3 to 0.6km) reducing porosity and permeability from an early stage. Growth started during a 50My pause in subsidence and the concretions nucleated on the detrital shell debris in the most porous and permeable depositional facies. Growth continued to 2.3km (early I & II) with later cement being precipitated at deeper depths (3.6km).

2. Carbon isotope values for calcite range from +3.7 to -11.7‰ PDB, bicarbonate supply was from variable admixtures of shell material (dissolution and reprecipitation) and oxidation of organic matter by fermentation followed by thermal decarboxylation.

3. Oxygen isotopes for the early calcites range from +19.7 to +24.3‰SMOW and for the later cements +14.9 to +15.9‰SMOW. The porewater during early diagenesis was dominantly meteoric (-7.0‰SMOW) which had replaced the depositional marine water and the isotopically derived nucleation temperatures were 11° to 70°C. Later cements may have been precipitated from isotopically similar water at temperatures up to 75°C or from a more evolved water at even higher temperatures.

4. $^{87}Sr/^{86}Sr$ ratios and thin section textures shows that detrital feldspars dissolved slowly during early concretion growth, and more abundantly to the end of concretion growth. This has changed the bulk sandstone from depositional 10% feldspar to present day 2% feldspar.

5. Calcite has increasing $^{87}Sr/^{86}Sr$ ratio due to the increased effect of the incorporation of radiogenic strontium. The concretion cores have higher strontium concentrations due to dissolution of shell debris.

6. Early concretion cements are Fe rich (0.8-3.0wt%) and dully luminescent. They are followed by precipitation of slightly later concretion cements which are Fe poor (0.4<wt%) and bright orange luminescent.

7. Dissolution of concretion upper rims and patchy non-concretionary calcite has produced extensive secondary porosity, which is partly infilled by dolomite rhombs and minor calcite and quartz cement.

2.13 ACKNOWLEDGEMENTS

Marathon Oil (U.K.) Ltd. provided the funding for this project and allowed access to their data and core of the South Brae Oilfield. This research was carried out at the Department of Geology and Applied Geology, University

of Glasgow, and the Isotopes Geology Unit, Scottish Universities Research and Reactor Centre (SURRC). The authors would like to thank Peter Hill and John Millar in Edinburgh University, for kindly allowing use of their microprobe and CL facilities. The authors would also like to thank Douglas Maclean (Glasgow University) for his help with the production of photomicrographs.

2.14 REFERENCES CITED

Baker, P. & Kastner, M. (1981) Constraints on the formation of sedimentary dolomite: Science, v.213, pp.214-216.

Baldwin, B. & Butler, C.O. (1985) Compaction curves: American Association of Petroleum Geologists Bulletin. v.69. pp.622-626.

Berner, R.A. (1968) Rate of concretion growth. Geochimica et Cosmochimica Acta, 32. pp.477-483.

Bigeleisen, J. & Mayer, M.G. (1947) Calculation of equilibrium constants for isotopic exchange reactions. Journal of Chemical Physics, 15. pp.261-267.

Bjorylkke, K., Ramm, M. & Saigal, G.C. (1989) Sandstone diagenesis and porosity modification during basin evolution. Geologische Rundschau, 78/1. pp.243-268.

Bjorkum, P.A. & Walderhaug, O. (1990) Geometrical arrangement of calcite cementation within shallow marine sandstones. Earth Science Reviews, v.29. pp.145-161.

Boles,J.R. & Ramseyer, K. (1987) Diagenetic carbonate in Miocene Sandstone Reservoir, San Joaquin Basin, California. American Association of Petroleum Geologists. v.71. pp.1475-1487.

Bryant, T.D. Kantorowicz, J.D. & Love, C.F. (1988) The origin and recognition of laterally continuous carbonate cemented horizons in the

Upper Lias Sands of southern England. Marine and Petroleum Geology. v.5. pp.108-133.

Burke, W.H., Denison, R.E., Hetherington, E.A., Koepnick, R.B., Nelson, H.F. & Otto, J.B. (1982) Variation of seawater 87Sr/86Sr throughout Phanerozoic time. Geology, v.10, pp.516-519.

Canfield, D.E., & Raiswell, R. (1991) Taphonomy: Releasing the Data locked in the Fossil Record, Volume 9 of Topics in Geobiology, in Allison, P.A. and Briggs, D.E.G. eds. Plenum Press, New York. pp.411-453.

Cornford, C. (1984) Source rocks and hydrocarbons of the North Sea,in Glennie, K.W., ed., Introduction to the Petroleum Geology of the North Sea, Blackwell, Oxford, pp.171-209.

Curtis, C.D. (1978) Possible links between sandstone diagenesis and depth related geochemical reactions occurring in enclosing mudstones. Journal of the Geological Society of London, v.135. pp.107-117.

Dempster, T.J. (1985) Uplift patterns and orogenic evolution in the Scottish Dalradian. Journal of the Geological Society of London, v.142. pp.111-128.

Dix, G.R. & Mullins, H.T. (1987) Shallow, subsurface growth and burial alteration of Middle Devonian calcite concretions. Journal of Sedimentary Petrology. v.57. pp.140-152.

Emery, D., Dickson, J.A.D, & Smalley, P.C. (1987) The strontium isotopic composition and origin of burial cements in the Lincolnshire Limestone (Bajocian) of central Lincolnshire, England. Sedimentology, v.34, pp.795-806.

Faure, G., (1986) Principles of Isotope Geology, (2nd ed.) John Wiley & Sons, Canada, pp.183-196.

Friedman, I. & O'Neil, J.R. (1977) Compilation of stable isotope fractionation factors of geochemical interest. In: Data of Geochemistry, sixth edition, M. Fleischer (ed). United States Geological Survey Professional Paper, 440-kk, 12pp.

Frost, C.D. & O, Nions, R.K. (1985) Caledonian magma genesis and crustal recycling. Journal of Petrology, v.26. pp.514-544.

Garrels, R.M. & Christ, C.L. (1965) Solutions, minerals and equilibria: New York, Harper and Row, 450p.

Gautier, D.L. (1982) Siderite concretions: indicators of early diagenesis in the Gammon Shale (Cretaceous). Journal of Sedimentary Petrology. v.52, pp.859-871.

Giles, M.R. (1987) Mass transfer and problems of secondary porosity creation in deeply buried hydrocarbon reservoir. Marine and Petroleum Geology, v.4. pp.188-204.

Giles, M.R., Stevenson, S., Martin, S.V., Cannon, S.J.C., Hamilton, S.J., Marshall, J.D. & Samways, G.M. (1992) The reservoir properties and diagenesis of the Brent Group: - A regional perspective. Diagenesis of the Brent Group, Geological Society Special Publication.pp.

Hamilton, P.J., Fallick, A.E., Macintyre, R.M. & Elliott, S. (1987) Isotopic tracing of the provenance and diagenesis of Lower Brent Group Sands,

North Sea.In Brooks, J., and Glennie, K. (Eds) Petroleum Geology of North West Europe, Graham & Trotman, London,pp.939-949.

Harms, J.C., Tackenberg, P., Pickles, E. & Pollock, R.E. (1981) The Brae oilfield area, in Illing, I.V., and Hobson, G.D., eds., Petroleum Geology of the Continental Shelf of North - West Europe, Heyden & Son, London, pp.352-357.

Haszeldine, R.S., Brint, J.F. Fallick., A.E. Hamilton, P.J. & Brown, S. (1991) Open and restricted hydrologies in Brent Group diagenesis: North Sea. In Geology of the Brent Group, Geological Society Special Publication No. 61, pp.From Morton, A.C., Haszeldine, R.S., Giles, M.R, and Brown, S. (eds).pp.

Haughton, P.D.W., Rogers, G. & Halliday, A.N. (1990) Provenance of Lower Old Red Sandstone conglomerates, S.E. Kincardineshire: evidence for the timing of Caledonian terrane accretion in central Scotland. Journal of the Geological Society of London, v.147. pp.105-120.

Hudson, J.D. & Andrews, J.E. (1987) The diagenesis of the Great Estuarine Group, Middle Jurassic, Inner Hebrides, Scotland. In J.D. Marshall (Ed.) Diagenesis of Sedimentary Sequences. Blackwell, Oxford, pp.259-276.

Irwin, H., Curtis, C.D. & Coleman, M. (1977) Isotopic evidence for source of diagenetic carbonates formed during burial of organic-rich sediments. Nature, v.269, pp.209-213.

Irwin, H. (1980) Early diagenetic carbonate precipitation and porefluid migration in the Kimmeridge Clay of Dorset, England. Sedimentology, v.27. pp.577-591.

Kantorowicz, J.D., Bryant, T.D. & Dawans, J.M. (1987) Controls on the geometry and distribution of carbonate cements in Jurassic sandstones: Bridport Sands, southern England and the Viking Group, Troll Field, Norway. In J.D. Marshall (Ed.) Diagenesis of Sedimentary Sequences. Blackwell, Oxford, pp.103-118.

Kelts, K. & Mackenzie, J.A. (1982) Diagenetic dolomite formation in Quaternary anoxic diatomaceous muds of Deep Sea Drilling Project, Leg 64, gulf of California. in Initial Reports of the Deep Sea Drilling Project, v.64. pp.553-569.

Lippmann, F. (1955) Ton, Geoden Minerale des Barreme von Hoheneggelsen, Geologisch Rundschau, v.43. pp.475-503.

Longstaffe, F.J, (1983) Diagenesis, IV. Stable isotope studies of diagenesis in clastic rocks. Geoscience Canada, 10. pp.45-58.

Mackenzie, A.S., Price, I., Leythaeuser, D., Muller, P., Radke, M. & Schaefer, R.G. (1987) The expulsion of petroleum from Kimmeridge Clay source rocks in the area of the Brae Oilfield, UK. In Brooks, J., and Glennie, K. (Eds) Petroleum Geology of North West Europe, Graham & Trotman, London, pp.865-877.

Marshall, D.J. (1988) Cathodoluminescence of geological materials. Chapter 7. pp.76-93. Unwin Hyman, Boston.

Mc Bride, E.F. (1988) Contrasting diagenetic histories of concretions and host rock, Lion Mountain Sandstone (Cambrian), Texas. Geological Society of America Bulletin, v.100. pp.1803-1810.

Moore, C.H. (1989) Carbonate diagenesis and porosity (Chapter 6). Developments in Sedimentology 46. Elsevier. pp.161-175.

Nielson, A.E. (1961) Diffusion controlled growth of a moving sphere. The kinetics of crystal growth in potassium perchlorate precipitation. Journal of Physical Chemistry, 65. pp.46-69.

Oertel, G. & Curtis, C.D. (1972). Clay Ironstone concretion preserving fabrics due to progressive compaction: Geological Society of America Bulletin. v.83, pp.2597-2606.

Pisciotto, K.A. & Mahoney, J.J. (1981) Isotopic survey of diagenetic carbonate, Deep Sea Drilling Project Leg 63, in Initial Reports of the Deep Sea Drilling Project, v.63. pp.595-609.

Raiswell, R. (1971) The growth of Cambrian and Liassic concretions, Sedimentology, v.17. pp.147-171.

Raiswell, R. (1987) Non-steady state microbiological diagenesis and the origin of concretions and nodular limestones. Diagenesis of Sedimentary Sequences (J.D. Marshall, ed.) Geological Society of London Special Publication 36. pp.41-54.

Reitsema, R.H. (1980) Dolomite and nahcolite formation in organic rich sediments: Isotopically heavy carbonates, Geochimica et Cosmochimica Acta, v.44, pp.2045-2049.

Reitsema, R.H. (1983) Geochemistry of North and South Brae areas, North Sea. In Brooks, J.(ed) Petroleum geochemistry and exploration of Europe. Geological Society of London. Special Publication 12. pp.203-212.

Schwarkzkopf, T.A. (1990) Relationship between petroleum generation, migration and sandstone diagenesis, Middle Jurassic, Gifhorn Trough, Germany. Marine and Petroleum Geology. v.7. pp.153-170.

Shackleton, N.J. & Kennett, J.P. (1975) Paleotemperature history of the Cenezoic and the initiation of Antartic glaciation: Oxygen and carbon analyses in DSDP sites 277, 279,281. In Kennett, J.P. and Howtz, R.E. (eds) Initial Report DSDP 24, Washington. pp.653-659.

Smith J.M. (1978) Carbonates - a guide to hydrocarbons. Journal of Geochemical Exploration, v. 10, pp.103-107.

Steuber, A.M., Pushkar, P. & Hetherington, E.A. (1984) A strontium isotopic study of Smackover Brines and associated solids, Southern Arkansas. Geochimica et Cosmochimica Acta. v.48. pp.1637-1649.

Stow, D.A.V., Bishop, C.D. & Mills, S.J. (1982) Sedimentology of the Brae oilfield, North Sea. Fan models and controls. Journal of Petroleum Geology. v.5, No.2, pp.129-148.

Thyne, G.D. & J.R. Boles. (1989) Isotopic evidence for origin of the Moeraki Septarian Concretions, New Zealand. Journal of Sedimentary Petrology. v.59. No.2. pp.272-279.

Turner, C.C., Cohen, J.M., Connell, E.R. & Cooper, D.M. (1987) A depositional model for the South Brae oilfield, In Brooks, J., and Glennie,

K. (Eds) Petroleum Geology of North West Europe, Graham & Trotman, London,pp.853-864.

Urey, H.C. (1947) The thermodynamic properties of isotopic substances. Journal of the Chemistry Society. pp.562-581.

Veizer, J., Holser, W.T. & Wilgus, C.K. (1980) Correlation of $^{13}C/^{12}C$ and $^{34}S/^{32}S$ and Secular Variations. Geochimica et Cosmochimica Acta. v.44, pp.579-589.

Veizer, J. (1983) Chemical diagenesis of carbonates- theory and application of trace element technique, in M.A. Arthur, T.F. Anderson, I.R. Kaplan, J. Veizer & L.S. Land, eds., Stable isotopes in sedimentary geology, S.E.P.M. Short Course 10, p.3-1-3-100.

Wilkinson, M. & Dampier, M.D. (1990) The rate of growth of sandstone hosted calcite concretions. Geochimica et Cosmochimica Acta. 54. pp.3391-3399.

Wilkinson, M. (1991) The concretions of the Bearreraig Sandstone Formation: geometry and geochemistry. Sedimentology, v.38. pp.899-912.

Ziegler, P.A. (1978) North-Western Europe: tectonics and basin development. Geologie Mijnbouw, v.57. pp.589-626.

2.15 TABLES

Table 2.1. Data used to calculate a compaction curve for the South Brae reservoir applying a geothermal gradient of 30°C/km. The equation used to calculate the burial depths for precipitation is taken from Baldwin & Butler 1985, Burial depth (kms) = 3.7ln (0.49/1-S)

Well no.	Depth T.V.D. (ft)	Minus Cement Porosity%	Solidity%	Calculated Burial (km)	Temperature °C
16/7a-A6	13412'	37.4	62.6	0.99	30
	13415'	44.4	55.6	0.36	11
	13419'	38.6	61.4	0.88	26.5
	13422'8"	23.8	76.2	2.75	82.5
16/7a-A11	13694'	28.2	71.8	2.04	61
	13702'4"	34.2	65.8	1.33	40
	13703'5"	32	68	1.57	47
	13707'9"	29.5	70.5	1.87	56
	13776'	38.2	61.8	0.92	27.5
	13778'	41.4	58.6	0.62	19
	13778'6"	35.8	64.2	1.16	35
16/7b-A19	13501'	32.4	67.6	1.53	46
	13501'5"	33.6	66.4	1.39	42
	13502'8"	31.2	68.8	1.67	50
	13504'	30	70	1.82	54.5
	13504'1"	27.6	72.4	2.12	64
	13506'	18.5	81.5	3.60	108
16/7a-A27	13526'	21.8	78.2	3.00	90
	13535'	28.8	71.2	1.97	59
	13536'	37.4	61.6	1.00	30
	13538'	26	74	2.34	70

Table 2.2. Summary of $\delta^{13}C$ and $\delta^{18}O$ values for calcite cements and shells from the Brae Formation in the South Brae Oilfield. (± values quoted for samples encompass range of replicate analysis)

Well no.	Depth TVD (ft)	$\delta^{13}C$ (‰ PDB)	$\delta^{18}O$ (‰PDB)	$\delta^{18}O$ (‰SMOW)	Type of cement
16/7a-A6	12997'9"	-9.5±.07	-7.36±.6	23.31±.62	Early
	12999'5"	-9.81	-6.45	24.26	Early
	13412'	-9.02	-9.86	20.74	Early
	13415'	+3.62±.04	-7.32±.03	23.36±.03	Early
	13419'	-.54±.24	-9.95±.46	20.64±.47	Early
	13422'8"	-9.92±.2	-13.06±.16	17.45±.15	Mix
	13462'3"	-10.59±.4	-14.55±.42	15.91±.44	Late
16/7a-A11	12712'6"	-9.50	-11.93	18.67	Mix
	13422'	-6.64	-6.28	24.44	Shell
	13632'	-10.10±.08	-15.24±.02	15.19±.02	Late
	13694'	-10.76±.01	-9.27±.05	21.36±.05	Early
	13702'4"	-9.26±.01	-7.82±.05	22.85±.05	Early
	13703'5"	-1.75	-8.80±..04	21.84±.04	Early
	13707'9"	-8.91±.4	-8.14±.50	22.01±.51	Early
	13719'	-7.97	-12.19	18.34	Mix
	13776'	-10.45±.01	-9.76±.01	20.85±.01	Early
	13778'	-5.65	-9.04±.11	21.17±.31	Early
	13778'6"	-10.52	-10.07	20.53	Early

Table 2. 2. continued

Well no.	Depth TVD (ft)	$\delta^{13}C$ (‰ PDB)	$\delta^{18}O$ (‰PDB)	$\delta^{18}O$ (‰SMOW)	Type of cement
16/7b-A19	13501'	-10.96	-10.89	19.68	Early
	13501'5"	-10.47	-11.95	18.60	Early
	13502'	-11.24	-13.04	17.47	Early
	13502'8"	-9.45	-15.52	14.91	Mix
	13504'	-10.79	-15.55	14.88	Mix
	13504'1"	-11.66	-15.08	15.36	Mix
	13506'	-10.53	-14..56	15.90	Mix
	13506'8"	-7.83±.25	-14.96±.01	15.48±.01	Mix
	13688'6"	-6.03	-12.03	18.51	Early
16/7a-A27	12904'	-11.03	-11.00	19.56	Shell
	13526'	-6.96	-15.26	15.20	Late
	13535'	-6.10	-10.45	20.13	Early
	13536'	-8.70	-10.90	19.67	Early
	13538'	-1.69	-9.72	20.89	Early
	13540'	-7.80	-8.37	22.28	Early

Table 2.3. Summary of strontium and rubidium values for calcite cements and shells from the Brae Formation in the South Brae Oilfield.

Well no.	Depth TVD (ft)	Rb (ppm)	Sr (ppm)	$^{87}Rb/^{86}Sr$	$(^{87}Sr/^{86}Sr)_{140}$
Calcite Cements					
16/7a - A6	†13412'	2.02	137.0	0.0428	0.71410±3
	†13415'	2.37	393.6	0.0175	0.71052±4
	†13419'	2.65	594.6	0.0129	0.71024±4
	†13422'	-	97.0	-	0.71368±21*
16/7a - A27	13526'	1.84	402.7	0.0132	0.72320±4
	†13536'	4.11	168.9	0.0704	0.71350±4
	†13538'	3.97	346.0	0.0332	0.71090±3
	†13540'	2.09	72.4	0.0834	0.71234±4
16/7a - A11	12712'6"	2.44	345.4	0.0204	0.71055±4
	13632'	6.43	77.9	0.2391	0.72120±3
	†13702'4"	2.07	68.9	0.0868	0.71166±4
	†13703'5"	1.46	229.4	0.0184	0.71101±4
	†13707'9"	5.4	203.4	0.0769	0.71295±4
	13719'	1.22	368.3	0.0095	0.71102±4
	†13776'	2.24	219.3	0.0295	0.71206±4
	†13778'	0.28	18.1	0.0454	0.71186±4
	†13778'6"	2.76	203.4	0.0393	0.71218±4

Table 2.3. continued.

Well no.	Depth TVD (ft)	Rb (ppm)	Sr (ppm)	$^{87}Rb/^{86}Sr$	$(^{87}Sr/^{86}Sr)_{140}$
16/7b - A19	†13500'	0.75	228.9	0.0094	0.71439±4
	†13501'	5.82	111.7	0.0728	0.71110±4
	†13501'5"	2.3	194.9	0.034	0.71083±4
	†13502'	0.0	235.7	0.0073	0.71077±5
	†13502'8"	2.52	192.9	0.0378	0.71075±4
	†13504'	3.85	192.9	0.0706	0.71098±6
	†13504'1"	1.23	203.0	0.0176	0.71090±8
	†13506'	6.85	108.7	0.1824	0.71400±7
	†13506'8"	1.22	262.5	0.0135	0.72044±3
	13688'6"	12.42	464.8	0.0774	0.71120±4
Shells					
16/7a - A27	12904'	1.06	1230.0	0.0025	0.70719±4
16/7a - A11	13422'	1.3	180.9	0.0208	0.70833±5

† Indicates concretion samples

* We have used the measured value as the initial ratio in the absence of Rb analyses

Note: All strontium isotope ratios have been corrected for rubidium decay over 140Ma.

Table 2.4. Summary of microprobe analyses for calcite cemented concretions from the Brae Formation in the South Brae Oilfield.

Well no.	Depth TVD (ft)	Ca (mol%)	Fe (mol%)	Mn (mol%)	Mg (mol%)
16/7a - A6	13412'	99.09	0.09	0.62	0.20
	13415'	96.47	2.43	0.54	0.56
	13419'	95.76	3.17	0.14	0.93
	13422'8"	99.32	0.18	0.28	0.22
16/7a - A11	13694'	98.94	0.05	0.69	0.32
	13702'	99.03	0.25	0.42	0.30
	13703'5"	98.48	0.60	0.56	0.36
	13707'4"	98.78	0.17	0.63	0.42
16/7a - A11	13776'	98.76	0.34	0.58	0.32
	13778'	98.03	0.81	0.76	0.40
	13778'6"	98.81	0.28	0.57	0.34
16/7a - A27	13531'	99.17	0.19	0.32	0.32
	13535'	99.27	0.24	0.22	0.27
	13536'	99.04	0.16	0.34	0.46
	13538'	99.06	0.15	0.20	0.59

2.16 FIGURE CAPTIONS & FIGURES

Figure 2.1 Location of Brae relative to major tectonic elements. The shaded areas contain thick Jurassic deposits (after Ziegler, 1978).

Figure 2.2 Schematic cross section showing approximate position of the wells sampled in the South Brae area.

Figure 2.3 Paragenetic sequence showing timing of major diagenetic events in the South Brae oilfield

Figure 2.4a-d Vertical porosity trends for wells 16/7a-A3, A6, A11, A27 & 16/7b-A19 showing overall decline with depth - controlled mainly by facies. Porosity data is from an internal Marathon report and is summarised in Chapter 4 (Table 4.4).

Figure 2.5 South Brae core photograph showing a conglomerate with a coarse grained sandy matrix, calcite cemented to the right and quartz cemented to the left 16/7a-A27, 13535' (T.V.D.). Scale on core is 2cm.

Figure 2.6a Cathodoluminescence photomicrograph of (Early I) ferroan dull luminescent concretionary calcite cement with a vein of a brighter cement (Early II). The feldspars have been dissolved to a minor extent and the detrital quartz grains remain unetched 16/7a-A6, 13419' (T.V.D.).

Figure 2.6b Cathodoluminescence photomicrograph of (Early II) non ferroan brightly luminescent concretionary calcite cement. The feldspar and quartz grains have been subjected to more leaching 16/7a-A6, 13412' (T.V.D.).

Figure 2.6c Cathodoluminescence photomicrograph of brightly luminescent late calcite cement. The calcite cement infills ex-feldspar sites, some quartz overgrowths and secondary porosity are evident 16/7a-A6 13462'3" (T.V.D.). Compare this texture with those of 2.6a & b.

Figure 2.7 Cathodoluminescence photomicrograph of early brightly luminescent patchy calcite cement in laminated fine grained sandstone; a lot of feldspar is still evident 16/7b-A19, 13688'6" (T.V.D.).

Figure 2.8 Crossed polars photomicrograph of poikilotopic calcite cement also displaying the effects of early dissolution on detrital quartz grains 16/7b-A19, 13501'(T.V.D.).

Figure 2.9 Cathodoluminescence photomicrograph showing calcite replacement of a dissolved coral fragment and feldspar grains (remnants are bright blue). The cement replacing the feldspar is a slightly darker orange than the main body of cement 16/7a-A11, 13776' (T.V.D.).

Figure 2.10 Back scatter image with false colour superimposed to highlight secondary porosity development at the top of a concretion 16/7a-A19, 13501' (T.V.D.). Quartz = Green, Calcite = Red, Pyrite = Yellow & Secondary Porosity = Purple.

Figure 2.11 Minus cement porosity data for concretions in wells 16/7a-A6, A11, A27 & 16/7b-A19 showing decreasing cement volumes and increasing compaction towards the concretion margins.

Figure 2.12 Cathodoluminescence photomicrograph of late fractures cross cutting detrital quartz grains and concretionary calcite cement. The cement infilling the fractures is brightly luminescent calcite 16/7a-A11, 13694' (T.V.D.).

Figure 2.13 Cathodoluminescence photomicrograph of late calcite cement infilling ex-feldspar sites 16/7a-A6, 13462'3" (T.V.D.).

Figure 2.14 Cathodoluminescence photomicrograph of late calcite cement infilling ex-feldspar sites and a late zoned rhomb of dolomite 16/7a-A6, 13462'3" (T.V.D.).

Figure 2.15 Cathodoluminescence photomicrograph of (Early I) dully luminescent cement in the centre of a concretion, bright orange cement occurs where feldspar grains have been replaced 16/7a-A6, 13419' (T.V.D.).

Figure 2.16 Cathodoluminescence photomicrograph of leached mica and feldspar replaced by (Early II) brightly luminescent orange cement in (Early I) dully luminescent cement 16/7a-A6, 13415' (T.V.D.).

Figure 2.17 Cathodoluminescence photomicrograph of woody material within a concretion. Plant material is quite commonly found in South Brae reservoir rocks 16/7a-A11, 13778'6" (T.V.D.).

Figure 2.18 Cathodoluminescence photomicrograph of increased compaction showing more grain to grain contact and fractured detrital grains, and also increased leaching of feldspar at concretion edge 16/7a-A11, 13694' (T.V.D.).

Figure 2.19 Brightly luminescent orange bioclast of dolomite in calcite cemented concretion 16/7b-A19, 13504' (T.V.D.).

Figure 2.20 Compaction curve for South Brae concretions from wells 16/7a-A6, A11, A27 & 16/7b-A19. Individual points in the concretions are given in feet and metres (T.V.D.) in Table 2.1.The Minus Cement Porosity (=1/solidity) where, S (solidity) is the volume of solid grains as a percent of total volume of sediment, was measured by

point counting for each concretionary sample. The depths of calcite precipitation were then calculated using empirically-derived compaction curves (Baldwin & Butler, 1985). Burial depth (kms) = 3.71n (0.49/(1-S)). By applying a geothermal gradient of 30°C/km (suitable for this reservoir), approximate temperatures of cementation were then calculated.

Figure 2.21 Carbon dioxide production within different diagenetic zones (after Irwin et al. 1977). Each depth process has a characteristic carbon isotope signature.

Figure 2.22 $\delta^{13}C$ values for the concretions of South Brae, exhibiting a spatial trend of more depleted $\delta^{13}C$ values towards the margins.

Figure 2.23 Cathodoluminescence photomicrograph of recrystallized brachiopod shell 16/7a-A27, 12904' (T.V.D.).

Figure 2.24 Distinct $\delta^{18}O$(SMOW) populations for early, mixed and late South Brae calcite cements. $\delta^{13}C$ values overlap suggesting similar organic sources.

Figure 2.25 Calcite $\delta^{18}O$ versus temperature and $\delta^{18}O$ porewater for South Brae concretions. The temperature range for calcite cements is illustrated for waters

a) $\delta^{18}O$=-1.2‰ (SMOW)

b)$\delta^{18}O$=-7.0‰ (SMOW)

The meteoric water interpretation is preferred. The isotopic fractionation equation used to derive these curves was determined by Friedman & O'Neil (1977).

Figure 2.26 Plot of $^{87}Sr/^{86}Sr$ values for Brae calcites versus $^{87}Sr/^{86}Sr$ of Upper Jurassic seawater (isotope values for seawater are from Burke et al. 1982) The calcites contain

strontium variably more radiogenic than Upper Jurassic seawater.

Figure 2.27 Systematic spatial distribution of $^{87}Sr/^{86}Sr$ in the South Brae concretions showing increasing enrichment in $^{87}Sr/^{86}Sr$ concurrent to growth.

Figure 2.28 Concretion centres showing higher strontium concentrations due to shell dissolution and less input from the radiogenic silicates.

Figure 2.29 $^{87}Sr/^{86}Sr$ versus $\delta^{13}C$ for South Brae concretions. With continued growth more radiogenic strontium has been taken in by the calcite cements.

Figure 2.30 Concretion centres 16/7a-A6, A11 & A27 have the highest wt% Fe and consequently are dully luminescent.

Figure 2.31 Burial curve for the Brae Formation (Oxfordian) in the South Brae field. The reconstructed burial curve is based on well 16/7a-8, using present day rock thicknesses. The burial curve has been decompacted and backstripped.

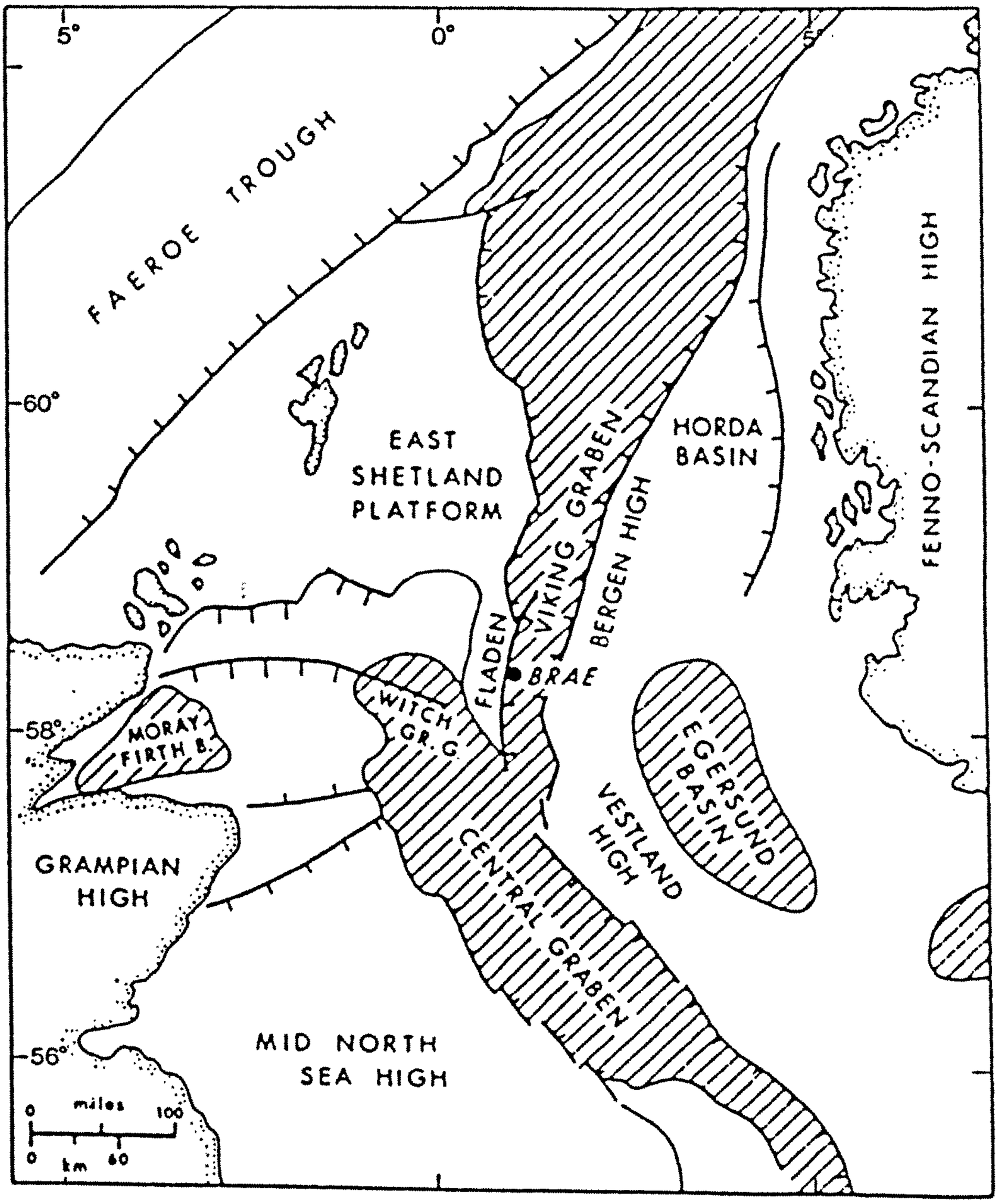
5°
0°
5°
60°
58°
56°
FAEROE TROUGH
EAST SHETLAND PLATFORM
VIKING GRABEN
BERGEN HIGH
HORDA BASIN
FENNO-SCANDIAN HIGH
FLADEN
BRAE
WITCH GR.
MORAY FIRTH B.
GRAMPIAN HIGH
CENTRAL GRABEN
VESTLAND HIGH
EGERSUND BASIN
MID NORTH SEA HIGH
0 miles 100
0 km 60

Figure 2.1.

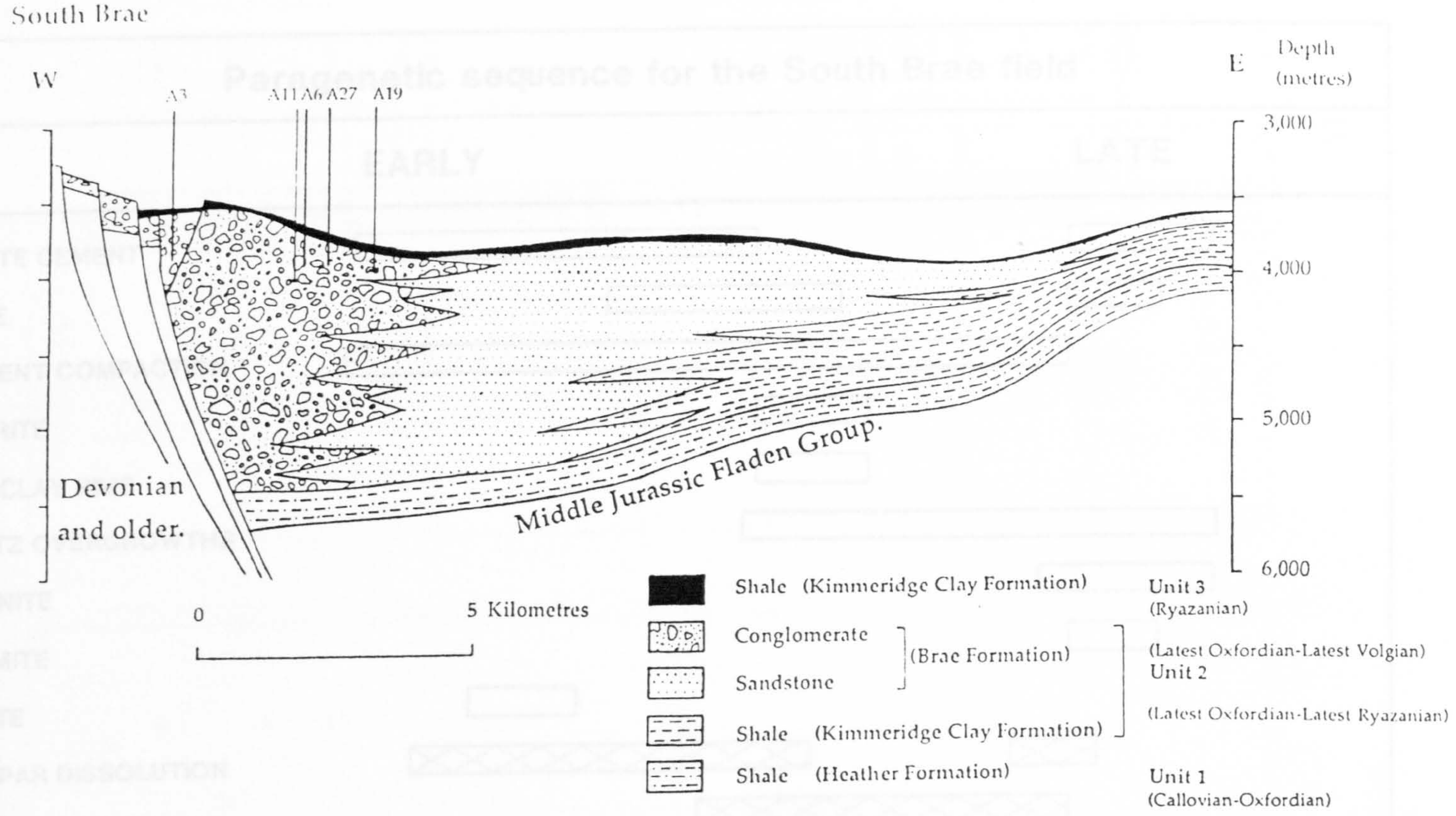
South Brae
W
E
Depth (metres)
A3
A11
A6
A27
A19
3,000
4,000
5,000
6,000
Devonian and older.
Middle Jurassic Fladen Group.
0
5 Kilometres
Shale (Kimmeridge Clay Formation)
Unit 3
(Ryazanian)
Conglomerate
(Brae Formation)
(Latest Oxfordian-Latest Volgian)
Unit 2
Sandstone
(Latest Oxfordian-Latest Ryazanian)
Shale (Kimmeridge Clay Formation)
Shale (Heather Formation)
Unit 1
(Callovian-Oxfordian)

Figure 2.2.

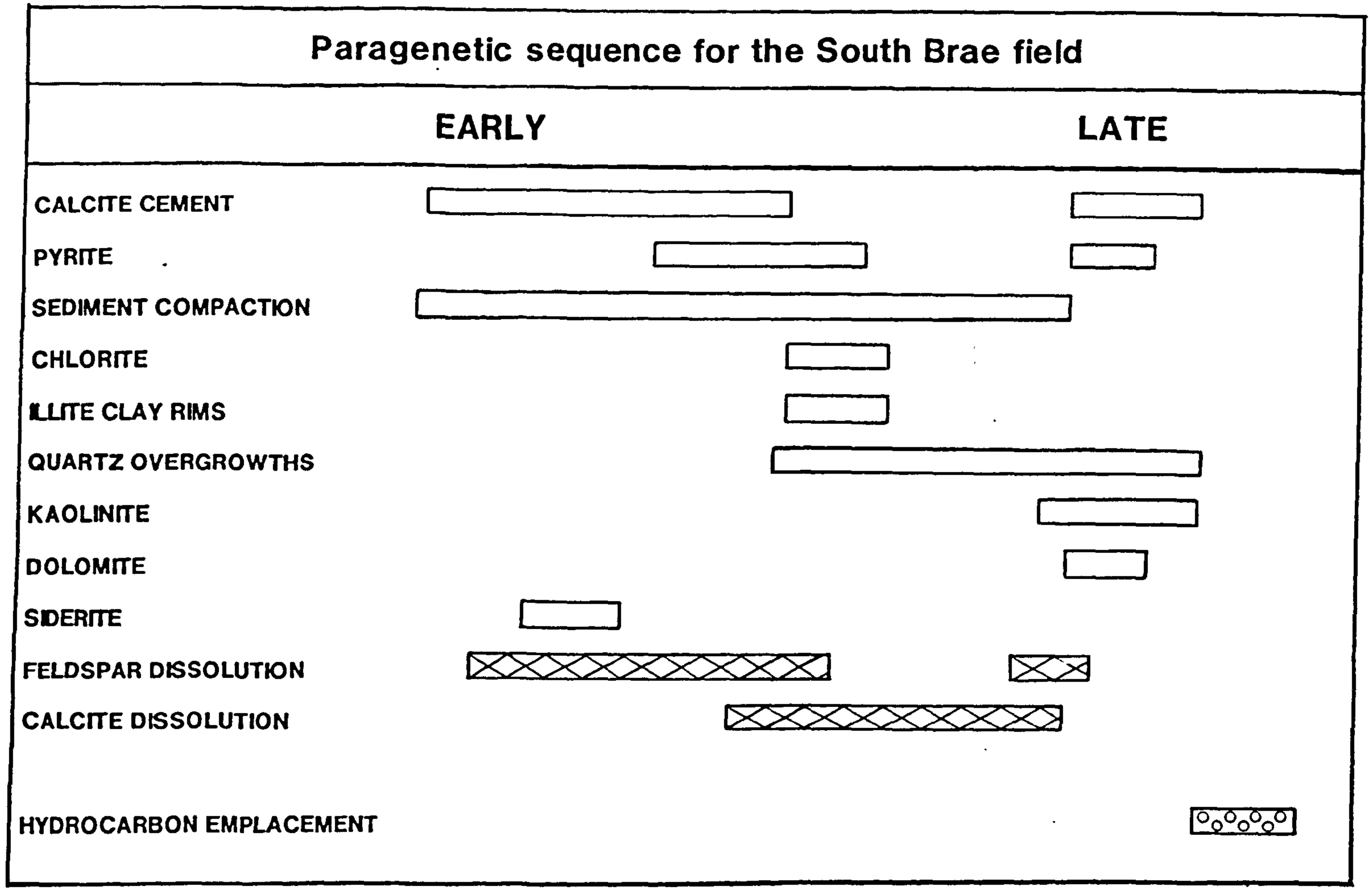
Paragenetic sequence for the South Brae field
EARLY
LATE
CALCITE CEMENT
PYRITE
SEDIMENT COMPACTION
CHLORITE
ILLITE CLAY RIMS
QUARTZ OVERGROWTHS
KAOLINITE
DOLOMITE
SIDERITE
FELDSPAR DISSOLUTION
CALCITE DISSOLUTION
HYDROCARBON EMPLACEMENT

Figure 2.3.

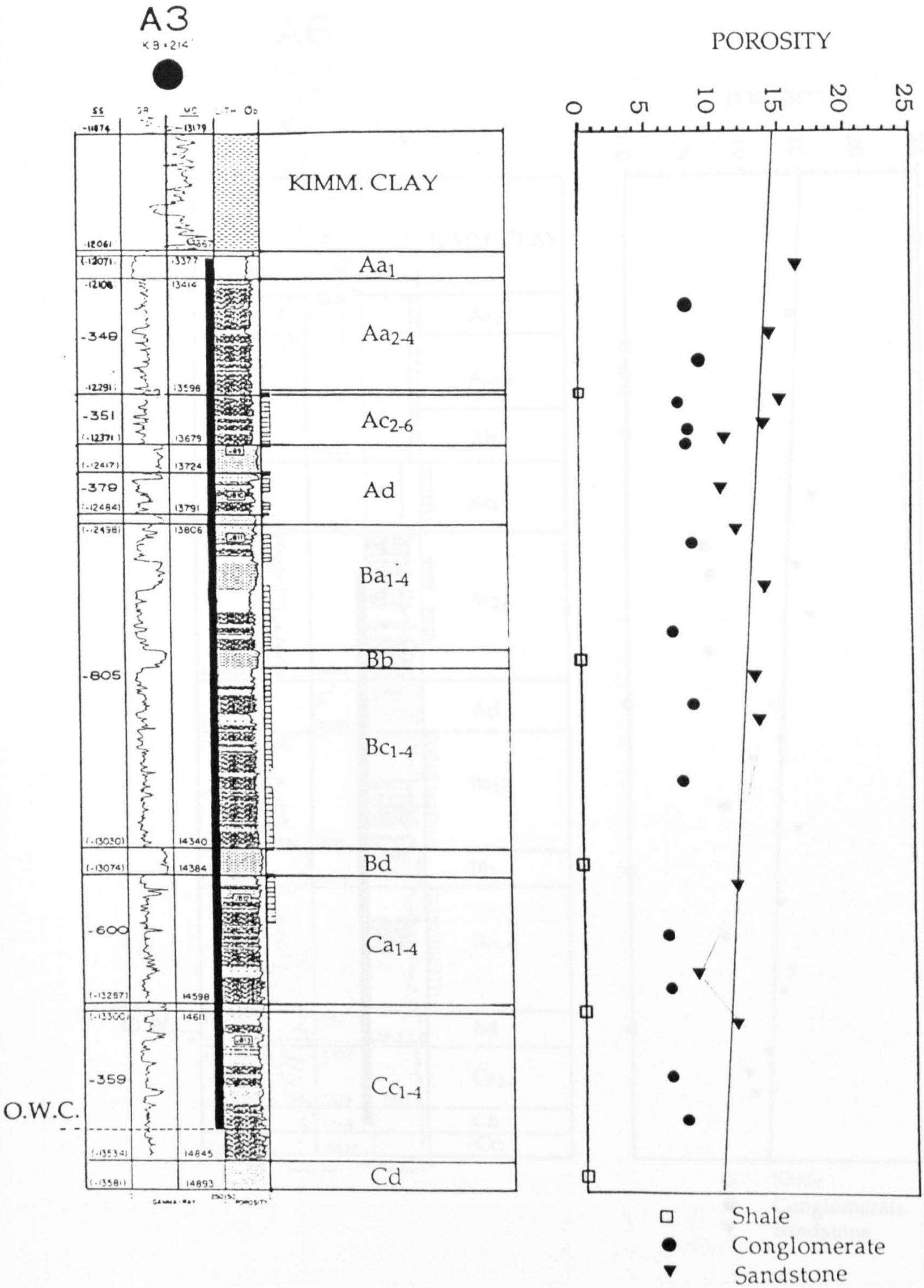
A3
KB = 214'
SS
-11874
SP
MS
-13179
Oo
-12061
(-12071)
-12108
-348
-12291)
-351
(-12371)
(-12417)
-378
(-12484)
(-12498)
-805
(-13030)
(-13074)
-600
(-13287)
(-13300)
-359
O.W.C.
(-13534)
(-13581)
13377
13414
13598
13679
13724
13791
13866
14340
14384
14598
14611
14845
14893
KIMM. CLAY
Aa1
Aa2-4
Ac2-6
Ad
Ba1-4
Bb
Bc1-4
Bd
Ca1-4
Cc1-4
Cd
GAMMA-RAY
POROSITY
0
5
10
15
20
25
Shale
Conglomerate
Sandstone

Figure 2.4a.

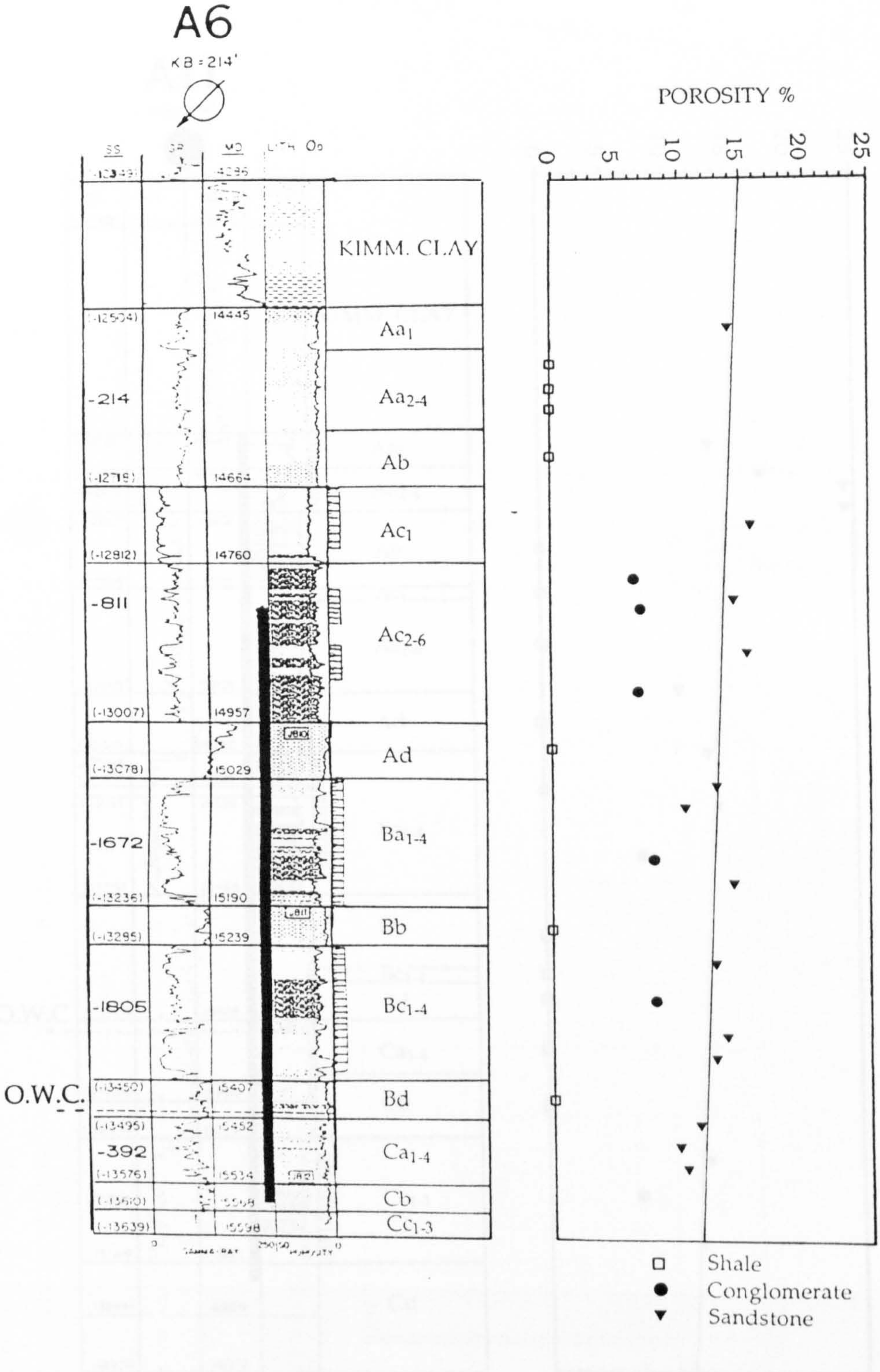
A6
KB = 214'
SS
VD
-12948
4086
KIMM. CLAY
(-12504)
14445
Aa1
-214
Aa2-4
(-12718)
14664
Ab
(-12812)
14760
Ac1
-811
Ac2-6
(-13007)
14957
(-13078)
15029
Ad
-1672
Ba1-4
(-13236)
15190
(-13285)
15239
Bb
-1805
Bc1-4
O.W.C.
(-13450)
15407
Bd
(-13495)
15452
-392
Ca1-4
(-13576)
15534
Cb
(-13610)
15598
Cc1-3
(-13639)
POROSITY %
0
5
10
15
20
25
Shale
Conglomerate
Sandstone

Figure 2.4b.

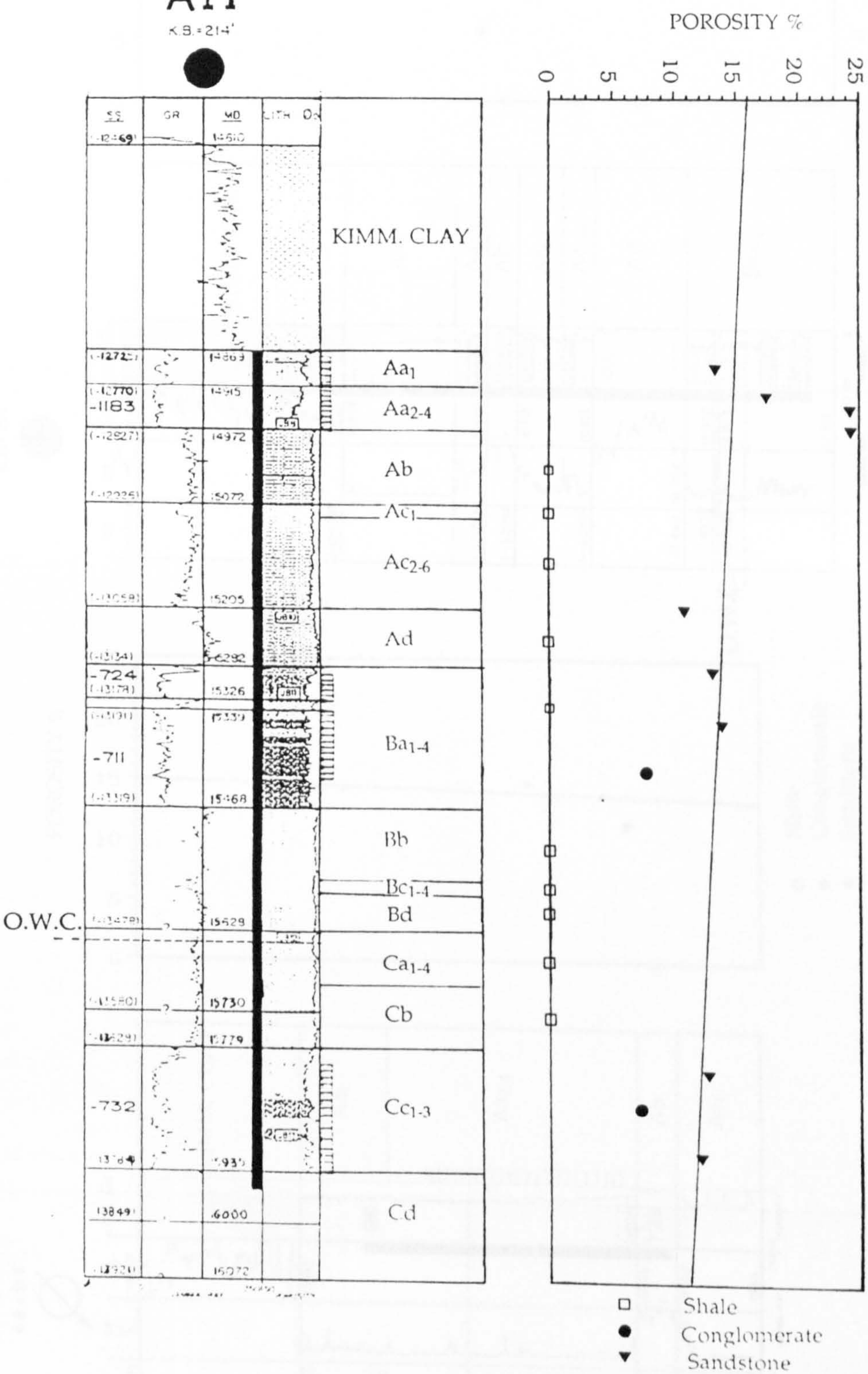
A11
K.B.=214'
SS
GR
MD
LITH
POROSITY %
0
5
10
15
20
25
KIMM. CLAY
Aa1
Aa2-4
Ab
Ac1
Ac2-6
Ad
Ba1-4
Bb
Bc1-4
Bd
Ca1-4
Cb
Cc1-3
Cd
O.W.C.
-1183
-724
-711
-732
Shale
Conglomerate
Sandstone

Figure 2.4c.

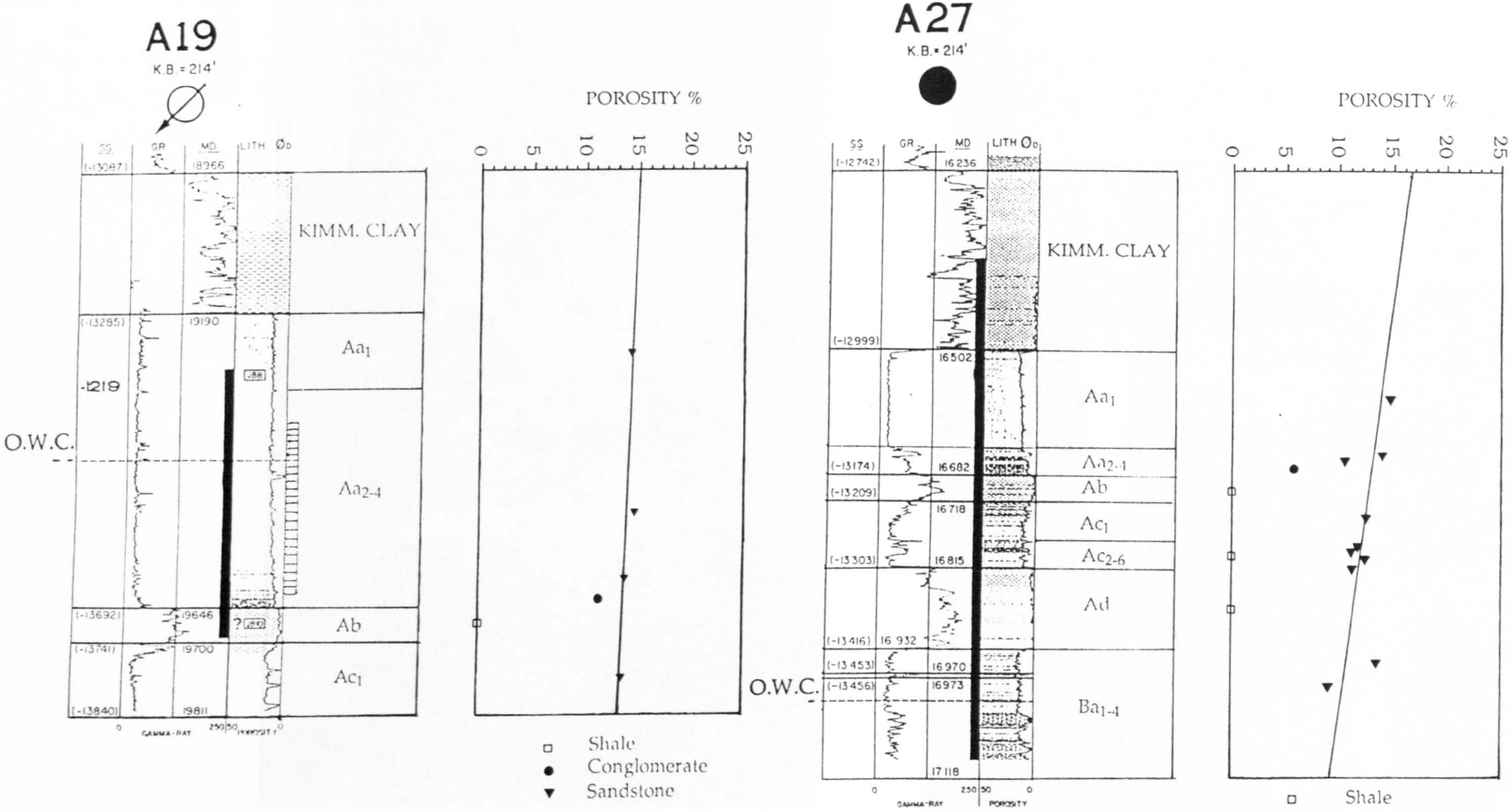
A19
K.B. = 214'
SS
GR
MD
LITH Ø
(-13087)
18266
KIMM. CLAY
(-13285)
19190
Aa1
-1219
O.W.C.
Aa2-4
(-13692)
19646
Ab
(-13741)
19700
Ac1
(-13840)
19811
0
GAMMA-RAY
250
50
POROSITY
0
POROSITY %
0
5
10
15
20
25
Shale
Conglomerate
Sandstone
A27
K.B. = 214'
SS
GR
MD
LITH Ø
(-12742)
16236
KIMM. CLAY
(-12999)
16502
Aa1
(-13174)
16682
Aa2-4
(-13209)
Ab
16718
Ac1
(-13303)
16815
Ac2-6
Ad
(-13416)
16 932
(-13453)
16970
O.W.C.
(-13456)
16973
Ba1-4
17118
0
GAMMA-RAY
250
50
0
POROSITY
POROSITY %
0
5
10
15
20
25
Shale
Conglomerate
Sandstone

Figure 2.4d.

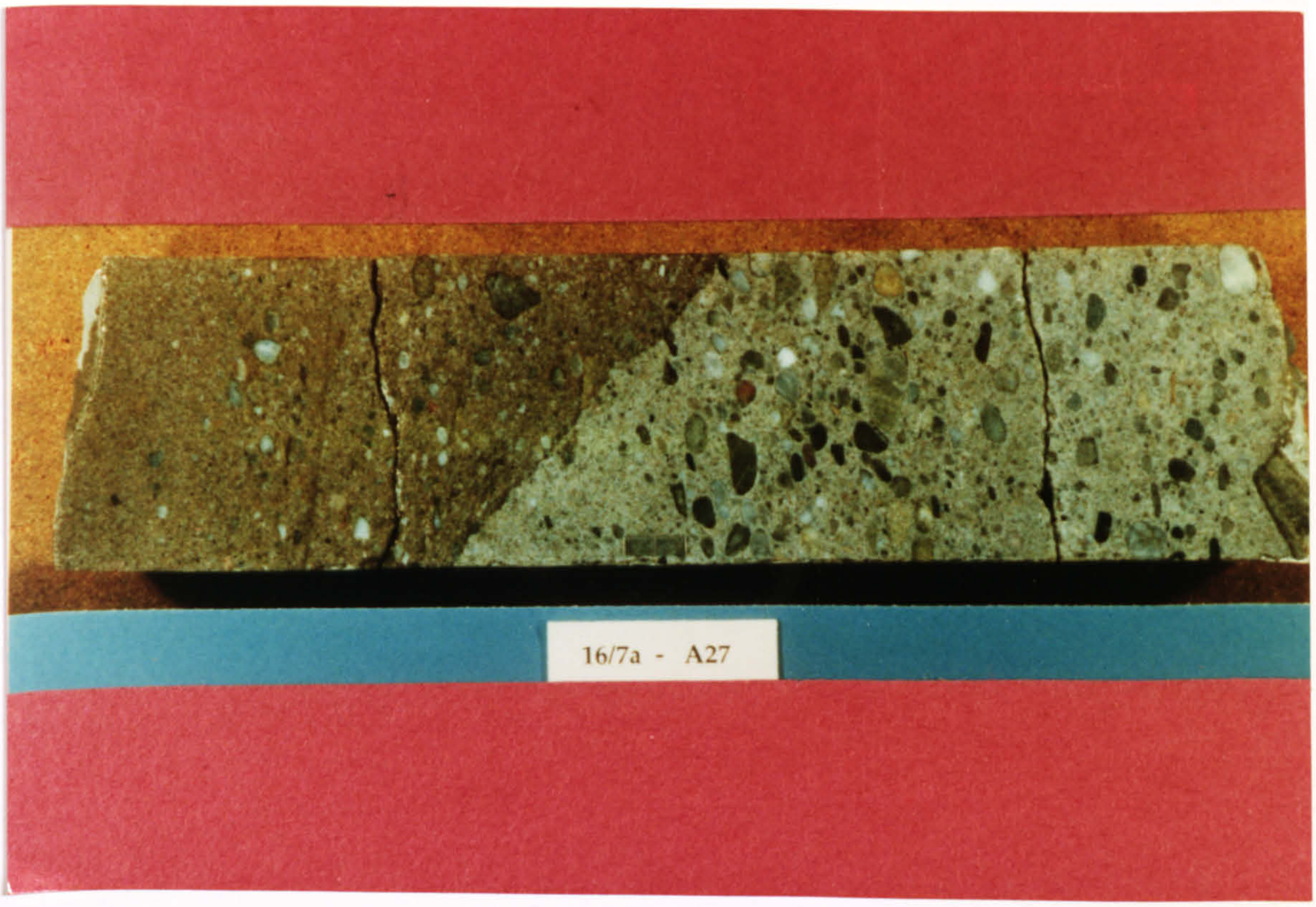

Figure 2.5.

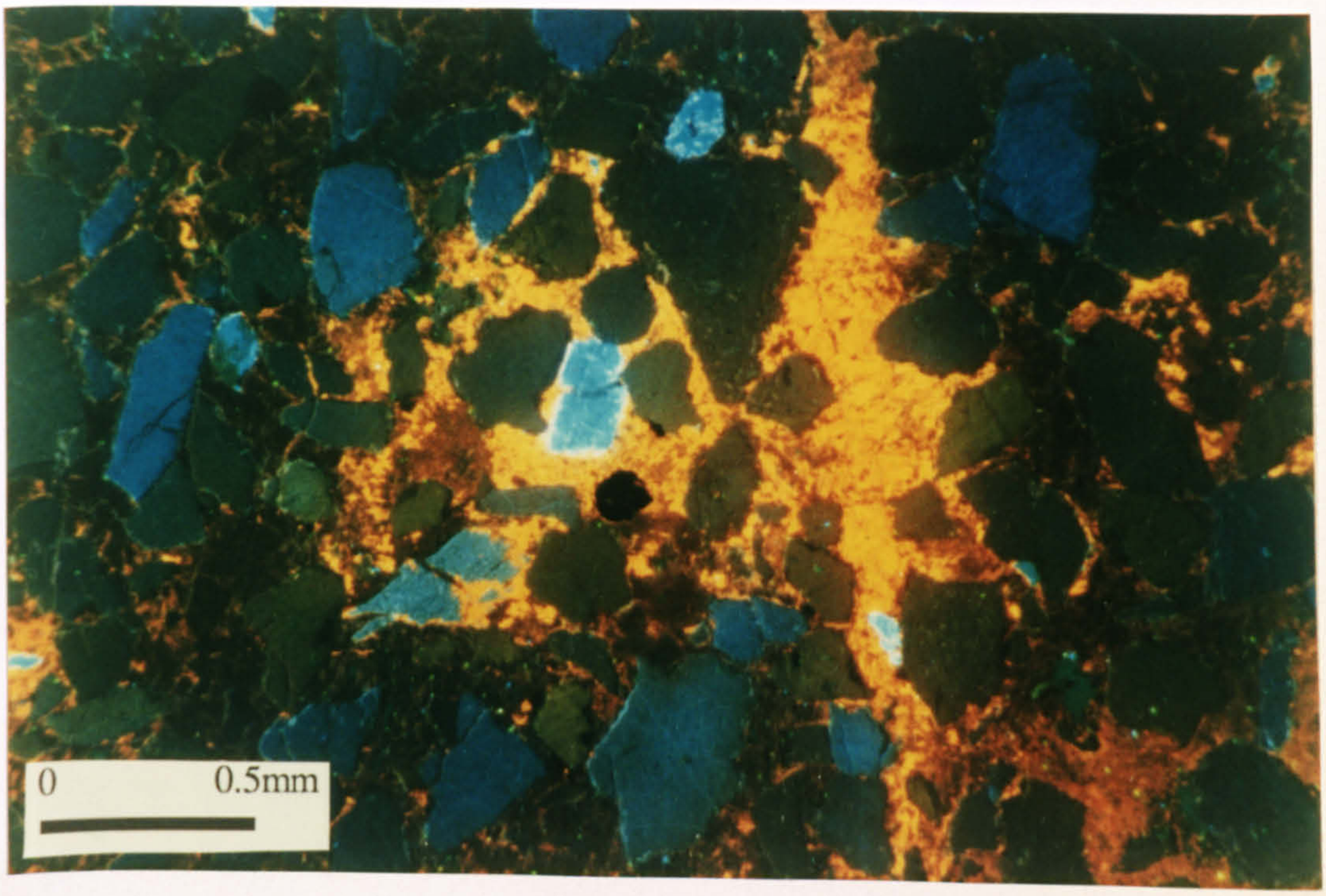

Figure 2.6a.

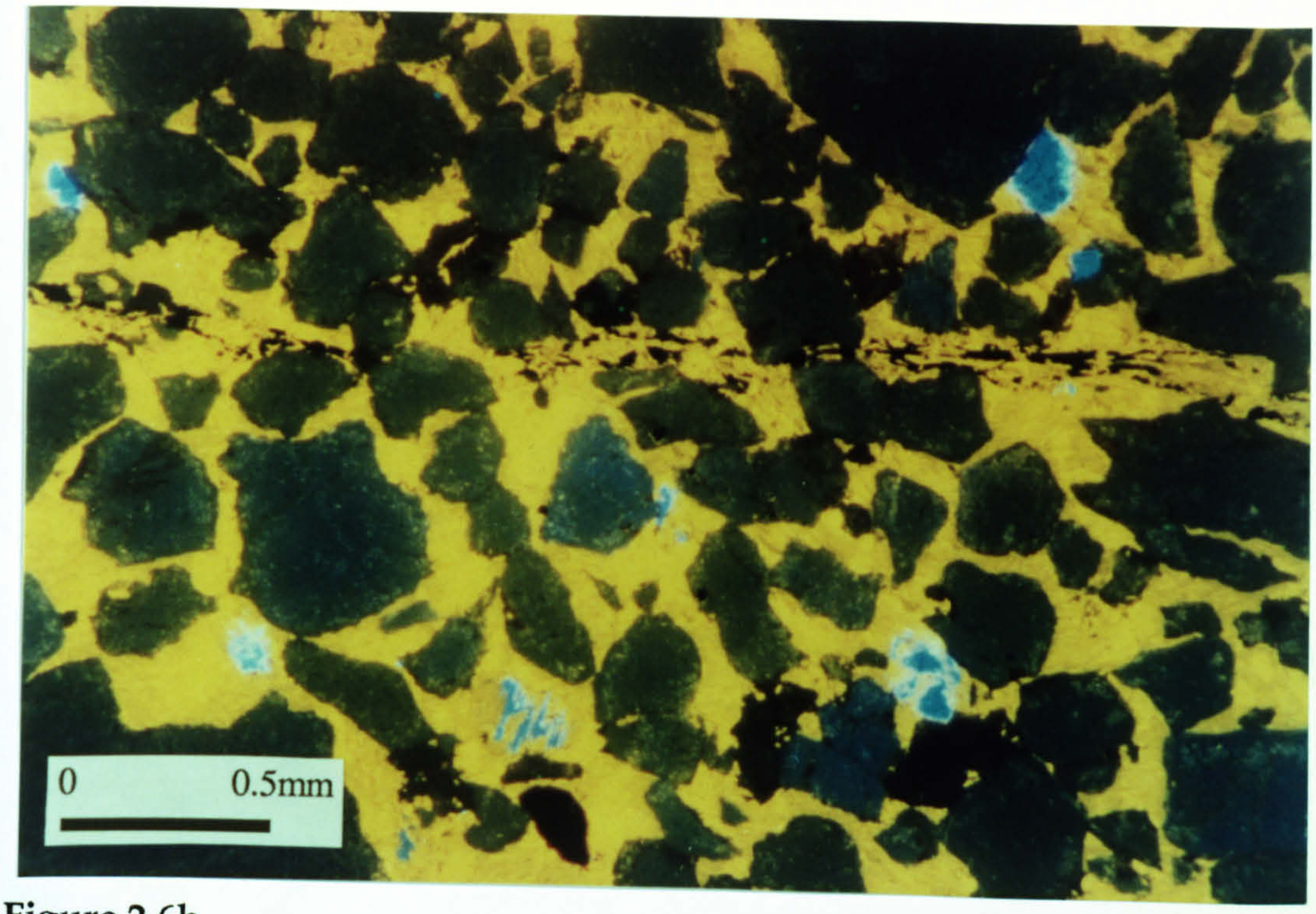

Figure 2.6b.

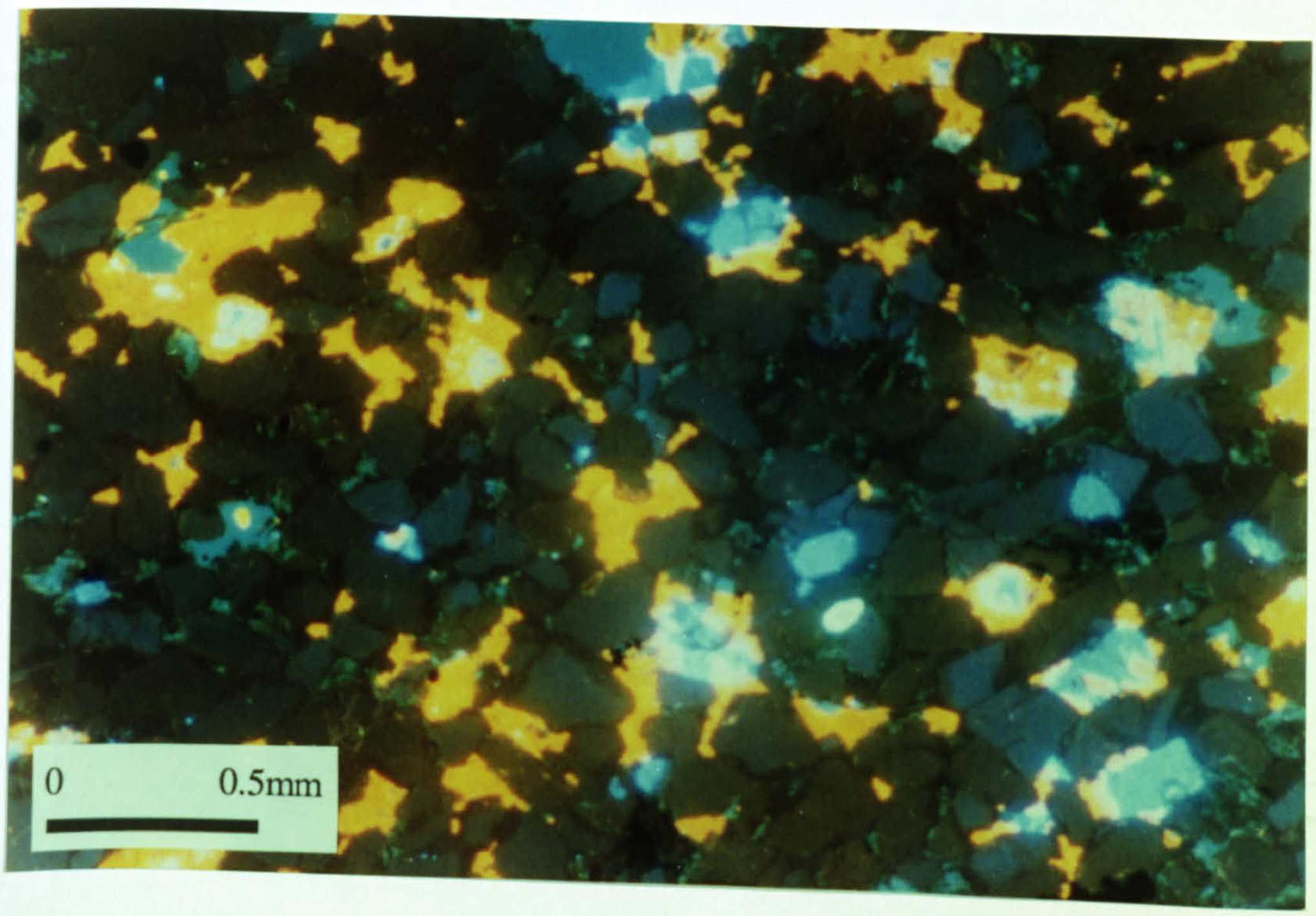

Figure 2.6c.

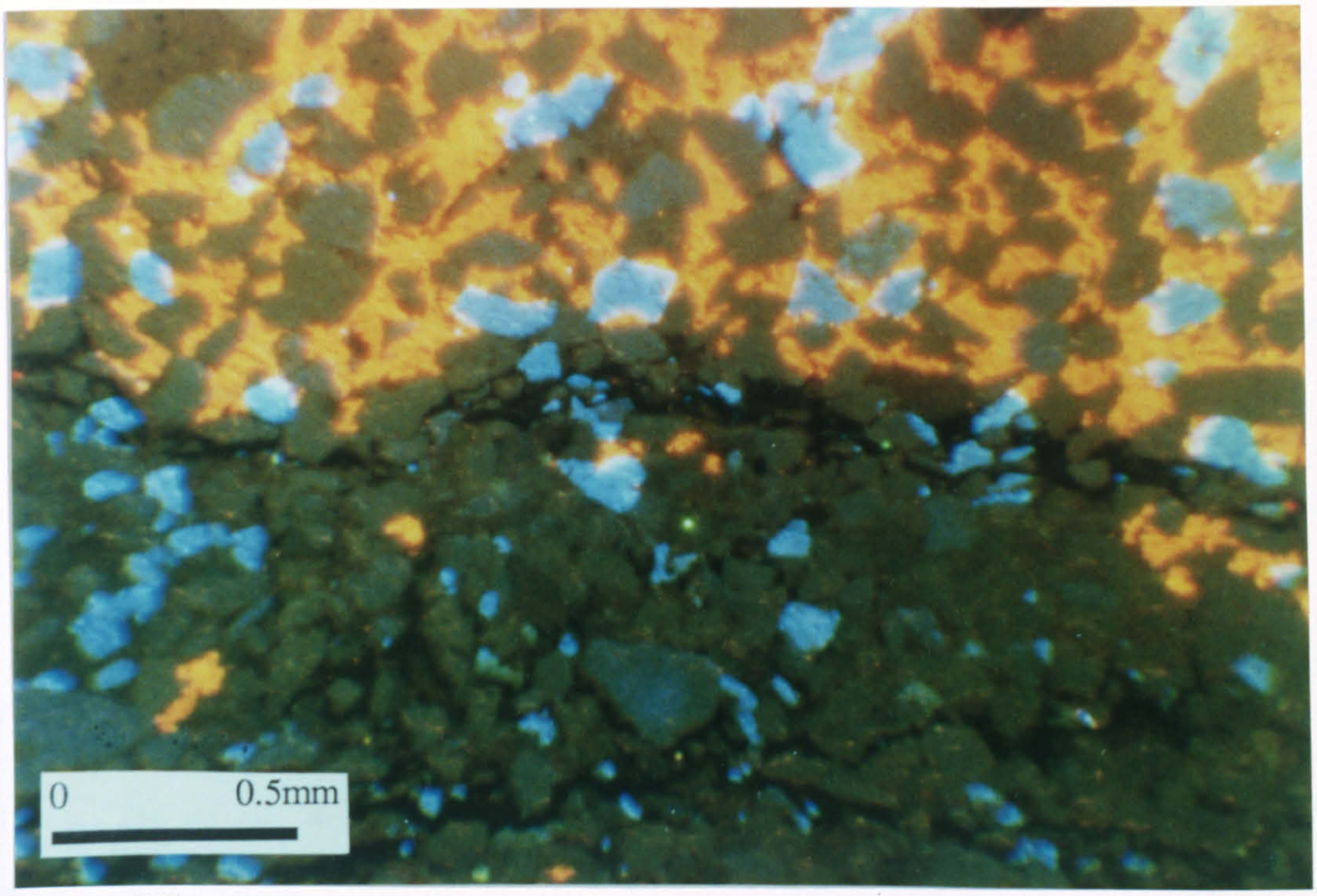

Figure 2.7.

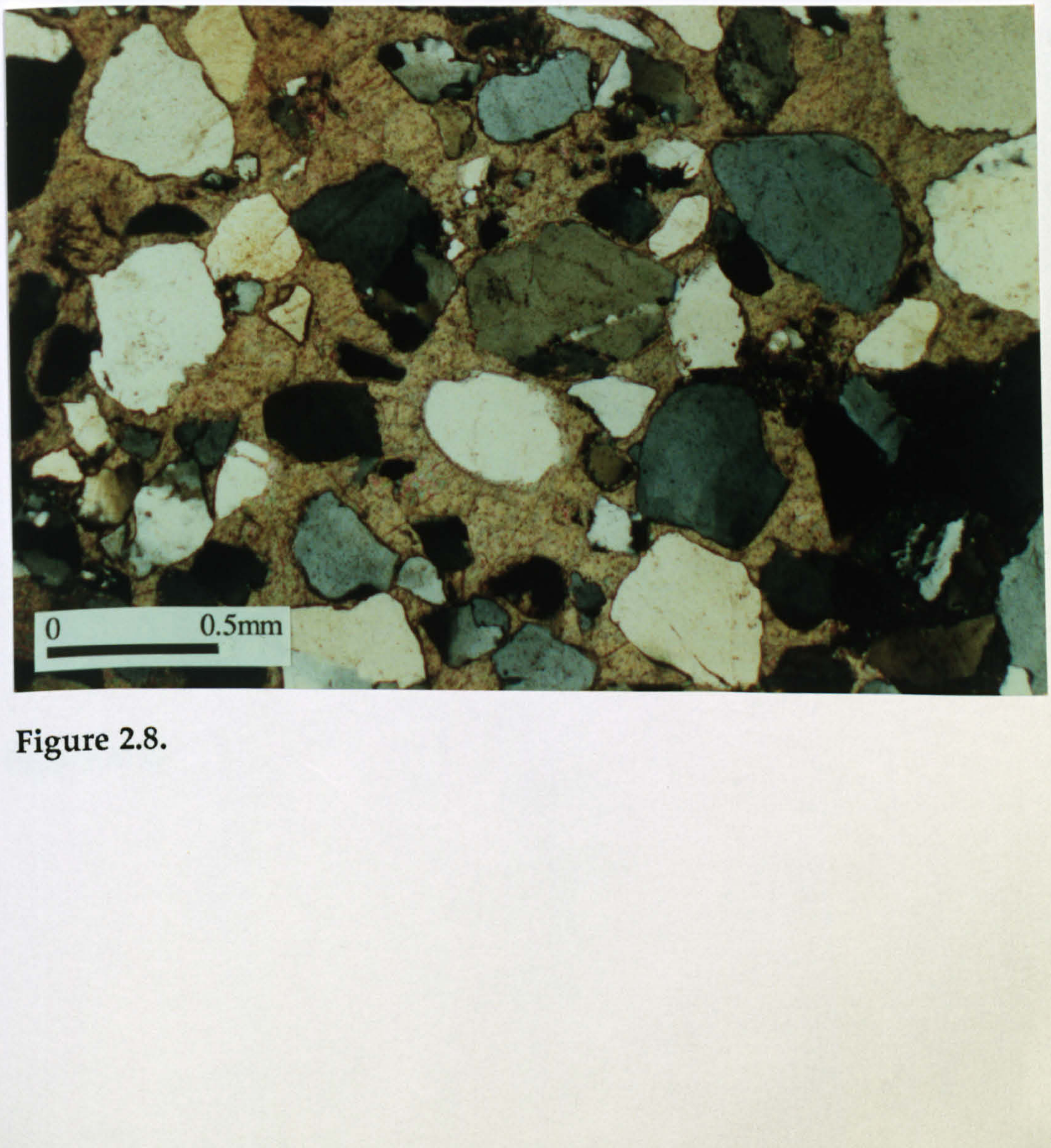

Figure 2.8.

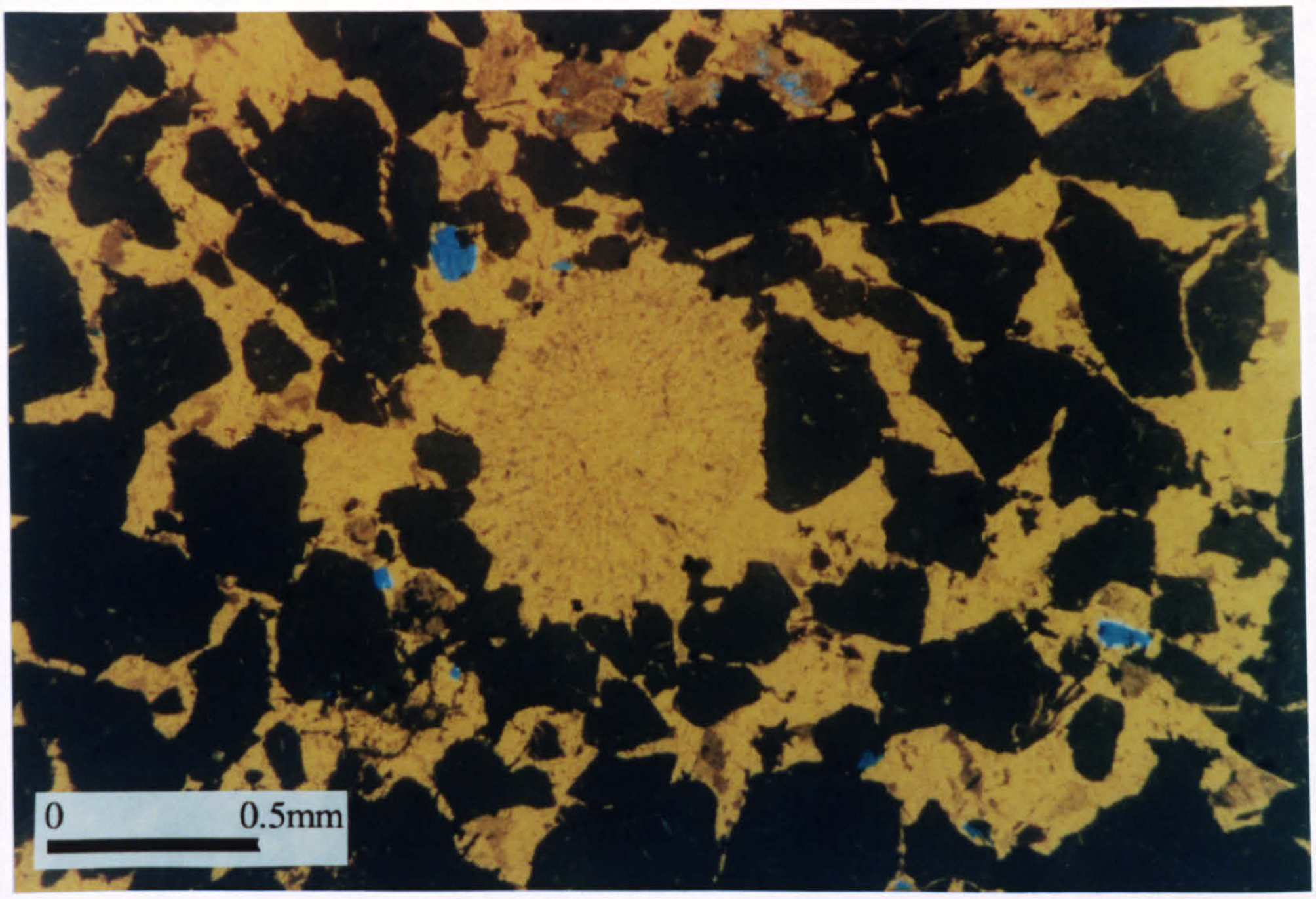

Figure 2.9.

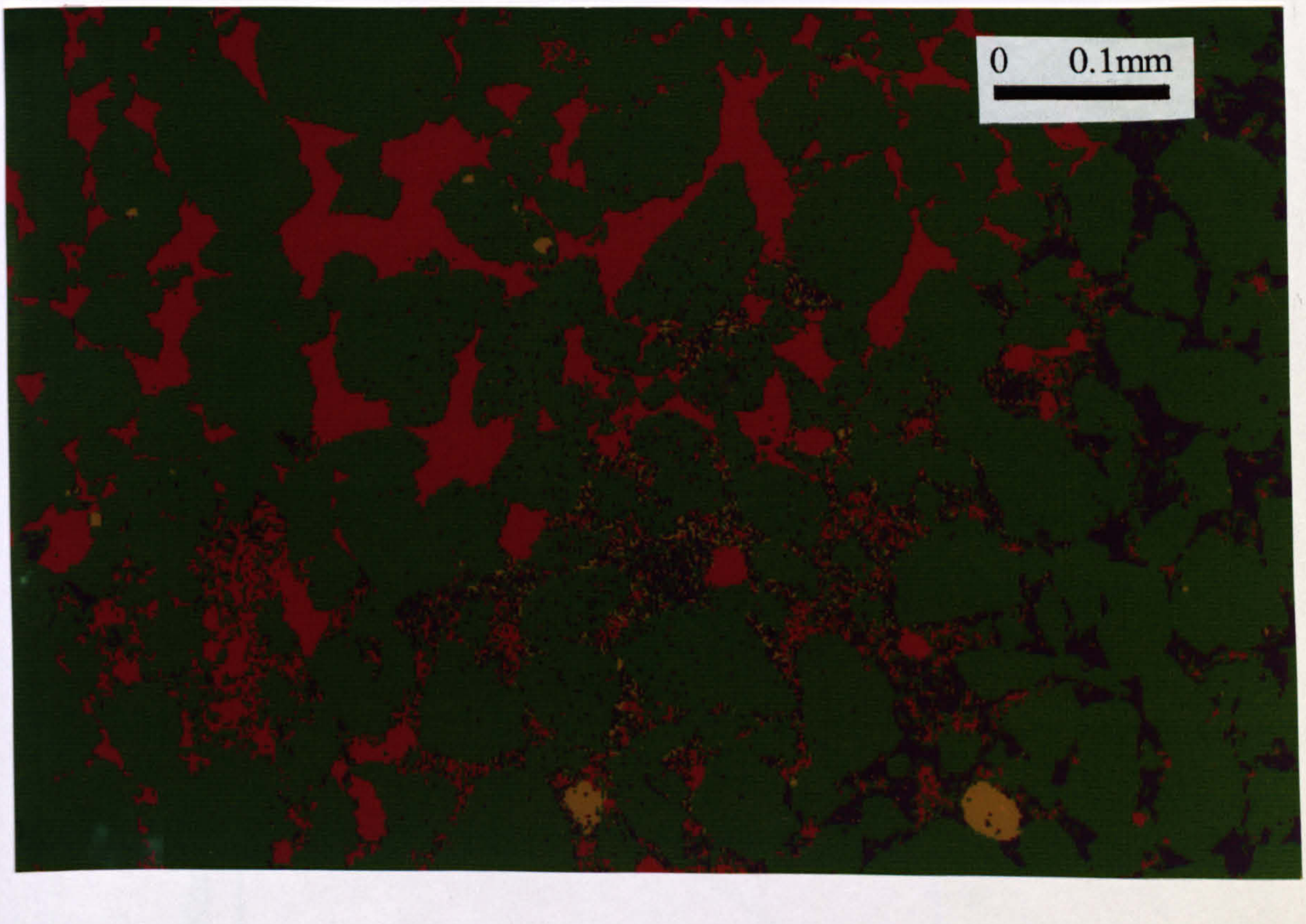

Figure 2.10.

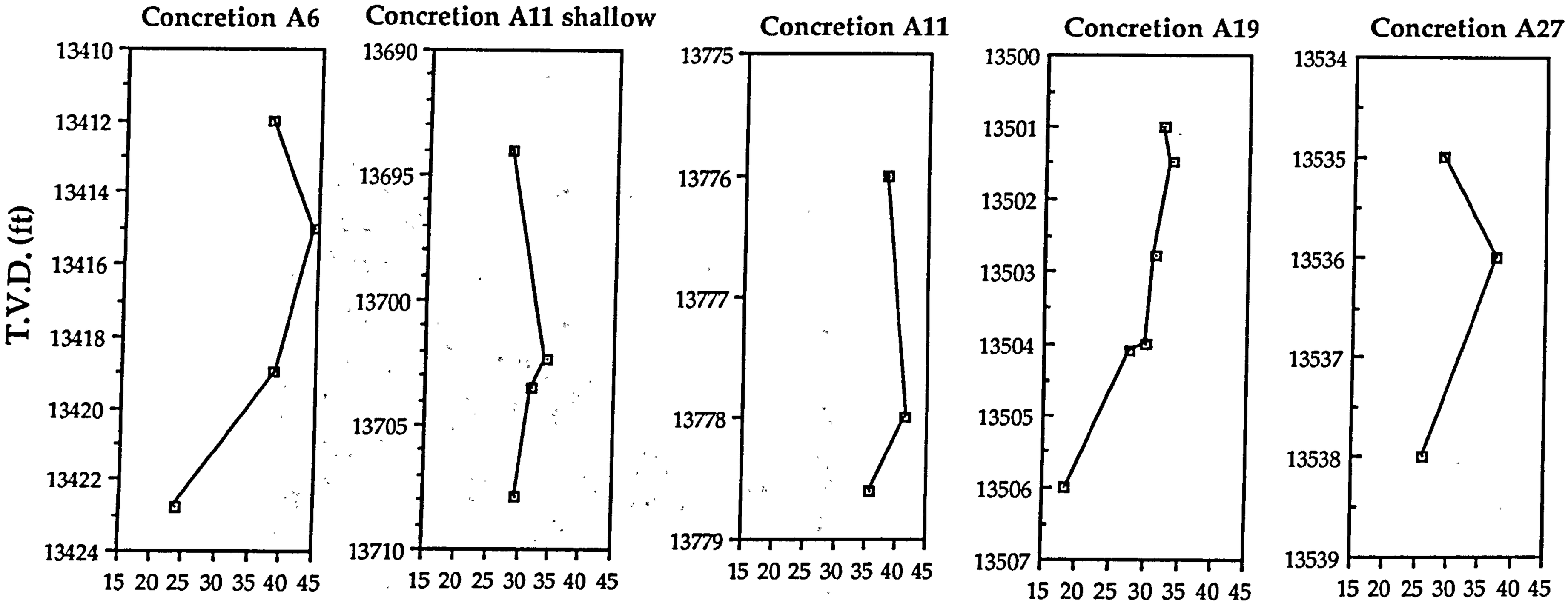
Concretion A6
Concretion A11 shallow
Concretion A11
Concretion A19
Concretion A27
T.V.D. (ft)
13410
13412
13414
13416
13418
13420
13422
13424
13690
13695
13700
13705
13710
13775
13776
13777
13778
13779
13500
13501
13502
13503
13504
13505
13506
13507
13534
13535
13536
13537
13538
13539
15 20 25 30 35 40 45
Minus Cement Porosity%

Figure 2.11.

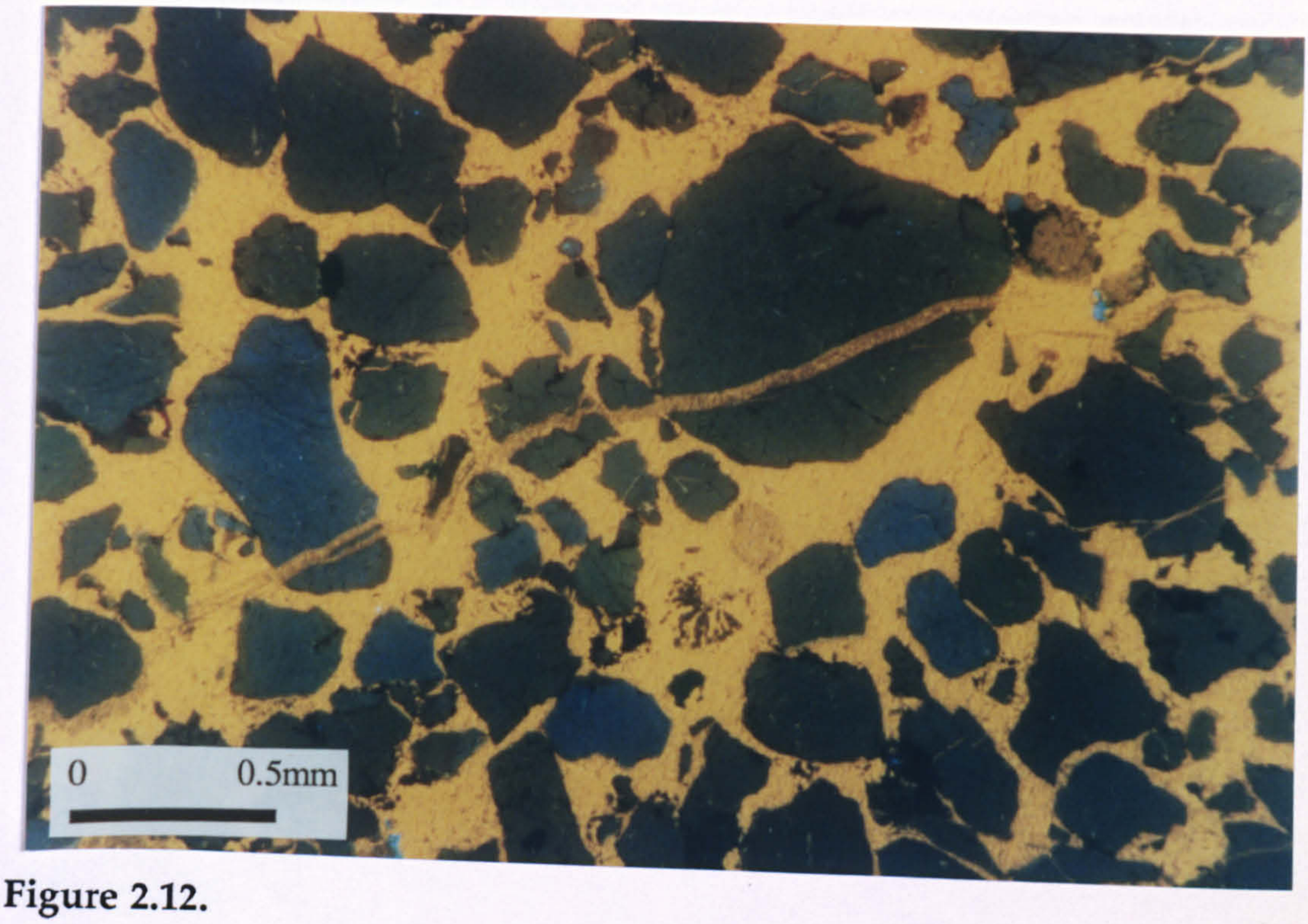

Figure 2.12.

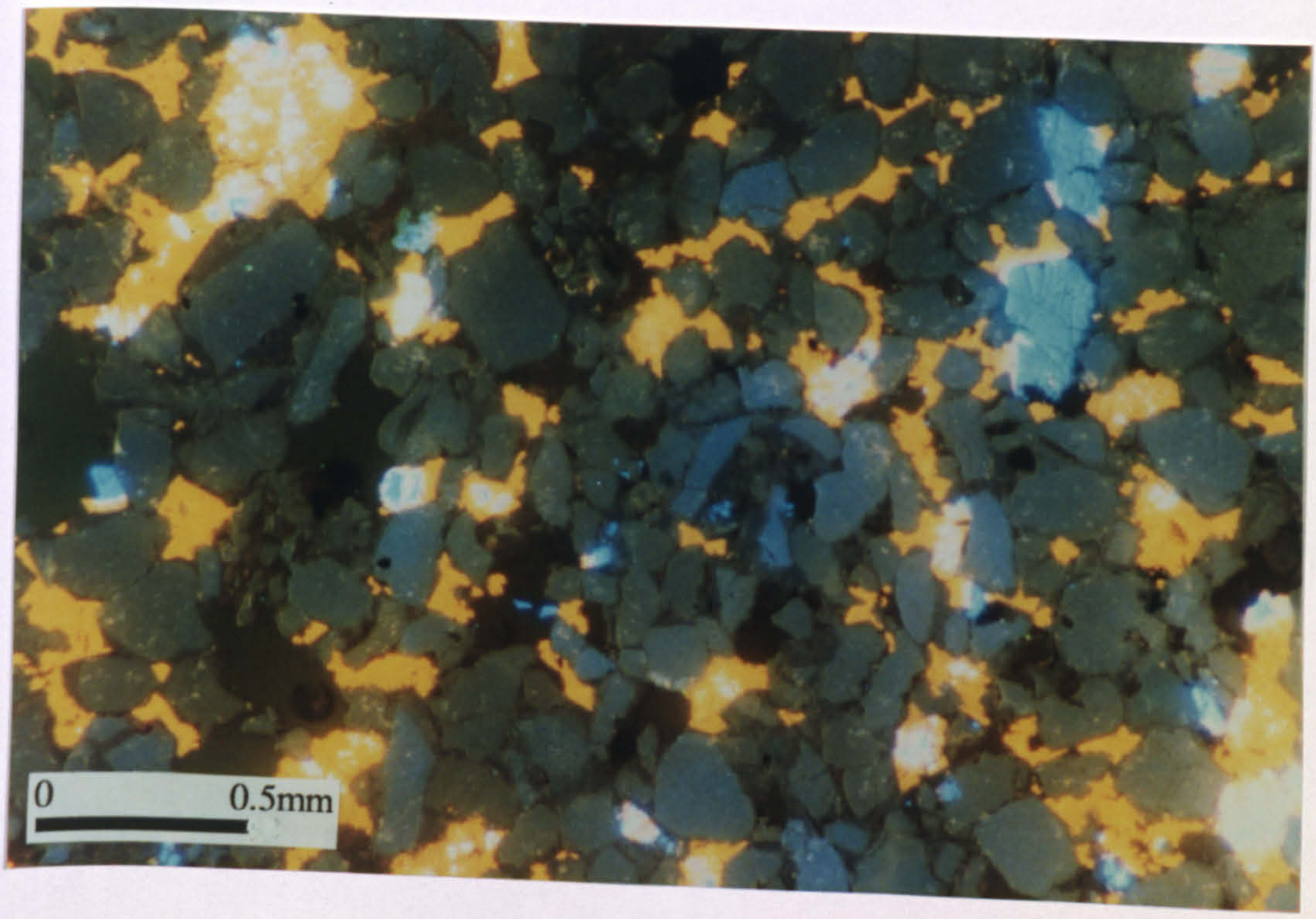

Figure 2.13.

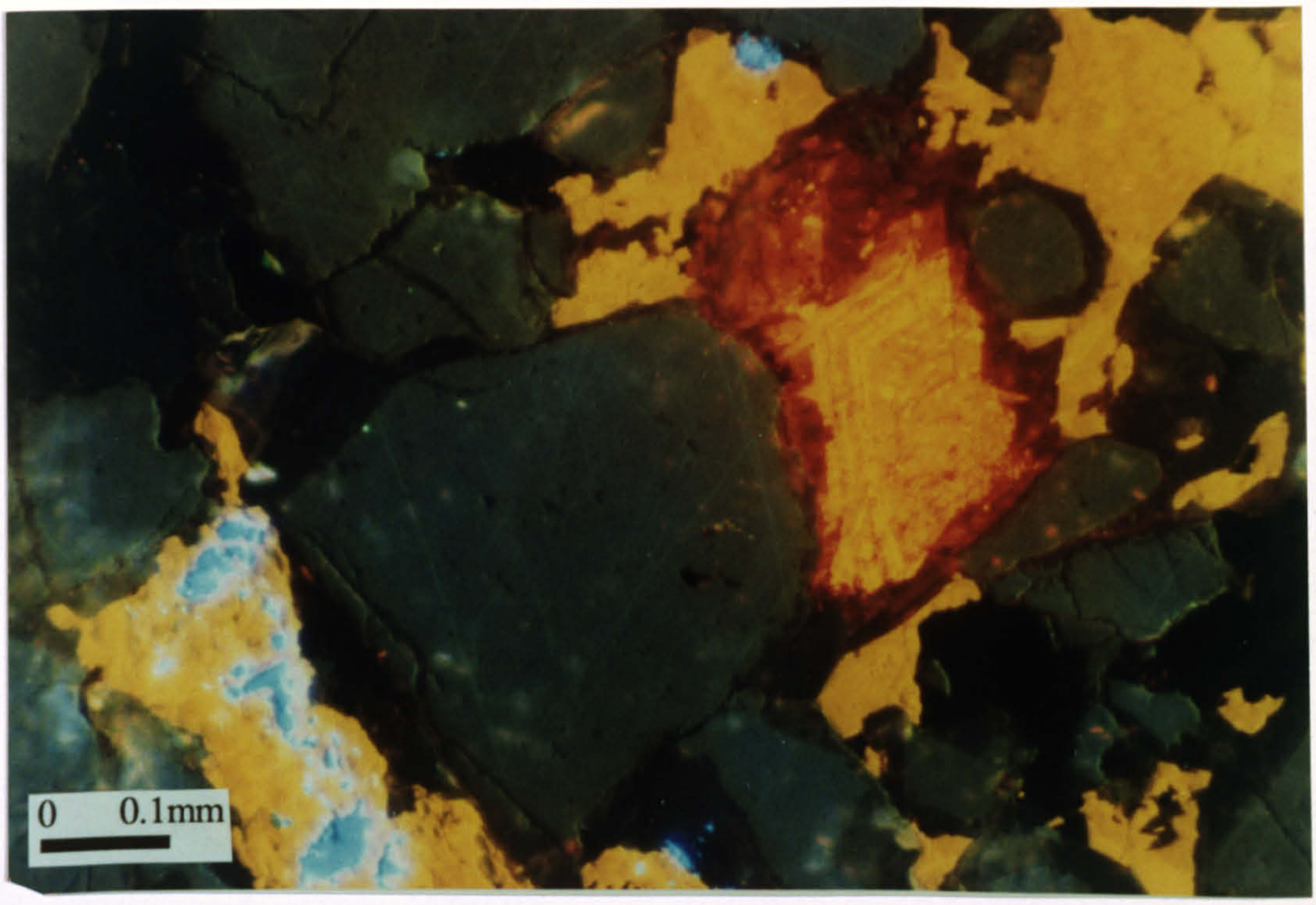

Figure 2.14.

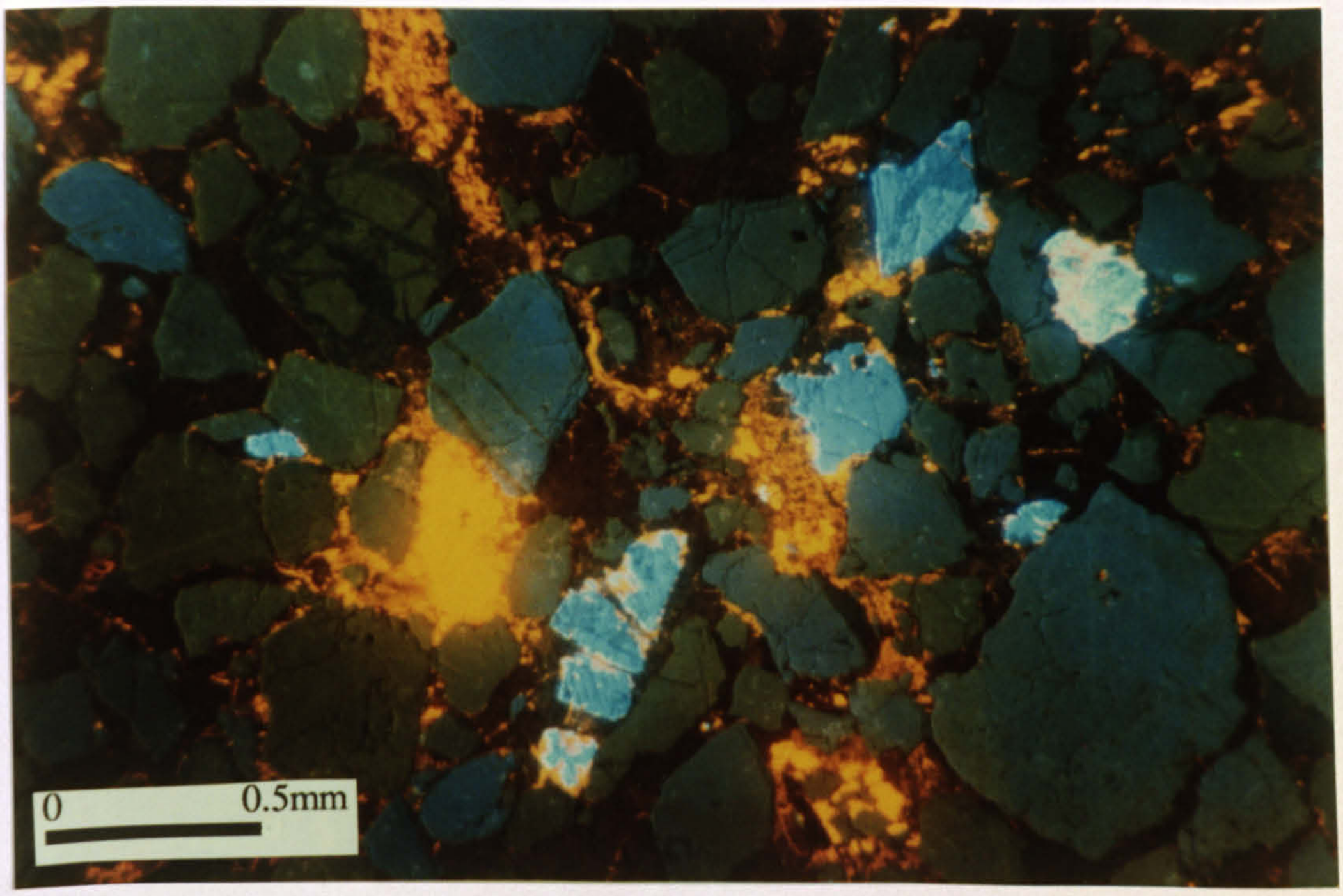

Figure 2.15.

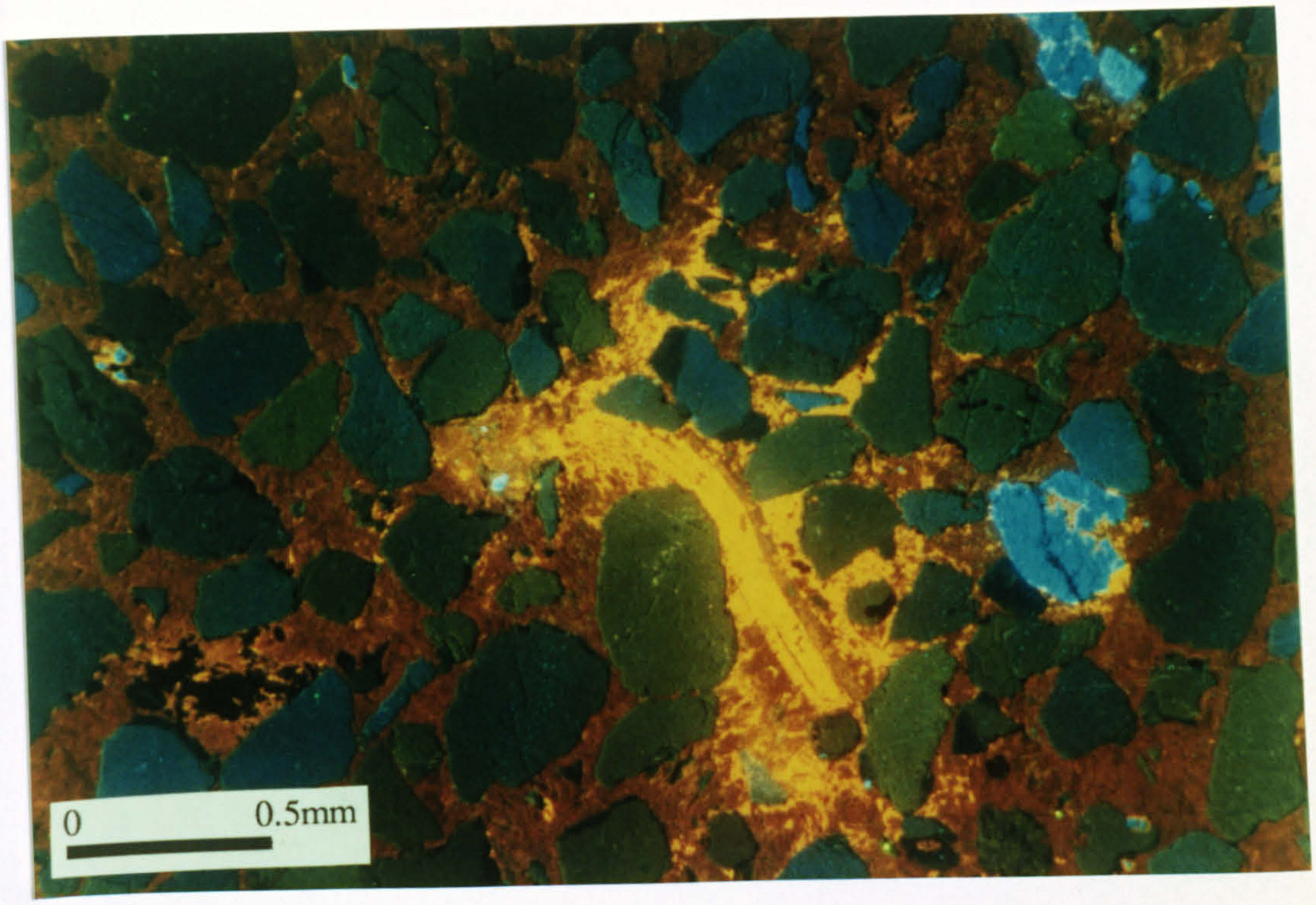

Figure 2.16.

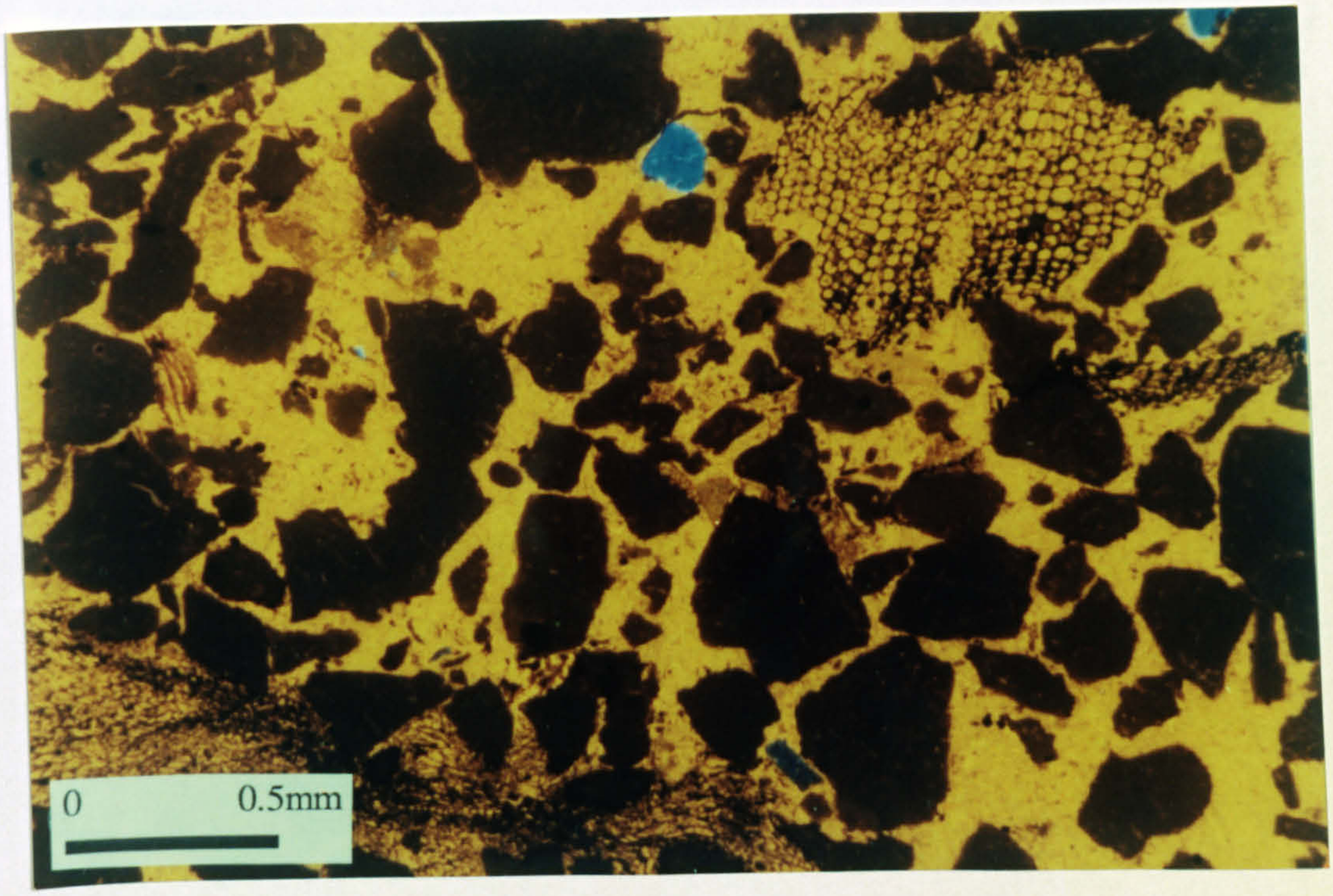

Figure 2.17.

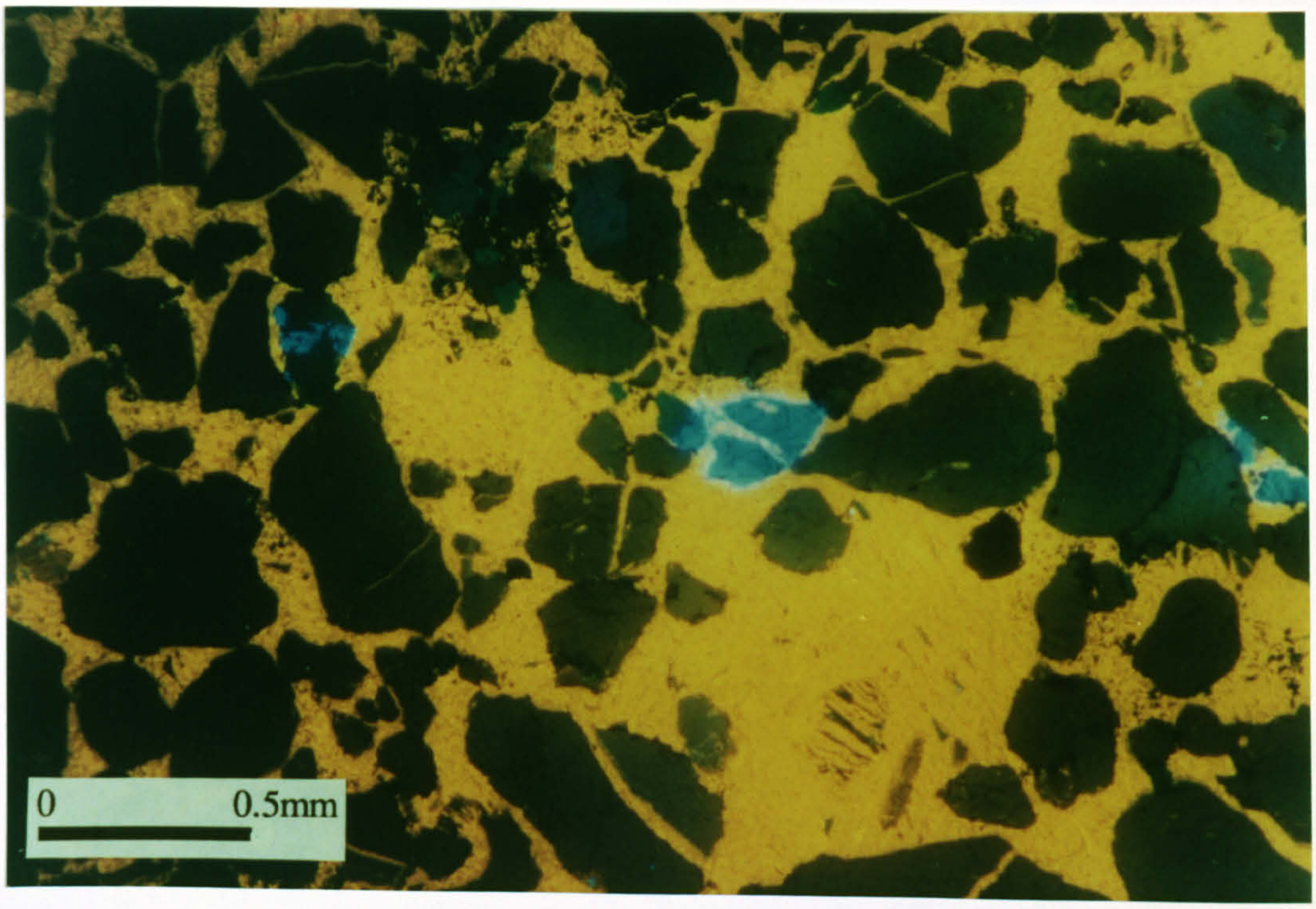

Figure 2.18.

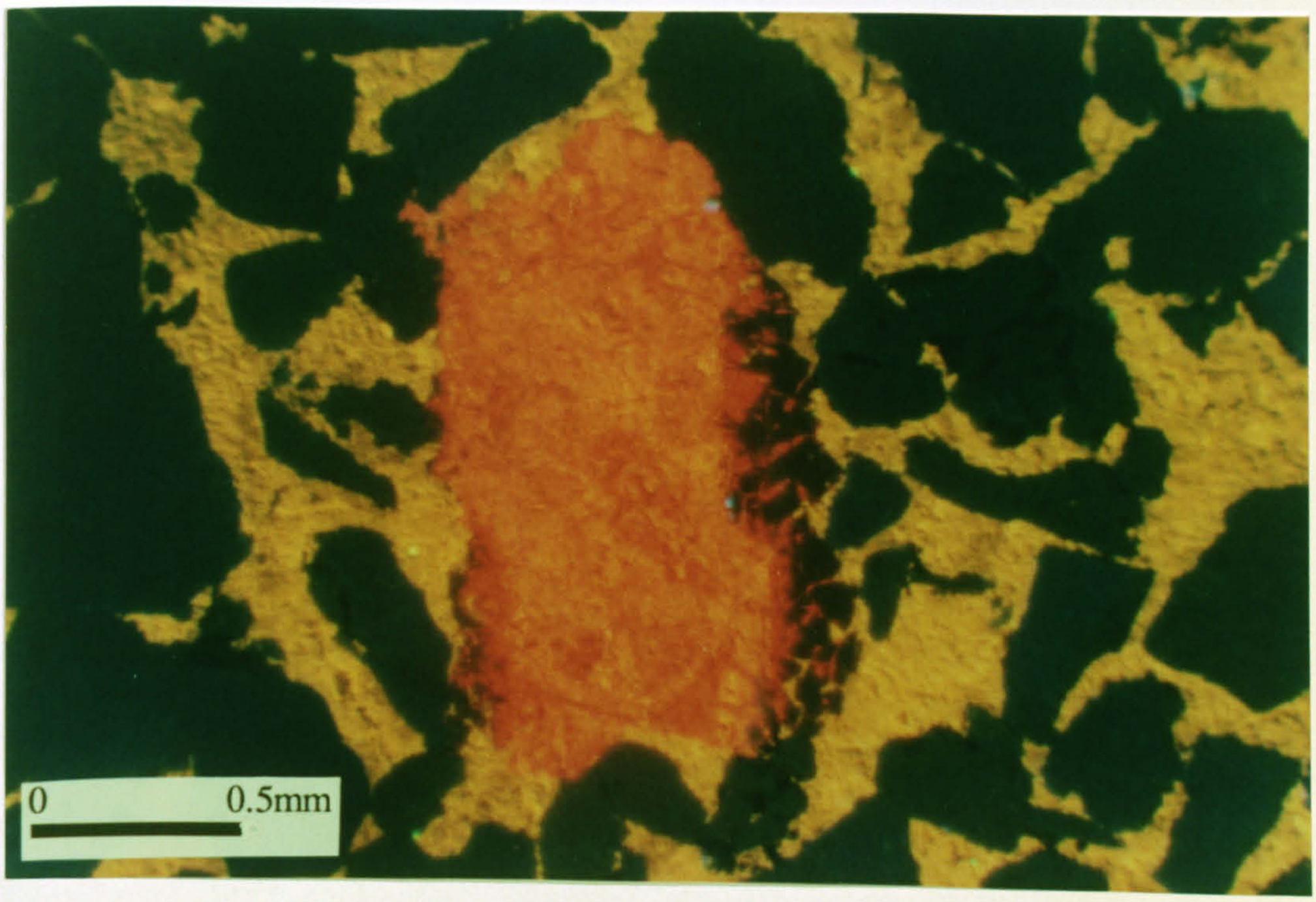

Figure 2.19.

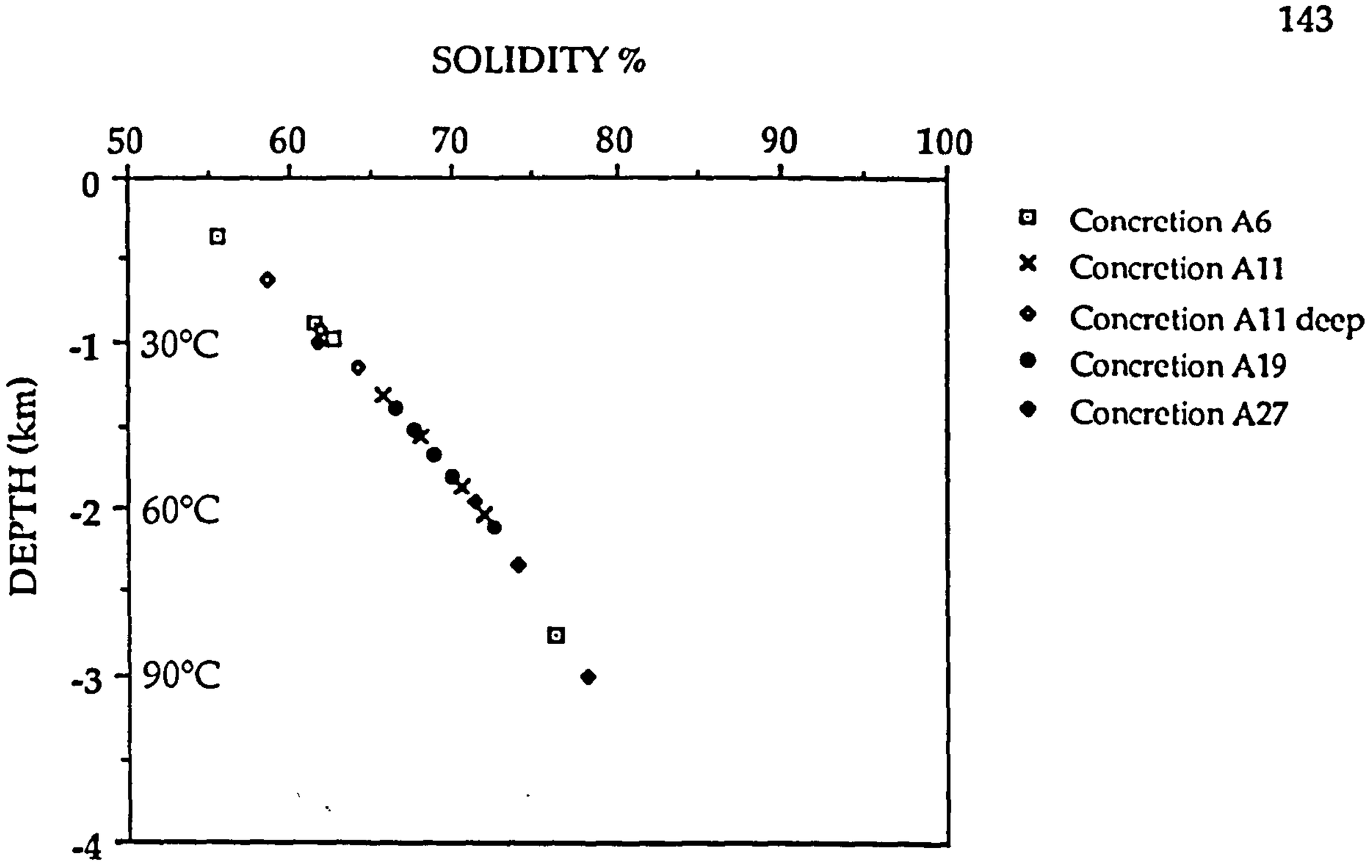
SOLIDITY %
50
60
70
80
90
100
0
-1
-2
-3
-4
DEPTH (km)
30°C
60°C
90°C
Concretion A6
Concretion A11
Concretion A11 deep
Concretion A19
Concretion A27

Figure 2.20.

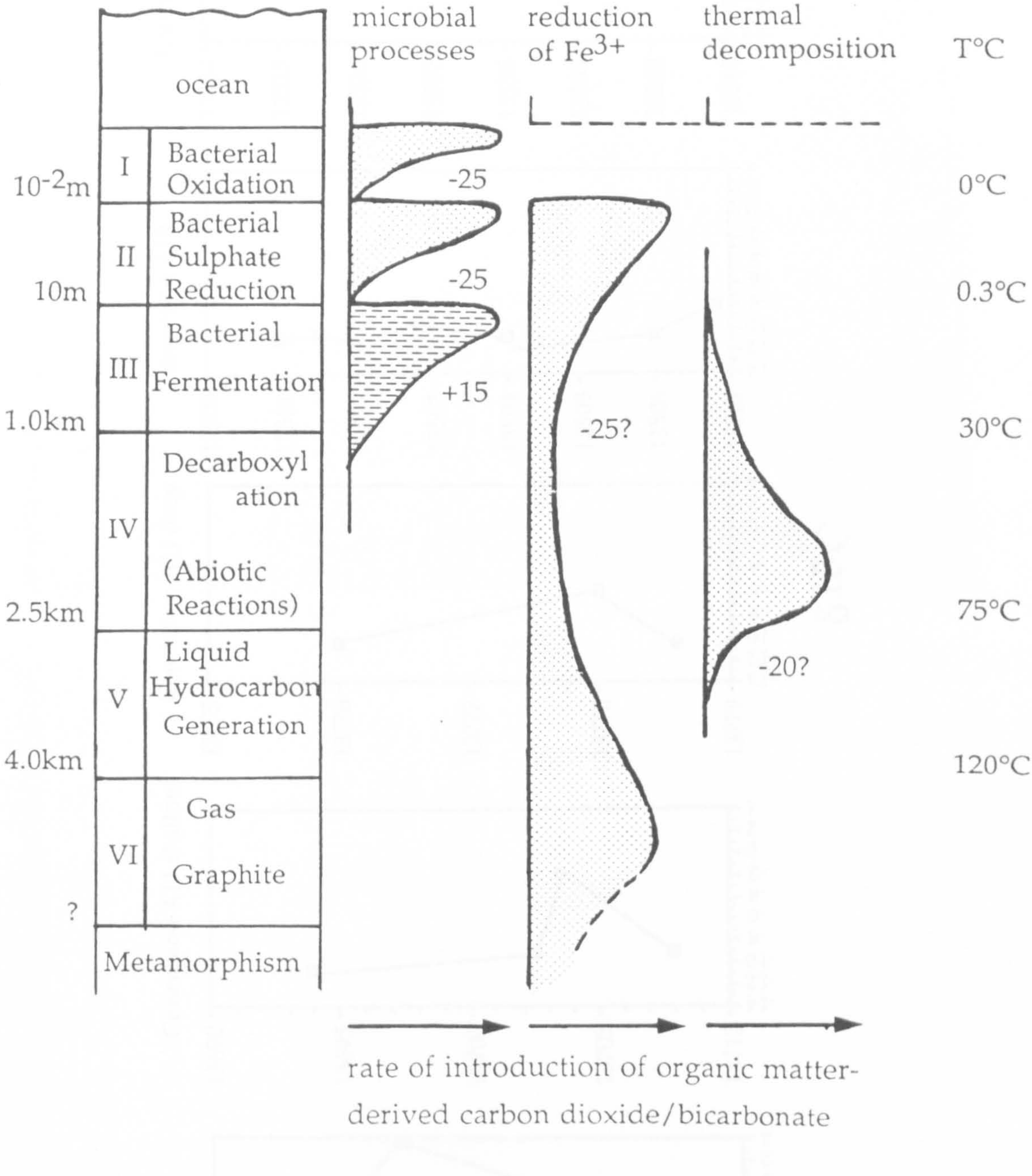
microbial processes
reduction of Fe^{3+}
thermal decomposition
T°C
ocean
I
Bacterial Oxidation
10^{-2}m
-25
0°C
II
Bacterial Sulphate Reduction
10m
-25
0.3°C
III
Bacterial Fermentation
+15
1.0km
-25?
30°C
IV
Decarboxyl ation
(Abiotic Reactions)
2.5km
75°C
V
Liquid Hydrocarbon Generation
-20?
4.0km
120°C
VI
Gas
Graphite
?
Metamorphism
rate of introduction of organic matter-derived carbon dioxide/bicarbonate

Figure 2.21

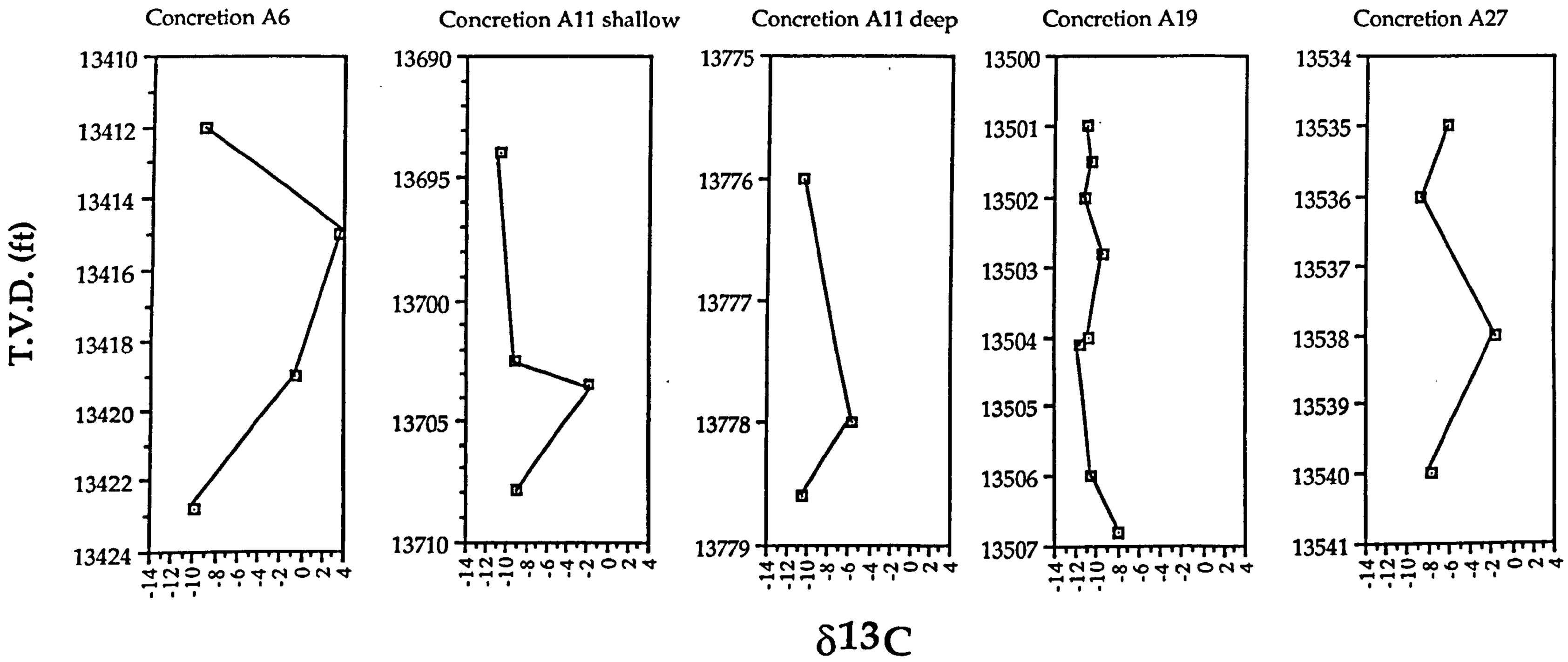
Concretion A6
Concretion A11 shallow
Concretion A11 deep
Concretion A19
Concretion A27
T.V.D. (ft)
13410
13412
13414
13416
13418
13420
13422
13424
13690
13695
13700
13705
13710
13775
13776
13777
13778
13779
13500
13501
13502
13503
13504
13505
13506
13507
13534
13535
13536
13537
13538
13539
13540
13541
-14
-12
-10
-8
-6
-4
-2
0
2
4
δ13C

Figure 2.22

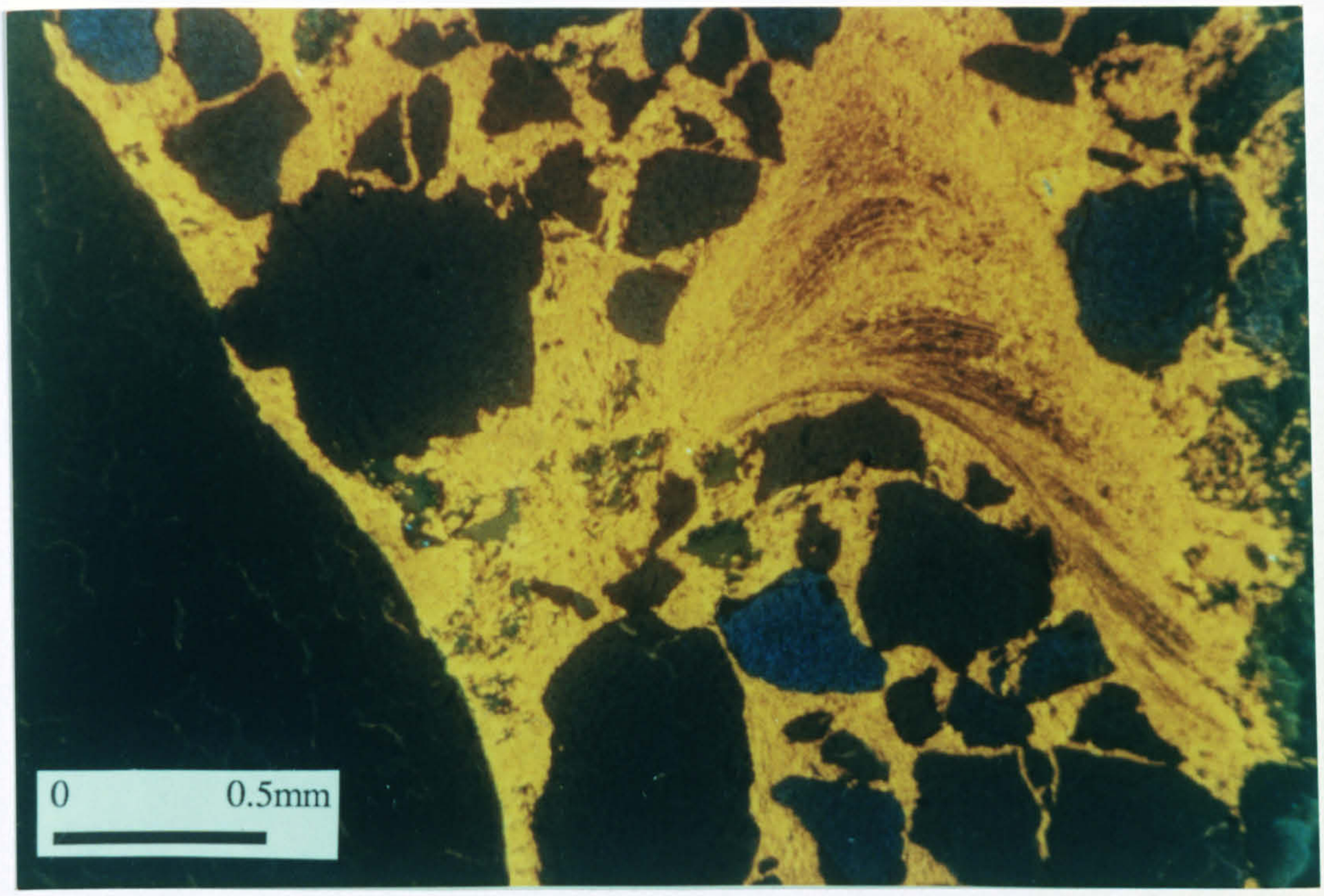

Figure 2.23.

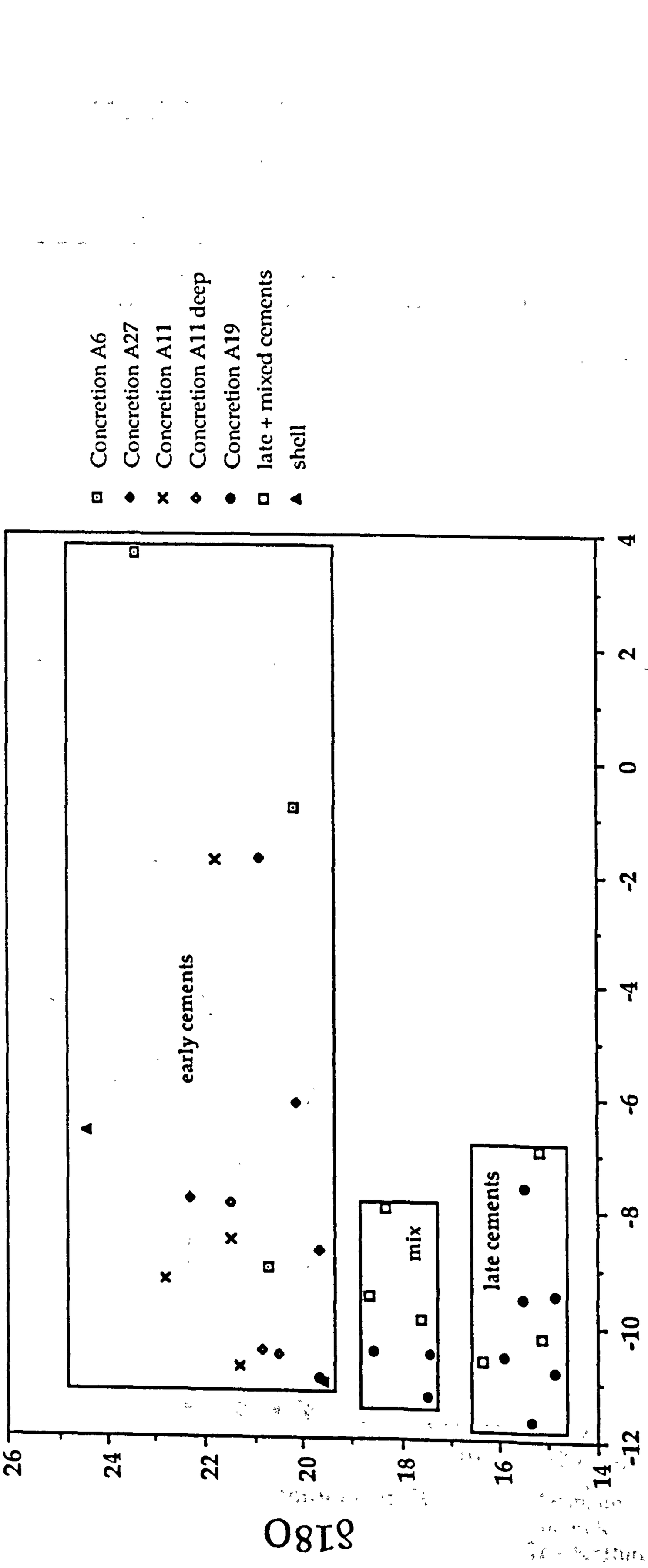
Concretion A6
Concretion A27
Concretion A11
Concretion A11 deep
Concretion A19
late + mixed cements
shell
early cements
mix
late cements
δ13C
δ18O
4
2
0
-2
-4
-6
-8
-10
-12
26
24
22
20
18
16
14

Figure 2.24.

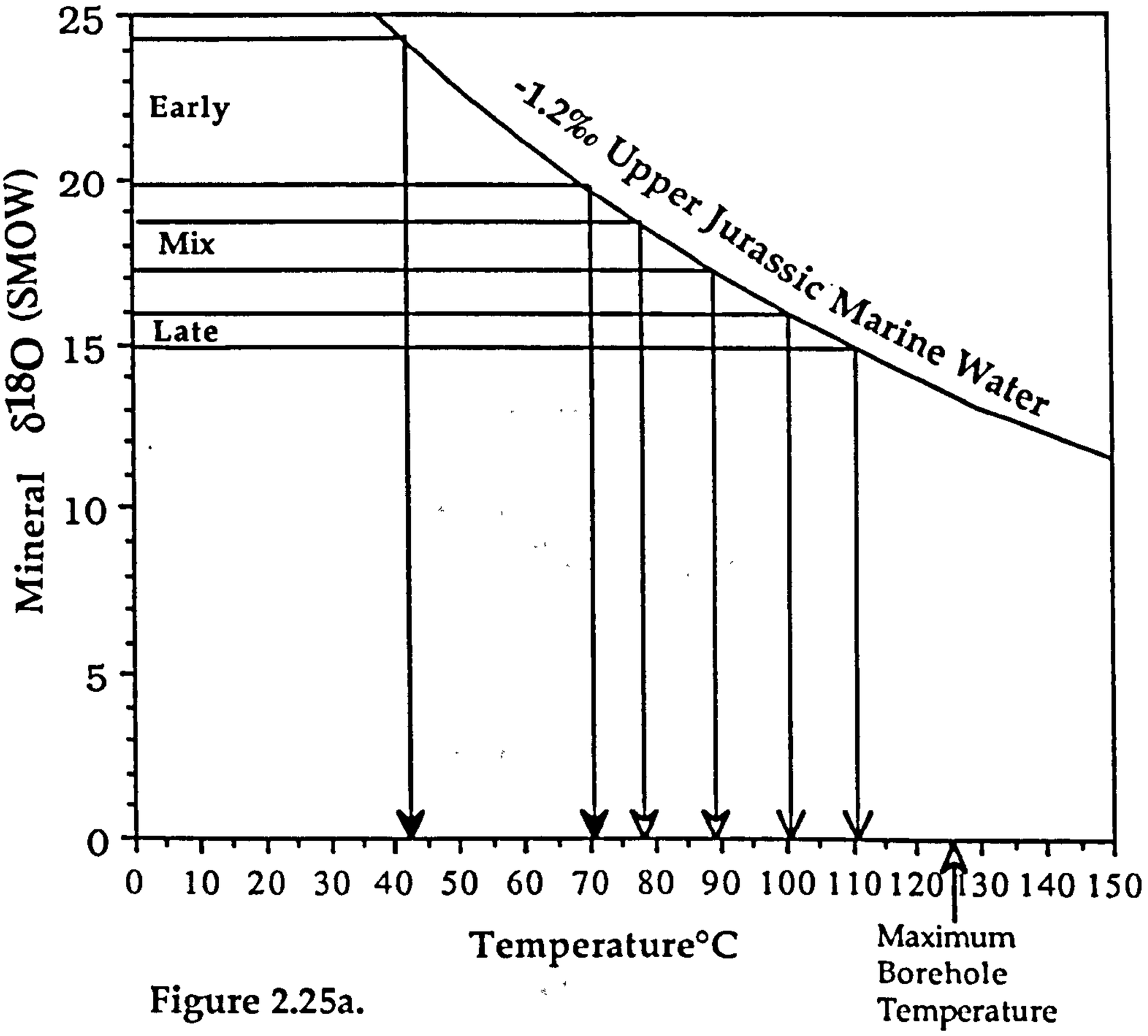

Figure 2.25a.

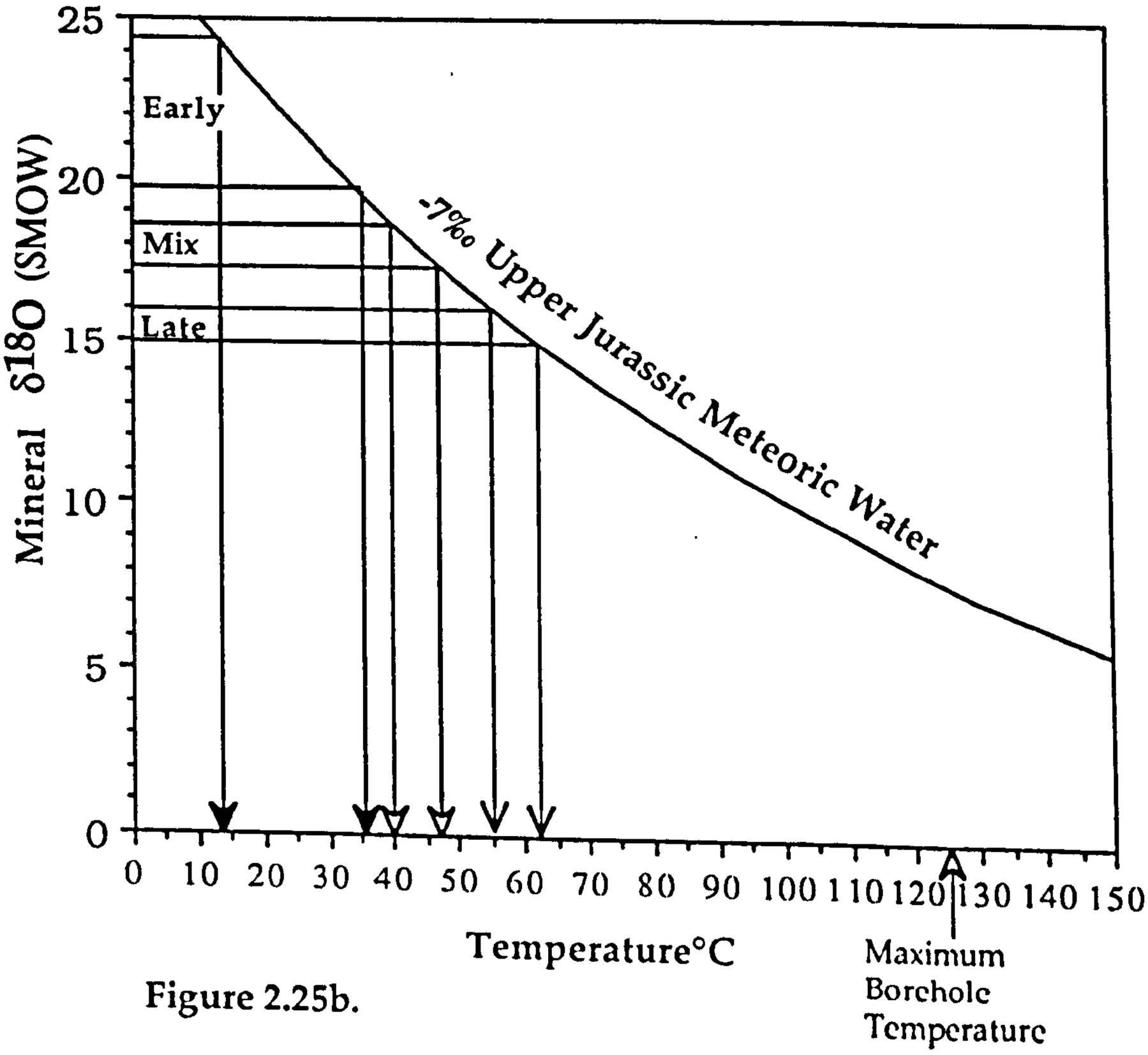

Figure 2.25b.

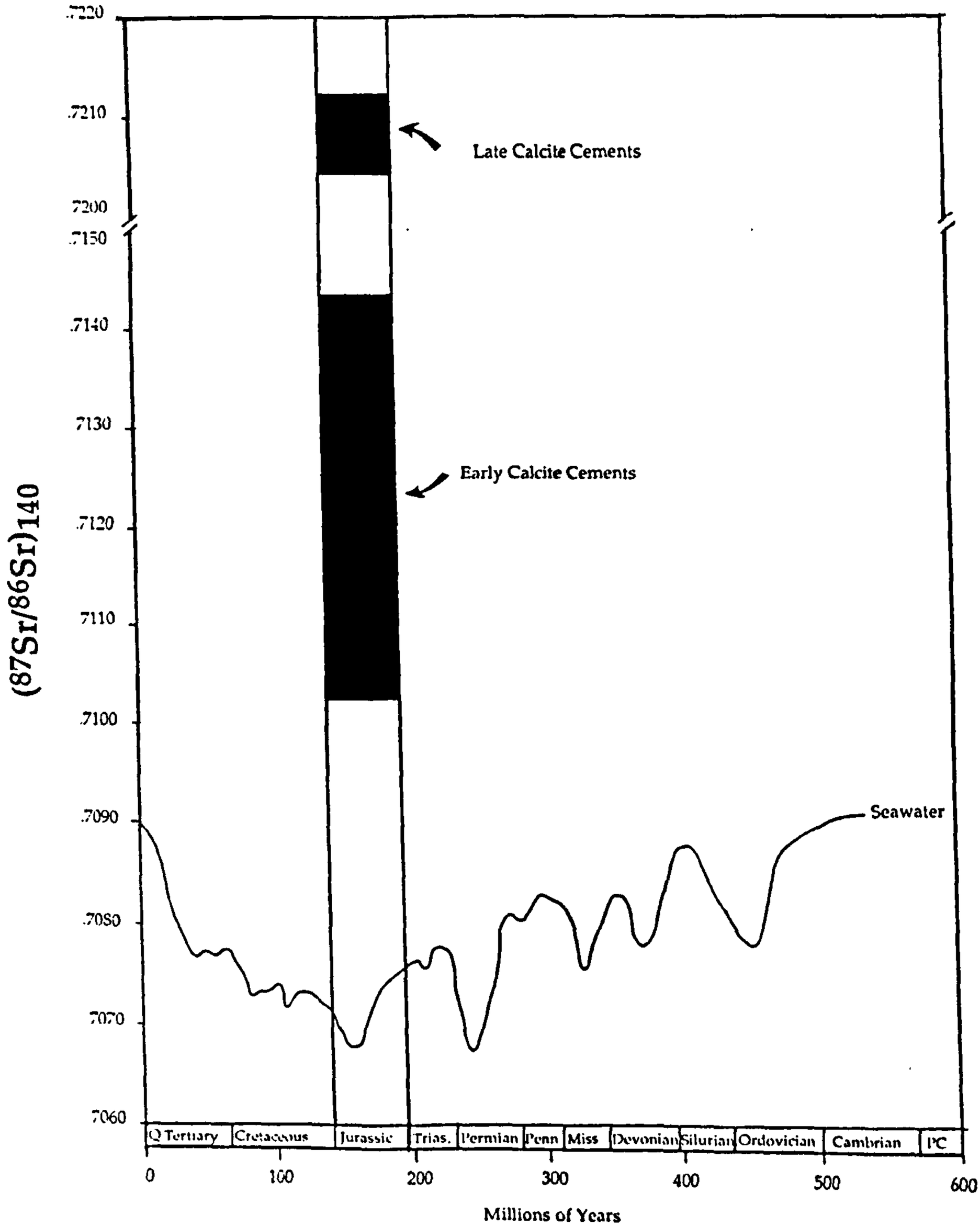
.7220
.7210
7200
.7150
.7140
7130
.7120
7110
.7100
.7090
.7080
7070
7060
(87Sr/86Sr)140
Late Calcite Cements
Early Calcite Cements
Seawater
Q Tertiary
Cretaceous
Jurassic
Trias.
Permian
Penn
Miss
Devonian
Silurian
Ordovician
Cambrian
PC
0
100
200
300
400
500
600
Millions of Years

Figure 2.26.

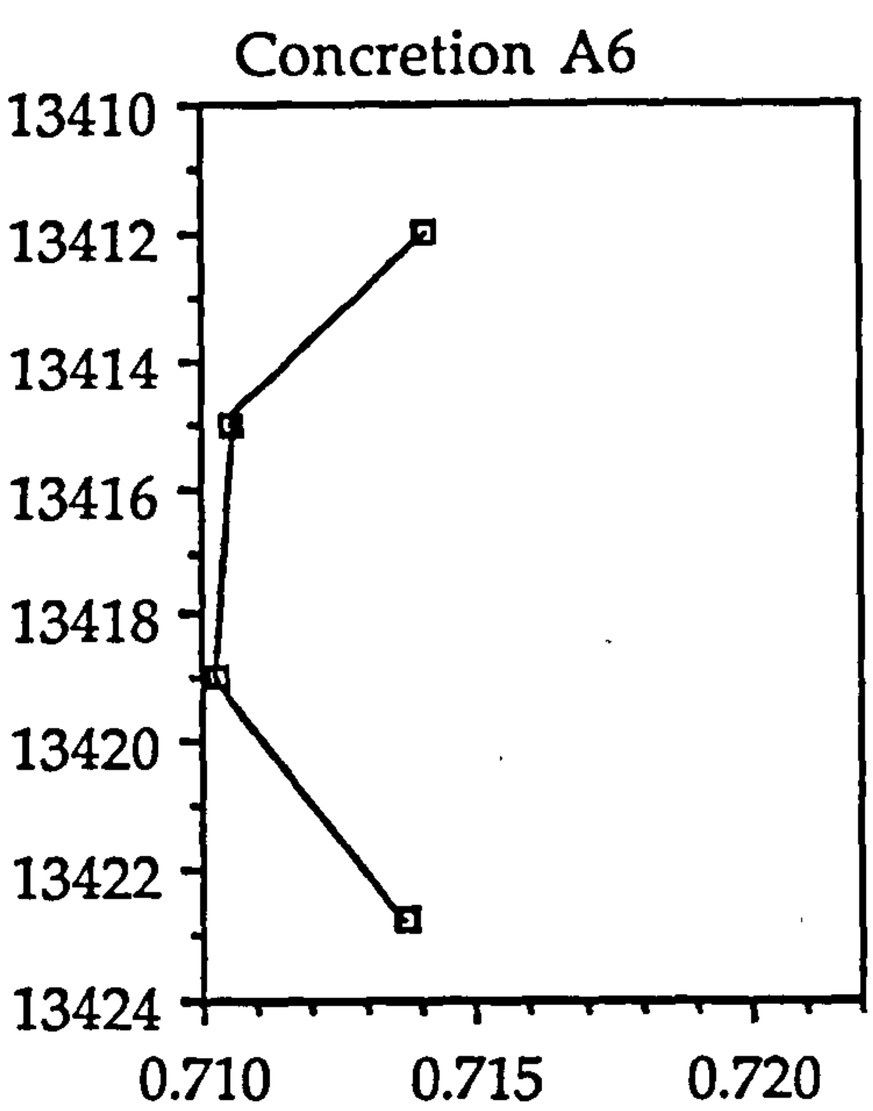

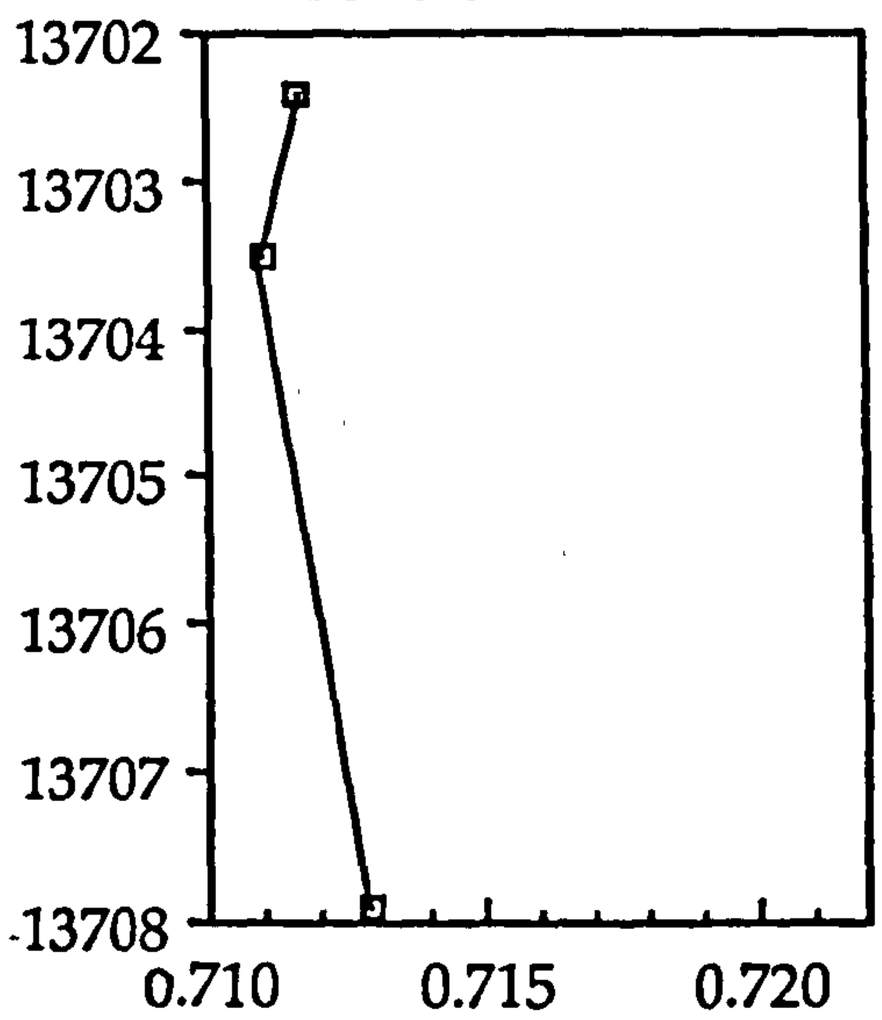

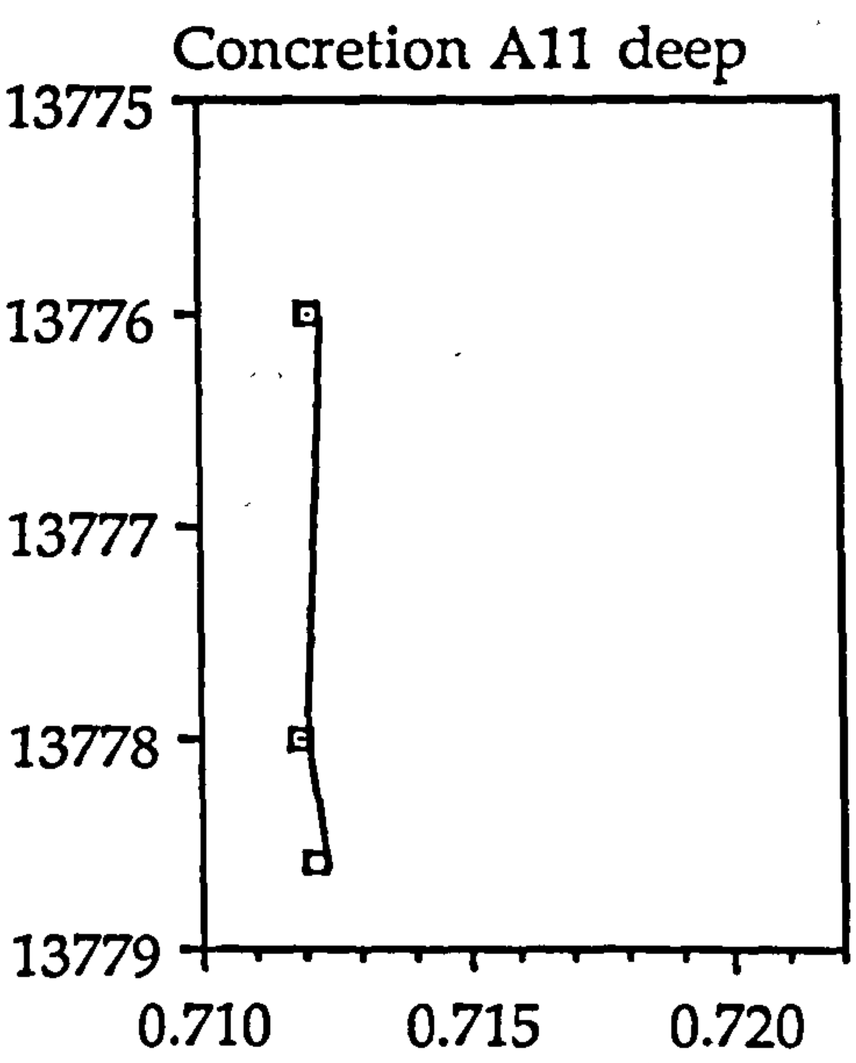

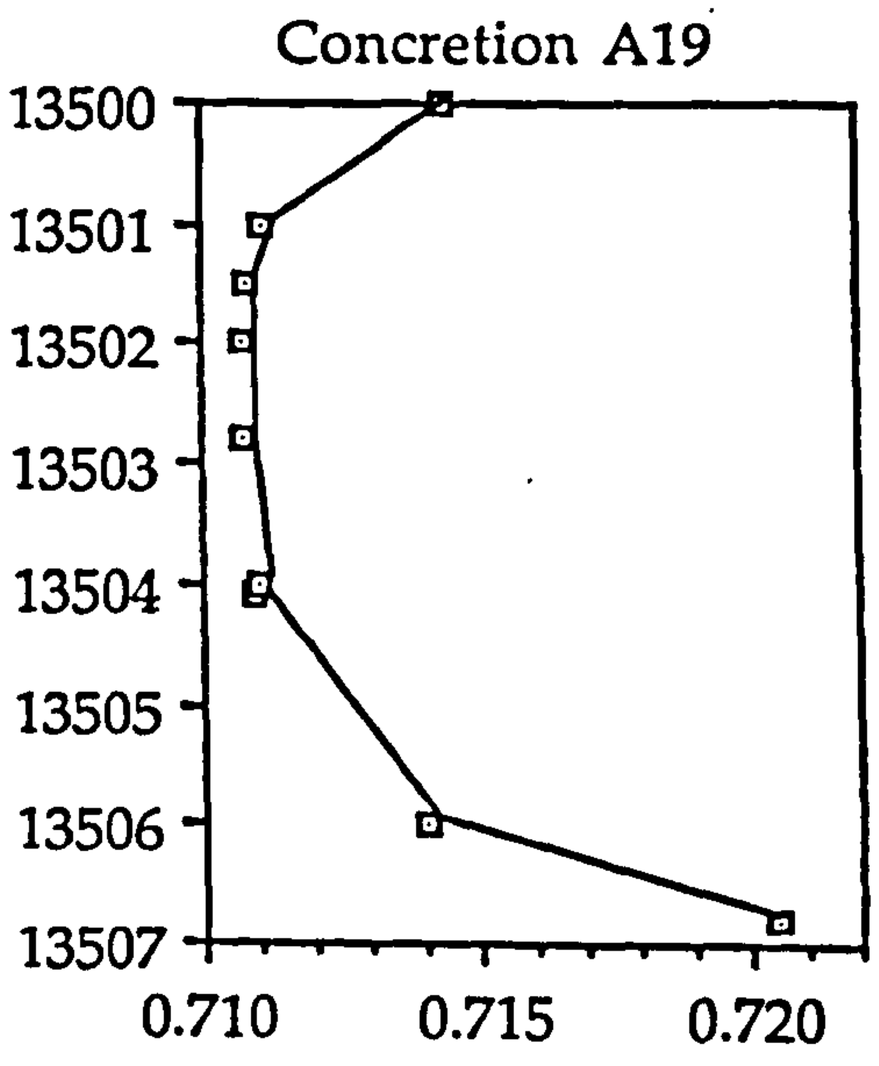

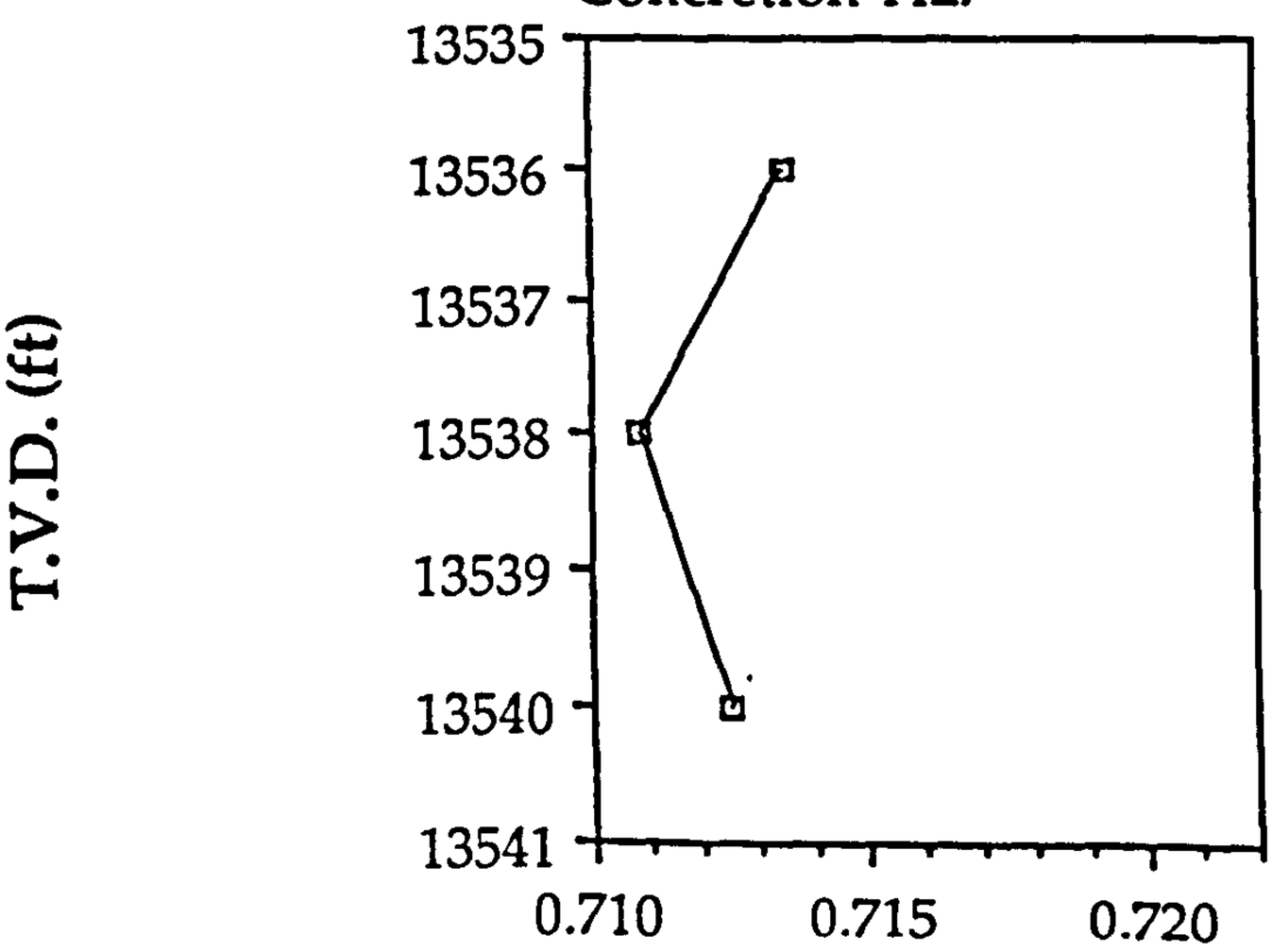

Figure 2.27. $(^{87}Sr/^{86}Sr)_{140}$

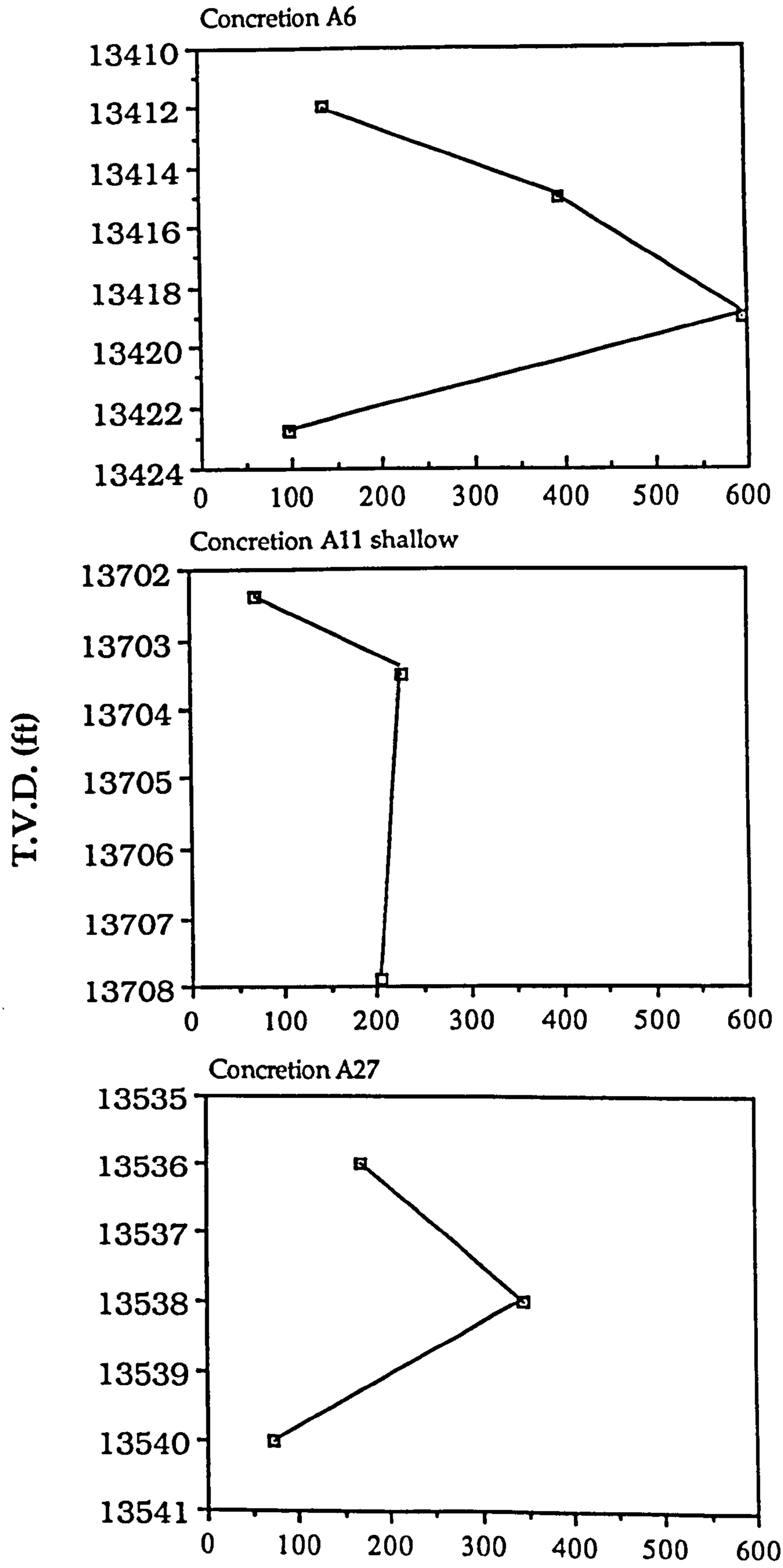
Concretion A6
13410
13412
13414
13416
13418
13420
13422
13424
0
100
200
300
400
500
600
Concretion A11 shallow
13702
13703
13704
13705
13706
13707
13708
0
100
200
300
400
500
600
T.V.D. (ft)
Concretion A27
13535
13536
13537
13538
13539
13540
13541
0
100
200
300
400
500
600
Sr ppm

Figure 2.28.

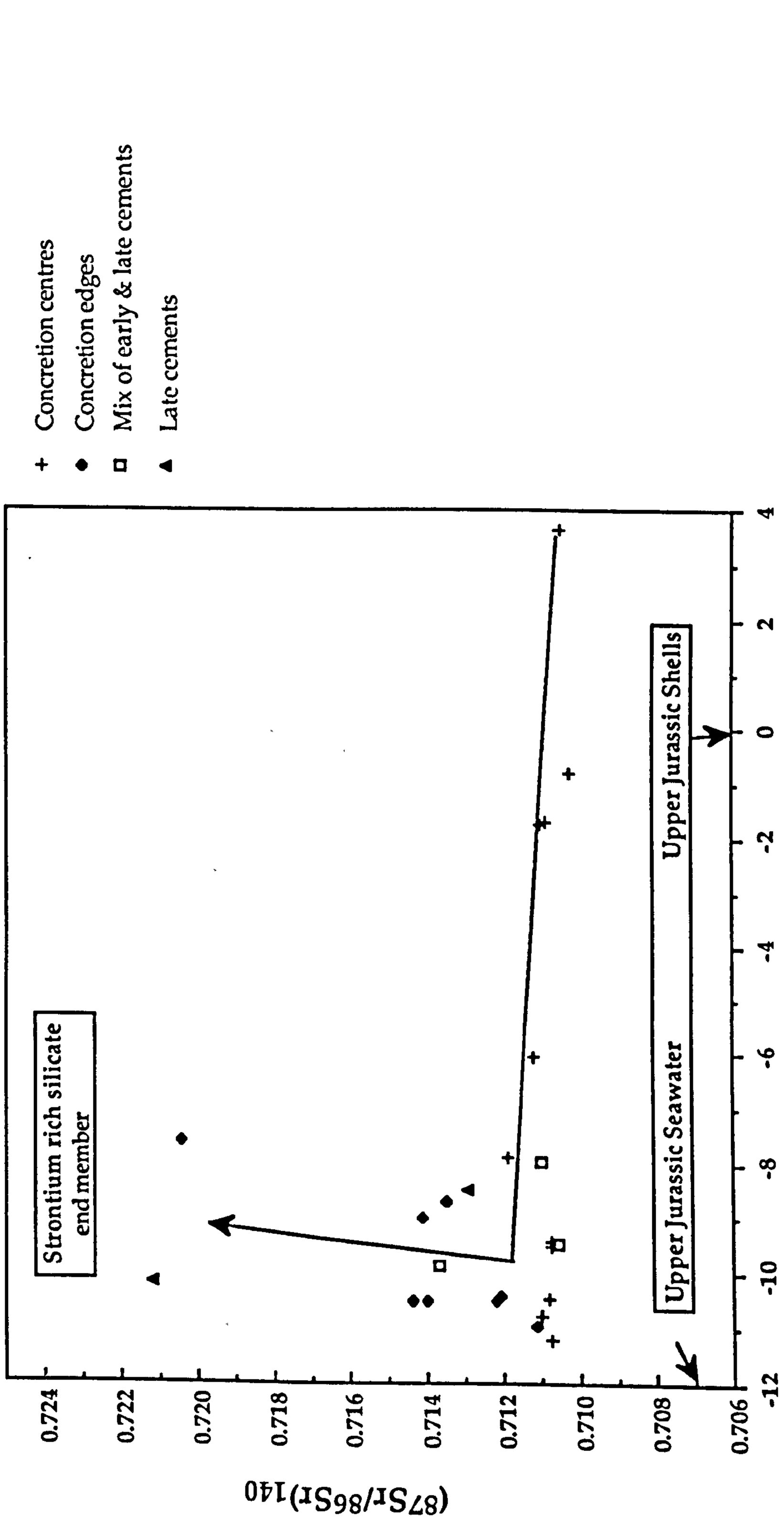
Concretion centres
Concretion edges
Mix of early & late cements
Late cements
Upper Jurassic Shells
Upper Jurassic Seawater
Strontium rich silicate end member
δ13C
(87Sr/86Sr)140
4
2
0
-2
-4
-6
-8
-10
-12
0.724
0.722
0.720
0.718
0.716
0.714
0.712
0.710
0.708
0.706

Figure 2.29

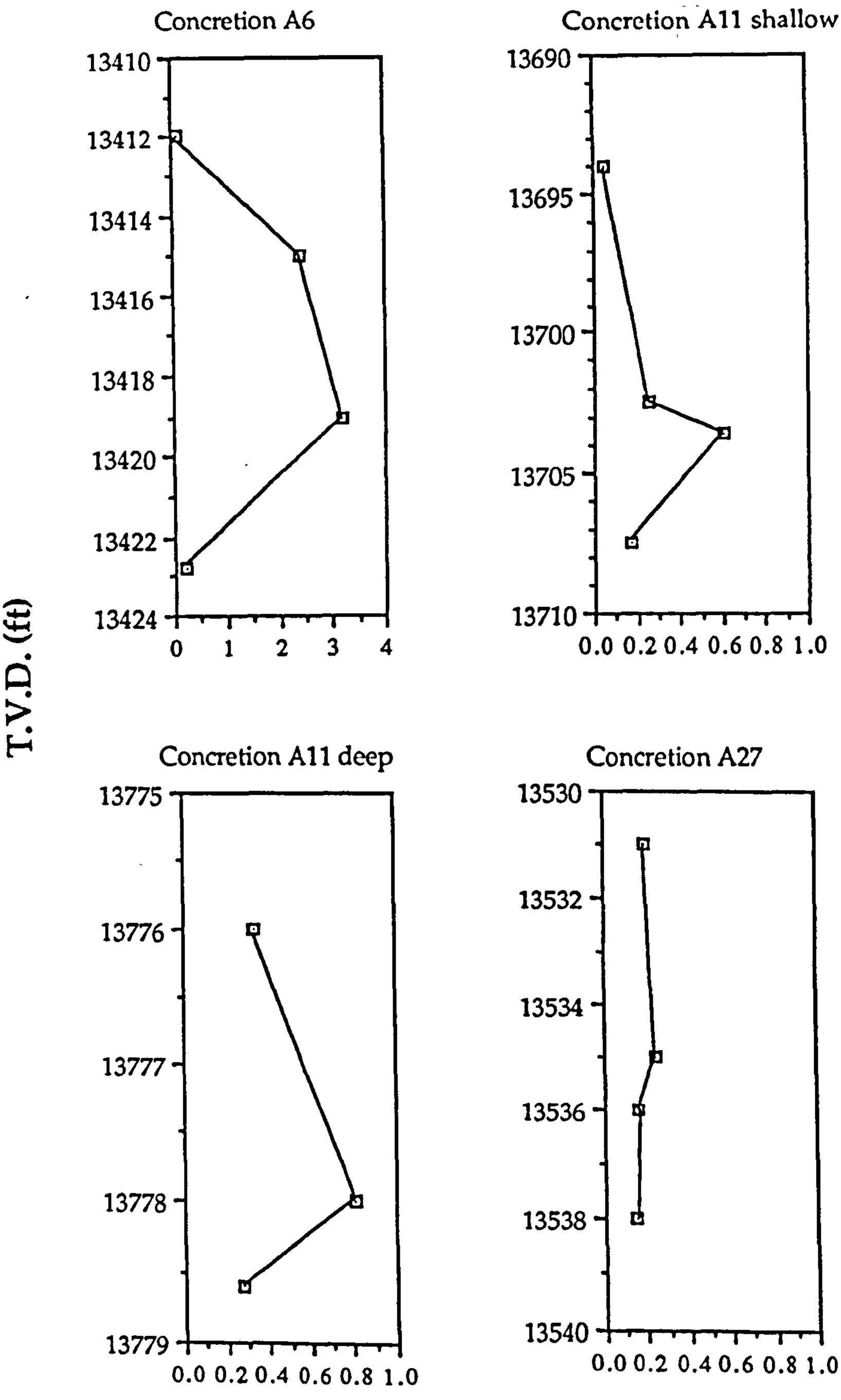
Concretion A6
13410
13412
13414
13416
13418
13420
13422
13424
0 1 2 3 4
Concretion A11 shallow
13690
13695
13700
13705
13710
0.0 0.2 0.4 0.6 0.8 1.0
T.V.D. (ft)
Concretion A11 deep
13775
13776
13777
13778
13779
0.0 0.2 0.4 0.6 0.8 1.0
Concretion A27
13530
13532
13534
13536
13538
13540
0.0 0.2 0.4 0.6 0.8 1.0
Fe wt%

Figure 2.30.

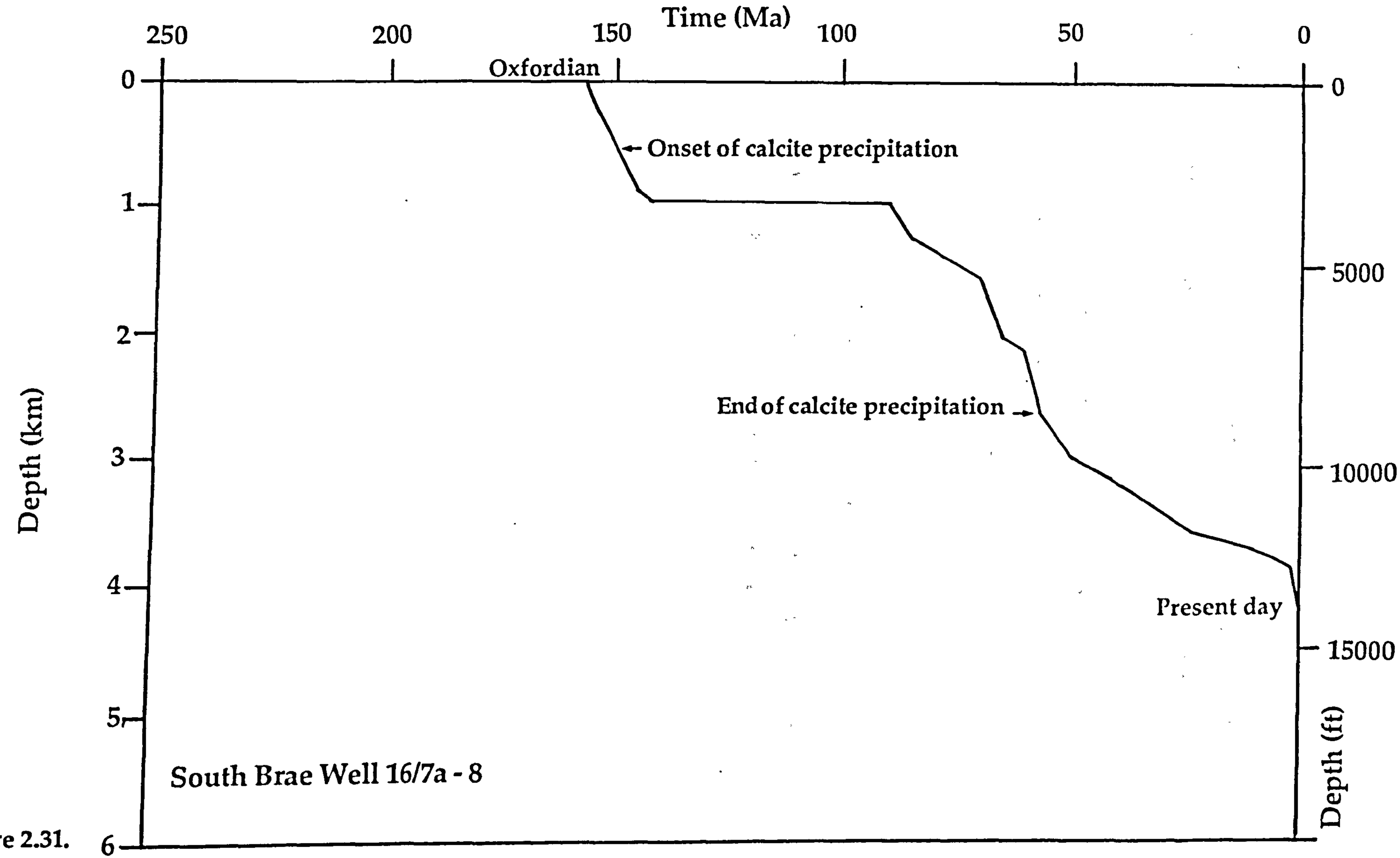
Time (Ma)
250
200
150
100
50
0
Oxfordian
Onset of calcite precipitation
End of calcite precipitation
Present day
South Brae Well 16/7a - 8
Depth (km)
0
1
2
3
4
5
6
Depth (ft)
0
5000
10000
15000

Figure 2.31.

DIAGENETIC QUARTZ CEMENTATION - A LAYERED POREFLUID: THE SOUTH BRAE OILFIELD, NORTH SEA

Órla M. Mc Laughlin, R. Stuart Haszeldine

Department of Geology and Applied Geology, University of Glasgow,

Glasgow G12 8QQ, Scotland

Anthony E. Fallick

Isotope Geology Unit, Scottish Universities Research and Reactor Centre,

East Kilbride, Glasgow G75 0QU, Scotland

3.1 ABSTRACT

The South Brae reservoir sandstones were cemented by quartz late in their diagenetic history, succeeding calcite cementation. The volume of quartz cement in the South Brae sandstones ranges from 0 (in the calcite cemented concretions) to 10.8% with a mean of 3.5%. Oxygen isotope analyses of quartz overgrowth were performed using the mass balance technique of Milliken et al.1981. The most obvious trend from our quartz data is that $\delta^{18}O$ of quartz overgrowths varies from the top to the bottom of each well. In each case the $\delta^{18}O$ values gets lower with increasing depth. We conclude that all overgrowths in any one well can not have precipitated from a single porefluid. Thus overgrowths in the shallow reservoir sandstones have precipitated from an isotopically different fluid (basinal $\delta^{18}O$ = +4‰SMOW) than overgrowths formed in the deeper reservoir sandstones (evolved meteoric -7 to +4‰SMOW). The greatest volume of quartz is interpreted to have precipitated at temperatures between 70°C and 110°C (2.3 to 3.7km). Temperatures were possibly hotter along the stratigraphic top of the sandstone aquifer, due to a finger of warm, basinal fluid flowing out and up from the basin towards the western boundary fault of the Viking Graben. Cementation occurred between (55 to 20Ma) Eocene to Mid Miocene. We suggest that quartz cementation occurred most rapidly during periods of overpressure release. Volumes of quartz cement are not different in the distinct porewaters.

3.2 INTRODUCTION

Cementation of reservoir sandstones by quartz is an important and common diagenetic process that as of yet is not fully understood. Many different and opposing interpretations have been made concerning the origins of quartz cement, timing of cementation, controls on cement distribution and the hydrologic conditions which transport the silica to the site of cementation. These unresolved problems were recently reviewed by McBride (1989) and he concluded that more quantitative case studies were necessary in order to establish a set of rules that govern quartz cementation.

This study of the South Brae reservoir sandstones provides an opportunity to address some of these questions. In this study, we have tried to evaluate the porewater present and its temperature. This has been achieved by $\delta^{18}O$ isotopic analysis of diagenetic overgrowths, paleotemperature measurements from fluid inclusions, and comparison of the paragenetic history with subsidence curves. We have also tried to evaluate the influence of the depositional environment and facies, grainsize, sorting and depth on quartz cementation. Using point count data we have attempted to estimate the amount of internally derived silica compared with the volume of silica imported from outside. We have also tried to determine the controls of silica distribution throughout the formation and relate this to the geometry of the fan and the channels within.

In the South Brae reservoir sandstones the well formed syntaxial authigenic quartz overgrowths reduced the primary porosity, but they have also helped preserve the porosity by mechanically strengthening the reservoir and preventing further compaction. This has also helped maintain an open network of pores for fluid migration. Extensive formation of quartz overgrowths which have become large enough to have destroyed reservoir quality is limited to the thinner sandstones which occur in predominantly shaly sequences.

The South Brae Formation is a submarine fan sequence comprising of conglomerates, sandstones and mudstones (Fig.3.1.). The sandstones petrographically examined and isotopically analysed in this study were from Facies 3 (medium to thick bedded sandstone) and Facies 4 (alternating thin bedded sandstone with interlaminated sandstone and mudstone) (Sect. 1.6). These sediments were deposited from turbidity currents of varying magnitudes in a marine environment (Turner et al. 1987). Following visual examination of core and thin sections, the samples chosen for isotopic analysis had the best developed diagenetic secondary overgrowths.

Oxygen isotope analysis ($\delta^{18}O$) of the authigenic quartz overgrowths is an important tool for constraining the temperature at which they were precipitated and the porefluid conditions at the time of their formation. Because in-situ isotopic analysis is still at an experimental stage, it is still necessary to physically separate or etch the detrital grain and the secondary overgrowth for analysis. The method used is similar to the technique described in Milliken et al. (1981).

The principal aims of this study were to measure the oxygen isotope compositions of quartz overgrowths from each of four wells (A3, A11, A19 & A27) which form a dip cross section through South Brae (Fig.3.1.). We then wanted to determine whether there is any systematic variation in isotopic composition between wells, with depth and reservoir zones. We subsequently attempted to determine the range of conditions under which the quartz authigenic phase could have formed using the measured isotopic data and equilibrium isotopic factors. We constrained these conditions further by integrating the data with cement stratigraphy and temperature estimates based on fluid inclusion measurements.

3.3 GEOLOGICAL SETTING & BURIAL HISTORY

In the South Brae Oilfield (Fig.3.2.) the reservoir sequence is the Brae Formation, it is of Upper Jurassic age and comprises thick units of sand-matrix conglomerate and sandstone, alternating with other thick units of mudstone and sandstone (Fig.3.1.). These sediments are commonly combined into large-scale fining upward sequences (Turner et al. 1987). The South Brae reservoir sequence is interpreted to have been deposited as the proximal part of a complex submarine fan system (Turner et al. 1987). These submarine fan sediments were deposited as syntectonic graben fill and they are overlain by, and laterally equivalent to the organically rich hemipelagic mudstones of the Kimmeridge Clay Formation (Roberts 1991). The South Brae reservoir rocks are the product of erosion of Devonian sandstones and possibly also younger sediments of the adjacent Fladen Ground Spur (Stow et al. 1982). In three dimensions, the coarse-grained

packages often occur as channel-like bodies which radiate basinward (becoming less conglomeratic and more sandy), these are separated by fine-grained interchannel areas (C.Turner, Marathon *pers. comm.* 1991) (Fig.3.3a & 3.3b.) .

Following deposition of the Upper Brae Formation as late stage graben fill, movement along the main boundary fault associated with antithetic faulting and differential compaction of the coarse clastic sequence led to the development of the South Brae structure in the early Cretaceous. Continued subsidence of the graben through the late Cretaceous and Tertiary was accompanied by a progressive transgression, this led to the deposition of thick sequences of marls, limestones and sandstones over a broad basin extending far beyond the South Viking Graben. Some re-activation of the graben margin faults led to the uplift of the graben flanks during the Paleocene. A subsequent widespread transgression occurred during late Palaeocene to early Eocene which resulted in flooding of the uplifted flanks. Hydrocarbon generation from the Kimmeridge Clay Formation began during the late Cretaceous or early Tertiary and continues to the present (Mackenzie et al. 1987).

A combination of lithostratigraphic, structural, biostratigraphic and reservoir pressure correlation techniques has been utilised by Marathon to delineate 4 major Zones in South Brae. Four reservoir zones have been designated A, B, C and D. Zone A is made up of the Upper Brae Formation, Zone B the Middle Brae Formation and Zones C/D make up the Lower Brae Formation. Each of these major zones has been subdivided into layers (eg.Aa, Ab, Ac and Ad), and sublayers (eg. Aa1, Aa2, Aa3) see Figure 3.4. This refined lithology

distribution should facilitate more accurate modelling of fluid flow in the reservoir as the zones are thought to follow the depositional stratification.

3.4 PETROGRAPHIC METHODS

Forty thin sections from four wells (16/7a-A3, 16/7a-A11, 16/7b-A19 & 16/7a-A27) from the South Brae field were examined using a standard polarizing microscope. The samples were impregnated with blue epoxy resin to highlight existing porosity and were then sectioned perpendicular to bedding. They were point counted with a minimum of 500 counts per section in order to determine modal percentages of detrital grains and authigenic cements, the same samples were also point counted for varying degrees of grain contact to try and determine quantitatively the degree of intergranular pressure solution. Textural relationships were examined in detail using a Cambridge Stereo Scan 360 Scanning Electron Microscope (SEM) equipped with a LINK energy dispersive analyser (EDS), cathodoluminescence analyses were performed on the SEM with a Monochrome Oxford Instruments CL. Bulk sandstone and mineral separate mineralogy analyses were accomplished using a Philips X-Ray Diffractometer (XRD).

Oxygen isotope analysis requires approximately 10mg of quartz sample, this was loaded into nickel reaction vessels, which were then outgassed at high vacuum at 250°C for one hour. The oxygen was liberated from the samples by oxidation reaction with ClF_3 (Borthwick & Harmon 1982) at 650°C. The oxygen was purified and reduced to CO_2 using a vacuum extraction line similar to that

described by Clayton & Mayeda, (1963). The CO_2 gas was analysed on a VG-SIRA 10 mass spectrometer and $\delta^{18}O$ compositions of the quartz are quoted relative to SMOW (Standard Mean Ocean Water). The oxygen yield for each sample was calculated by comparing the initial weight of the sample with the number of micromoles of gas produced. The replicate analysis of inter-laboratory standard NBS#28 produced an average $\delta^{18}O$ value of 9.9‰±0.31 (SMOW).

3.5 DETRITAL MINERALOGY

The sandstones examined from the South Brae reservoir formation are mainly quartz arenites (Fig.3.5.). Quartz is the most abundant component of these rocks, forming from 27 to 85% of the detrital mineralogy. Monocrystalline quartz is the dominant type but polycrystalline quartz grains are present and constitute up to 5% of the samples examined. As would be expected, the polycrystalline varieties become more common as grain size increases. In some of the coarser sandstones small quartz granules and pebbles are common. Feldspar comprises 0 to 5% of the total composition and is therefore only a minor component. K-feldspar is the most common type of feldspar in these sandstones, although small amounts of plagioclase have been found. Muscovite and a few heavy minerals namely zircon, apatite, rutile and sphene occur in trace amounts. Rock fragments are mainly clasts of Devonian sandstones and quartzites and some fragments of schists and mudstones.

3.6 DIAGENESIS

The sequence of diagenetic events in the South Brae reservoir (Fig.3.6.) was determined using cement stratigraphy from polarizing microscope, cathodoluminescence, SEM and microprobe studies. The generalized sequence of diagenetic events was minor compaction of the sediments followed closely by early calcite cementation. Following carbonate cementation, minor amounts of pyrite, chlorite and illite formed. These in turn were followed by a long term phase of authigenic quartz precipitation. A dissolution event occurred next, removing some feldspar, fossils and carbonate cement. The final phase was precipitation of late authigenic clays and some small amounts of calcite into the newly formed secondary pores.

3.6.1 Early Cements

Calcite cements were the first to precipitate following deposition of the sediments (McLaughlin et al. Chapter 2). Compaction of the sediments either occurred after the commencement of cementation or perhaps in some cases contemporaneously. The calcite-cemented coarse-grained sandstones and conglomerates, formed concretions observed to range from 0.8 to 4.0m in diameter. The cement is poikilotopic and the detrital grains have an open texture and appear to float within the concretions. The volume of cement increases from the margins to the centres ranging from 19 to 45%. The decrease in the volume of cement present in the concretions is due to continuing compaction over time. Some authigenic pyrite was seen as framboids within the concretions, its formation is contemporaneous with calcite precipitation. The fluid which precipitated the calcite cement

simultaneously leached detrital quartz and feldspar grains and shell fragments in the surrounding areas. The detrital quartz grains were only slightly etched but the feldspar grains and the shell fragments in places were totally replaced by calcite. Estimates of precipitation temperatures for the (early I & II) calcite cements range from 11 to 70°C at burial depths of 0.3 to 2.3km from a meteoric fluid (see Chapter 2 for further discussion and photomicrographs of early cements).

Authigenic quartz and authigenic clays were not found inside the concretions, but small amounts were found in a number of quartz cemented sandstones. Illite and chlorite were precipitated prior to quartz cementation and were found occasionally as coatings on detrital quartz grains. A few tiny pyrite inclusions were found within quartz overgrowths suggesting that they grew contemporaneous to quartz overgrowth formation.

3.6.2 Quartz Cement

Post depositional authigenic quartz overgrowths were observed in most samples and serve as a primary cement. The volume of quartz cement in the South Brae sandstones ranges from 0 to approximately 11% (Fig.3.7.). Overgrowths have reduced the primary porosity, but they have also prevented further compaction by strengthening the sandstones - this is particularly common in the the coarse-grained sandstones. The finer-grained sandstones suffer more compaction effects and quartz overgrowth formation is usually quite extensive (Fig.3.8.).The overgrowths range in size from individual tiny crystal euhedra of 5-30μm to grain rimming cements 60μm thick (Fig.3.9.). Large euhedral overgrowths have been observed protruding into

secondary pores (Fig.3.10.), and overgrowths on the quartz granules and pebbles in the coarser sandstones are also quite common.

A few very small overgrowths were found on quartz grains within a calcite cemented concretion which could imply that there was a small time overlap of quartz and calcite cementation. Because these overgrowths are commonly abraded they are more likely to be predepositional and these overgrowths and their detrital grains may be imported form the original source area. The quartz cementation event was widespread and long term although most of the authigenic quartz overgrowth formation appears to have ceased prior to a dissolution event as evidenced by dissolution pores with no quartz overgrowths protruding into them (Fig.3.11.), occasionally we find quartz overgrowths terminating in secondary pores. In some of the thin sections there are small porous areas with no quartz overgrowths which indicates that calcite previously existed in these areas and inhibited overgrowth development. The calcite cement was then later removed by later dissolution.

Quartz overgrowths develop by precipitation of silica from aqueous solution, producing well ordered, low alpha quartz (McBride, 1989). Quartz overgrowths form in optical continuity and with the same crystallographic orientation as the detrital cores, this is also the case for the polycrystalline quartz and the quartz pebbles. In thin section quartz overgrowths can be identified by their prismatic terminations (if space permits their development), but most of the overgrowths in the South Brae samples share compromise boundaries or develop triple junctions with adjacent grains (Fig.3.12.). Usually the authigenic quartz can be distinguished by its 'clean' appearance

compared to the abundant inclusions in the detrital grain. A poorly developed line of small fluid inclusions often occurs along the detrital grain/overgrowth boundary (Fig.3.13.). In some instances the presence of a thin illite rim which coats the detrital grain can be used as an indicator of the detrital grain margin. But these 'dust lines' are not always present making it difficult to distinguish between detrital grain and overgrowth (Fig.3.14.). The percentages in Table 1.3. (point count data) should therefore be considered minima.

Cathodoluminescence of polished thin sections (Fig.3.15.) showed both dark red/brown quartz grains (indicative of a metamorphic source) and blue colours (indicative of a plutonic source, Zinkernagel 1978). The quartz overgrowths were non luminescent. SEM cathodoluminescence studies of the same samples allowed distinction of the authigenic and detrital quartz. The detrital grains luminesced brightly while the overgrowths did not (Fig.3.16.). Quartz cementation was occasionally seen to be polyphase, at least two distinct CL zones were noted (Fig.3.17.). These zones are not abraded, and it seems that there was no hiatus in their precipitation.

3.6.3 Late Cements

Following quartz overgrowth formation a late dissolution event occurred creating variable quantities of secondary porosity. The outer limits of the calcite cemented concretions were dissolved, and carbonate clasts, shell fragments and detrital feldspar grains also suffered varying amounts of dissolution. The most feldspar dissolution occurred in the coarse grained sandstones. Because the earlier quartz overgrowths had prevented intense compaction the enhanced primary porosity of the sediments perhaps allowed the

movement of the leaching fluids.

Subsequent to the formation of the secondary porosity, small amounts of pore-filling kaolinite and illite were precipitated. Some late stage cubic pyrite can also be found in the secondary pores and minor amounts of quartz (Fig.3.18.), calcite and dolomite rhombs have been observed.

3.7 OXYGEN ISOTOPE ANALYSIS OF DIAGENETIC QUARTZ

Oxygen isotope of quartz overgrowth analyses were performed using the mass balance technique of Milliken et al.1981. This involves the analysis of two aliquots, one which consists of the detrital cores and attached overgrowth and the other in which the overgrowths have been at least partially leached away using concentrated hydrofluoric acid. This method requires that the ratio of diagenetic quartz overgrowth to detrital quartz grain in each sample be measured accurately. To achieve this, thin sections were made of each aliquot and they were then imaged using the SEM equipped with a CL. The photographs of the detrital and authigenic quartz were then traced onto paper and image processed with a package called Image 1.41 using an Apple Mackintosh Computer and a Scan Jet Plus Scanner. Later an alternative method was developed to eliminate the use of photographs. The CL SEM images were transferred directly to the Apple Mackintosh Computer, they were then processed using a package called Adobe Photo Workshop which allowed the images to be laser printed. This method proved much faster than the previous technique and the laser printer images were of excellent quality. The oxygen isotopic composition of the quartz overgrowths was

calculated by a mass balance equation.

The interpretation of oxygen isotopic data for authigenic quartz cement may be complicated by certain intrinsic factors. These factors are discussed at length in Fisher and Land (1986) and Brint et al.(1991). The main causes of concern are 1) the $\delta^{18}O$ of the detrital quartz grain may vary up to 1.5‰; 2) calculation of the isotopic composition of the authigenic cement requires an extrapolation from the values of the detrital grain and detrital grain plus overgrowth to the final overgrowth value. Further complications include the problem of inherited overgrowths from earlier sedimentary cycles and distinct growth zones, which can be observed using CL. These zones can represent different temperatures, and porewaters of variable $\delta^{18}O$ values. The technique we use cannot resolve these inherent problems, but the $\delta^{18}O$ values for the quartz cements are probably accurate up to ±2‰. This error is based on the reproducibility of $\delta^{18}O$ to ±.2‰ and a point counting error of 2% for 300 counts (Folk 1974).

3.8 OXYGEN ISOTOPE RESULTS

$\delta^{18}O$ compositions were measured for 24 samples of authigenic quartz for four wells (16/7a-A3, 16/7a-A11, 16/7b-A19 & 16/7a-A27) in the South Brae reservoir and vary from 17.16‰ to 25.3‰ SMOW (Table 3.1.). The initial quartz samples analysed from well 16/7b-A19 were measured for different size fractions, 160-250µm, 250-500µm and

500-1000μm. Slight variations in the calculated $\delta^{18}O$ for the overgrowths existed, the differences ranged from +0.72 to 0.87‰SMOW. The remaining samples analysed measured 250-750μm as this was the most representative size fraction, and it also gave the best reproducibility when the results were extrapolated to 100% overgrowth. Duplicates of each sample were also analysed, samples which had unacceptably low yields and/or poor conversions were discarded. The wide range (17.1 to 25.3‰SMOW) in overgrowth oxygen isotope compositions (Table.3.1) suggests that these values could have been produced by several combinations of porefluid composition and temperature. These conditions can be constrained somewhat by previous quantitative data which indicates that most quartz cement is introduced after sandstones have been buried 1 to 2km and at temperatures of 50°C and greater (McBride 1989).

In South Brae the quartz overgrowths form after the calcite cementation event; in Chapter 2 we calculated that the calcite cements were precipitated at temperatures < 75°C and down to depths of 2.3km. This would imply that the succeeding quartz overgrowths were precipitating from fluids of over 75°C and at depths greater than 2.3km.

The present day bottom hole temperature is approximately 120°C (J.Crane, Marathon *pers. comm.* 1991) the temperature varies between boreholes ie. 127°C in 16/7a-A3 and 113°C in 16/7b-A19, these are probably the highest temperatures and the deepest burial the reservoir has reached. When present day temperatures for a number of South Brae wells were plotted against present day burial depths a large scatter of points resulted, unusually there was no

correlation of depth with temperature (Fig.3.19.). We therefore must presume that some or all of the present day temperatures measured are incorrect and are therefore not entirely dependable. Applying a geothermal gradient of 30°C/km, bottom hole temperatures can be calculated. The bottom of the deepest well 16/7a-A11 (4204.5m) has a calculated temperature of 126°C and the base of the shallowest well (4100.5m) 16/7a-A3 has a calculated temperature of 123°C.

From the paragenetic sequence we know that a dissolution event and a minor late cementation event postdates quartz overgrowth formation, so quartz precipitation was possibly no hotter than 120°C. By combining the quartz oxygen isotope data with the calcite isotope values (pre and post quartz), and homogenization temperatures and salinities for fluid inclusions in the quartz overgrowths we are able to constrain the type of porefluid and temperature of quartz formation.

3.9 OXYGEN ISOTOPE INTERPRETATION

The most obvious trend from our quartz data is that the $\delta^{18}O$ of the quartz overgrowths varies from the top to the bottom of each well. In each case the $\delta^{18}O$ values gets lighter with increasing depth (Fig.3.20.). The range difference of $\delta^{18}O$ for the overgrowth values varies from 3.9‰ to 8.1‰ from the top of the reservoir to the bottom (Fig.3.21.) We are encouraged to accept the validity of this data set as our extrapolated core values fall into a tight cluster (Fig.3.20.), with a mean of 10.7±1.4‰SMOW.

For these overgrowths to have been precipitated from a single fluid, a temperature difference of 20 to 45°C would be required. If we assume

a geothermal gradient of 30°C/km for the South Brae reservoir rocks, then this temperature difference is very high, as the largest sampling interval is a mere 400m. For the overgrowths to have precipitated from a single fluid we would need to invoke a geothermal gradient of 62.5°C/km.

We conclude from these observations that all overgrowths in any one well can not have precipitated from a single porefluid. Thus overgrowths in the shallow reservoir sandstones have precipitated from an isotopically different fluid than overgrowths formed in the deeper reservoir sandstones.

We can impose temperature constraints on the precipitation of the quartz overgrowths from our cement stratigraphy. Calculations show that the early calcite cements were precipitated at temperatures up to 75°C (see Chapter 2), these cements petrographically predate authigenic quartz therefore quartz cementation should occur at even hotter temperatures. Current calculated reservoir temperatures range between 123-126°C, and because the reservoir is presently at its deepest burial this puts a top temperature constraint on quartz cementation.

When the $\delta^{18}O$ of the quartz overgrowths are plotted in their respective reservoir zones for all the wells, we find that there is a grouping of the $\delta^{18}O$ values for individual zones ie. a crude form of compartmentalisation (Fig.3.22.). The overgrowths sampled are from reservoir layers Aa_1, Aa_{2-4} and Ac_1 (Upper Brae) separated from Middle Brae by a major fieldwide shale layer Ad. Layer Ba_{1-4} is a reservoir layer separated from Lower Brae by another shaly interval.

Ca_{1-4} and Cc_{1-3} are also reservoir layers. The shaly intervals are mostly non-reservoir.

The $\delta^{18}O$ overgrowth values for each zone were plotted in a porewater versus temperature plot (Fig.3.23a-i.), we were then able to determine the type of porefluid present in each layer. The $\delta^{18}O$ composition of the water was calculated using the temperature of quartz precipitation derived from the range of homogenization temperatures from fluid inclusions in the quartz overgrowths. The measured $\delta^{18}O$ for quartz cement and the oxygen isotope fractionation equation for quartz-water were determined by Friedman and O'Neil, 1977.

$$(\delta \text{ quartz} - \delta \text{ water}) = 3.38 \text{ X } 10^6 (T^{-2}) - 2.90$$

Where δ quartz = isotopic composition of quartz (relative to SMOW), δ water = isotopic composition of the water from which the quartz precipitated (relative to SMOW) and T = the temperature of formation in degrees Kelvin.

3.9.1. Estimation of quartz growth conditions.

We know that in each of the four wells studied, a vertical trend of increasing $\delta^{18}O$ upwards is seen in the overgrowths (Fig.3.20.). This can not be explained by a down well increase of temperature under equilibrium conductive conditions, with a single evolved fluid. For example a 0‰ porefluid gives ~75°C in the Kimmeridge Clay, but would unreasonably imply ~140°C in zone Cd (Fig.3.23a.). Choosing a more negative $\delta^{18}O$ fluid (-3‰) for the Kimmeridge Clay to limit zone Cd temperatures to present reservoir maximum of 120°C, consequently implies quartz growth below 60°C in the Kimmeridge Clay, which is unreasonably cold (considering its present depth).

Therefore we choose to construct an ad-hoc model to illustrate the temperature and $\delta^{18}O$ porefluid principles which satisfy our data. To do this, we must vary both temperature and $\delta^{18}O$, keep the temperature above 70-80°C and below 120°C, and respect the end member porefluid boundaries of -7 (meteoric) to+5‰(basinal). The most satisfactory model we have produced is one of warm basinal water overlying cooler meteorically-derived water. This model also fits the finishing conditions for calcite cementation of an evolved meteoric fluid, 75°C deduced in Chapter 2 and links to the conditions for secondary porosity development in Chapter 4. Ours may not be the only model, but it is a feasible one. Figures 3.23a-i illustrate feasible interpretations.

<u>Kimmeridge Clay Formation</u>

The overgrowths analysed in the Kimmeridge Clay Formation were from a thick sandstone in 16/7a-A27, they gave $\delta^{18}O$ values typical of overgrowths precipitated from a basinal type fluid (+4‰ SMOW) at temperatures of approximately 105°C (Fig.3.23a.).

<u>Zone Aa_1</u>

$\delta^{18}O$ values were measured for wells 16/7a- A3, A11, A27 & 16/7b-A19. A19 overgrowths are precipitated from a basinal type fluid (+3‰ SMOW) at approximately 119°C. Because A19 is the most distal well, this is where the basinal fluid initially enters the reservoir and is hottest and most focused. As the fluid moves west-ward in this zone it progressively cools and the $\delta^{18}O$ values become lighter as mixing occurs.The overgrowths from A3, A11 and A27 were precipitated from a basinal type fluid at temperatures of

approximately 90° to 105°C (Fig.3.23b.).

Zone Aa_{2-4}

16/7b-A19 has two distinct sets of overgrowth values. The shallowest overgrowths have been precipitated from a basinal fluid at temperatures between 105-107°C, while the lighter and deeper overgrowths (situated beneath a large concretion - forming a possible barrier) have precipitated from a lighter marine type fluid (-2.5‰SMOW) at similar temperatures. Overgrowths in 16/7a-A11 & A3 have also precipitated from a marine type fluid with a possible $\delta^{18}O$ of -2.5 to -1.5‰ (SMOW) at temperatures of 92 and 72°C respectively (Fig.3.23c.).

Zone Ac_1

Overgrowths in 16/7a-A27 were precipitated from a mixed basinal/marine porefluid with a $\delta^{18}O$ of +0.0‰ (SMOW) at temperatures close to 91°C (Fig.3.23d.).

Zone Ad

Overgrowths in 16/7a-A27 have been precipitated from a mixed basinal/marine fluid with a $\delta^{18}O$ of +0.0‰ (SMOW) at temperatures of 92°C, overgrowths in 16/7a-A3 have been precipitated from an isotopically lighter fluid (-2.8‰ SMOW) at slightly cooler temperatures (Fig.3.23e.).

Zone Ba_{1-4}

In 16/7a-A27 the overgrowths have been precipitated from a marine fluid at approximately 93°C, overgrowths in 16/7a-A11 have precipitated at a similar temperature but from an isotopically lighter

fluid with a $\delta^{18}O$ of -3‰ (SMOW) (Fig.3.23f.).

Zone Ca_{1-4}

Overgrowths in 16/7a-A3 have precipitated from a marine/meteoric fluid around 82°C (Fig.3.23g.).

Zone Cc_{1-3}

Overgrowths in 16/7a - A3 have been precipitated from a marine/meteoric fluid at 84°C (Fig.3.23h.).

Zone Cd

The $\delta^{18}O$ values for 16/7a - A11 suggest that they have been precipitated from a marine/meteoric mixed fluid with a mean T_h value of 98°C (section 3.10) and a likely $\delta^{18}O$ value of -4.5‰SMOW (Fig.3.23i.).

3.9.2. Discussion and Model

We assume that overgrowths within these different layers grew at similar temperatures. The maximum temperature range expected from a normal temperature gradient across all these depths would be 15°C. This temperature range is not sufficient to produce the measured variation in overgrowth $\delta^{18}O$ with a single porefluid. For our model we have assumed an initial temperature for the basinal fluid; the first pulse of fluid which entered the uppermost Zone A in the basinward well A19 was most likely the hottest. Using a geothermal gradient of 30°C/km we then calculated the porewater temperatures for the remaining zones (Fig.3.24a.). The examples below assume that quartz grew at temperatures from approximately 105/119°C in KCF and Aa_1, decreasing to 98°C (mean of fluid

inclusion measurements) in Zone Cd. For each of these temperatures, we can deduce a porewater $\delta^{18}O$ in equilibrium (Table.3.2.). End member possible fluids are (-1.2‰) marine (Shackleton & Kennett, 1975), (-7.0‰) meteoric (Hamilton et al. 1987, Hudson & Andrews, 1987) and (+2 to +5.0‰) basinal (Egeberg & Aagard 1989, Wilkinson et al.1992).

The range of overgrowth $\delta^{18}O$ values suggests a possible model of a hot basinal fluid entering the reservoir. In South Brae the basinal fluid cools en route (to the western edge of the graben) due to movement and mixing with interstitial fluids, and quartz cementation occurs. Because Zone A is the most permeable the fluid has passed through this layer first and the overgrowths have the highest $\delta^{18}O$ values, they have been precipitated by a hot, isotopically heavy fluid (+4.0 to +2.0‰ SMOW). As the fluid moves westwards it cools slightly and mixes with interstitial water thus becoming isotopically lighter (Fig.3.24b.). In the deeper less permeable layers the water becomes isotopically lighter due to mixing and consequently the $\delta^{18}O$ overgrowth values are lower (Fig.3.24c.). It is unlikely that silica was carried into the reservoir by the hot basinal fluid as no additional silica cement has been observed along the flow paths, it is more likely that the silica was internally derived. The sources of silica are discussed in 3.11.

3.10 FLUID INCLUSION ANALYSIS

Fluid inclusion studies on quartz overgrowths provide us with information on the temperature, salinity and composition of the diagenetic fluid which precipitated the authigenic quartz. Only

primary two phase aqueous liquid-vapour fluid inclusions were observed (Roedder, 1984), no hydrocarbon fluid inclusions were found. Some of the quartz grains had prominent dustrims, others did not. These dustrims largely consist of fluid inclusions, although most of the inclusions are too small to enable homogenization temperature measurement.

Fluid inclusion measurements were made on a Linkam Th 600 heating/freezing stage used in conjunction with a Leitz- Dialux 20 - EB binocular microscope fitted with a long working distance condenser lens at magnifications of x1250. Homogenization temperatures, salinities and eutectic measurements were made on inclusions lying along the boundary between the overgrowth and the detrital grain. Most of the inclusions measured had diameters greater than 5μm but less than 10μm. All measured inclusions were isolated, with no signs of necking or decrepitation.

In well 16/7a-A11 at 13791'4" (T.V.D.) twenty five T_h measurements were made on inclusions which came from a single quartz grain (Table 3.3.). The temperatures ranged from 82°C to 114°C with a mean of 98.2°C (Fig.3.25.). A T_e value ranging between -40 to -30°C implies the porefluid was a NaCl-$MgCl_2$ salt system mixture (Crawford, 1981). The final melting of ice (T_m)values range from -10 to -7°C which gives calculated salinities of 10.5-13.9 wt% eq. NaCl (Potter, 1977).

Haszeldine & Osborne (1993) have inferred that homogenization temperatures in quartz can be reset over geological time, so that the coolest temperatures measured may best approximate the temperature of quartz growth. Thus the entrapment of the earliest

(and coolest) inclusions in the quartz overgrowths gave temperatures which started at 82°C, suggesting that the quartz cementation could have started at approximately this temperature. The lowest inclusion temperatures are in accordance with our cement stratigraphy ie. maximum calcite cementation occurred at 75°C with quartz precipitation immediately following. The highest T_h temperature is 114°C which is just slightly cooler than the current reservoir bottom hole temperature in this well (117.2°C) at 13921' (T.V.D.S.S.). The $\delta^{18}O$ values for the overgrowths in this zone and the average homogenization temperature, allow us to postulate that the porefluid was a mixed marine/meteoric fluid. This prediction also correlates with our fluid inclusion temperature and salinity measurements.

The pH of present day South Brae formation brine has been estimated by Marathon to be between 4.5 and 4.8 (J. Hardy, Marathon *pers. comm.* 1991). Formation water analysis revealed that water composition varies with depth. With increasing depth there is an increase in all the dissolved solids; these include sodium, calcium, magnesium, barium and strontium (see Table 1.2).

3.11 SOURCES OF QUARTZ CEMENT

Sources of silica sufficient to account for the total volume of quartz cement in the South Brae sandstones have not been fully identified, but much of the silica is probably internally derived. The volume of quartz cement ranges from 0% in the calcite cemented concretions to 10.8% in the coarser grained sandstones, but an average of 3.5% is calculated for the wells examined (Fig.3.7.). Four possible silica

sources for this late cement have been identified;

1) dissolution of quartz grains by pressure solution. Pressure solution in South Brae occurs mainly in the very fine grained sandstones, and between contacts of rock fragments (also noted by McBride, Diggs & Wilson, 1988).

2) silica released due to the compaction of interdigitating shales and siltstones. In the South Brae reservoir the shale/sandstone ratio is high with the reservoir layers separated by shales and the whole reservoir overlain by the Kimmeridge Clay Formation. Shaw and Primmer (1991) noted in the Kimmeridge Clay Formation in the Brae area, that quartz grains showed evidence of corrosion yet there was never any evidence of quartz overgrowths. They suggested that the silica had not been locally reprecipitated but had been mobilized, and could be a potential source for quartz cementation in adjacent sandstones.

3) silica liberated during mineral reactions. Feldspar dissolution occurred contemporaneous with the formation of the calcite concretions but prior to quartz cementation, we also noted that the detrital quartz grains within the concretions are embayed and corroded. Later (post-calcite) dissolution of feldspar is particularly prevalent in the top reservoir zones. Quartz overgrowths were found growing into secondary pore spaces so it is possible that late feldspar dissolution may have provided a silica source.

4) silica which may be dissolved in circulating porefluids due to flow over quartz grains in the sandstones (Leder & Park, 1986). Robinson & Gluyas (1992) also noted that dissolved silica is always available in sandstone pores due to equilibrium dissolution of silicate mineral grains and Rimstidt & Barnes (1980) suggested that it is unlikely that porefluids in clastic sequences could remain undersaturated with

respect to quartz for long.

3.11.1. Discussion

Since South Brae lies on the westernmost edge of the Viking Graben (Fig.3.2.), it might be hypothesized that any Graben-wide circulation of hot waters up major faults would be most noticeable here, by analogy with the situation proposed for Tartan which lies on a major E-W fault system (Burley et al.1989). To distinguish between these four sources is not possible with the present data set. However, the layering of the formation water by $\delta^{18}O$, and by salinity and $^{87}Sr/^{86}Sr$ (see Chapter 1) suggests porewaters have also remained layered during the timespan of quartz growth. Additionally, the growth temperatures deduced from $\delta^{18}O$ measurements and from fluid inclusion analyses are compatible with normal burial temperatures. Thus we can exclude large-scale advective transport of silica (Leder & Park. 1986, Burley et al.1989).

All the remaining three options have probably contributed to the South Brae quartz cement

1) Quartz-quartz pressure solution is seen in thin sections (Fig.3.26.) and is estimated to have dissolved 1-2% of the rock. Comparing Figure 3.27. and Figure 3.28. it can be seen that silica dissolution is more intense in finer grained sandstones, and must have been transported to sites of precipitation in coarser sandstones. As the porefluids are, and have been, layered this implies some type of diffusive or ionic drive. Although, pressure solution appears capable of producing almost half of the observed quartz cement, the question of timing of pressure solution relative to quartz cementation remains. Because compaction of the fine-grained beds would have

proceeded faster than that of the coarse-grained beds it is likely that the internally derived silica was available about the time of quartz cementation.

2) Silica released from compaction in mudrocks is demonstrated by the more intense cementation of the KCF sandstone, compared to the sandstone in the main reservoir sequence. (Imagine a short diffusion route to KCF sandstone versus a long route to the main reservoir.)

3) Silica from early (pre and syn concretion) feldspar dissolution has been lost to the system, along with aluminium. Post calcite feldspar dissolution of up to 4%, could have provided 1-2% silica, which fits with the amount of quartz overgrowth seen growing into secondary pores.

3.12. INFLUENCE OF OVERPRESSURE

South Brae is only slightly overpressured (900psi), Buhrig (1989) noted that it is a 'restricted system' (Fig.3.29.). The current formation pressure at 12740ft T.V.S.S. (3884m) is 7128psi (Roberts 1991). Because the field is only slightly overpressured (considering its present depth) it suggests that pressure has been released recently. The overpressure today is probably due to lithostatic pressure build-up of the very rapid 280m of subsidence in the past 2Ma (Fig.3.30.). An additional 1000psi overpressure must be inherited from the immediately preceding ~ 2000m of subsidence during the past 60Ma. Episodes of partial release of overpressure during this timespan would have permitted fluids to drain out of the reservoir. Driven by sediment compaction, they moved upwards and outwards from the surrounding Kimmeridge Clay of the South Viking Graben. These produced the isotopic and temperature layering deduced from the quartz overgrowths. Episodic

quartz cementation related to overpressure release and pressure solution in the Brae sandstone, are likely to be recorded by the incremental growth zonation seen in the quartz overgrowths on CL (Fig.3.17.). After 2Ma, South Brae has become effectively sealed and its porefluids and oil have been temporarily trapped.

Large overpressures minimise grain to grain overburden stress, and so minimise pressure solution. We suggest that quartz cementation occurred most rapidly during periods of overpressure release. The CL stratigraphy seen on a submicron scale is probably a record of this (Fig.3.17.). Luminescent zones in quartz are commonly attributed to variations in aluminium and trace element concentrations (Sprunt 1981, Matter & Ramseyer 1985), but they could also suggest episodic cementation from formation waters of variable composition (Land et al.1987, McBride 1989).

Overpressure release also drains pressure and porefluid from the surrounding KCF basin fill, via permeable aquifers of the Brae Formation Sandstone reservoirs, intimately fingering into the less permeable mudrocks. During overpressure release, these basinal fluids must have flowed laterally out of the Graben via Brae sandstones, and presumably up the western boundary fault of the South Brae Oilfield.

Such fluid would be 1) warmer than South Brae formation waters (coming from deeper in the graben; 2) less saline (having not interacted with so much mica and feldspar) and not been exposed to the saline fluids arriving upwards through the South Brae sands from Zechstein evaporite dissolution deeper at the graben edges.

Thus the expelled KCF graben fluids would be expected to 'float' over the cooler, denser South Brae porewaters. A record of these expelled fluids is seen in the $\delta^{18}O$ profiles deduced from the South Brae aquifers. Here the higher $\delta^{18}O$ basinal fluids occur preferentially towards the top of the South Brae reservoir package, and also occur towards the top of each unit within that package eg. Aa_{2-4} in 16/7a-A19. We envisage a model where basinal porewater layers extend up and out through the aquifers (Fig.3.31.).

It is important to emphasize that no additional silica cement has been observed along these flow paths. This suggests that water moved, but was neither hot enough, nor volumetrically large enough to transport large volumes of silica. Silica sources were decoupled from water sources, and silica was probably derived diffusively from the sources 1-3 listed above in see 3.11

3.13 MODEL FOR QUARTZ CEMENTATION

Petrographic, isotopic and fluid inclusion data all suggest that quartz cementation in the south Brae reservoir occurred under varying temperatures and fluid conditions. We have proposed a simple schematic model for quartz cementation (Fig.3.31.). The hot basinal water which caused quartz precipitation initially fingered into the most porous zone Aa_1, consequently the temperatures for cementation are much higher in this zone than in the deeper zones. The basinal fluid floated through the top of the reservoir as it was hotter and less dense than the interstitial porefluids. As the porefluid moved towards the western margin of the Viking graben it cooled

and became isotopically lighter due to increased mixing with surrounding interstitial porefluids. The overgrowths in the west of the reservoir are isotopically lighter and have been precipitated from a cooler lower $\delta^{18}O$ porefluid. The lower zones were precipitated from a similar evolving basinal fluid which became isotopically light with depth and distance from the centre of the basin. Internal silica sources, as discussed in Sect. 3.11 appear to have been sufficient to supply the total volume of quartz present in South Brae. We believe that the silica did not move on any large scale, but was redistributed on a local scale.

3.14 CONCLUSIONS

1) Quartz cementation succeeded calcite precipitation. The greatest volume of quartz overgrowths were precipitated at temperatures between 70°C to 110°C, at 2.3 to 3.7km burial.

2) $\delta^{18}O$ values for the quartz overgrowths in the four wells have a repeated trend ie. the $\delta^{18}O$ values get lower with increasing depth. It is not possible for these overgrowths to have been precipitated from a single fluid, hence we have invoked a model where the overgrowths were precipitated from a compactional driven fluid moving laterally upwards out of the basin. This gradually mixed with interstitial porefluids to become isotopically lighter and cooler with depth and distance from the basin centre.

3) Internal silica sources appear to have been sufficient to supply the total volume of authigenic quartz present in South Brae. No enhanced silica cement occurs at the reservoir top or base, suggesting

silica transport was decoupled from fluid type and fluid flow.

4) Fluid inclusion studies provided us with precipitation temperatures ranging from 82° to 114°C, these are correlative with the $\delta^{18}O$ overgrowth values and the calculated $\delta^{18}O$ for the porewaters.

5) Quartz cementation occurred most rapidly during periods of overpressure release. Cementation may have been halted due to the reservoir becoming sealed and overpressured, this would have limited fluid movement through the oilfield, and permitted hydrocarbon accumulation to occur.

6) Cementation occurred between the Eocene and Mid Miocene (55-20Ma) when subsidence rates were similar to present day (thermal subsidence).

3.15 ACKNOWLEDGEMENTS

Marathon Oil (U.K.) Ltd. provided the funding for this project and allowed access to their data and core of the South Brae Oilfield. This research was carried out at the Department of Geology and Applied Geology, University of Glasgow, and the Isotopes Geology Unit, Scottish Universities Research and Reactor Centre (SURRC). The authors would like to thank Peter Ainsworth (Glasgow University) for his assistance with mineral separation and SEM piloting. The authors would also like to thank Douglas Maclean (Glasgow University) for his help with the production of photomicrographs.

3.16 REFERENCES

Borthwick, J. & Harmon, R.S. (1982) A note regarding ClF_3 as an alternative to BrF_5 for oxygen isotope analysis: Geochimica et Cosmichima Acta, v.46. pp.1665-1668.

Brint, J.F., Hamilton, P.J., Haszeldine, R.S., Fallick, A.E. & Brown, S. (1991) Oxygen isotopic analysis of diagenetic quartz overgrowths from the Brent sands: A comparison of two preparation methods. Journal of Sedimentary Petrology, v.61. pp.527-533.

Buhrig, C. (1989) Geopressured Jurassic reservoirs in the Viking Graben: modelling and geological significance. Marine and Petroleum Geology, v.6. pp.31-48.

Burley, S.D., Mullis, J. & Matter, A. (1989) Timing diagenesis in the Tartan Reservoir (UK North Sea): constraints from combined cathodoluminescence microscopy and fluid inclusion studies. Marine and Petroleum Geology, v.6. pp.98-120.

Clayton, R.N. & Mayeda, T.K. (1963) The use of bromine pentafluoride in the extraction of oxygen from oxides and silicates for isotope analysis. Geochimica et Cosmochimica Acta, v.27. pp.43-52.

Crawford, M.L. (1981) Phase equilibria in aqueous fluid inclusions, in Short Course in Fluid Inclusions: Applications to Petrology, L.S.

Holliser and M.L. Crawford, eds. Mineralogical Association of Canada, pp.75-100.

Egeberg, P.K. & Aagard, P. (1989) Origin and evolution of formation waters from oil fields on the Norwegian shelf. Applied Geochemistry, v.4. pp.131-142.

Fisher, R.S. & Land, L.S. (1986) Diagenetic history of Eocene Wilcox sandstones, South-Central Texas: Geochimica et Cosmochimica Acta, v.50. pp.551-561.

Folk, R.L. (1974) Petrology of Sedimentary Rocks: Austin, Texas, Hemphill Book Store, 174p.

Friedman, I. & O'Neil, J.R. (1977) Compilation of stable isotope fractionation factors of geochemical interest. In: Data of Geochemistry, sixth edition, M. Fleischer (ed). United States Geological Survey Professional Paper, 440-kk, 12pp.

Hamilton, P.J., Fallick, A.E., Macintyre, R.M. & Elliott, S. (1987) Isotopic tracing of the provenance and diagenesis of Lower Brent Group Sands, North Sea.In Brooks, J., and Glennie, K. (Eds) Petroleum Geology of North West Europe, Graham & Trotman, London, pp.939-949.

Harris, J.P., & Fowler, R.M. (1987) Enhanced prospectivity of the Mid-Late Jurassic sediments of the South Viking Graben, Northern North Sea. In Brooks, J., and Glennie, K. (Eds) Petroleum Geology of North West Europe, Graham & Trotman, London, pp.879-898.

Haszeldine, R.S., & Osborne, M. (1993) Fluid inclusion temperatures in diagenetic quartz reset by burial: implications for oilfield cementation. American Association of Petroleum Geology Memoir. Diagenesis and basin development. In press.

Hudson, J.D. & Andrews, J.E., (1987) The diagenesis of the Great Estuarine Group, Middle Jurassic, Inner Hebrides, Scotland. In J.D. Marshall (Ed.) Diagenesis of Sedimentary Sequences. Blackwell, Oxford, pp.259-276.

Land, L.S., Milliken, K.L., & McBride, E.F. (1987) Diagenetic evolution of Cenozoic sandstones, Gulf coast of Mexico sedimentary basin. Sedimentary geology, v.50, pp.195-225.

Leder, F., & Park, W.C. (1986) Porosity reduction in sandstone by quartz overgrowth. Bulletin of the American Association of Petroleum Geologists, v.70, pp.1713-1728 .

Mackenzie, A.S., Price, I., Leythaeuser, D., Muller, P., Radke, M. & Schaefer, R.G. (1987) The expulsion of petroleum from Kimmeridge clay source rocks in the area of the Brae Oilfield. U.K. In Brooks, J., and Glennie, K. (Eds) Petroleum Geology of North West Europe, Graham & Trotman, London, pp.865-877.

Matter, A., & Ramseyer, K. (1985) Cathodoluminescence microscopy as a tool for provenance studies of sandstones. In: G.G. Zuffa (ed), Provenance of Arenites. Reidel, Dordrecht, pp.191-211.

McBride, E.F. 1963. A classification of common sandstones. Sedimentary Petrology, v.33, pp.664-669.

McBride, E.F. (1989) Quartz cement in sandstone: A Review. Earth Science Reviews, v.26, pp.69-112.

McBride, E.F., Diggs, T.N., & Wilson, J.C. (1988) Compaction of Wilcox and Carrizo sandstones (Paleocene-Eocene) to 4420m, Texas gulf Coast. Journal of Sedimentary Petrology, v.61, pp.73-85.

Milliken, K.L., Land, L.S., & Loucks, R.G. (1981) History of burial diagenesis determined from isotopic geochemistry, Frio Formation, Brazoria County, Texas. Bulletin of the American Association of Petroleum Geologists, v.65. pp.1397-1413.

Potter, R.W. 1977. Pressure correction for fluid inclusion homogenization temperatures based on the volumetric properties of the system NaCl-H_2O. United States Geological Survey Journal of Research, v.5, pp.603-608.

Rimstidt, J.D. & Barnes, H.L. (1980) The kinetics of silica-water reactions. Geochimica et Cosmochimica Acta, v.44, pp.1683-1699.

Robinson, A.G. & Gluyas, J.G. (1992) The duration of quartz cementation in sandstones, North Sea and Haltenbanken basins. Marine and Petroleum geology, v.9. pp.324-327.

Roberts, M.J. (1991) The South Brae Field, Block 16/7a, UK North Sea. Geological Society Memoirs No. 14. From Abbotts, I.L. (ed) United

Kingdom Oil and Gas Fields. Geology Society of London Press. pp.55-62.

Roedder, E. 1978. Experimental evidence that fluid inclusions do not leak. Economic Geology, v.63, pp.715-730.

Shackleton, N.J. & Kennett, J.P. (1975) Paleotemperature history of the Cenezoic and the initiation of Antartic glaciation: Oxygen and carbon analyses in DSDP sites 277, 279,281. In Kennett, J.P. and Howtz, R.E. (eds) Initial Report DSDP 24, Washington. pp.653-659.

Shaw, H.F. & Primmer, T.J. (1991) Diagenesis of mudrocks from the Kimmeridge Clay Formation of the Brae Area, UK North Sea. Marine and Petroleum Geology, v.8. pp.270-277.

Sprunt, E.S. (1981) Causes of quartz luminescence colours. Scanning Electron Microscopy, Part 1, SEM Inc. Chicago. pp.525-535.

Stow, D.A.V., Bishop, C.D, & Mills, S. J. (1982) Sedimentology of the Brae oilfield, North Sea. Fan models and controls. Journal of Petroleum Geology, v.5, No.2, pp.129-148.

Turner, C.C., Cohen, J.M., Connell, E.R. & Cooper, D.M. (1987) A depositional model for the South Brae oilfield, In Brooks, J., and Glennie, K. (Eds) Petroleum Geology of North West Europe, Graham & Trotman, London,pp.853-864.

Wilkinson, M., Crowley, S.F. & Marshall, J.D. (1992) Model for the evolution of oxygen isotope ratios in the porefluids of mudrocks

during burial. Marine and Petroleum Geology, v.9, pp.98-105.

Ziegler, P.A. (1978) North-Western Europe: tectonics and basin development. Geologie Mijnbouw, v.57. pp.589-626.

Zinkernagel, U. (1978) Cathodoluminescence of quartz and its application to sandstone petrology. Contributions to Sedimentology, v.8. pp.1-69.

Chapter 3. Diagenetic quartz cementation- A layered porefluid

Table 3.1. Summary of percentage overgrowth in the un/leached aliquots, the respective $\delta^{18}O$ mineral values and the extrapolated core and overgrowth values for quartz cemented sandstones in the South Brae Oilfield.

Size Fraction	Depth T.V.D.(ft) (M.D.)	$\delta^{18}O$‰ Leached	$\delta^{18}O$‰ Unleached	% Overgrowth Leached	% Overgrowth Unleached	Extrapolated Core $\delta^{18}O$‰	Extrapolated Overgrowth	Reservoir Zone $\delta^{18}O$‰
16/7a-A3								
250-750µm	13444'1" (14755'1")	12.68	14.46	11.80	31.27	11.59	20.78	Cc_{1-3}
250-750µm	13086'2" (14396'2")	13.29	13.99	10.66	29.45	10.20	20.68	Ca_{1-4}
250-750µm	12433'2" (13740')	12.76	13.50	17.44	24.00	10.79	22.07	Ad
250-750µm	12111'5" (13418'5")	13.42	15.50	7.20	25.34	11.75	24.06	Aa_{2-4}
250-750µm	12080' (13387')	13.00	14.92	8.30	22.89	11.90	25.06	Aa_1
16/7a-A11								
250-750µm	13791'4" (15936'4")	11.95	13.24	19.00	39.30	10.73	17.12	Cd
250-750µm	13238' (15387')	13.58	14.70	7.50	9.16	13.19	18.36	Ba_{1-4}
250-750µm	13190'3" (15338'3")	13.97	14.82	26.61	39.21	12.14	18.61	Ba_{1-4}
250-750µm	13164'6" (15312'6")	12.16	13.65	25.45	41.00	9.72	19.30	Ba_{1-4}

Table 3.1. continued.

Size Fraction	Depth T.V.D.(ft) (M.D.)	$\delta^{18}O$‰ Leached	$\delta^{18}O$‰ Unleached	% Overgrowth Leached	% Overgrowth Unleached	Extrapolated Core $\delta^{18}O$‰	Extrapolated Overgrowth $\delta^{18}O$‰	Reservoir Zone
250-750µm	12813' (14958')	12.18	13.20	18.05	28.87	10.47	19.90	Aa2-4
250-750µm	12790' (14935')	12.26	13.37	24.49	34.72	9.76	20.15	Aa2-4
250-750µm	12750' (14895')	12.97	14.51	24.10	33.87	9.14	24.60	Aa1
250-750µm	12712'6" (14875'6")	11.36	12.18	8.13	19.70	10.13	25.29	Aa1
<u>16/7b-A19</u>								
250-750µm	13660'	12.39	12.92	20.28	28.0	10.99	17.88	Aa2-4
160-250µm	13660' (19605')	12.73	13.29	17.34	28.22	11.8	17.16	Aa2-4
500-750µm	13630'	11.79	12.36	21.01	28.37	10.16	17.96	Aa2-4
250-500µm	13630'	12.11	12.81	20.73	30.17	10.57	17.99	Aa2-4
160-250µm	13630' (19567')	12.21	12.90	16.71	25.25	10.88	18.83	Aa2-4
250-750µm	13460'3" (19380'3")	12.24	13.99	10.94	27.74	11.09	21.59	Aa2-4
500-750µm	13415'	13.30	13,50	27.52	31.11	9.69	22.80	Aa2-4
250-500µm	13415' (19337')	13.85	15.46	26.20	39.60	10.67	22.80	Aa2-4

Table 3.1. continued.

Size Fraction	Depth T.V.D.(ft) (M.D.)	$\delta^{18}O$‰ Leached	$\delta^{18}O$‰ Unleached	% Overgrowth Leached	% Overgrowth Unleached	Extrapolated Core $\delta^{18}O$‰	Extrapolated Overgrowth $\delta^{18}O$‰	Reservoir Zone
160-250µm	13415' (19337')	14.08	14.98	24.54	30.70	10.96	23.66	Aa_{2-4}
250-750µm	13355' (19270')	11.75	13.66	15.53	30.40	9.76	22.58	Aa_1
<u>16/7a-A27</u>								
250-750µm	13554'4" (17072'4")	14.03	15.15	21.22	34.06	12.17	20.90	Ba_{1-4}
250-750µm	13413'6" (16929'6")	13.05	15.12	19.28	37.77	10.76	22.60	Ad
250-750µm	13240' (16746')	10.93	13.59	3.06	25.05	10.55	22.65	Ac_1
250-750µm	13061' (19564')	11.24	13.26	6.50	21.33	10.35	23.97	Aa_1
250-750µm	12987' (16490')	11.97	14.00	2.00	16.70	11.84	24.77	Kimm.
250-750µm	12978' (16481')	12.70	14.63	14.78	28.37	10.60	24.80	Kimm.

Table 3.2. Water type from which the South Brae quartz overgrowths have been precipitated. In the Upper Jurassic basinal water had a $\delta^{18}O$ of +4‰ (SMOW), marine water had a $\delta^{18}O$ of -1.2‰ (SMOW) and meteoric water had a $\delta^{18}O$ of -7‰ (SMOW).

Well	Kimm.	Aa_1	Aa_{2-4}	Ac_1	Ad	Ba_{1-4}	Ca_{1-4}	Cc_{1-3}	Cd
A27	basinal +4	basinal +4	-	marine 0	marine 0	marine -1.5	-	-	-
A3	-	basinal +2	marine -1.5	-	mar/met -2.8	-	mar/met -3.2	mar/met -2.8	-
A11	-	basinal +3	marine -2.5	-	-	mar/met -4	-	-	mar/met -4.5
A19	-	basinal +3.5	basinal +2 marine -2.5	-	-	-	-	-	-

Table 3.3.

Fluid inclusion data from 16/7a-A11 South Brae Oilfield. The inclusions came from a single quartz grain, all lie along the boundary between the overgrowth and the detrital grain and measured <10μm in size.

Depth T.V.D. (ft)	(m)	T_h (°C)	Salinity (wt.%eq.NaCl)	T_m (°C)	T_e (°C)
13791'4"	4204.5	109°	10.5-13.9	-10 to -7°	-40 to -30
		94°			
		102°			
		97°			
		86°			
		103°			
		114°			
		106°			
		109°			
		108°			
		86°			
		96°			
		95°			
		89°			
		97°			
		85°			
		99°			
		82°			
		94°			
		90°			
		104°			
		99°			
		108°			
		105°			
		99°			

3.18 FIGURE CAPTIONS & FIGURES

Figure 3.1 Schematic cross section of the South Brae submarine fan, showing approximate position of the wells sampled, 16/7a-A3, A6, A11, A27 & 16/7b-A19.

Figure 3.2 Location of Brae relative to major tectonic elements. The shaded areas contain thick Jurassic deposits (after Ziegler, 1978).

Figure 3.3a Generalized facies map of (Cc) Lower Brae Formation reservoir defined by two apron shaped conglomeratic complexes (after internal Marathon report).

Figure 3.3b Generalized facies map of (Ac) Upper Brae Formation reservoir, made up of channelized conglomerates which are separated by shaly islands (after internal Marathon report).

Figure 3.4. Brae Formation type section well 16/7a-8, a composite fining upwards 'mega sequence' 500m thick, apex upward triangles define the seven reservoir layers (after Harris & Fowler 1987). Also included is the new zonation nomenclature recently defined by Marathon.

Figure 3.5 Framework - grain compositions from South Brae, wells 16/7a-A3, A6, A11, A27 & 16/7b-A19. Classification after Mc Bride, 1963. Point count data in table 1.3.

Figure 3.6 Paragenetic sequence showing timing of major diagenetic events in the South Brae Oilfield.

Figure 3.7 Histogram showing the volume of quartz cement in the South Brae Oilfield.

Figure 3.8 Cartoon to illustrate the difference in the amount of porosity preserved in coarse and fine-grained sandstones.

Figure 3.9 Photomicrograph of grain rimming quartz cement. The overgrowths have distinct geometric edges and in some cases a dust line can be seen which encloses the detrital grain and separates it from the authigenic quartz 16/7a-A27, 13554'4" (T.V.D.).

Figure 3.10 Plane polarized light photomicrograph showing a quartz overgrowth protruding into a secondary dissolution pore, 16/7b-A19, 13410' (T.V.D.).

Figure 3.11 Plane polarized light photomicrograph showing a large secondary dissolution pore which has no quartz overgrowths growing into it, 16/7b-A19, 13405' (T.V.D.).

Figure 3.12 Photomicrograph showing quartz overgrowths form a triple junction, 16/7a-A3, 13444'1" (T.V.D.).

Figure 3.13 Plane polarized light photomicrograph which distinguishes between detrital and authigenic quartz due to the existence of a well developed dustrim, 16/7a-A27, 12987' (T.V.D.) The black interstitial material is bitumen.

Figure 3.14 Plane polarized light photomicrograph showing a distinct lack of dustrims making it difficult to distinguish detrital and authigenic quartz, 16/7b-A19, 13630' (T.V.D.) This sample contains abundant pyritohedrons.

Figure 3.15 Cathodoluminescence photomicrograph showing a rock fragment which contains dark red/brown quartz grains (metamorphic source) and blue quartz grains (plutonic source), 16/7a-A6, 12996'6" (T.V.D.).

Figure 3.16 Scanning Electron Microscope cathodoluminescence photomicrograph of mounted quartz grains, the detrital grain luminesces brightly while the overgrowths are dull, 16/7a-A27, 12978' (T.V.D.).

Figure 3.17 Scanning Electron Microscope cathodoluminescence photomicrograph of polyphase quartz cementation, 16/7a-A11, 13791'4" (T.V.D.).

Figure 3.18 Photomicrograph of late stage calcite cement in which the quartz overgrowths are enclosed, 16/7a-A6, 13462'3" (T.V.D.).

Figure 3.19 Plot showing the bottom hole temperatures measured for a number of South Brae wells against the present day burial depth. The temperatures show no correlation, with depth as would be expected.

Figure 3.20 Plot showing the depths of quartz samples from wells 16/7a-A3, A11, A27 & 16/7b-A19 and their $\delta^{18}O$ core and overgrowth values. While the $\delta^{18}O$ values of the core samples remain constant, the overgrowth values get lighter with the increasing depth.

Figure 3.21 Plot showing the depths of quartz samples, the $\delta^{18}O$ values of the overgrowths and the range of $\delta^{18}O$ change for each well.

Figure 3.22 $\delta^{18}O$ values of authigenic quartz for wells 16/7a-A3, A11, A27 & 16/7b-A19 are plotted in their respective reservoir zones, there exists a broad grouping of $\delta^{18}O$ values for several zones.

Figure 3.23a-i Equilibrium relationship between $\delta^{18}O$ of porewater, $\delta^{18}O$ of quartz and temperature for different zones in the South Brae oilfield. The curved line depicts all theoretically possible combinations of temperature and water composition from which a quartz overgrowth of a given composition could have formed.The straight line depicts the water type which may have precipitated the overgrowths, the arrowed line indicates the temperature at which the overgrowth may have grown. The isotopic fractionation equation used to derive these curves was determined by Friedman & O'Neil (1977).

Figure 3.24a Graph illustrating the four wells analysed and the connecting reservoir zones, with calculated porewater precipitation temperatures. The temperatures for

cementation are contoured. To the east (ie. towards the centre of the basin) the fluid finger is at its hottest, as it travels west towards the graben margin it cools.

Figure 3.24b Graph illustrating the four wells analysed and the connecting reservoir zones, with the calculated $\delta^{18}O$ of the cementing porefluids. The porefluids are isotopically heavy in the upper reservoir zones and isotopically lighter in the deeper zones, particularly close to the western graben margin. The contours are complicated possibly due to the position of the wells in the fan (ie. channel/inter-channel), making the plumbing more complex.

Figure 3.24c Graph illustrating the four wells analysed and the connecting reservoir zones, with the measured $\delta^{18}O$ of the quartz overgrowths. The contour lines appear complex, but there is an overall trend within the four wells. The $\delta^{18}O$ values for the overgrowths get isotopically lighter with depth. The higher shallower values are due to precipitation from a basinal fluid, while the deeper overgrowths have been precipitated from an isotopically lighter mixed fluid.

Figure 3.25 Histogram of homogenization temperatures from fluid inclusions from a single quartz grain in 16/7a-A11; 13791'4" (Zone Cd). The inclusions measured lie along the boundary between the overgrowth and the detrital grain. The values can be found in table 3.3.

Figure 3.26 Photomicrograph showing a shale with quartz-quartz and quartz-chert pressure solution features, 16/7a-A6, 13243' (T.V.D.).

Figure 3.27 Photomicrograph of clay rich siltstone showing silica dissolution between fine-grained quartz grains, 16/7a-A3, 13072'5" (T.V.D.).

Figure 3.28 Photomicrograph of quartz overgrowths in a coarse grained sandstone, there is some slight dissolution between the overgrowths but none between the detrital grains, 16/7a-A11, 12712'6" (T.V.D.).

Figure 3.29 Plot of formation overpressures versus aquifer depth (UK sector) after Buhrig, 1989. South Brae moderately overpressured relative to the hydrostatic gradient.

Figure 3.30 Burial curve for well 16/7a-8 South Brae showing time spans and relevant temperatures of quartz cementation, hydrocarbon generation and overpressure build up. The burial curve has been decompacted and backstripped.

Figure 3.31 Cartoon illustrating the pore-fluid regime existing in South Brae from the Eocene to the Miocene when quartz cementation was taking place. Wavy arrows indicate large flows of basinal fluid entering and penetrating the aquifer. The basinal fluid floats as it is less saline and hotter than the surrounding interstitial porefluids. The short arrows indicate no flow, they represent the diffusion of silica on a small scale.

South Brae

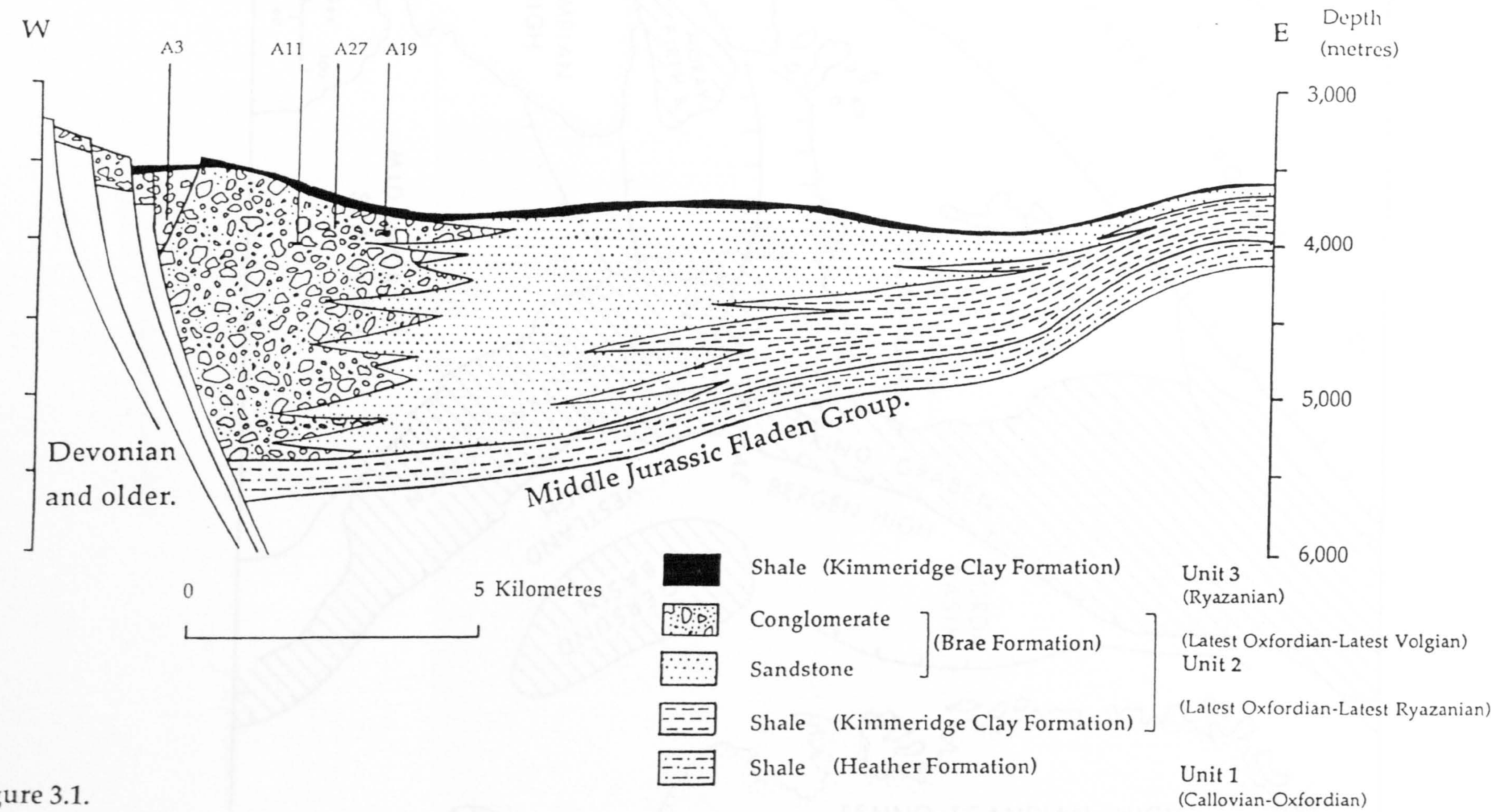

Figure 3.1.

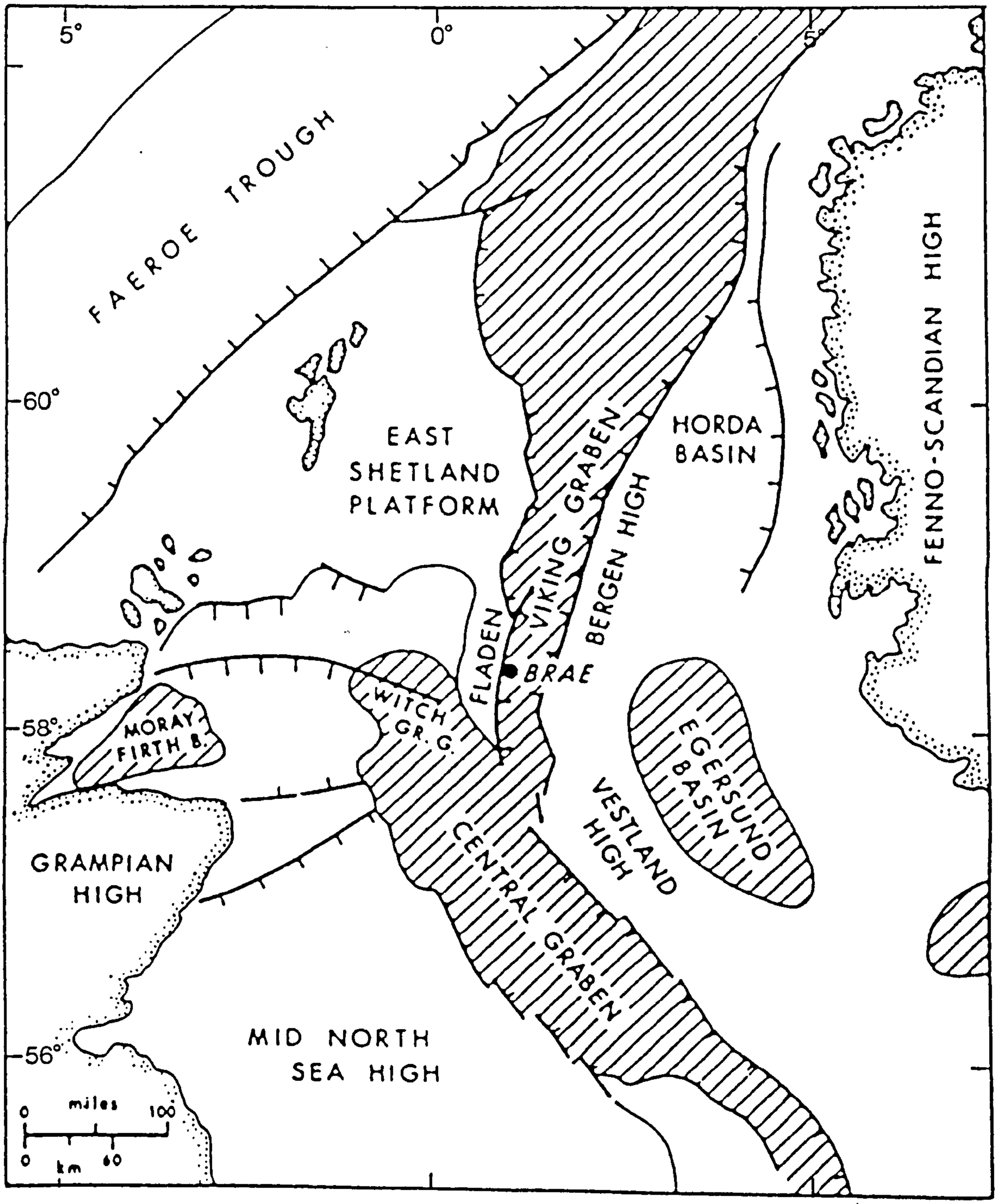
5°
0°
5°
60°
58°
56°
FAEROE TROUGH
EAST SHETLAND PLATFORM
HORDA BASIN
FENNO-SCANDIAN HIGH
VIKING GRABEN
BERGEN HIGH
FLADEN
BRAE
WITCH GR.
MORAY FIRTH B.
GRAMPIAN HIGH
CENTRAL GRABEN
VESTLAND HIGH
EGERSUND BASIN
MID NORTH SEA HIGH
0 miles 100
0 km 60

Figure 3.2.

Lower Brae Formation (Ce) Generalised Facies Map

Fault

16/7a (Marr)

16/12a (Lasmo)

16/12c (Open)

16/7b (BP)

A1

A3

A4

A6

A17

A19

Basement

Shale with Sandstone

Conglomerate

Sandstone

1 mile

1Km

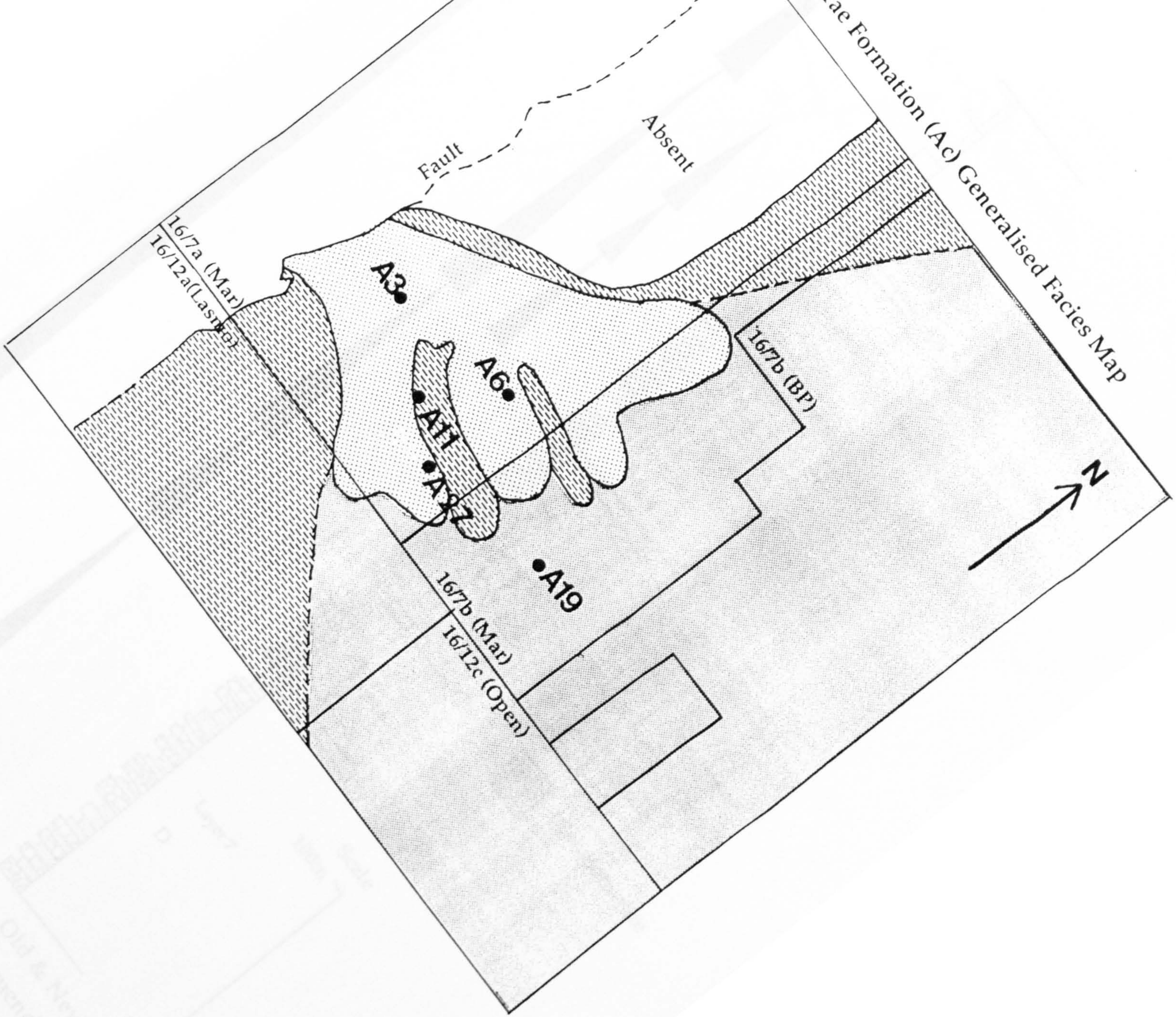

Figure 3.3b. Ae Formation (Ac) Generalised Facies Map

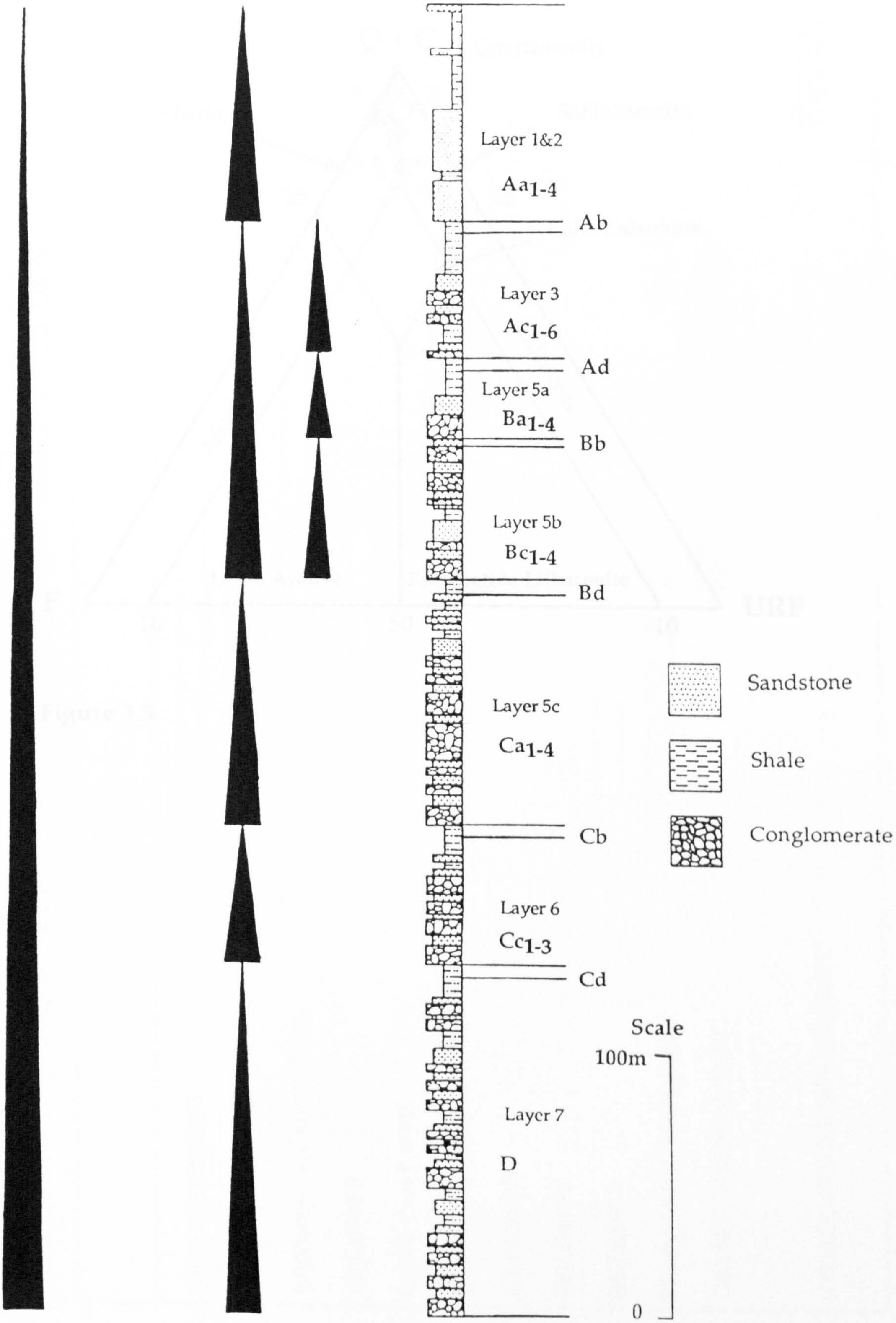
Layer 1&2
Aa1-4
Ab
Layer 3
Ac1-6
Ad
Layer 5a
Ba1-4
Bb
Layer 5b
Bc1-4
Bd
Layer 5c
Ca1-4
Cb
Layer 6
Cc1-3
Cd
Layer 7
D
Sandstone
Shale
Conglomerate
Scale
100m
0
Old & New
Nomenclature

Figure 3.4.

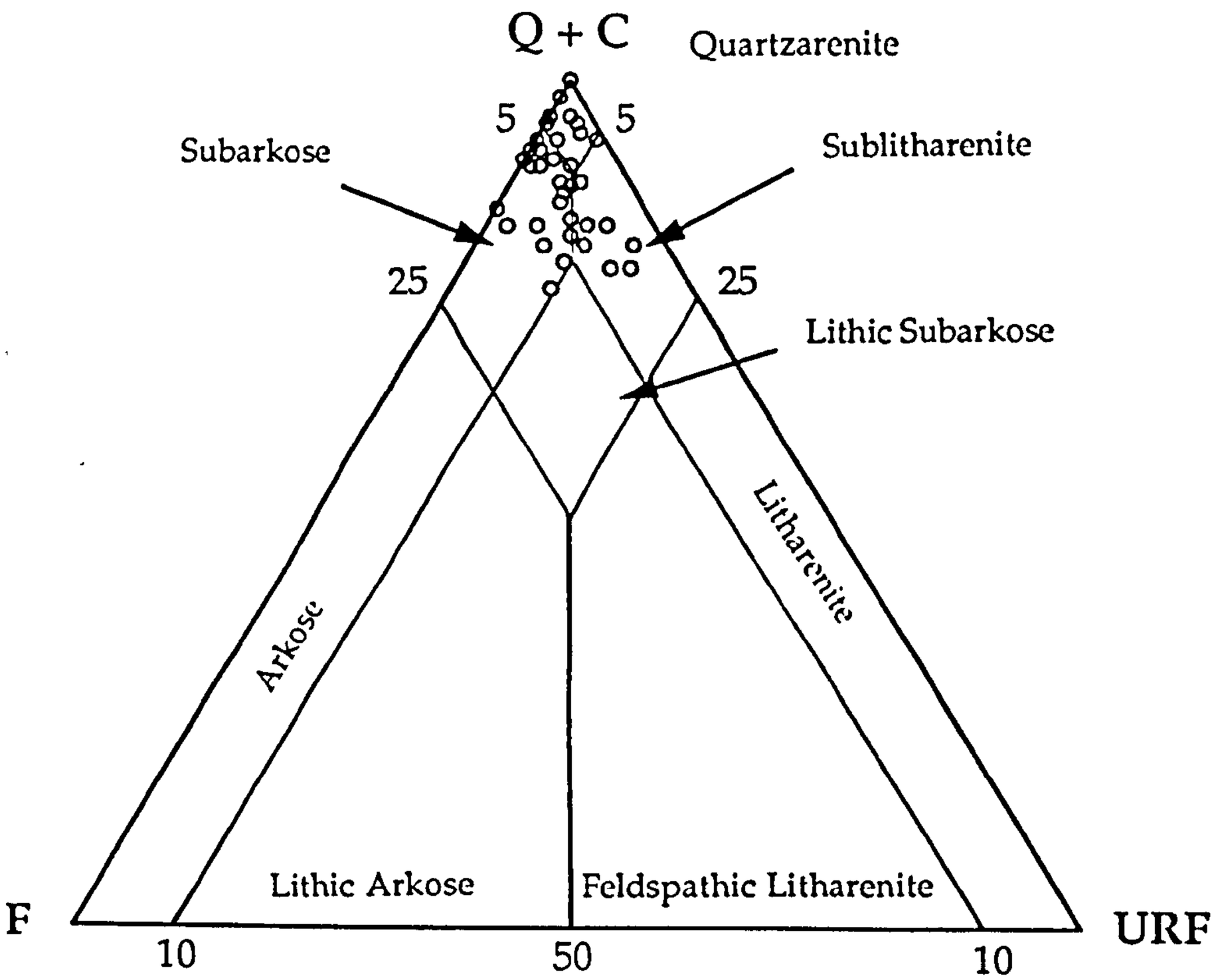
Q + C
Quartzarenite
5
5
Subarkose
Sublitharenite
25
25
Lithic Subarkose
Arkose
Litharenite
Lithic Arkose
Feldspathic Litharenite
F
URF
10
50
10

Figure 3.5.

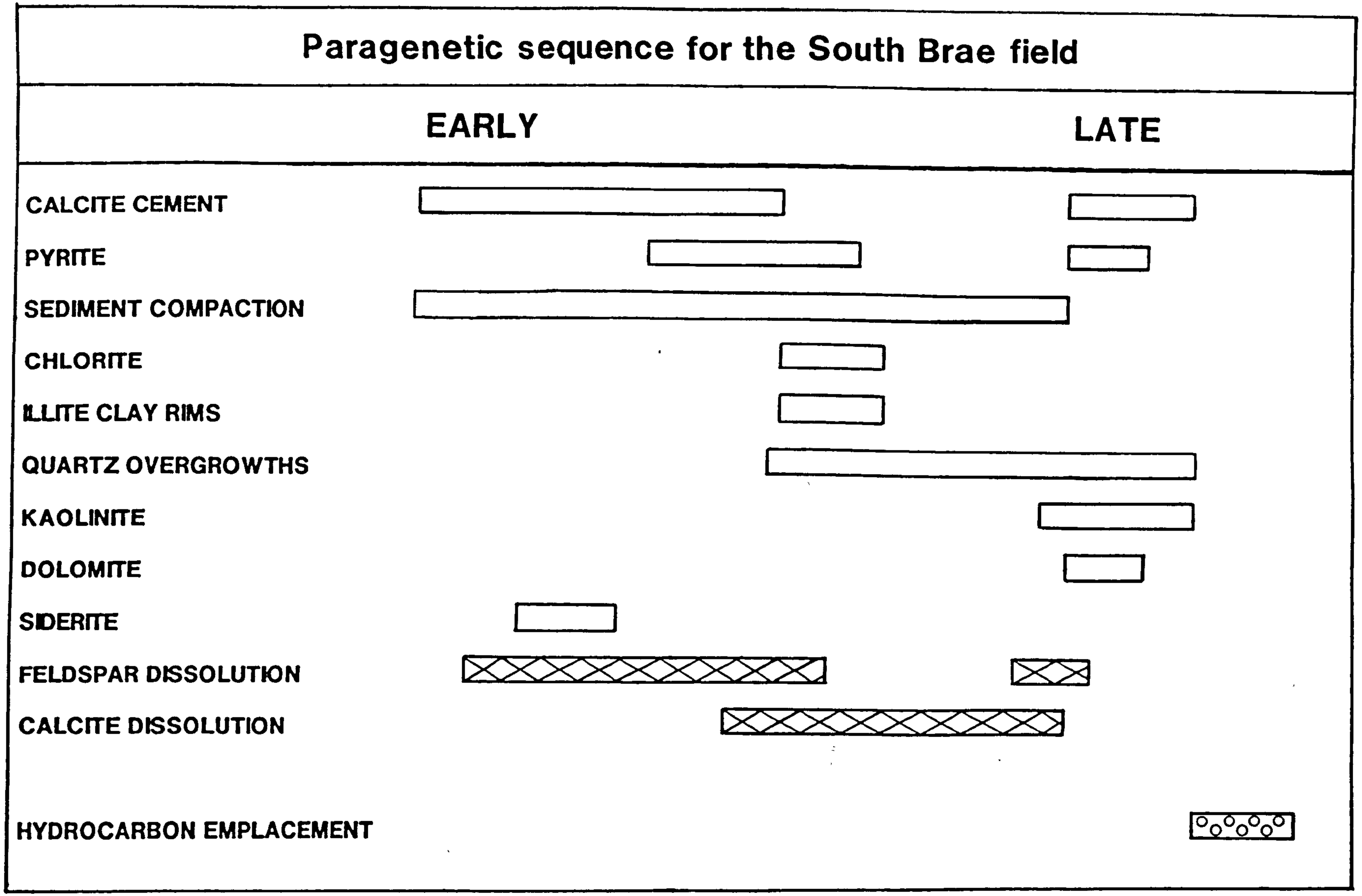
Paragenetic sequence for the South Brae field
EARLY
LATE
CALCITE CEMENT
PYRITE
SEDIMENT COMPACTION
CHLORITE
ILLITE CLAY RIMS
QUARTZ OVERGROWTHS
KAOLINITE
DOLOMITE
SIDERITE
FELDSPAR DISSOLUTION
CALCITE DISSOLUTION
HYDROCARBON EMPLACEMENT

Figure 3.6.

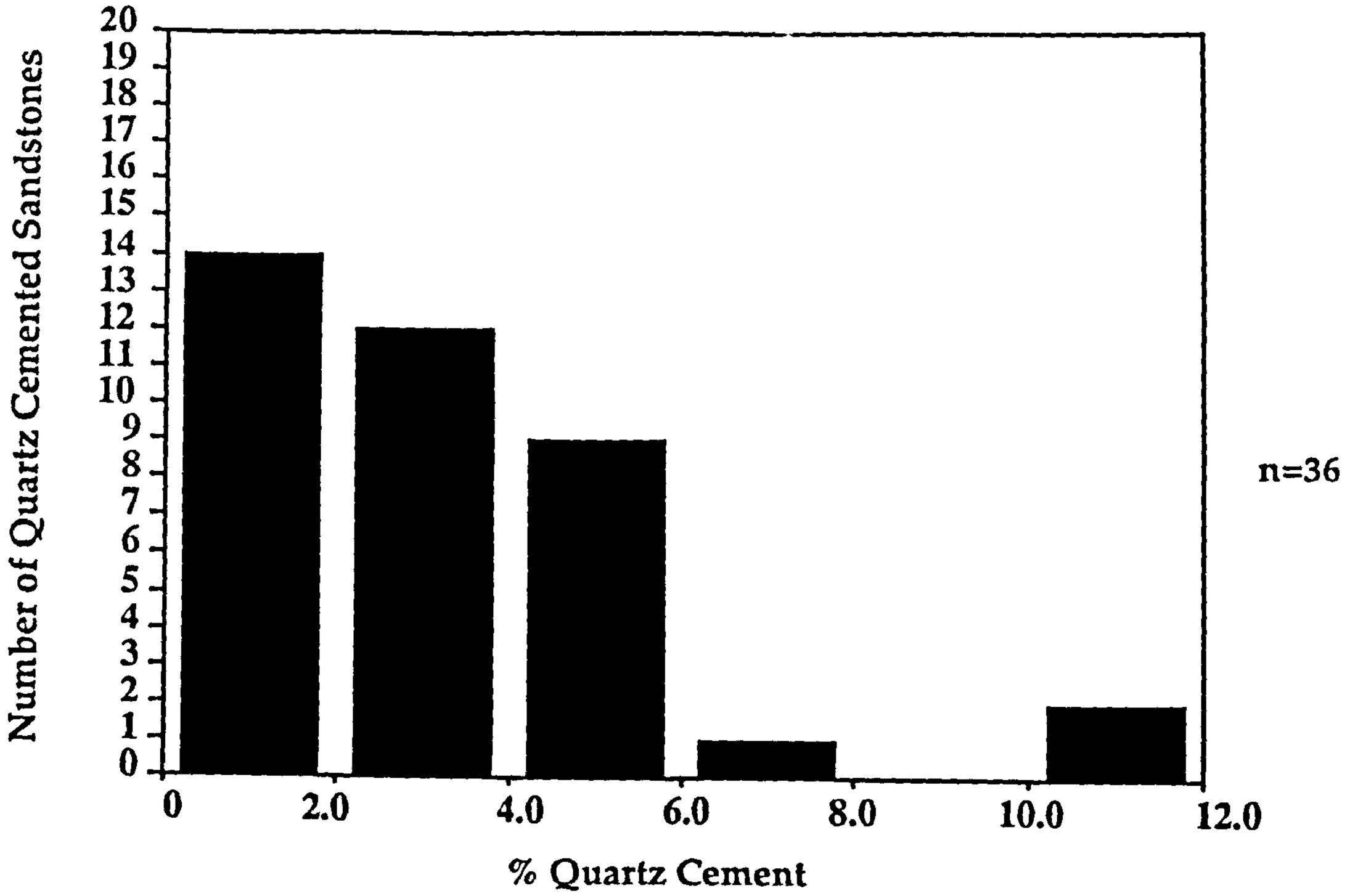
Number of Quartz Cemented Sandstones
20
19
18
17
16
15
14
13
12
11
10
9
8
7
6
5
4
3
2
1
0
0
2.0
4.0
6.0
8.0
10.0
12.0
% Quartz Cement
n=36

Figure 3.7.

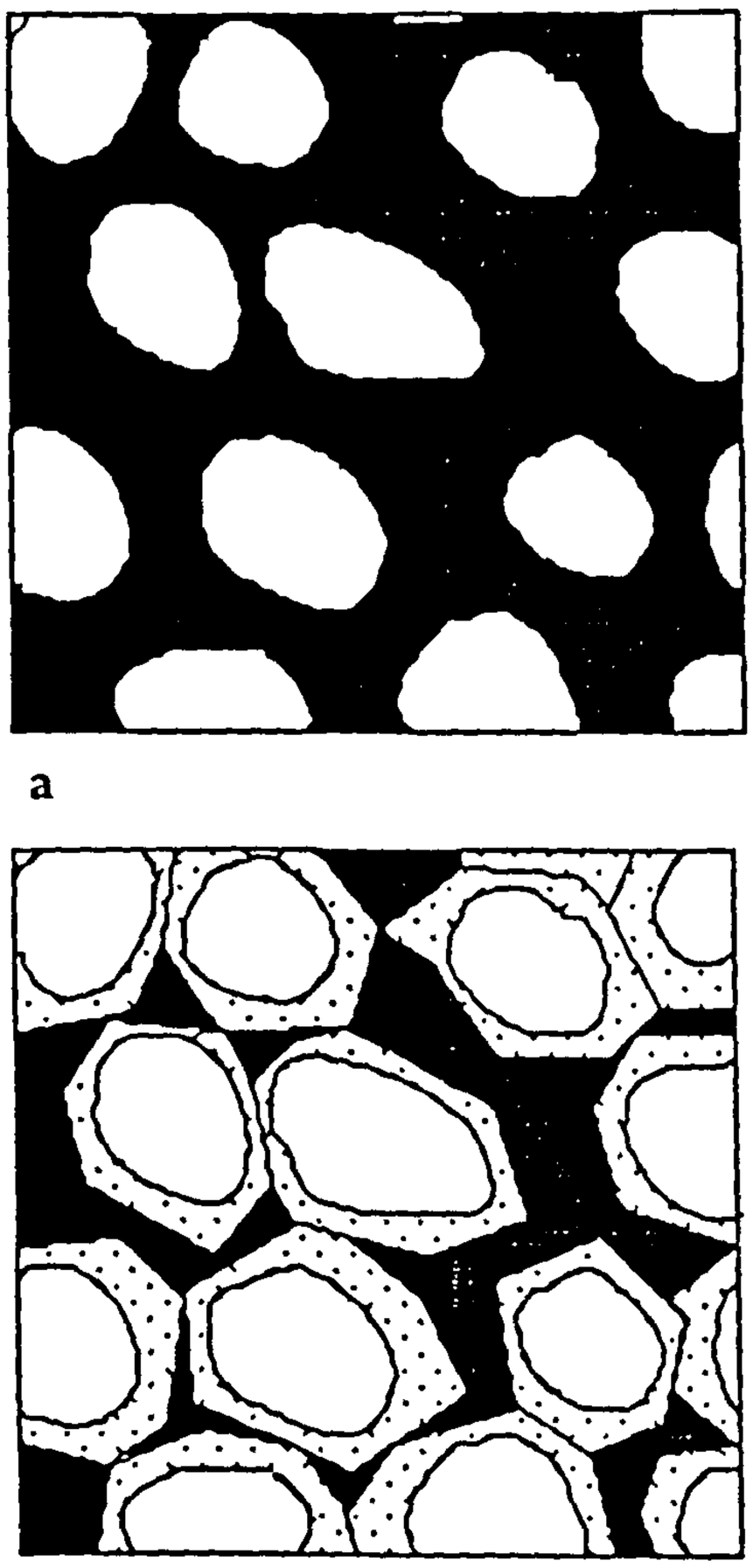

a

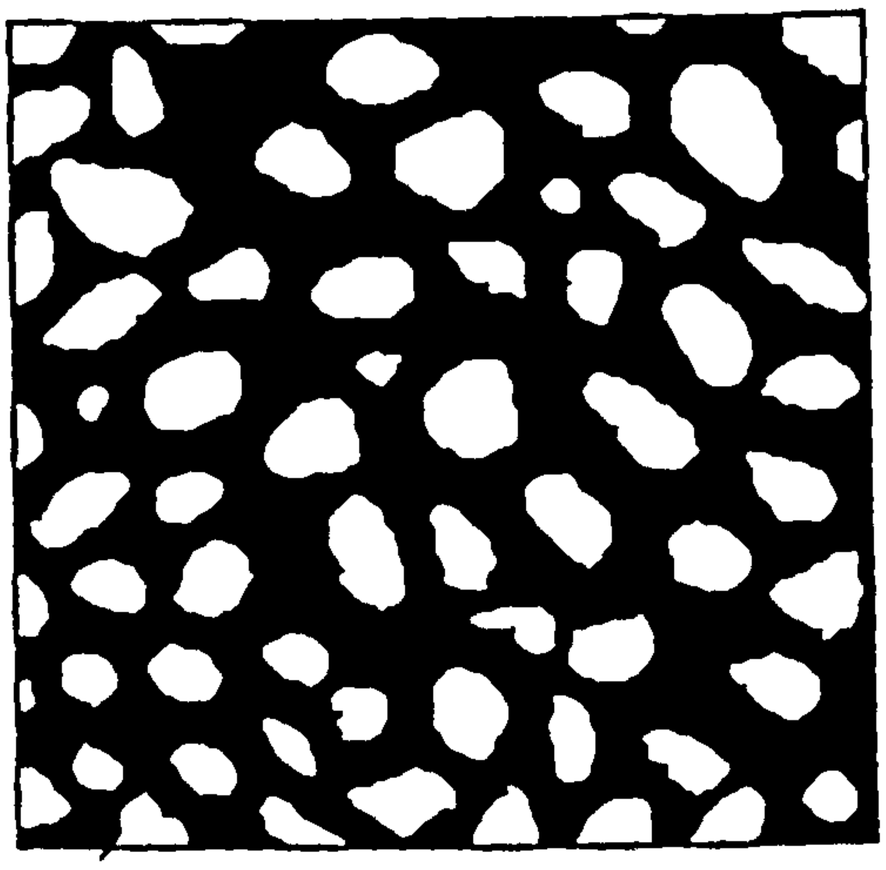

b

c

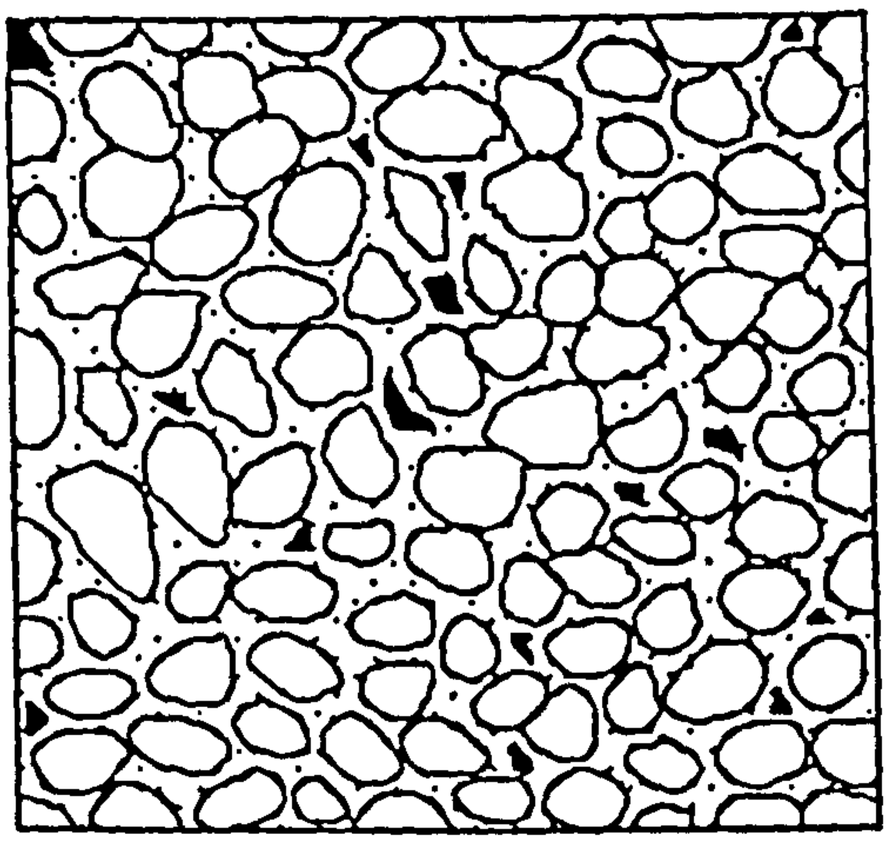

d

0 0.5mm

Figure 3.8.

Primary porosity

Detrital quartz

Diagenetic quartz

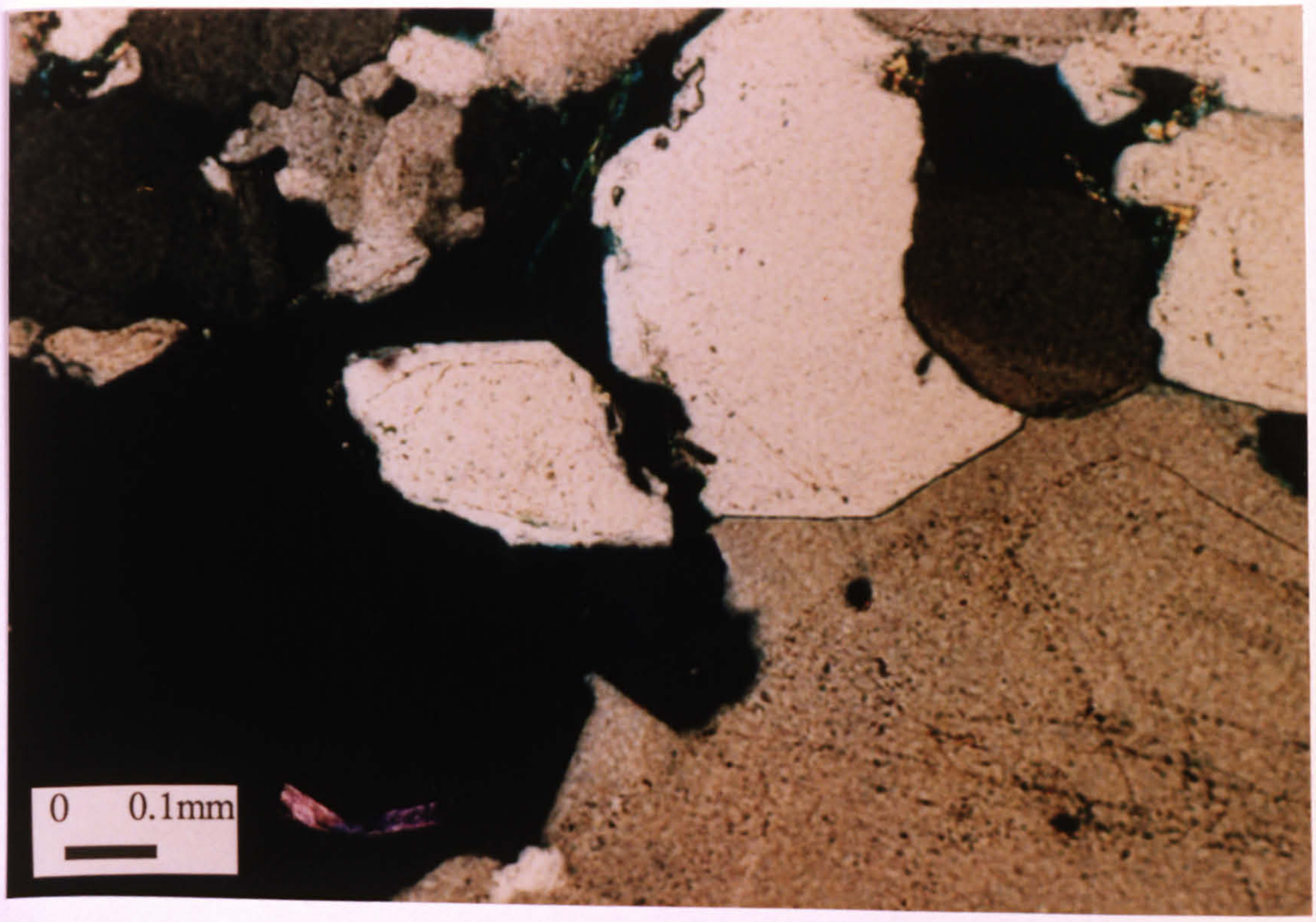

Figure 3.9.

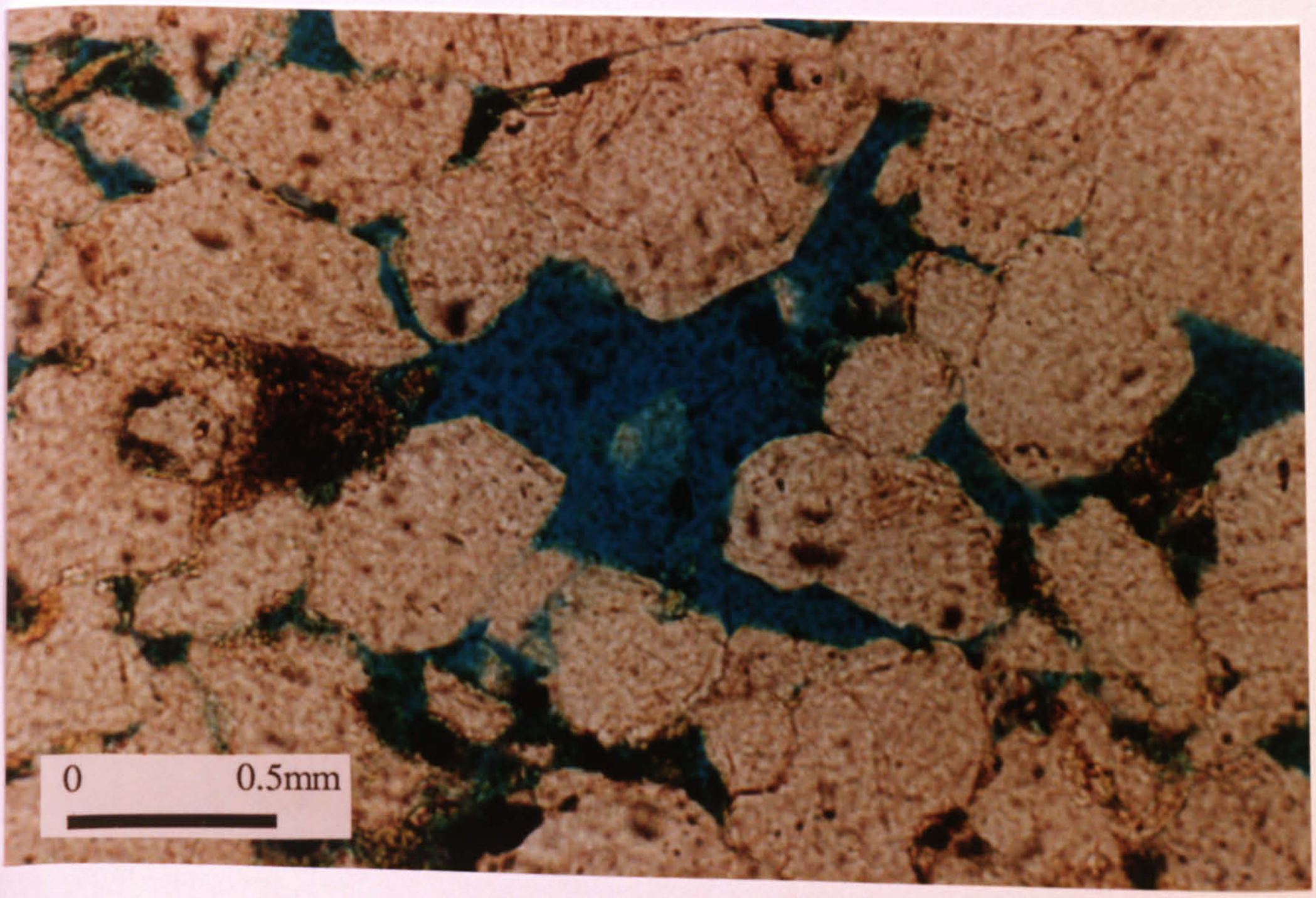

Figure 3.10.

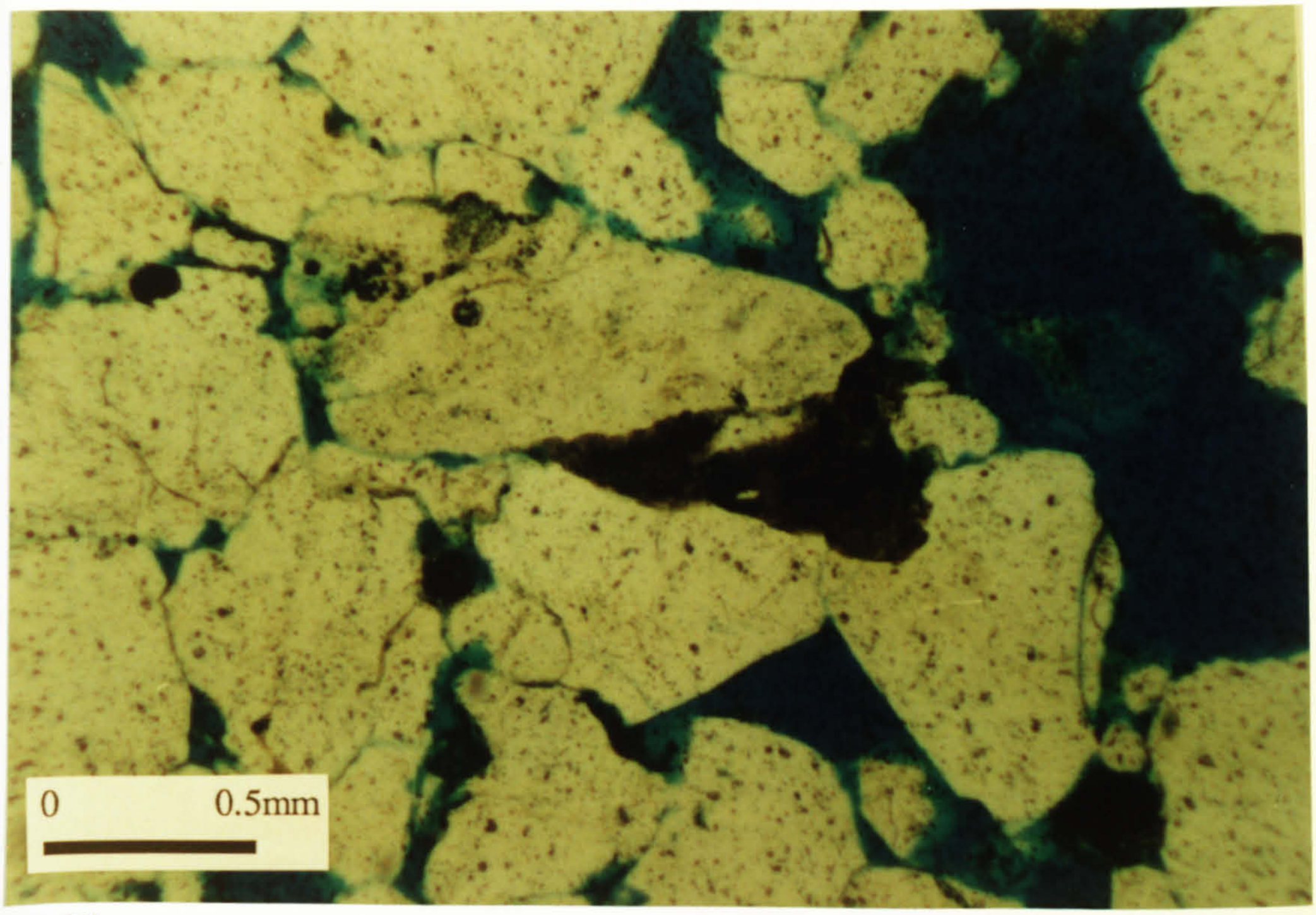

Figure 3.11.

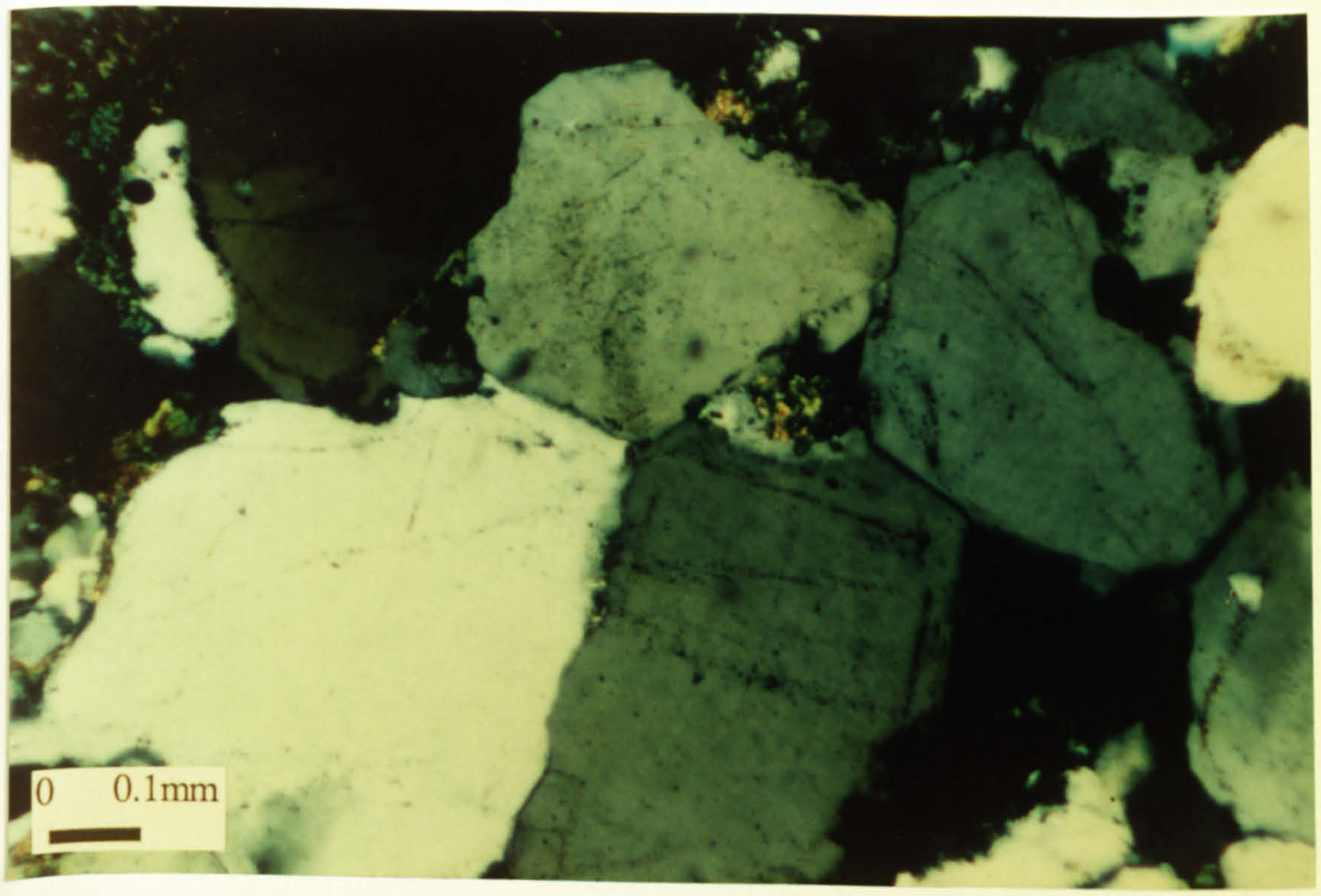

Figure 3.12.

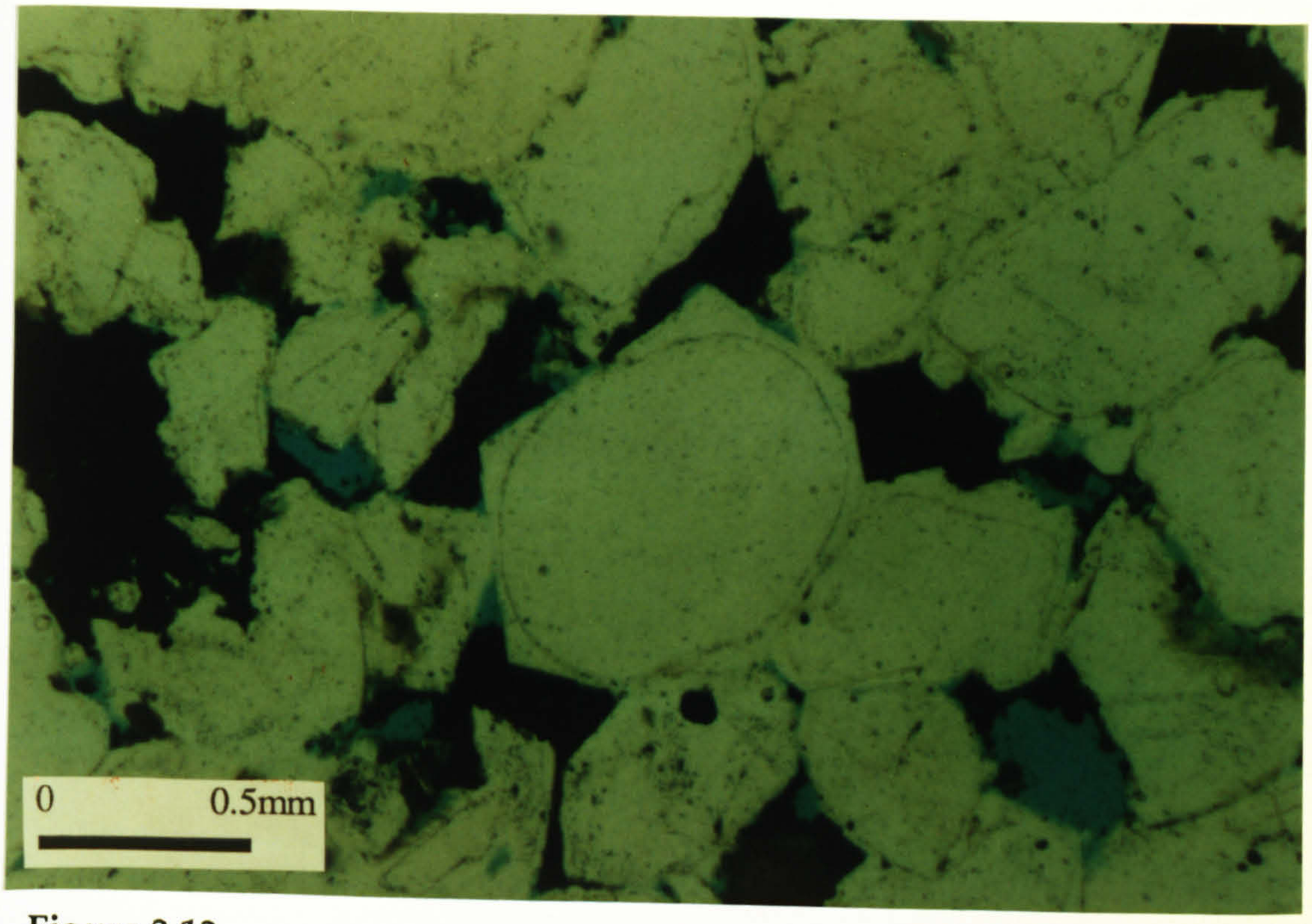

Figure 3.13.

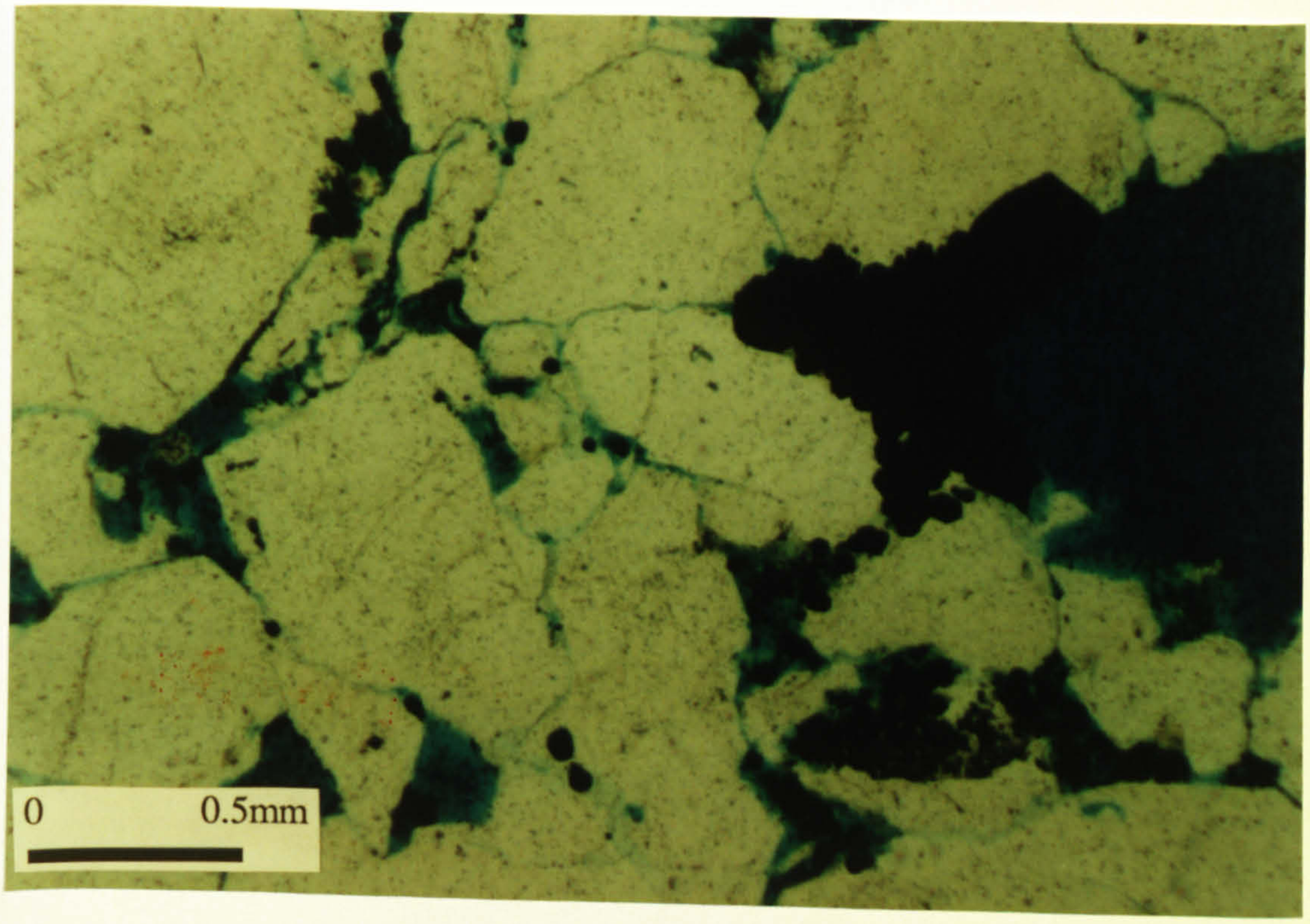

Figure 3.14.

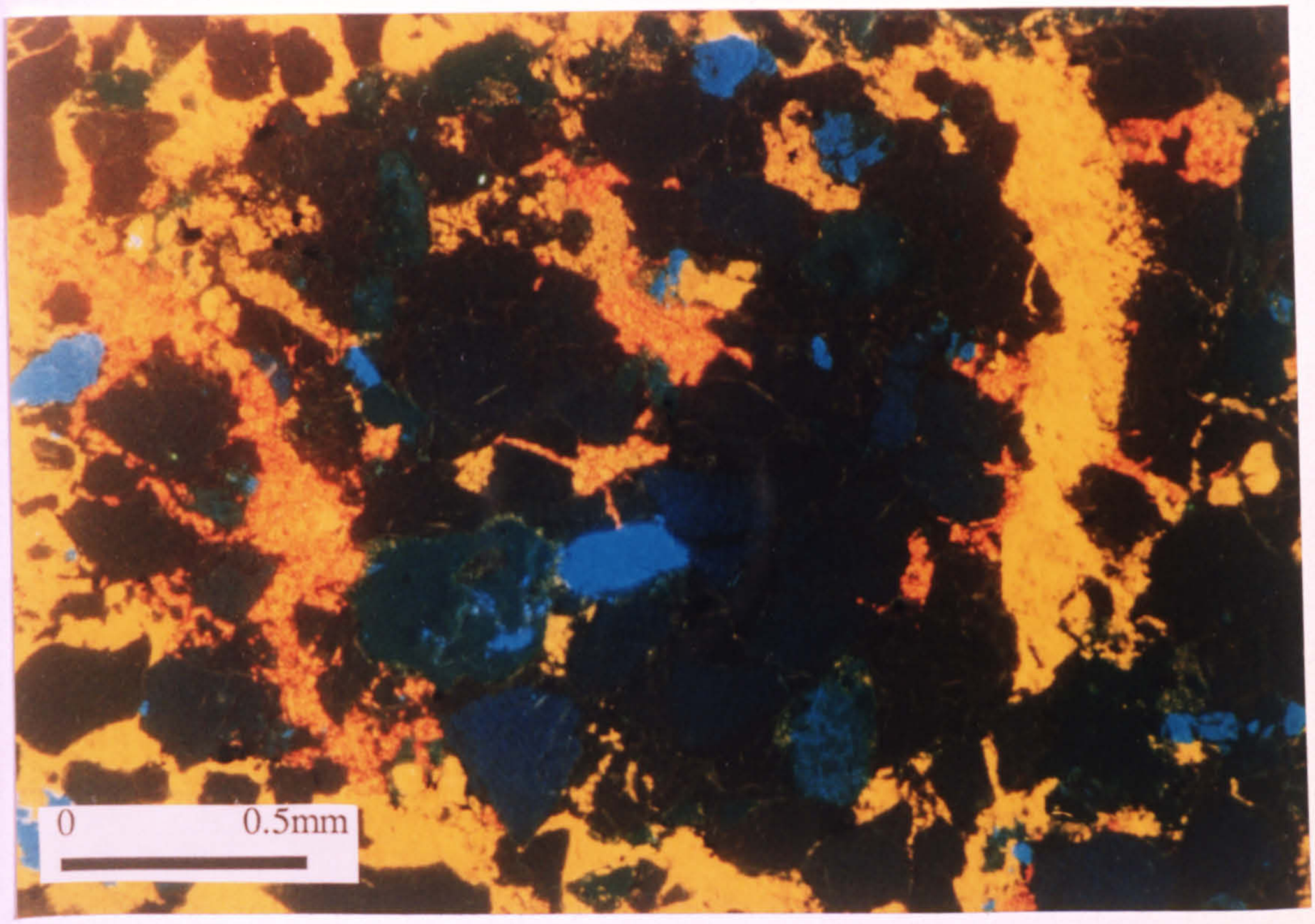

Figure 3.15.

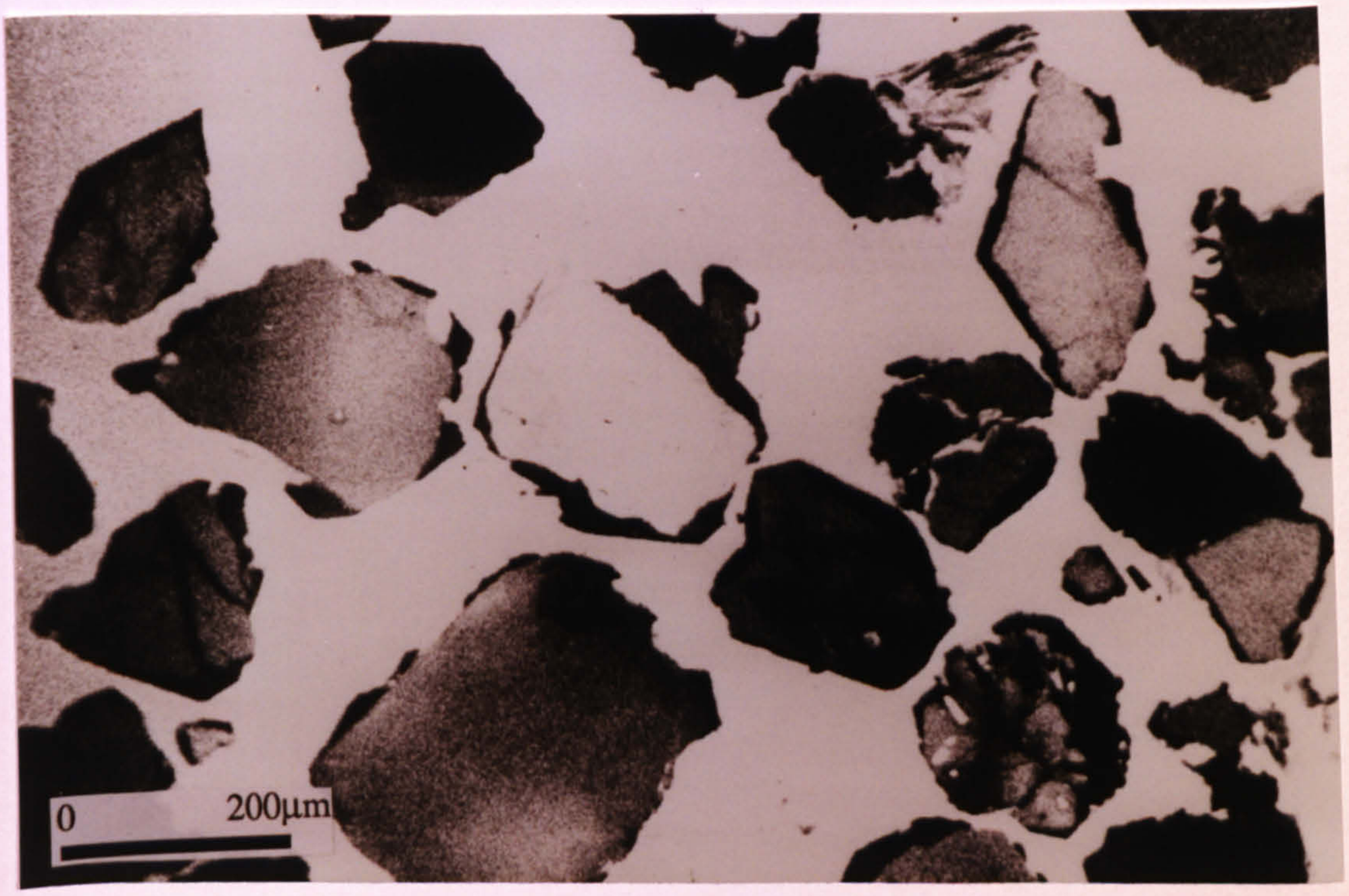

Figure 3.16.

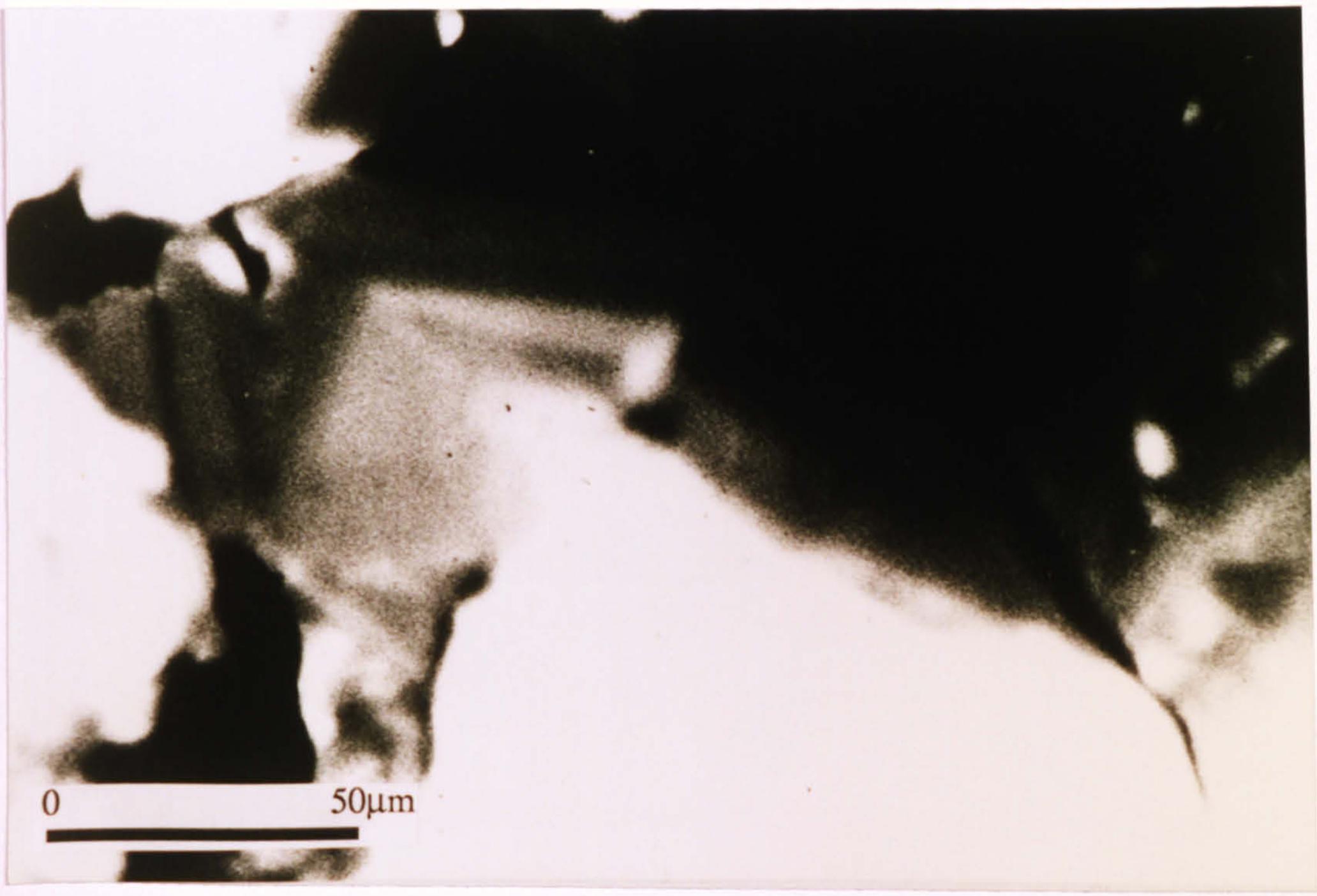

Figure 3.17.

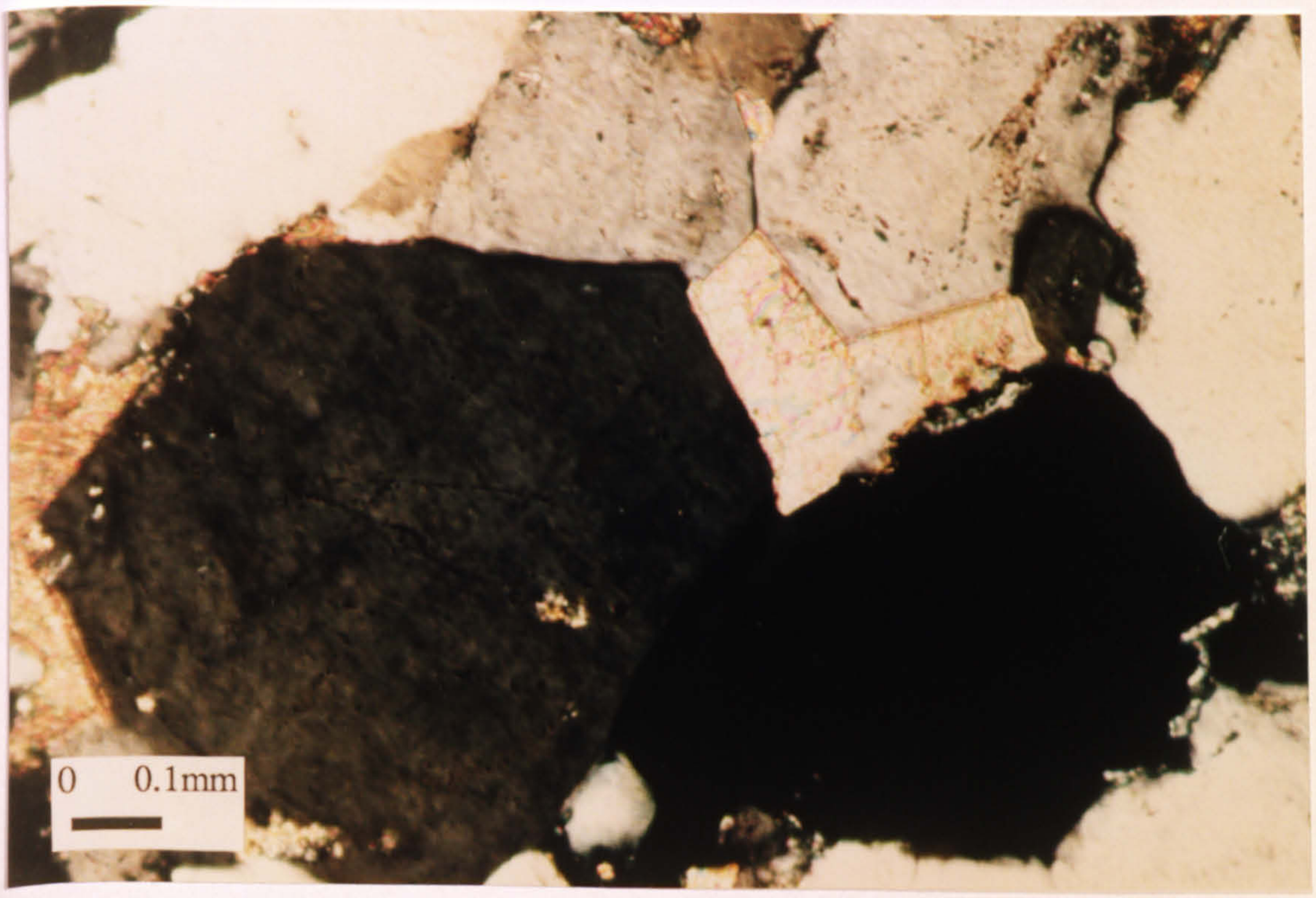

Figure 3.18.

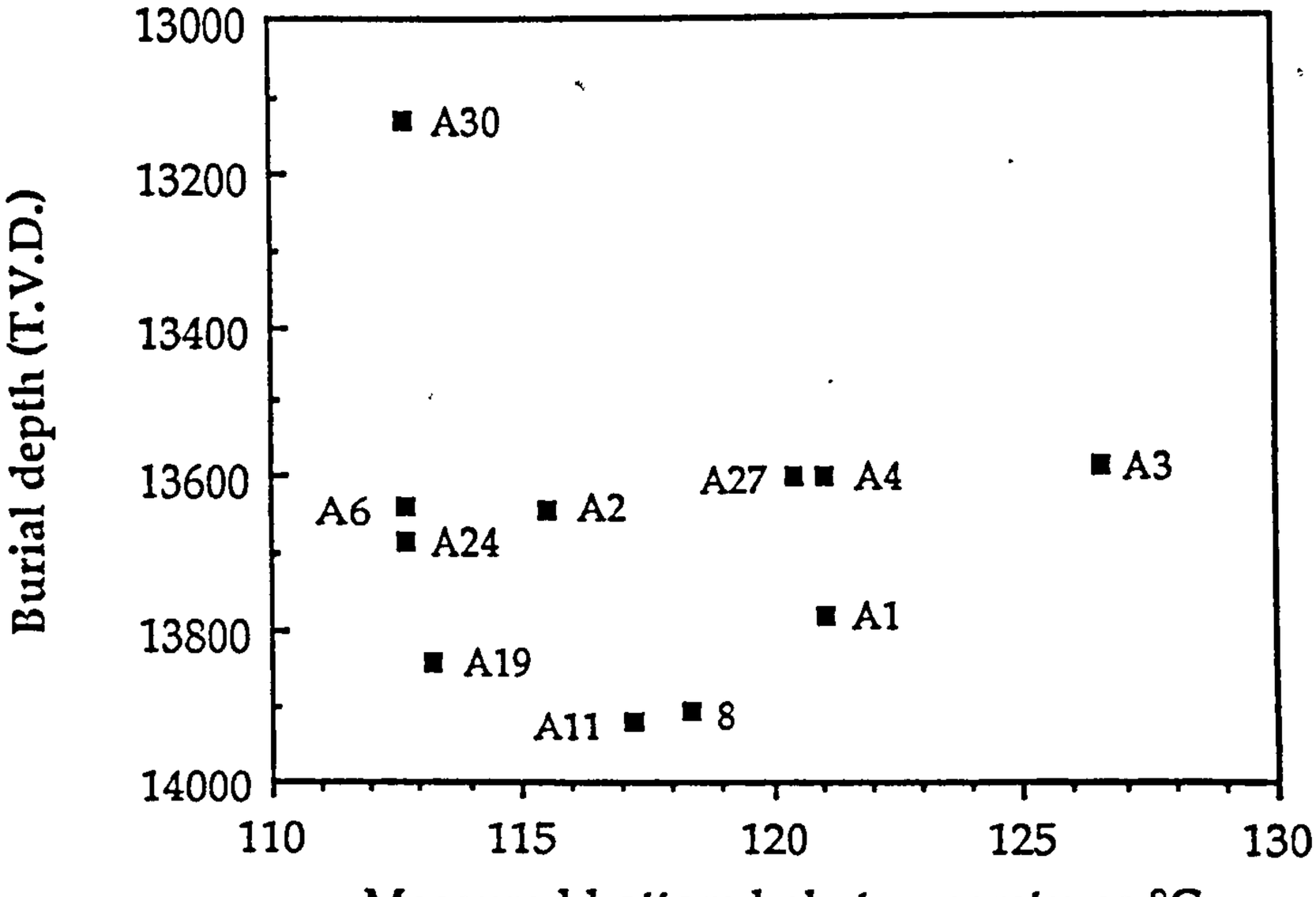
13000
13200
13400
13600
13800
14000
Burial depth (T.V.D.)
A30
A6
A24
A2
A27
A4
A3
A1
A19
A11
8
110
115
120
125
130
Measured bottom hole temperatures °C

Figure 3.19.

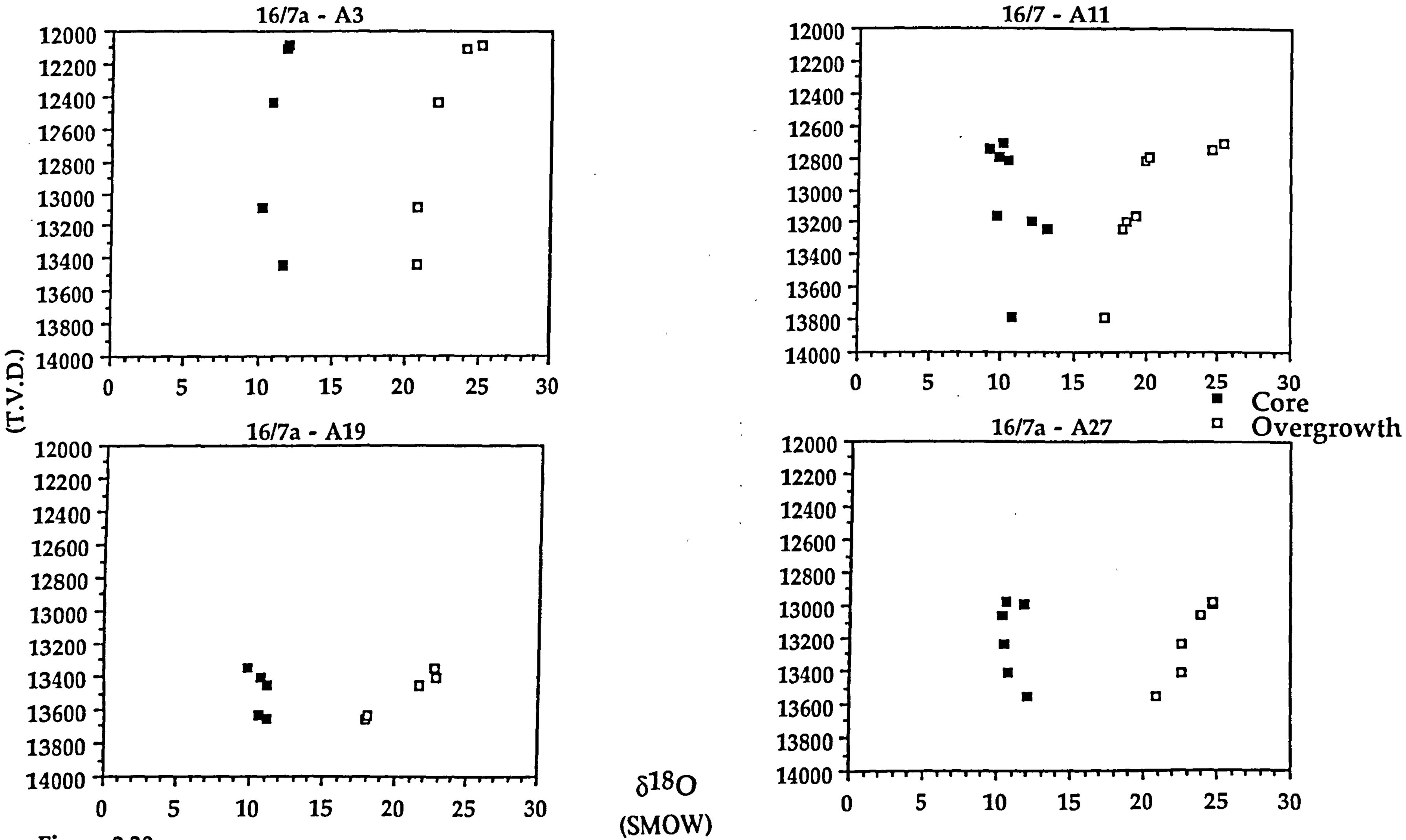
16/7a - A3
16/7 - A11
16/7a - A19
16/7a - A27
12000
12200
12400
12600
12800
13000
13200
13400
13600
13800
14000
0
5
10
15
20
25
30
(T.V.D.)
Core
Overgrowth
δ18O
(SMOW)

Figure 3.20.

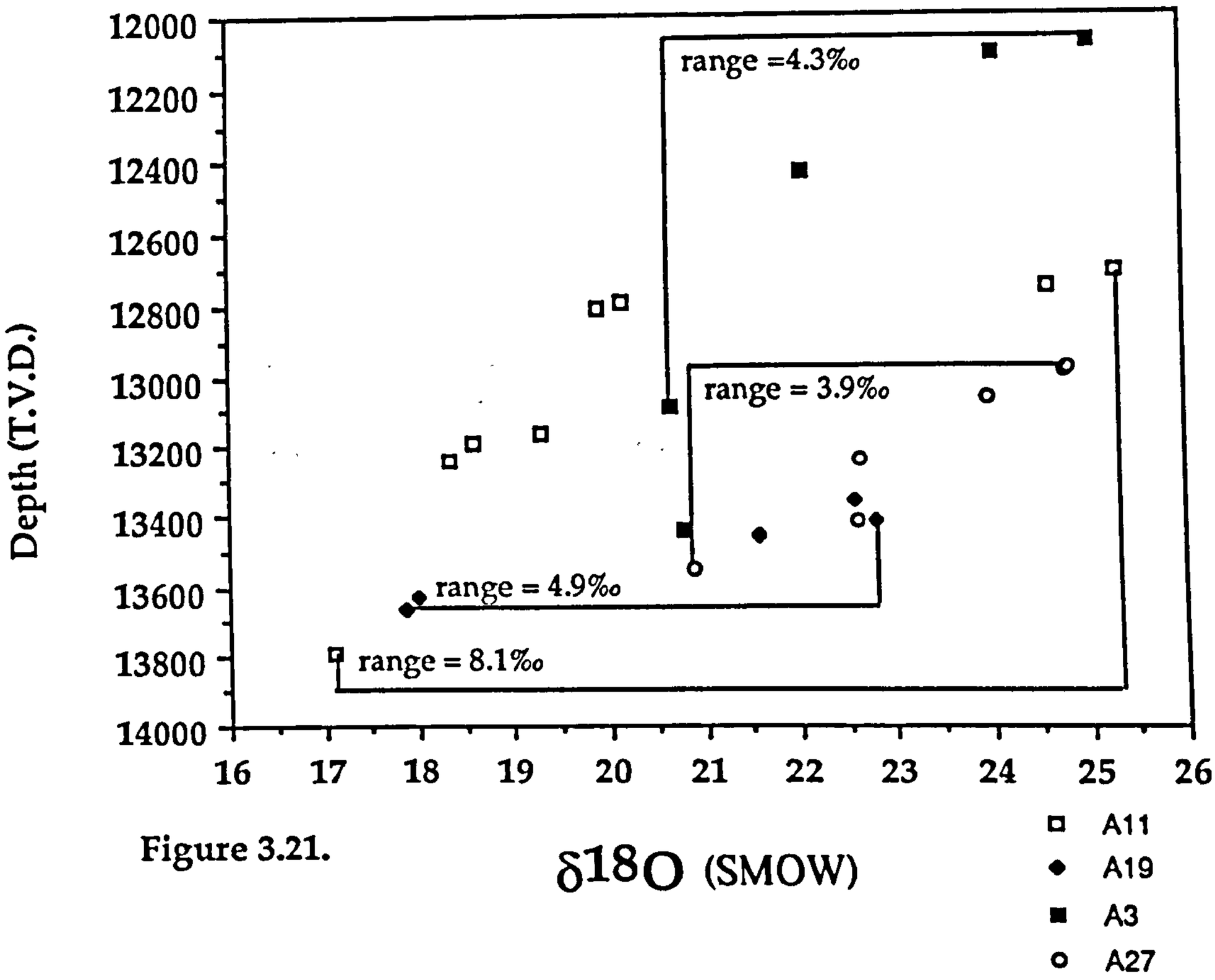

Figure 3.21.

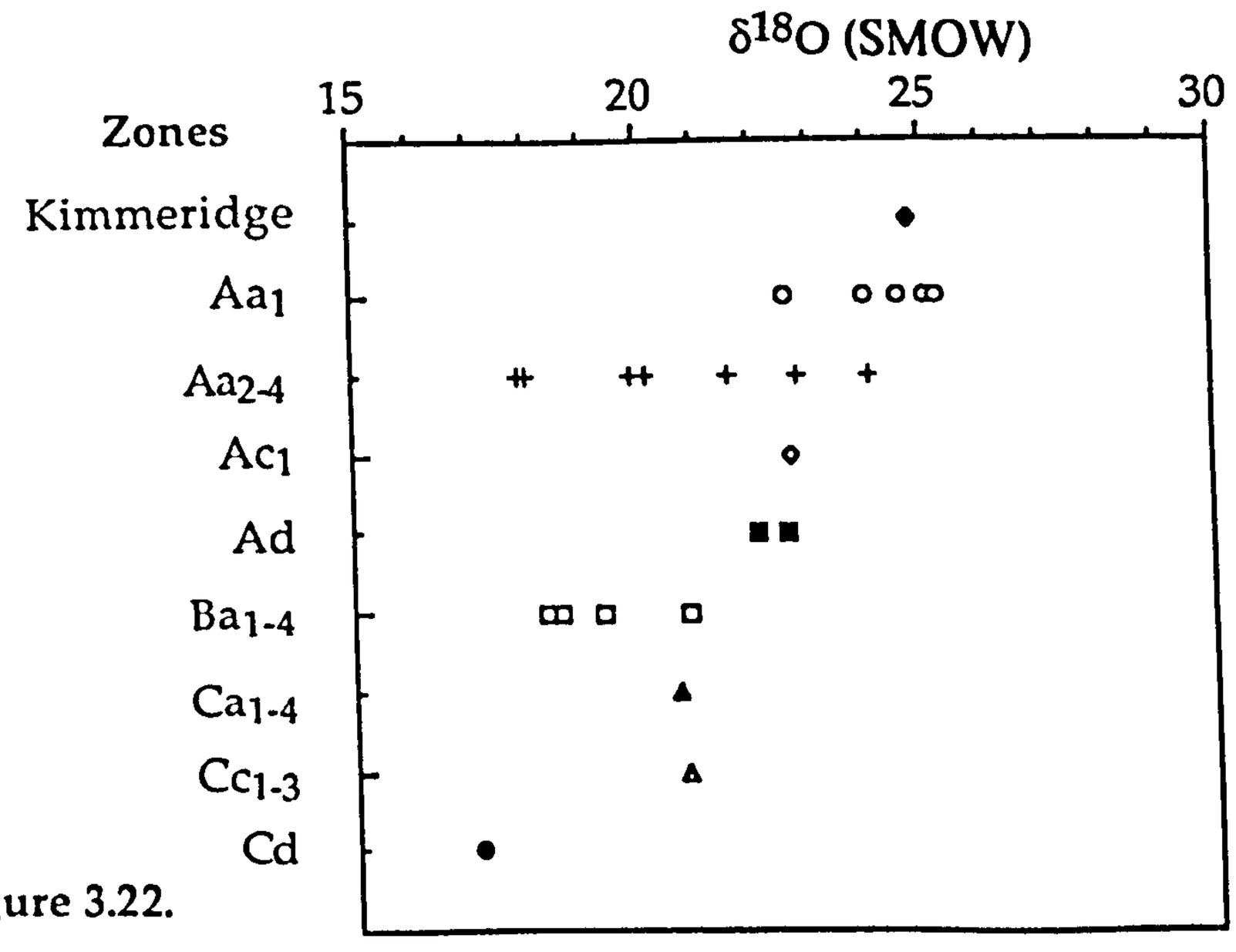

Figure 3.22.

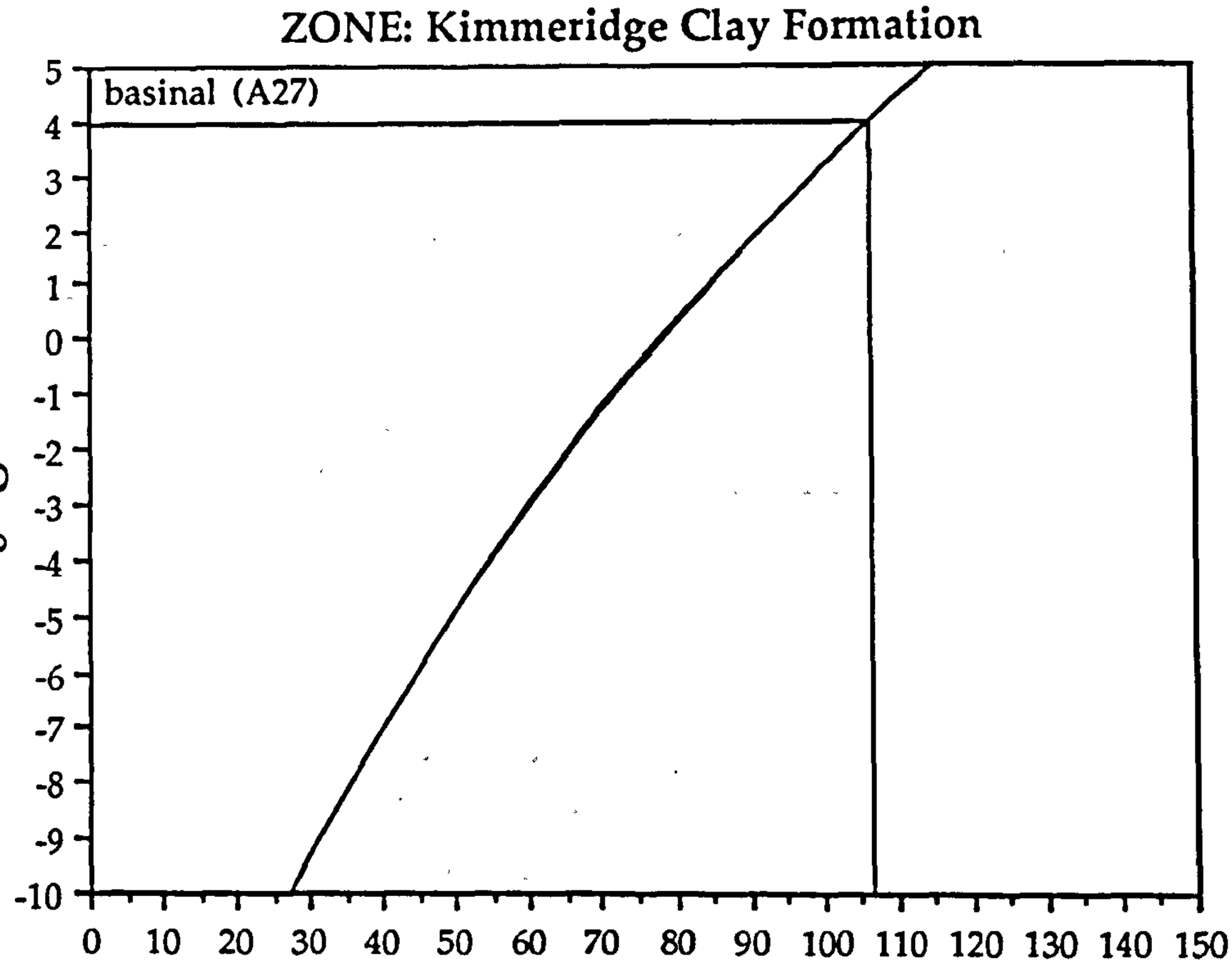

Figure 3.23a.

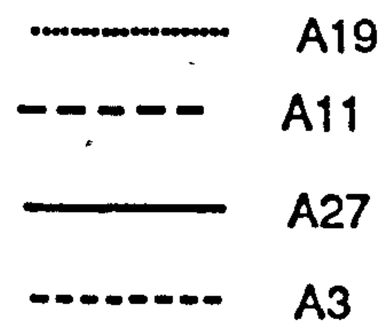

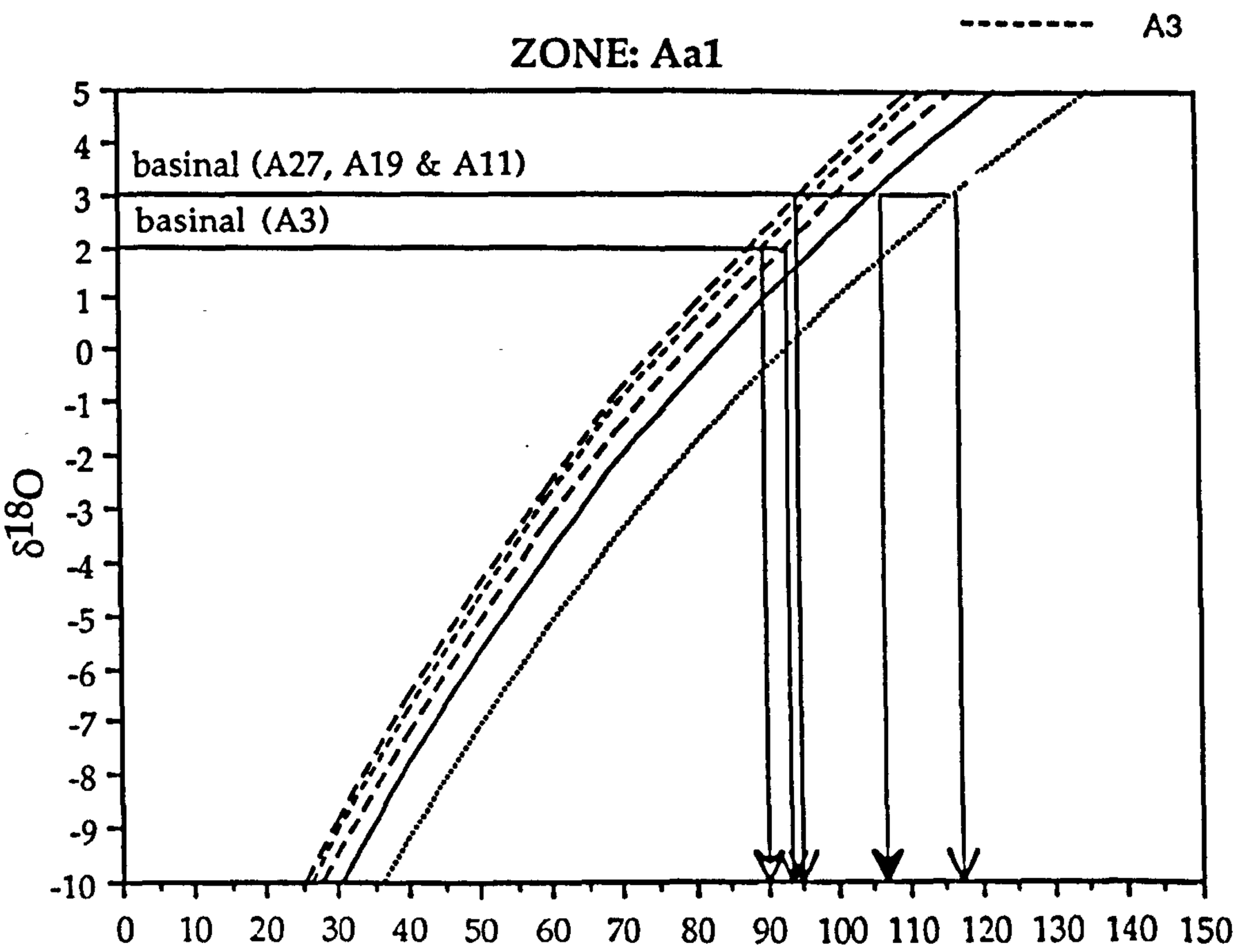

Figure 3.23b.

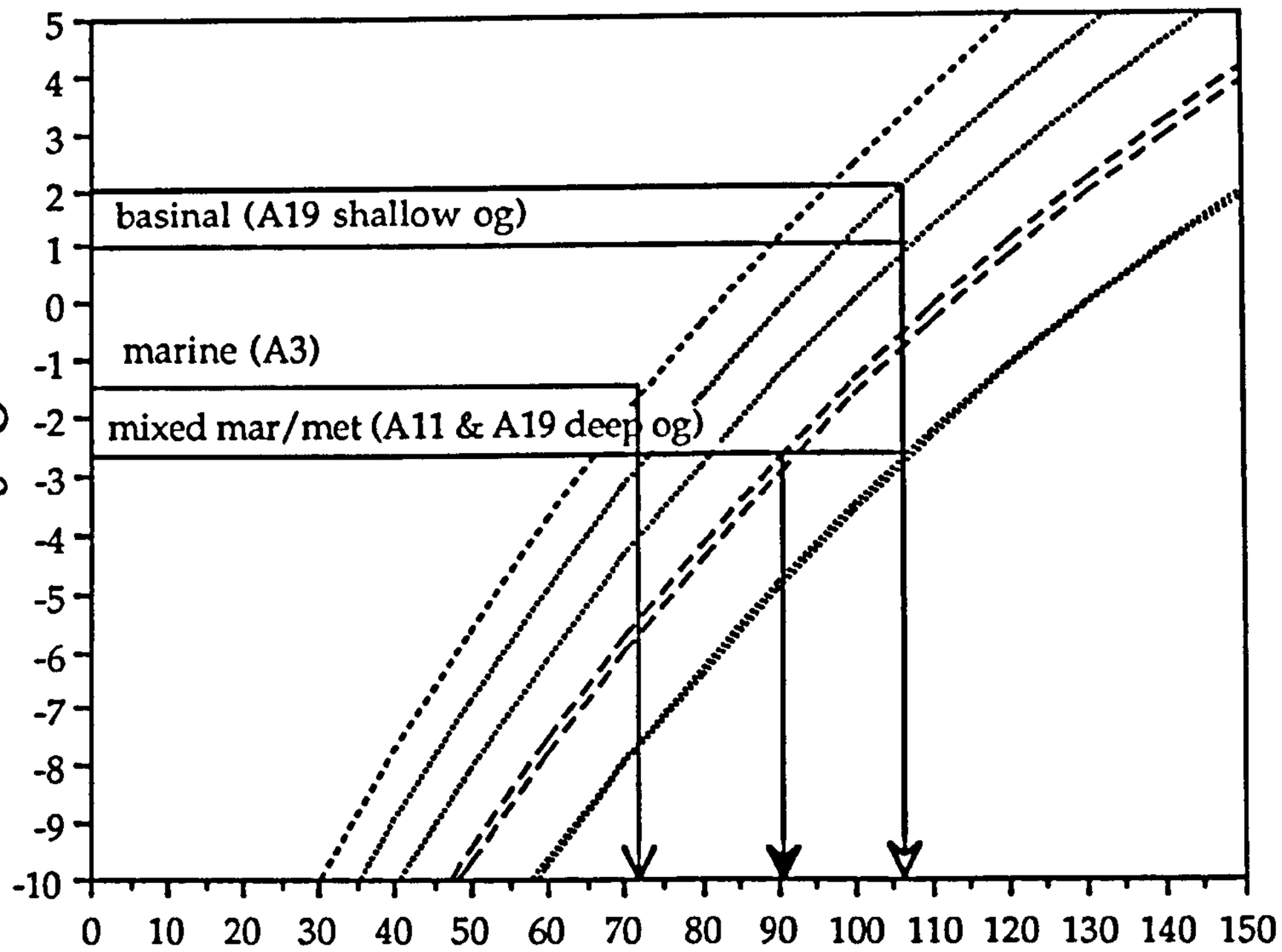

Figure 3.23c.

A19
A11
A27
A3

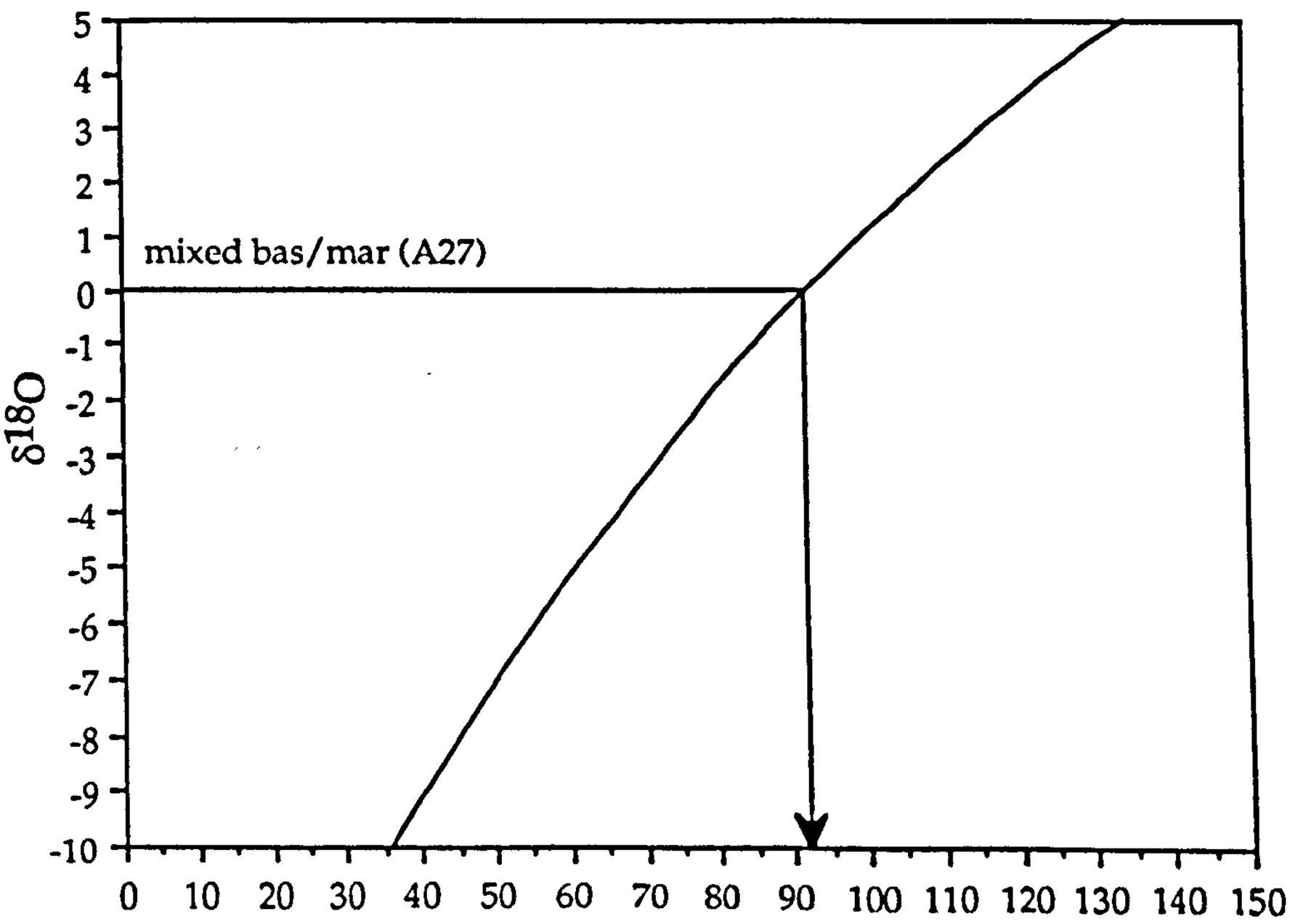

Figure 3.23d.

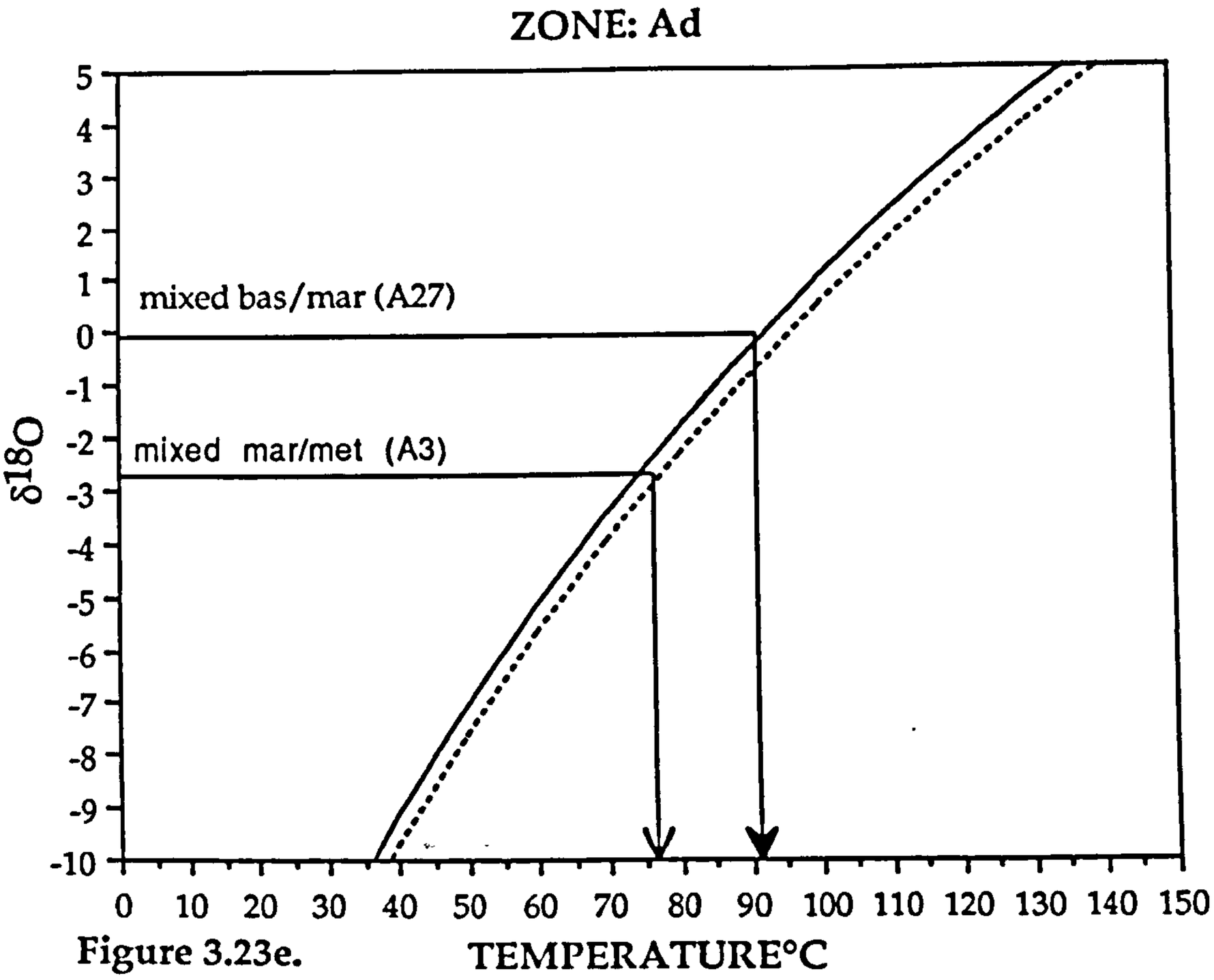

Figure 3.23e.

A19
A11
A27
A3

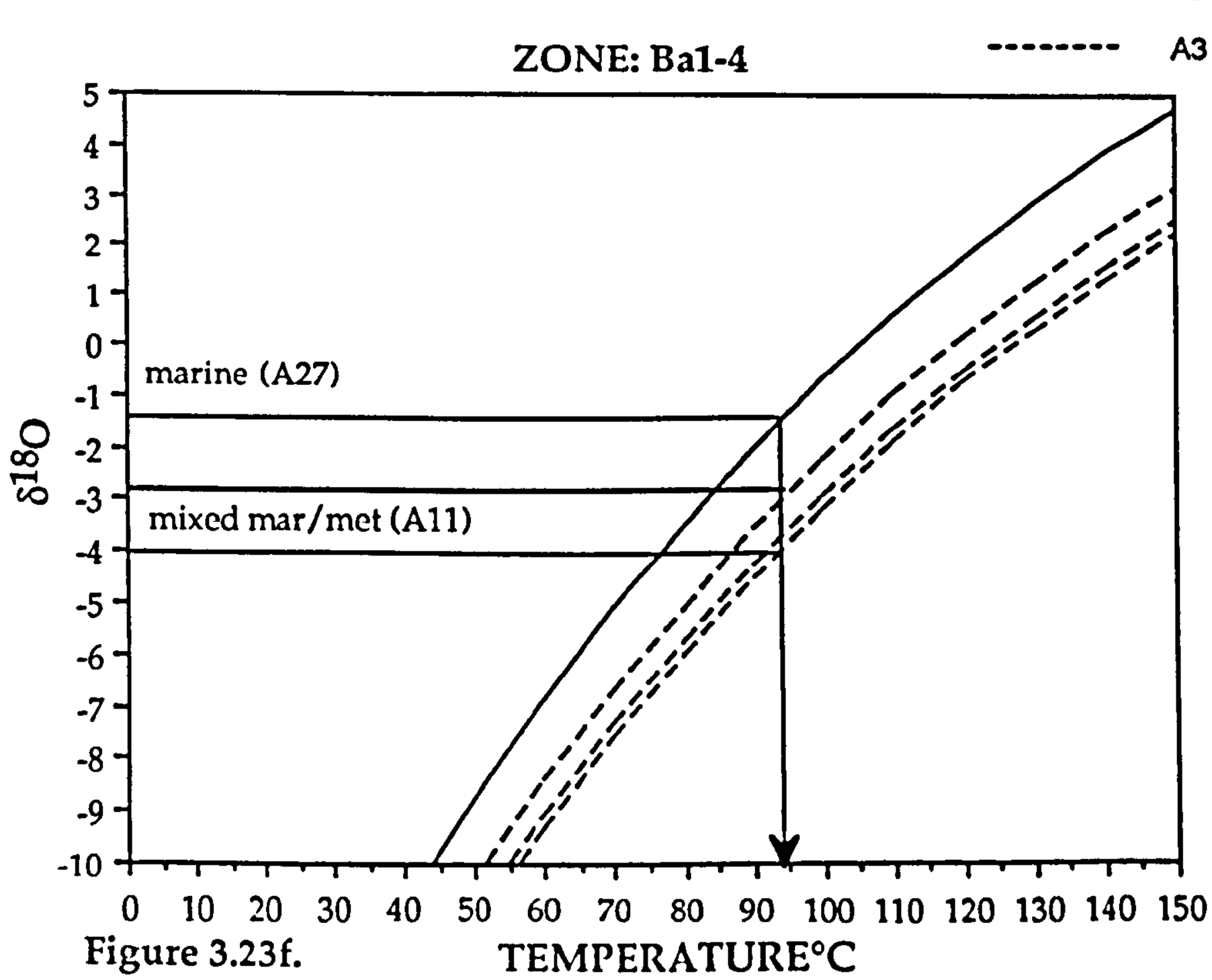

Figure 3.23f.

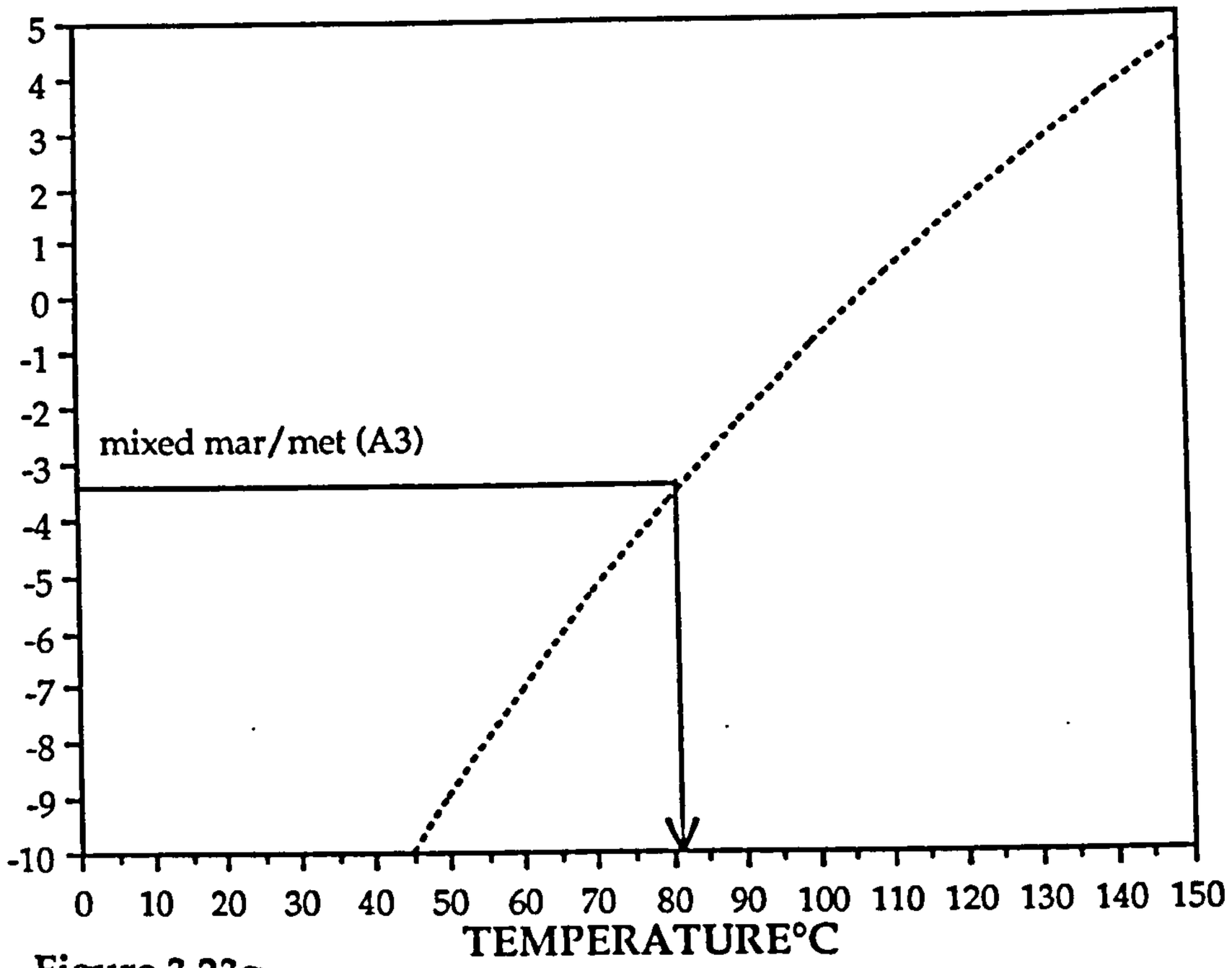

Figure 3.23g.

--------- A3

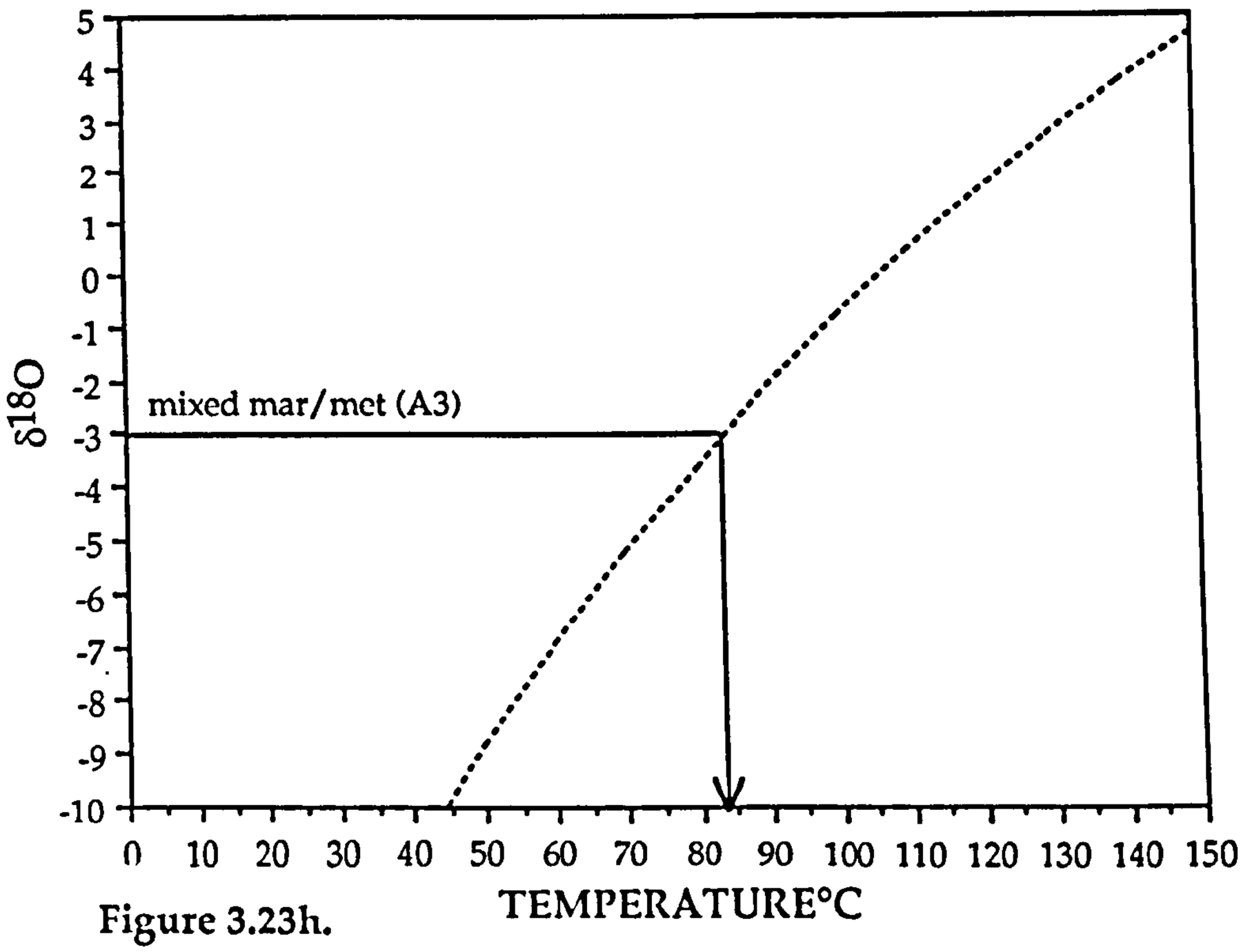

Figure 3.23h.

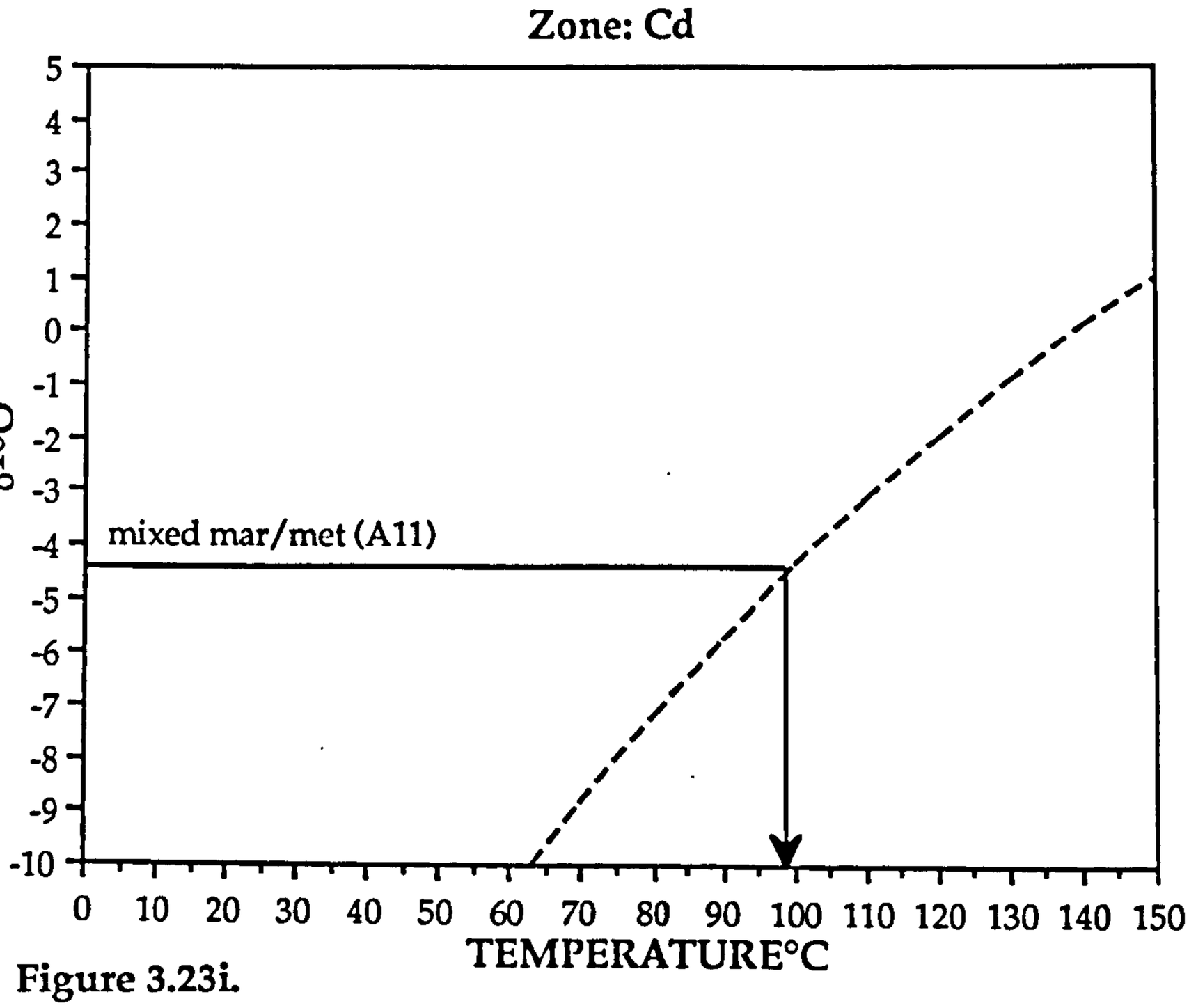
Zone: Cd
δ18O
5
4
3
2
1
0
-1
-2
-3
-4
-5
-6
-7
-8
-9
-10
mixed mar/met (A11)
0 10 20 30 40 50 60 70 80 90 100 110 120 130 140 150
TEMPERATURE°C
A11

Figure 3.23i.

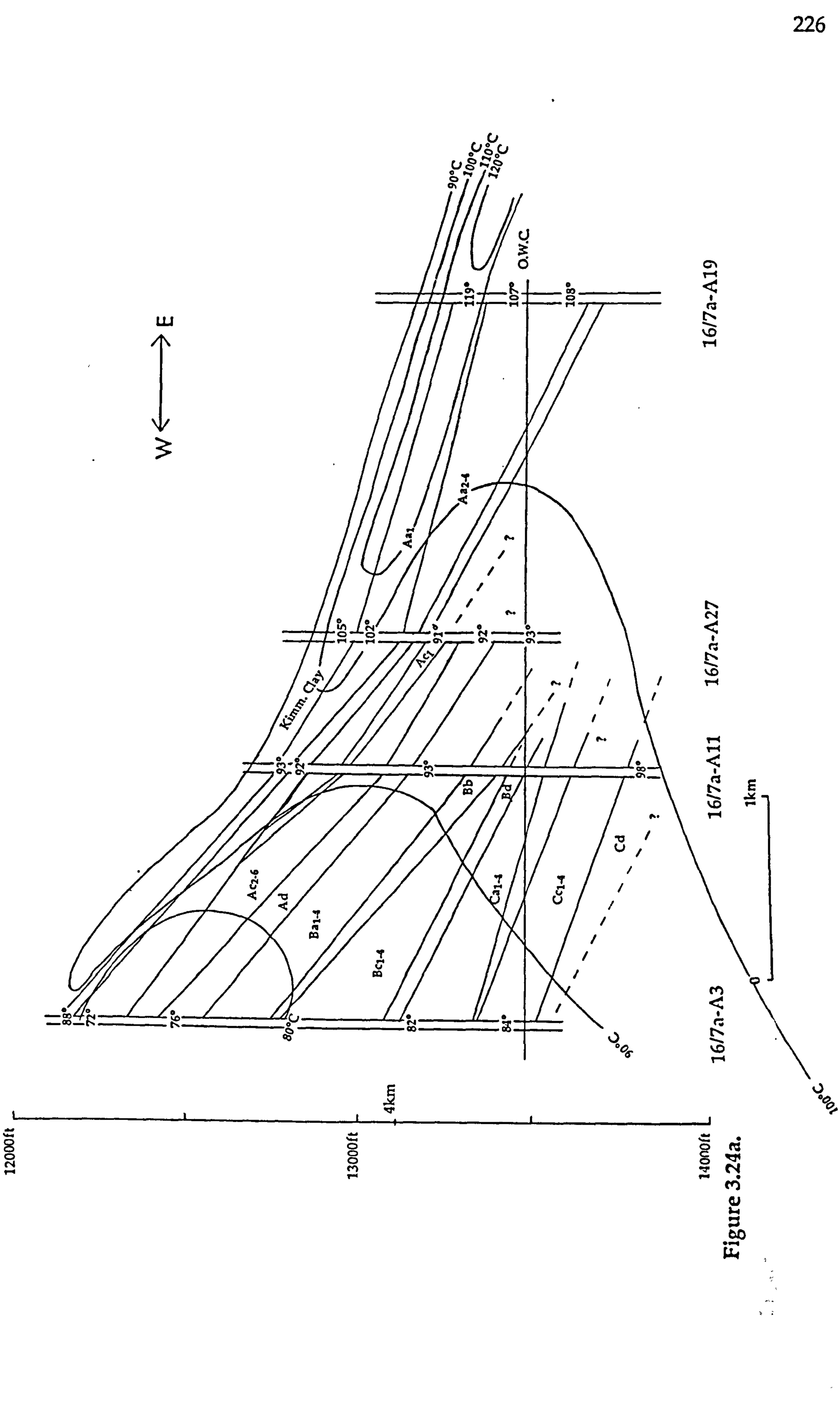
W
E
90°C
100°C
110°C
120°C
O.W.C
119°
107°
108°
16/7a-A19
Aa1
Aa2-4
105°
102°
91°
92°
93°
Ac1
Kimm. Clay
?
93°
92°
93°
98°
Bb
Bd
Cd
16/7a-A11
Ac2-6
Ad
Ba1-4
Bc1-4
Ca1-4
Cc1-4
88°
72°
76°
80°C
82°
84°
90°C
16/7a-A3
1km
0
100°C
12000ft
13000ft
4km
14000ft

Figure 3.24a.

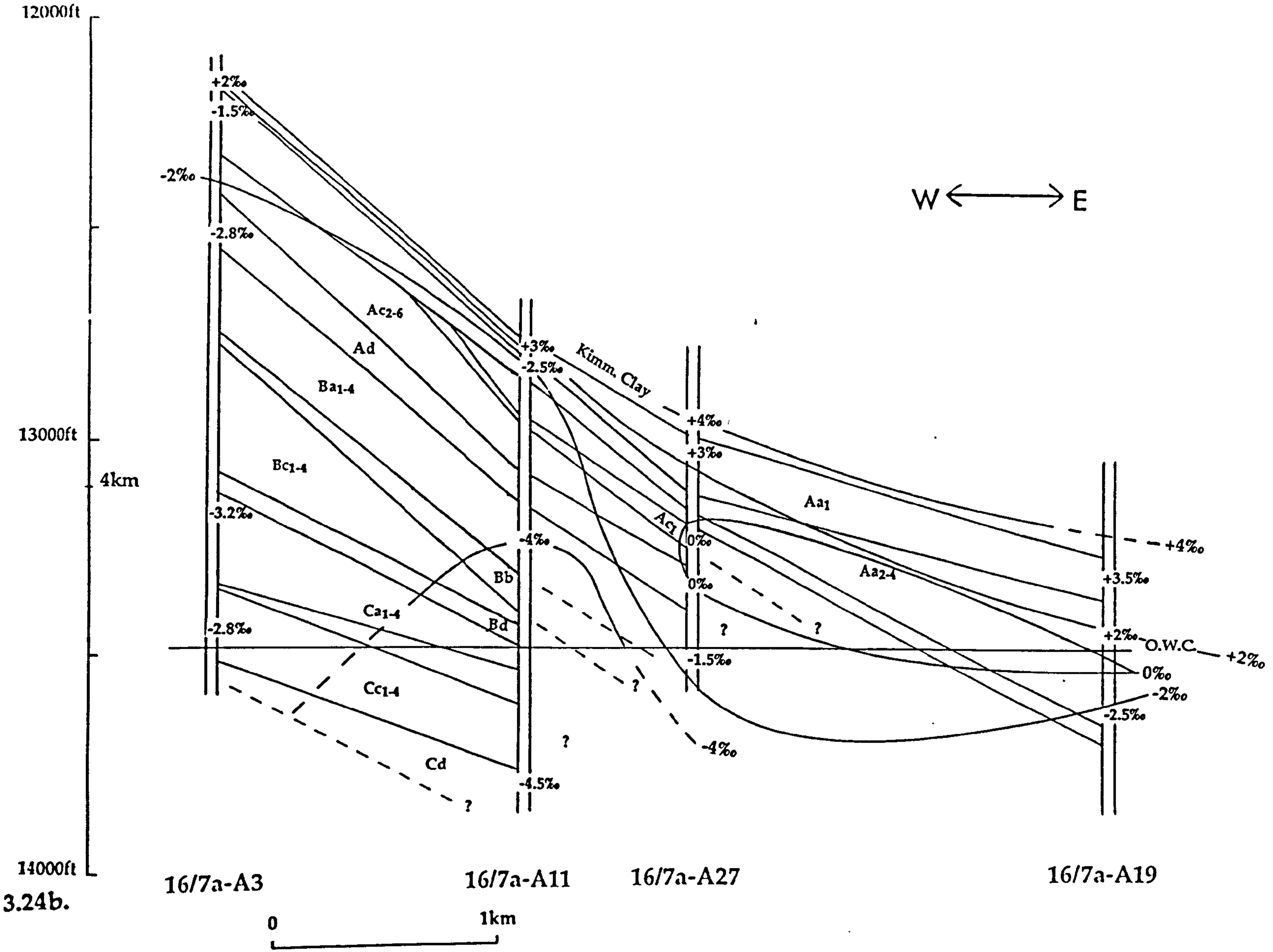
12000ft
13000ft
4km
14000ft
W ⟷ E
+2‰
-1.5‰
-2‰
-2.8‰
Ac2-6
Ad
Ba1-4
Bc1-4
-3.2‰
Ca1-4
-2.8‰
Bd
Cc1-4
Cd
?
-4.5‰
+3‰
-2.5‰
Kimm. Clay
-4‰
Bb
?
?
?
-4‰
+4‰
+3‰
Aa1
Ac1
0‰
Aa2-4
0‰
+4‰
+3.5‰
+2‰
O.W.C.
+2‰
-1.5‰
0‰
-2‰
-2.5‰
16/7a-A3
16/7a-A11
16/7a-A27
16/7a-A19
0
1km

Figure 3.24b.

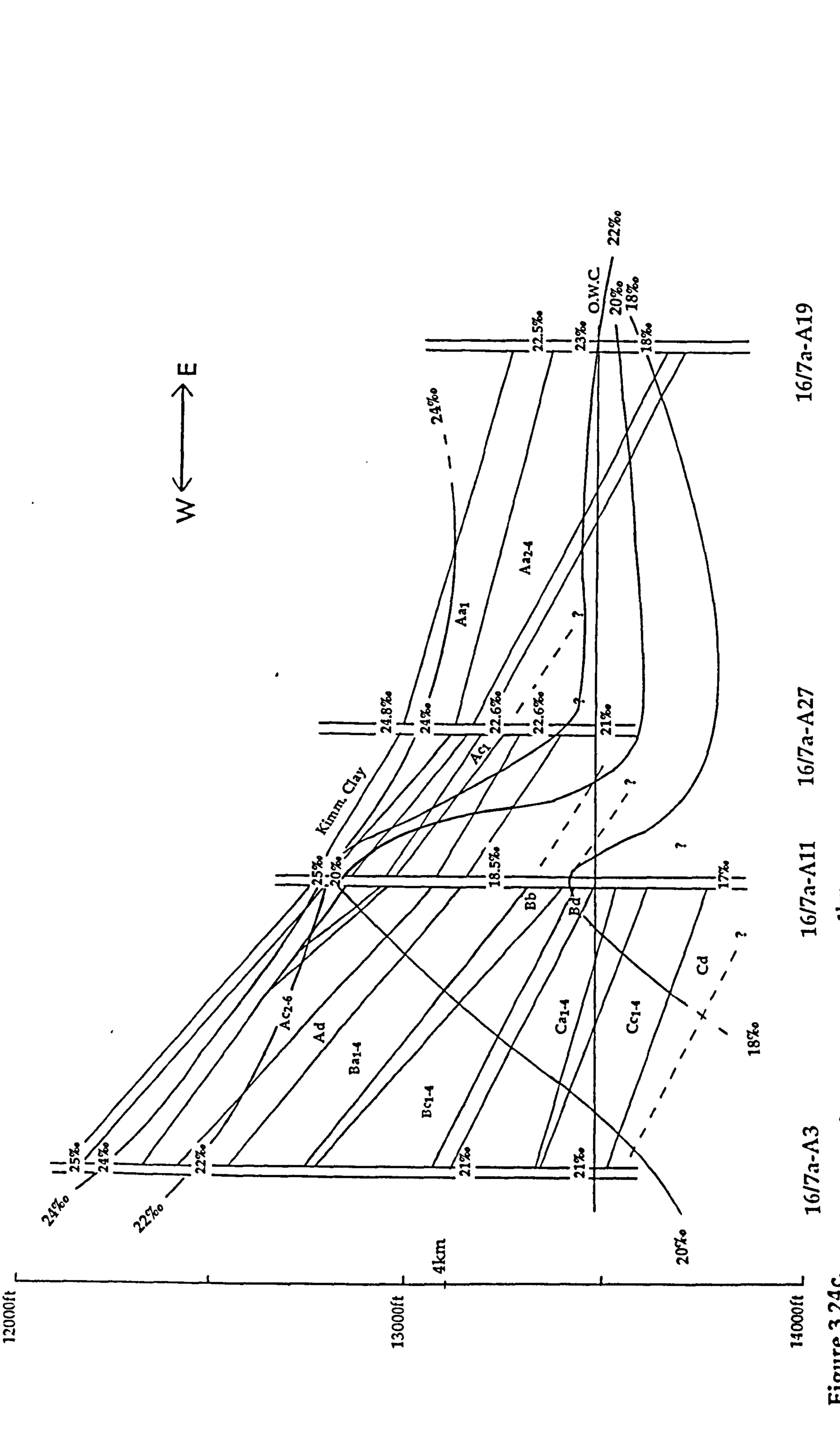
W
E
16/7a-A19
16/7a-A27
16/7a-A11
16/7a-A3
O.W.C
22‰
20‰
18‰
22.5‰
23‰
18‰
24‰
24.8‰
24‰
22.6‰
22.6‰
21‰
Aa1
Aa2-4
?
Kimm. Clay
Ac1
25‰
20‰
18.5‰
17‰
Ac2-6
Ad
Ba1-4
Bc1-4
Bb
Bd
Ca1-4
Cc1-4
Cd
?
?
?
18‰
25‰
24‰
22‰
21‰
21‰
20‰
24‰
22‰
0
1km
4km
12000ft
13000ft
14000ft

Figure 3.24c.

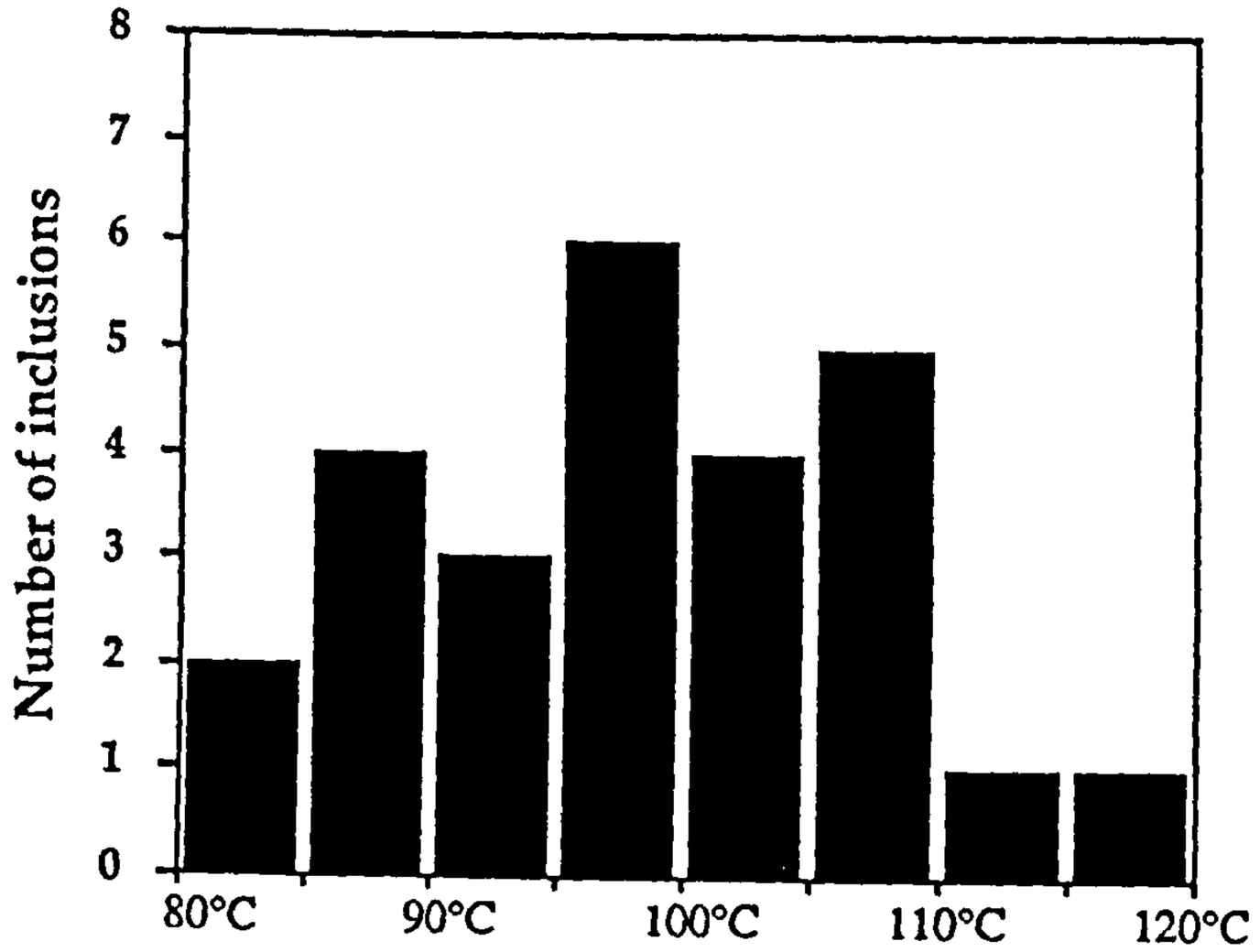
Number of inclusions
0
1
2
3
4
5
6
7
8
80°C
90°C
100°C
110°C
120°C
n=25
Homogenization Temperature °C

Figure 3.25.

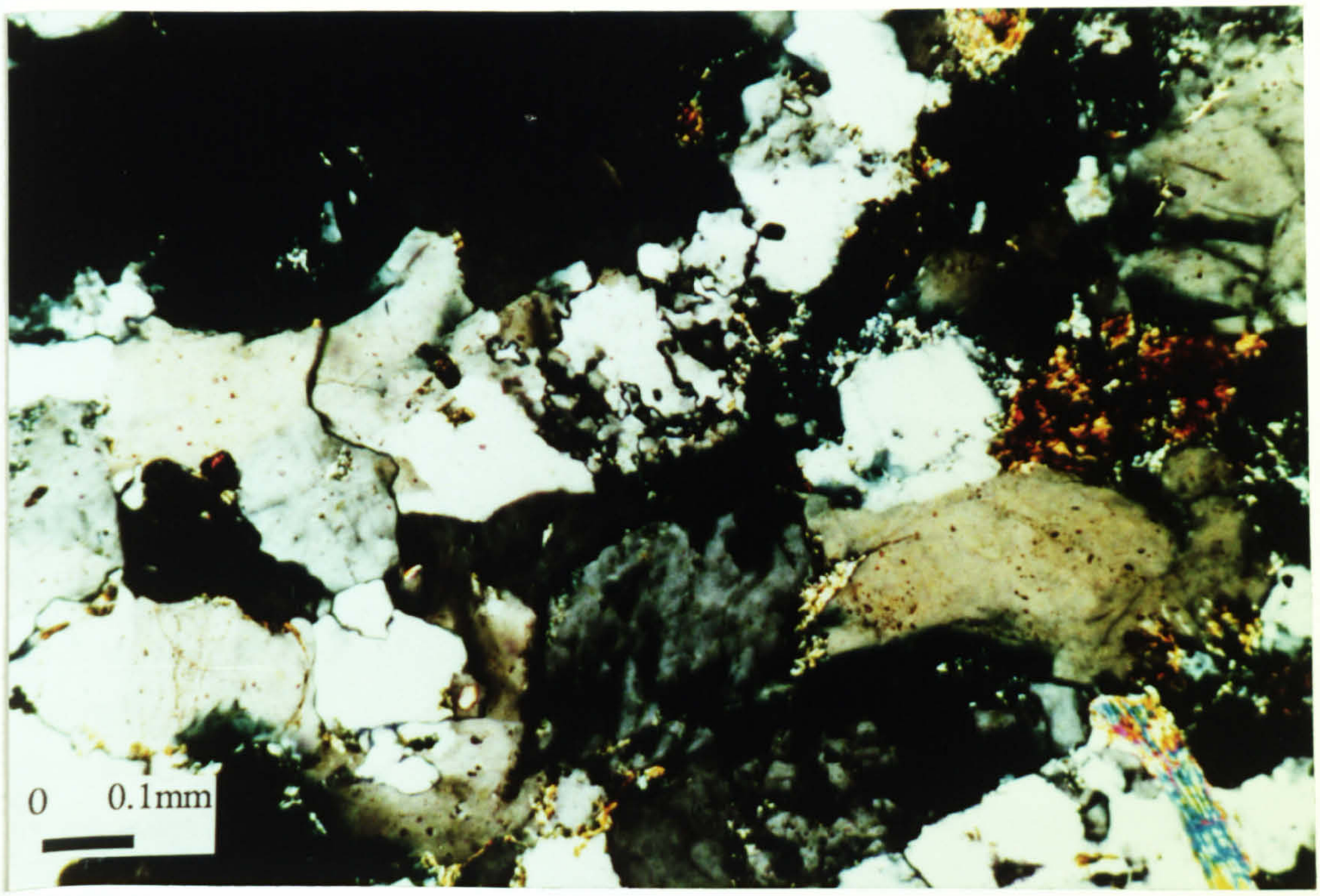

Figure 3.26.

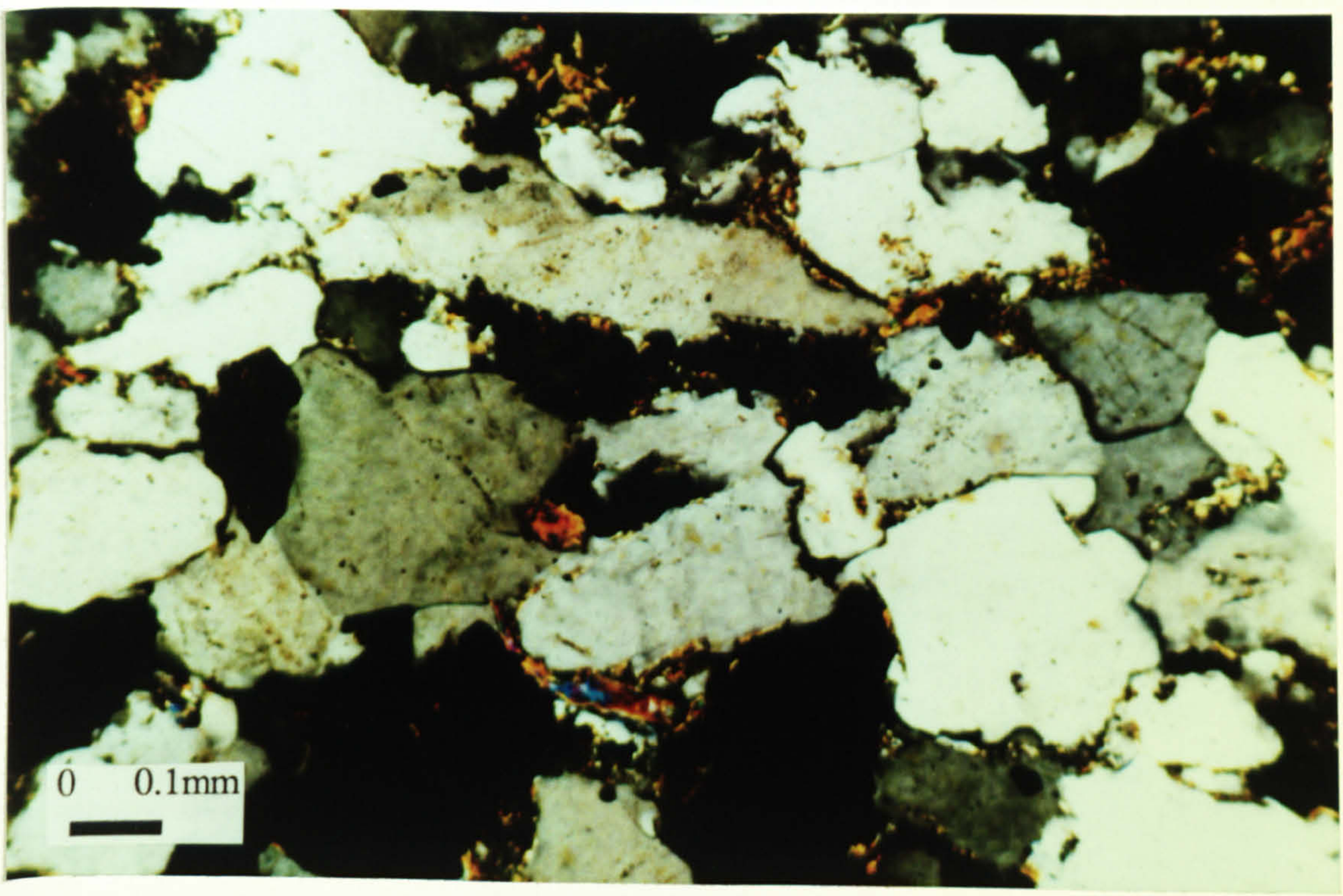

Figure 3.27

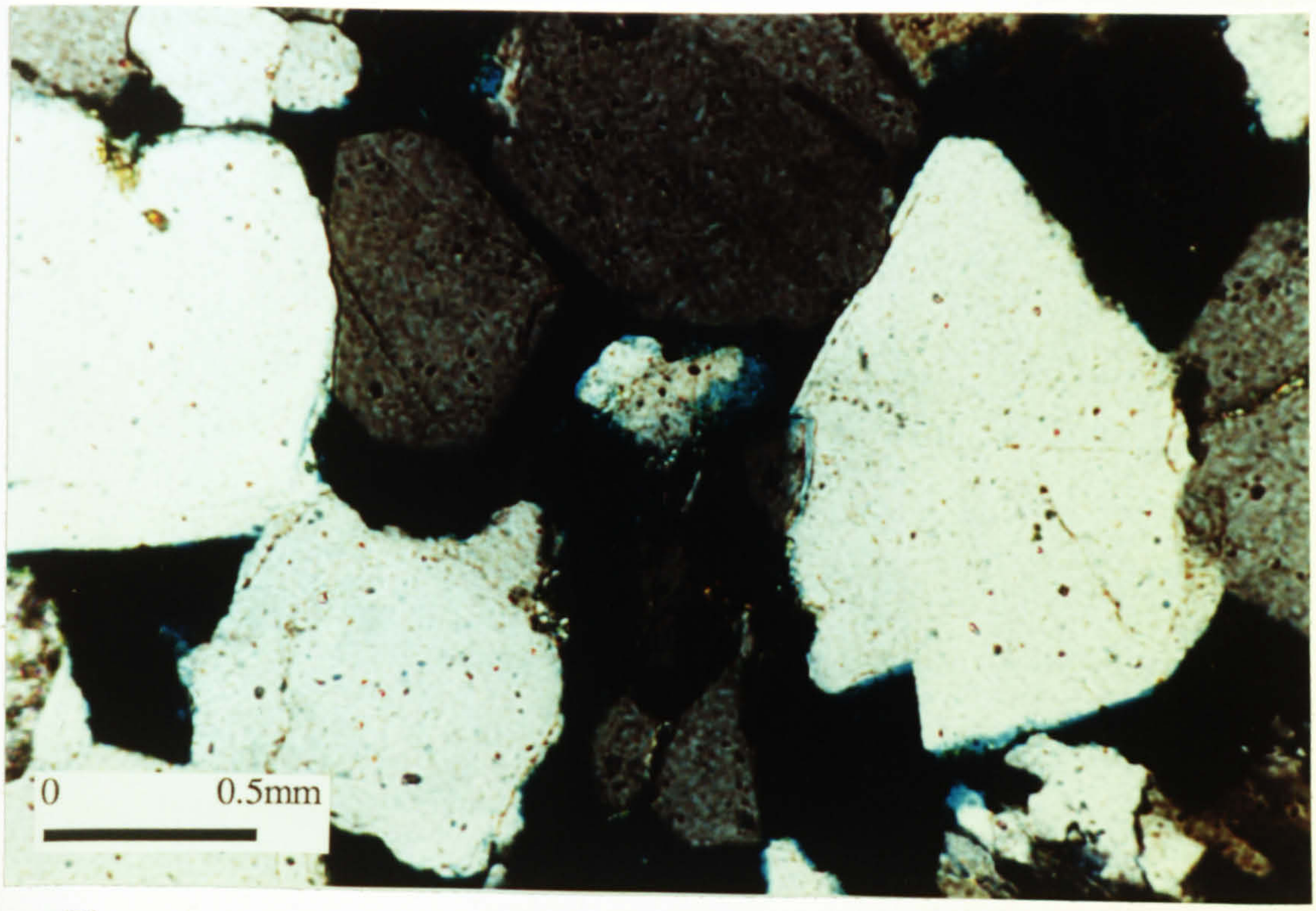

Figure 3.28.

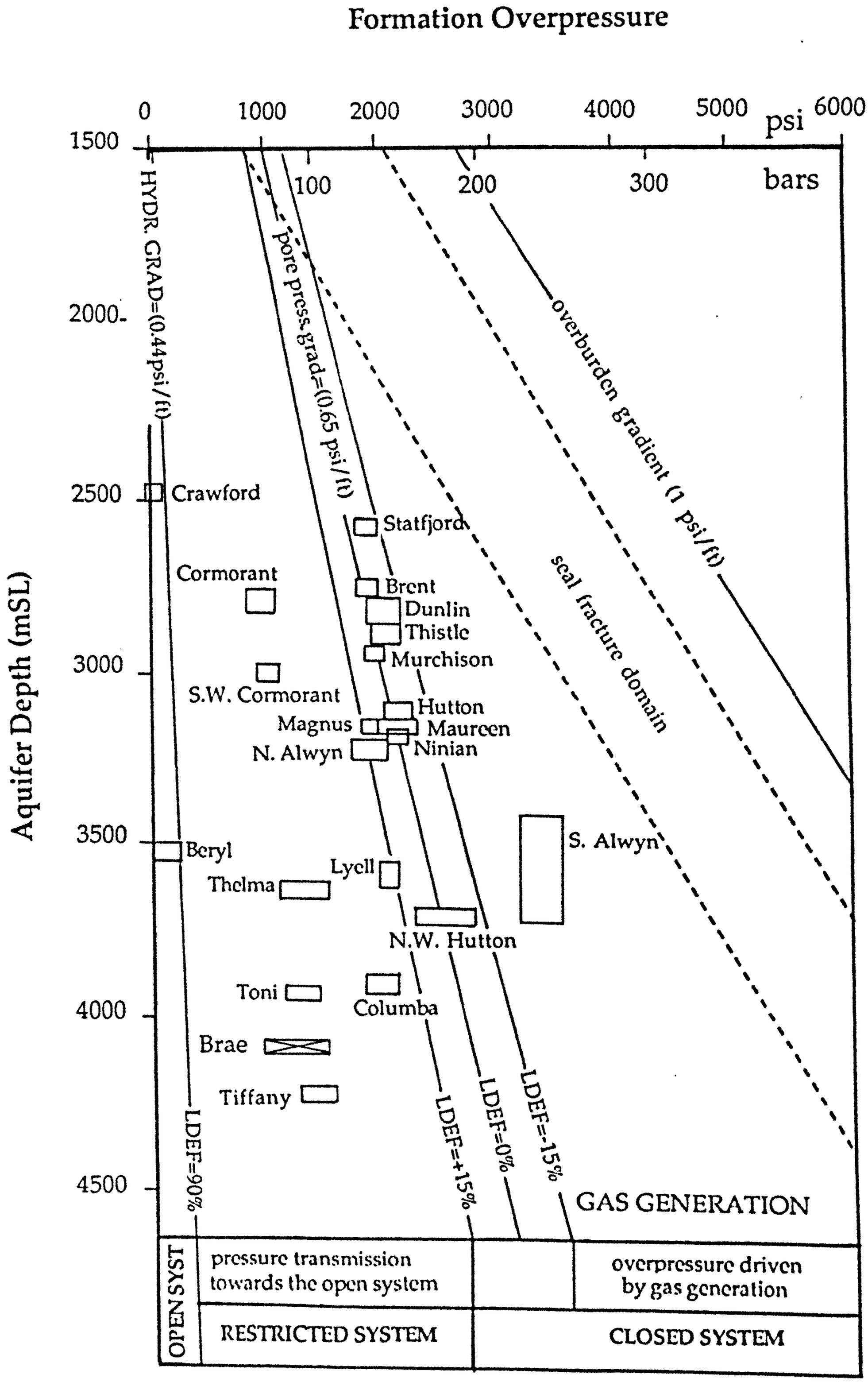
Formation Overpressure
0
1000
2000
3000
4000
5000
psi
6000
1500
100
200
300
bars
2000
HYDR. GRAD=(0.44psi/ft)
pore press.grad=(0.65 psi/ft)
overburden gradient (1 psi/ft)
seal fracture domain
Aquifer Depth (mSL)
2500
Crawford
Statfjord
Cormorant
Brent
Dunlin
Thistle
3000
Murchison
S.W. Cormorant
Hutton
Magnus
Maureen
N. Alwyn
Ninian
3500
Beryl
Lyell
Thelma
S. Alwyn
N.W. Hutton
Toni
Columba
4000
Brae
Tiffany
LDEF=90%
LDEF=+15%
LDEF=0%
LDEF=-15%
4500
GAS GENERATION
OPEN SYST
pressure transmission towards the open system
overpressure driven by gas generation
RESTRICTED SYSTEM
CLOSED SYSTEM

Figure 3.29.

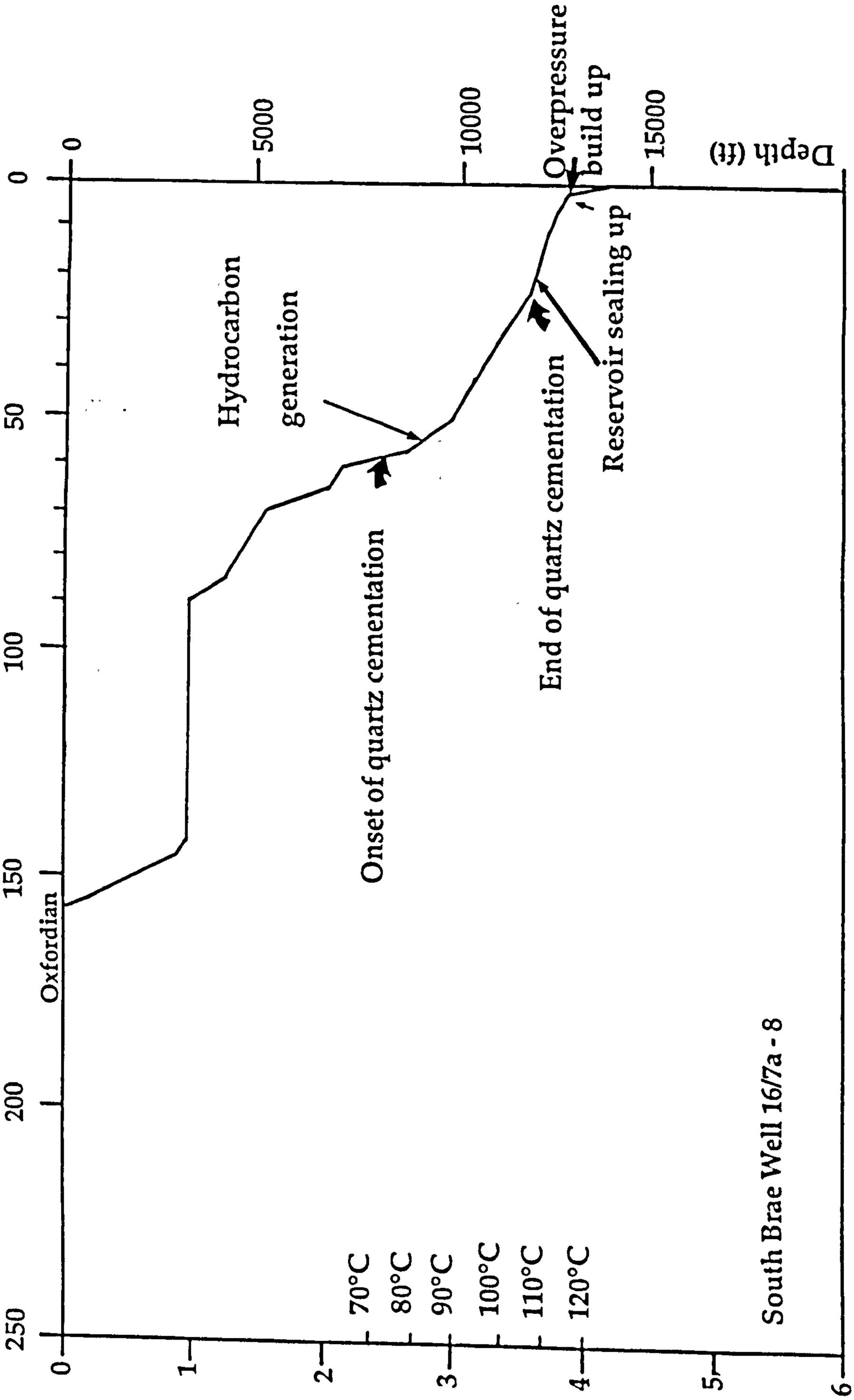
Depth (ft)
0
5000
10000
15000
Overpressure build up
Hydrocarbon generation
Onset of quartz cementation
End of quartz cementation
Reservoir sealing up
Time (Ma)
0
50
100
150
200
250
Oxfordian
South Brae Well 16/7a - 8
70°C
80°C
90°C
100°C
110°C
120°C
Depth (km)
0
1
2
3
4
5
6

Figure 3.30.

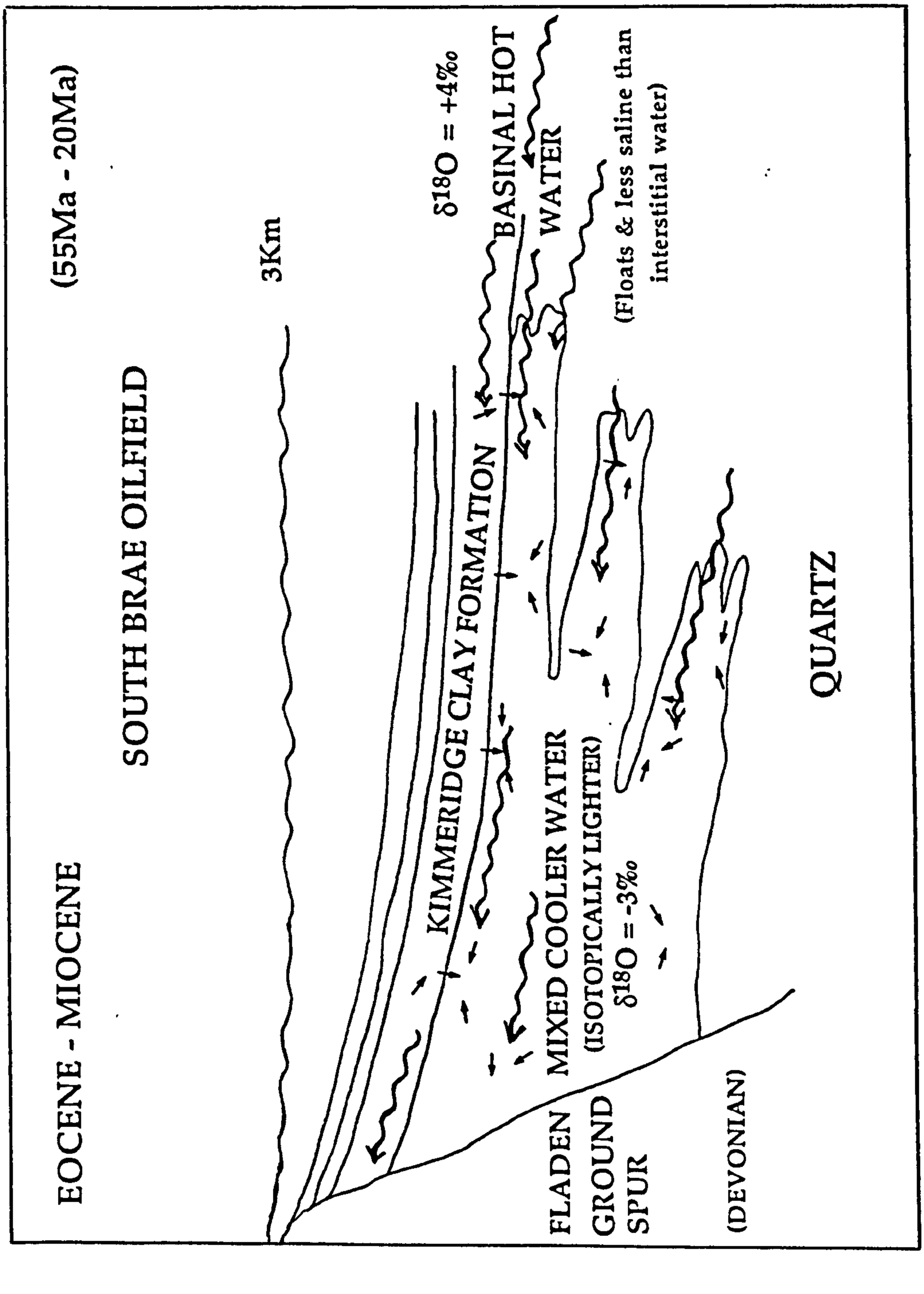
EOCENE - MIOCENE
SOUTH BRAE OILFIELD
(55Ma - 20Ma)
3Km
δ18O = +4‰
BASINAL HOT WATER
(Floats & less saline than interstitial water)
KIMMERIDGE CLAY FORMATION
MIXED COOLER WATER
(ISOTOPICALLY LIGHTER)
δ18O = -3‰
FLADEN GROUND SPUR
(DEVONIAN)
QUARTZ

Figure 3.31.

SECONDARY POROSITY AND REGIONAL FLUID EXPULSION IN DEEP BURIAL: SOUTH BRAE, NORTH SEA

Órla M. Mc Laughlin, R. Stuart Haszeldine

Department of Geology and Applied Geology, University of Glasgow,

Glasgow G12 8QQ, Scotland

Anthony E. Fallick

Isotope Geology Unit, Scottish Universities Research and Reactor Centre,

East Kilbride, Glasgow G75 0QU, Scotland

4.1 ABSTRACT

Secondary porosity, formed by the dissolution of both carbonate and silicate minerals (particularly K-feldspar) is widely developed in the South Brae reservoir sandstones. A combination of diagenetic events has resulted in a reservoir which is composed mostly of reduced primary porosity with lesser enhanced secondary porosity. The preservation of the secondary porosity is due to the late timing of its generation and infill by hydrocarbons.

Secondary porosity averages 8.2% of the total thin section porosity, it is present at all depths, but makes up the greatest percentage of total porosity (7-17% whole rock) in zone Aa_1 and Aa_{2-4}. The amount of porosity and its distribution throughout these sandstones differs due to the influences of grain size, lithology and stratigraphic position. The porosity zone is possibly related to a basinal fluid migration pathway, these aggressive fluids were possibly expelled from the interdigitating Kimmeridge Clay.

4.2 INTRODUCTION

The geological setting of the South Brae oilfield is a submarine fan (Fig.4.1.) which is currently undergoing active burial, there are no significant unconformities indicating post-depositional uplift or subaerial exposure. Present day burial conditions are believed to represent the maximum pressure-temperature conditions.

Petrographic analyses of seventy sandstone thin sections from five wells in the Brae Formation in the South Brae Oilfield area (Fig.4.2.) suggest that the secondary porosity was created by the post-depositional leaching of detrital and authigenic minerals, based on the textural criteria outlined by Schmidt & McDonald (1979). Precise quantification of secondary porosity is difficult as it can often be misidentified as primary porosity. The minerals that underwent dissolution include K-feldspar, plagioclase, quartz, mica, authigenic calcite cement and shell debris. Textural evidence for mineral dissolution includes oversized and elongate pores, corroded grain margins and partially dissolved detrital grains. Petrographic observations show that there is often not enough authigenic clay to account for the aluminium removed from the dissolved feldspar within the sandstones (see Sect. 4.5.).

The effect of secondary porosity development on reservoir properties ultimately depends on the amount of dissolution which occurs, and the subsequent infilling of these pores by precipitation of authigenic cements. Variations in the secondary porosity for similar sandstone bodies within the reservoir provide us with information about the lateral continuity of sandstone layers, and the "plumbing" of the reservoir. The ability to predict where such leached zones occur and their geometry is of critical

interest to the petroleum geologist.

4.3 INITIAL POROSITY AND PERMEABILITY

When deposited, up to 50% of the volume of sands can be intergranular pore space (Gluyas & Coleman 1992). This figure is dependent on grainsize and sorting. Lower initial porosity estimates range between 40% and 42% (Sclater & Christie 1982 and Houseknecht 1988 respectively). In South Brae porosity generally decreases with depth due to compaction and the precipitation of authigenic cements (Table 4.1.). Point counts of thin sections show early concretionary calcite cement contents of 20 to 45% (Fig.4.3.); this represents the sandstone porosity during calcite growth, showing that these concretions started to form prior to substantial sediment compaction (Table 4.2.). Decreasing carbonate cements (Fig.4.3.) from the centre to the exterior of the concretions (45-19%) reflect decreasing pore space volume during concretion growth due to continuing compaction (see Chapter 2) (similar to concretions described by Oertel & Curtis, 1972).

The most important controlling factor for the preservation and development of porosity in South Brae is the environment of deposition. This initially controls the relative permeabilities by determining sorting and the composition of the sand ie. amounts of feldspar, clay matrix and rock fragments. The highest porosities occur in the coarse-grained clean sandstone unit in Zone A. These sandstones today still form the easiest expulsion pathways for pore fluids. The fine-grained sandstones in the rest of the reservoir, such as Ad, had low depositional porosities and permeabilities. These show little or no dissolution of feldspar, and they have suffered increased compaction. Such factors may have reduced the

ability of aggressive diagenetic fluids to circulate easily. Some microporosity can be found in the conglomerates, as many of the rock fragments are porous (Fig.4.4a&b.). These clasts are disconnected vugs within a calcite cemented matrix so a poor permeability results, and consequently they have little effect on the overall porosity of a well.

4.4 SECONDARY POROSITY

4.4.1. Early redistributional secondary porosity

Within the early calcite cemented concretions we see evidence of redistributional secondary porosity (Giles & de Boer 1990), in which feldspar and fossil shells have been dissolved and detrital quartz grains partially leached, but an identical volume of early calcite cement has been precipitated in their place. This isochemical conservation of cementing Ca^{++} ions is most likely to happen when the porewaters are close to equilibrium with the majority of the minerals of the rock, or where the porewaters have been in contact with the rock for a long period of time (Bjorlykke 1984).

The fossil shells in most of the concretions have been recrystallized, this is particularly obvious when the thin sections are examined by CL (Fig.4.5.). In the centre of the concretions feldspar is preserved to a greater extent (Fig.4.6.) than feldspar present in the margins, which suggests that as the concretions grew, feldspar dissolution increased. In some cases the entire grain is replaced by calcite (Fig.4.7.), whilst in other examples, small detrital remnants survive and are engulfed by authigenic calcite (Fig.4.8.). Detrital quartz grains are also commonly leached in the concretions (Fig.4.9.). They show ragged edges and embayments, and are increasingly leached towards the margins of the concretions. Mica grains are slightly affected by this leaching event, they become frayed at the edges and expand outwards

(Fig.4.10.); occasionally they appear kaolinitized at the grain extremities showing textures similar to those described by Bjorlykke et al. 1979 and Boles & Johnson 1983. This mica texture predates calcite cementation.

Where the feldspar and rock fragments have been dissolved completely, they leave an obvious grain-sized pore in the sandstone which shows little evidence of the precursor grain (Fig.4.11.). The dissolution remnants of the feldspars are typically delicate structures, and they seldom show mechanical disruption or crushing as one might expect during the early stages of compaction. The relationship between the pore-filling calcite cement and the dissolution pore provides us with direct timing evidence for early secondary dissolution and replacement. No additional effective porosity can be demonstrated to have resulted from this process. However only very minor quantities <1% of diagenetic kaolinite and quartz formed at this time. Thus we think that some silica and aluminium have been exported from the sandstone.

4.4.2 Late secondary porosity

Late secondary porosity was formed after the main bulk of quartz cementation (Fig.4.12.) but before quartz, late calcite and dolomite growth had finished. The detrital components which were subject to dissolution include feldspar, calcareous fossil fragments, carbonate clasts and micas (Table 4.3.). Dissolution of feldspar grains ranges from none (in fine-grained sandstones) to totally dissolved and appears to be compositionally controlled, with plagioclase (Fig.4.13.) suffering less dissolution (Fig.4.14a&b). Comparison of feldspar contents in calcite cemented concretions (Table 4.1.) suggests that original feldspar contents in similar non-calcite cemented sandstones have been reduced by up to 50%, which has resulted in an enhanced secondary porosity increase of 2-5%. We noticed that some of the concretionary calcite cement was also dissolved in

the samples we examined, but it was restricted to the outer margins of the concretions (Fig.4.15. & 4.16.). Authigenic quartz is occasionally found precipitated inside secondary pores indicating that some of the leaching was contemporaneous with quartz precipitation (Fig.4.17.). Dissolution in the sandstones was variable in extent and resulted in slightly enhanced porosities in some areas due mainly to a depositional lithological control.

This porosity is not redistributional, as no late calcite cement corresponding to dissolved calcite occurs locally. The oversized pores subsequent to silicate dissolution may be due to additional dissolution of calcite cement which has replaced original silica grains during shallow burial. Local export of calcite cement has occurred, and these ions have either formed minor late dolomite and calcite throughout the sandstone, or have been exported totally from the sandstone.

4.5 FORMATION OF SECONDARY POROSITY ASSOCIATED WITH PRECIPITATION OF KAOLINITE

Authigenic kaolinite is only very rarely observed in secondary pores in association with relict grains of feldspar, a phenomenon also observed by Nedkvitne & Bjorlykke (1992). This is not consistent with the theory of secondary porosity, ie. feldspar dissolution is associated with concurrent kaolinite precipitation. An equation from Giles & de Boer (1990) relates the amount of feldspar to the volume of kaolinite and quartz produced:

$$2KAlSi_3O_8 + 2H_2CO_3 + 9H_2O = 2K^+_{(aq)} + Al_2Si_2O_5(OH)_4 + 4H_4SiO_4 + 2HCO_3^-$$

2K feldspar + fluid = fluid + kaolinite + 4 quartz

Giles and de Boer (1990) postulate that this reaction would probably happen where the waters had a silica content that put them in equilibrium with α-quartz and an aluminium content in equilibrium with a clay mineral - this

is the expected result of burial leaching of feldspars especially in a reservoir where the formation water has been in contact with the rocks for a considerable period of time.

Assuming that aluminium is conserved in this reaction, approximately 45 volume percent of the feldspar should be precipitated as kaolinite, this does not correspond with the pointcounted values of secondary feldspar porosity (5% average of whole rock) and kaolinite (<1%). The amount of kaolinite present is much too low to achieve a mass balance with secondary porosity by the above reaction. We also find that less kaolinite precipitates in the sandstones with the highest porosities, which suggests that the aluminium is being removed in solution. The low content of kaolinite in the entire South Brae Oilfield (C.Turner, Marathon *pers. comm.* 1991) suggests that the aluminium has been transported out of the reservoir - a possible site for redistribution of aluminium could be the Miller Oilfield which lies to the East of South Brae. However this field also contains very little kaolinite, and where present rarely exceeds 0.5% by volume (Gluyas, 1985). Thus it is more likely that aluminium has been exported to adjacent mudrocks, or upwards and westwards out of the system (although we have no geological evidence for either hypothesis).

Because of the low solubilities of aluminium from kaolinite in neutral pH waters (Curtis, 1983), it is very difficult to understand how the ions from the dissolved feldspar can be removed (although we do not know the pH of the South Brae waters at this time), either large quantities of water are removing the aluminium to the surface via faults or else the aluminium is being organically complexed which would increase its solubility very significantly (Surdam et al. 1984).

4.6 CONTROLS ON DISTRIBUTION OF SECONDARY POROSITY

Depositional facies type and distribution control total porosity and to a lesser extent permeability. Feldspar dissolution is most abundant in the coarse grained sandy lithologies, where a lack of significant compaction and the development of quartz overgrowths maintained open porespaces (Fig. 4.18.); these sandstones provide a conduit for the migration of dissolving fluids. The highest porosity (24.2%) and permeability values (961mD) are found in the sandy matrix conglomerates and massive sandstones, except where early calcite cementation has occurred.

In the fine-grained and siltier lithologies, increased compaction prevents and restricts the movements of the dissolving fluids and therefore these lithologies show less dissolution of feldspar and hence lower porosities. The finer grained sandstones have low to medium porosities and the permeabilities are also lower due to the existence of mudstone laminae (Fig.4.19.).

In general both parameters show an overall decrease with depth. As sorting becomes poorer and the section becomes more conglomeratic towards the base there is a reduction in porosity. The vertical porosity distribution shows a distinct vertical trend (Fig.4.20a-d.). Each figure shows a decline of porosity with depth. The vertical gradients within each well are similar/identical, ranging from 8.2 - 9.5%km^{-1} porosity loss. If well A3 and A19 are overlain (Fig.4.21.) and the vertical trend for A3 is projected, we can see that A19 has too much porosity for the depth it is currently at (3.0%km^{-1}). Therefore we expect A19 to be more quartzose than A3, and Miller to be more quartzose than South Brae. The average porosity values for each zone can be found in Table 4.4 and Figure 4.22. The general trend

in the reservoir is of increased porosity in the upper zones and the wells closer to the basin centre. Zone Aa_{2-4} in well A11 has an exceedingly high porosity value, this is probably due to the dissolution of a concretionary body. The lack of consistency of the porosity values attests to the complex nature of the reservoir system, the position of the well with respect to channels/interchannels and its diagenetic variations. In Figure 4.23 the total porosity values for each well were calculated from the vertical trends (derived from Fig.4.21.), the values were then contoured to illustrate the dissolving fluids pathway. The fluid pathway appears slightly complex due to the low porosity values in well A27. These lower porosity values are due to the large amount of conglomerate material making up the section. The conglomeratic material tends to have lower porosity than sandstones.

4.7. SOURCE OF AGGRESSIVE FLUIDS

The pore geometries of the Brae Formation sandstones which were produced by selective mineral dissolution signify two secondary porosity events. An early porosity event occurred contemporaneous with early calcite cementation, and took place between shallow to moderate depths. Temperature during its formation was probably similar to that at which calcite cementation occurred 15-75°C. A later porosity event occurs at elevated temperatures and at greater depths. It appears to have been contemporaneous with quartz cementation, but in other places quartz cementation had stopped - this event probably occurred at temperatures close to 100°C (Fig.4.24.). The source of the fluids which have caused this post depositional leaching are unknown but porewaters capable of dissolving minerals have two principal origins 1) meteoric or 2) basinal.

4.7.1 Meteoric Water

Dissolution caused by meteoric ground water is commonly an early diagenetic event forming at relatively shallow burial, normally less than 1000m (Bjorlykke et al. 1989). Secondary porosity by meteoric water dissolution requires a throughflow of porewater that is undersaturated with respect to one or more minerals present in the sandbody (Bjorlykke 1984). The leaching capacity of a meteoric water will depend upon the amount of dissolved CO_2 and the reactions that have occurred as it passes through the reservoir (Giles & Marshall, 1986). Mixing corrosion may enhance the leaching potential, particularly at low temperature and in fractured rocks. Mixing corrosion was originally described by Bogli (1964), it is most likely to occur at sites where meteoric water mixes with seawater or basinal brines. It arises when two solutions of different compositions which are both in equilibrium with a given mineral are mixed, the result is a solution either under or oversaturated with respect to the mineral in question. Leaching will result when the solution is undersaturated.

Meteoric water flushing is possibly the dissolving agent for early secondary porosity in South Brae as it mixed with the interstitial porefluids, this porewater then proceeded to precipitate concretionary calcite for which the $\delta^{18}O$ values display a distinct meteoric signature.

4.7.2 Connate Water- Basinal Brine

Connate water is the depositional porewater buried with sediments; it can be forced upwards by the compaction of sediments. Its flow is limited by the amount of water contained in the underlying sedimentary sequence in the basin. The total average upwards flow of porewater has been calculated as 10^4 - 10^5 $cm^3 . cm^{-2}$ for a bed of sandstone from the time of deposition to 3km burial (Bjorlykke 1984). Secondary dissolution has been ascribed to ascending compactional waters containing a number of solvent constituents (Carothers & Kharaka 1978, Surdam et al. 1984 and Giles &

Marshall 1986).

Leaching has been attributed to the CO_2 released from maturing kerogen due to decarboxylation forming carbonic acid in porewater. The amount of CO_2 that is released, is dependent on the type of kerogen present in the source rock (Bjorlykke 1984). The acidic fluids are thought to migrate to the reservoir, and by dissolving carbonate and feldspar create secondary porosity. However, studies by Bjorlykke (1980,1984) & Lundegard et al. (1984) have shown that even if all the CO_2 generated could escape from the source rocks, there is still insufficient volume to account for the large amounts of observed secondary porosity.

In the South Brae calcite-cemented concretions we have evidence that CO_2 was being produced from organic matter by thermal maturation, this CO_2 has been incorporated into the diagenetic calcite. The carbon isotope signatures range from +3.66 to -11.66‰ (PDB), and the CO_2 from the organic source has a considerable input. Therefore much of the CO_2 generated from organic matter ends up as carbonate concretions and not as a leaching agent.

Carothers & Kharaka (1978) showed that oilfield waters can contain considerable amounts of dissolved aliphatic monocarboxylic acids. Surdam et al. (1984) hypothesized from their experiments with acetic acid solutions that secondary porosity is the natural consequence of the interaction of organic and inorganic reactions during progressive diagenesis.

Giles and de Boer (1989) postulated that porewaters were initially in equilibrium with calcite at depth; when forced to rise through an aquifer these cool due to their movement up through the basin. As they ascend

they become cooler, they also become undersaturated with respect to calcite and are then capable of dissolving it. Upon migrating the formation water may become oversaturated with respect to silica and silica cementation may accompany leaching, the fluids may also be no longer in equilibrium with feldspar. A rising porewater with leaching ability may be the cause for the late secondary porosity in South Brae. Giles (1987) postulated that high permeability pathways give rise to narrow intense zones of leaching. If this is the case it appears that the fluid may have been focused in the top layer of the field ie. Zone A, as this is where secondary porosity is most prevalent. It was possibly forced through this zone as it was the most porous and permeable on deposition, and extends furthest into the basin. Figure 4.25a&b show the distribution of calcite cements for four different zones in South Brae Oilfield. It is apparent that the deeper zones contain more calcite cement than the shallower zones Aa_{1-4} and Ac_{2-6}. This may be due to the preferential removal of calcite from the most porous zones by dissolving basinal fluids. This same aquifer was possibly a pathway for hot isotopically heavy waters being driven by sediment compaction out of the basin as shown by $\delta^{18}O$ evidence in our diagenetic quartz model (see Chapter 3). These fluids were probably less saline and less dense and floated on top of the heavier saline porewaters.

Giles and de Boer (1989) calculated that the formation waters need a pH below 7 before they can become undersaturated with respect to calcite at reservoir temperatures. Carbon dioxide and carboxylic acids can shift the pH of the formation water towards an acidic value and into the pH range in which cooling will result in significant undersaturations. South Brae formation waters currently have a pH of 4.5 - 4.8 (J.Hardy, Marathon *pers. comm.*) and it is most likely that the dissolving waters would have had a similar pH.

4.8 PATHWAYS FOR AGGRESSIVE FLUIDS

Magara (1976) suggested that compactional porewater preferentially flows in highly permeable and extensive sandstones. According to such a model, most leaching would be expected to occur in the most laterally extensive sandstone layer. Many other authors agree that maximum leaching by porewaters will occur in sandstones having the highest primary porosity (Giles 1987). Giles and de Boer (1989) suggest that a large interval between the starting point and the aquifer is necessary for a dissolving fluid to have the potential to leach (ie. the time to cool down), this interval may possibly be a fault plane. They also suggest that secondary porosity could occur during episodic release of formation water during faulting or overpressure release.

4.9. CONCLUSIONS

1) Early secondary porosity was due to meteoric flushing-water driven by hydraulic head. This fluid was initially undersaturated with respect to silica and calcite; thus, feldspar and quartz grains were leached and high Mg calcite shells were also dissolved. A concretionary calcite cement was then precipitated in these sites and shells were recrystallized.

2) Late secondary porosity was due possibly to the movement of compactional basinal fluids out of the basin, laterally through the reservoir. These fluids were focused through the uppermost aquifer which is also the most porous sandstone of the field (Fig.4.22.). As the fluid moved upwards it began to cool and possibly became undersaturated with respect to calcite cement and feldspar, causing leaching (Giles & de Boer, 1989). A layer of moving warm undersaturated porewater over more saline

cooler, static water may have existed during quartz cementation, and the short episode of secondary porosity generation. The time span of secondary porosity generation was short (little quartz cement post dates late secondary porosity), and must represent a rapid basinal expulsion period and the drop from overpressure to hydrostatic pressure (Fig.4.24.).

3) The aluminium released into this leaching solution was to a major extent removed from the sandstones. Large quantities of water may have carried the aluminium out of the reservoir or it may have been complexed. The ultimate fate of the dissolved and transported aluminium is a problem, as no trace is found in the adjacent Miller field to the east, we must assume it was carried up the faults on the western side of the South Brae field. This process has modified the bulk sandstone mineralogy from a sub-arkose to a diagenetic quartz arenite.

4) It is very difficult to quantify the exact volumes of secondary porosity created by leaching, as some of the material dissolved may be reprecipitated elsewhere in the sandstone. However plots of porosity versus depth and point count data suggest that up to 14% secondary porosity was formed. This may locally comprise 75% of the effective porosity.

4.10. ACKNOWLEDGEMENTS

Marathon Oil (U.K.) Ltd. provided the funding for this project and allowed access to their data and core of the South Brae Oilfield. This research was carried out at the Department of Geology and Applied Geology, University of Glasgow, and the Isotopes Geology Unit, Scottish Universities Research and Reactor Centre (SURRC). The authors would also like to thank Douglas Maclean (Glasgow University) for his help with the production of photomicrographs.

4.11. REFERENCES CITED

Bjørlykke, K., Elverhoi, A. & Malm, A.O. (1979) Diagenesis in Mesozoic sandstones from Spitsburgen and the North Sea - A comparison. Geologische Rundschau, v.68, pp.1152-1172.

Bjørlykke, K. (1980) Clastic diagenesis and basin evolution- Revista del Instituo Geologas, Diputacion Provincial Universidad de Barcelona, 34, pp.21-44.

Bjørlykke, K. (1984) Formation of secondary porosity: how important is it ? In: McDonald, D.A. & Surdam, R.C. (eds.), Clastic Diagenesis. Memoir American Association of Petroleum Geologists, Special Publication, 37, pp. 277-286.

Bjorlykke, K. Ramm, M. and Saigal, G.C. (1989) Sandstone diagenesis and porosity modification during basin evolution. Geologische Rundschau, v.78/1. pp.243-268.

Bögli,A. (1964) Mischungskorrosion, ein Beitrag zum Verkastungsproblem. Erdkunde, v. 18, pp. 83-92.

Boles, J.R. & Johnson, K.S. (1983) Influence of mica surfaces on porewater pH. Chemical Geology, v.43, pp.303-317.

Carothers, W.W. & Kharaka, Y.K. 1978. Aliphatic acid ions in oil-field waters-implications for origin of natural gas. Bulletin of the American Association of Petroleum Geology, v.62, pp. 2441-2453.

Curtis, C.D. (1983) Link between Al mobility and destruction of secondary porosity. American Association of Petroleum Geologists Bulletin, v.67, pp.380-384.

Giles, M.R. & Marshall, J.D. (1986) Constraints on the development of secondary porosity in the subsurface: re-evaluation of processes. Marine and Petroleum Geology, v. 3, pp. 243-255.

Giles, M. R. (1987) Mass transfer and problems of secondary porosity creation in deeply buried hydrocarbon reservoirs. Marine and Petroleum Geology, v.4. pp.188-204.

Giles, M. R., & de Boer, R. B (1989) Secondary porosity: creation of enhanced porosities in the subsurface from the dissolution of carbonate cements as a result of cooling formation waters. Marine and Petroleum Geology, v.6. pp.261-269.

Giles, M. R., & de Boer, R. B (1990). Origin and significance of redistributional secondary porosity. Marine and Petroleum Geology, v.7, pp. 378-397.

Gluyas, J. (1985) Reduction and prediction of sandstone reservoir potential, Jurassic, North Sea. Philosophical Transactions of The Royal Society, v.315. pp.187-202.

Gluyas, J., & Coleman, M. (1992) Material flux and porosity changes during sediment diagenesis. Nature, v.356. pp.52-54.

Houseknecht, D.W. (1987) Assessing the relative importance of compaction processes and cementation to reduction of porosity in sandstones. American Association of Petroleum Geologists Bulletin, v. 71, pp.633-642.

Lundegard, P.D., Land, L.S. & Galloway, W.E. (1984) Problem of secondary porosity: Frio Formation (Oligocene), Texas Gulf Coast. Geology, v. 12, pp. 399-402.

Magara, K. (1976). Water expulsion from clastic sediments during compaction, directions and volumes. Bulletin of the American Association of Petroleum Geologists, v. 60, pp. 543-553.

Nedkvitne, T., & Bjorlykke, K. (1992). Secondary porosity in the Brent Group (middle Jurassic), Hulda field, North Sea: Implication for predicting lateral continuity of sandstones? Journal of Sedimentary Petrology, v. 62(1), pp. 23-34.

Oertel, G., & Curtis, C. D. (1972). Clay-ironstone concretion preserving fabrics due to progressive compaction. Bulletin of the American Association of Petroleum Geologists, v. 83, pp. 2597-2606.

Schmidt, V., & McDonald, D. A. (1979). Texture and recognition of secondary porosity in sandstones. In P. A. Scholle & P. R. Schluger (Eds.), Aspects of Diagenesis (pp. 209-225). Tulsa, Oklahoma: Society of Economic Palaeontologists and Mineralogists. Special Publications.

Sclater, J.G., & Christie, P.A.F. (1982) Continental stretching: an explanation of the post-Mid Cretaceous subsidence of the Central North Sea Basin. Journal of Geophysical Research, v. 85, pp.3711-3739.

Stoker, S., and Brown, S. (1987) Coarse clastic sediments of the Brae field and adjacent areas, North Sea: a core workshop. British Geological Survey. Hydrocarbons Research Programme.

Surdam, R.C., Boese, S.W. & Crossey, L.J. 1984. The chemistry of secondary porosity. In: McDonald, D.A. & Surdam, R.C. (eds.), Clastic diagenesis. 37, American Association of Petroleum Geologists, pp.127-150.

4.12 TABLES

Table 4.1.
Volume percent feldspar (plagioclase & K-feldspar) and total porosity for quartz and calcite cemented sandstones in the South Brae Oilfield, North Sea, U.K. 500 point counts were made on each section. Zone Aa_1 etc. refer to stratigraphic layers downwards.

	Average Feldspar %		Average Total Porosity%
Zone	Calcite Cemented	Quartz Cemented	Quartz Cemented
Kimm.	-	3.5	14.3
Aa_1	-	3.3	12.3
Aa_{2-4}	4.6	3.0	13.6
Ab	-	-	19.0*
Ac_{2-6}	-	5.6	12.8*
Ad	10.6*	5.8*	16.6*
Ba_{1-4}	3.9	4.1	8.4
Bc_{1-4}	3.6	-	-
Ca_{1-4}	5.0*	-	-
Cc_{1-3}	4.9	3.0	7.4
Cd	5.8*	-	-

*One sample only

Table 4.2.

Point count data for volume percent of calcite in calcite cemented concretions, decreasing amounts of calcite reflect the decreasing amount of available space for its precipitation.

Well no.	Depth T.V.D. (ft)	Calcite Cement %
16/7a-A6	13412'	37.4
	13415'	44.4
	13419'	38.6
	13422'8"	23.8
16/7a-A11	13694'	28.2
	13702'4"	34.2
	13703'5"	32.0
	13707'9"	29.5
	13776'	38.2
	13778'	41.4
	13778'6"	35.8
16/7b-A19	13501'	32.4
	13501'5"	33.6
	13502'8"	31.2
	13504'	30.0
	13504'1"	27.6
	13506'	18.5
16/7a-A27	13526'	21.8
	13535'	28.8
	13536'	37.4
	13538'	26.0

Table 4.3.

Summary of porosity analysis from thin sections from wells 16/7a-A3, A11, A19 & A27, based on 500 point counts per sample. All depths given are T.V.D. (ft).

Well (sample)	Zone	Total Ø	Primary Ø	Secondary Ø			
				Micro Ø	Feldspar Ø	Cement Ø	Total Secondary Ø
A3 12080'	Aa_1	11.6	5.3	1.9	4.2	0.2	6.3
A3 12111'5"	Aa_{2-4}	9.2	5.8	2.1	1.3	0.0	3.4
A3 124333'2"	Ad	11.0	6.2	1.9	2.3	0.6	4.8
A3 13441'1"	Cc_{1-3}	9.0	2.3	2.4	2.7	1.6	6.7
A11 12750'	Aa_1	13.0	6.5	1.3	4.4	0.8	6.5
A11 12828'	Ab	19.0	5.1	1.3	7.7	4.9	13.9
A11 13678'9"	Cc_{1-3}	14.6	3.7	2.0	5.7	3.2	10.9
A19 13355'	Aa_1	19.0	8.7	0.2	9.0	1.1	10.3
A19 13415'	Aa_{2-4}	19.4	7.6	1.0	8.5	2.3	11.8
A19 13630'	Aa_{2-4}	14.8	6.0	1.0	6.3	1.5	8.8
A27 13061'	Aa_1	12.4	6.3	0.1	4.9	1.1	6.1
A27 13413'6"	Ad	16.6	8.8	0.8	5.8	1.2	7.8
A27 13554'4"	Ba_{1-4}	12.6	3.8	0.4	7.3	1.1	8.8

Table 4.4. Average helium porosity values for zones within South Brae Oilfield, the porosities are from an internal Marathon report (1991). They are mean values for each zone.

	Aa_1	Aa_{2-4}	Ab	Ac_{1-6}	Ad	Ba_{1-4}	Bb	Bc_{1-4}	Bd	Ca_{1-4}	Cb	Cc_{1-3}	Cd
A3	16.3	10.4	-	10.4	10.4	10.1	-	10.5	-	8.1	-	8.4	-
A6	14.0	-	-	11.1	-	11.3	-	11.9	-	10.4	-	-	-
A11	13.3	21.9	-	10.6	-	11.5	-	-	-	-	-	10.6	-
A19	14.2	13.2	-	13.4	-	-	-	-	-	-	-	-	-
A27	14.8	9.9	-	11.7	-	11.4	-	-	-	-	-	-	-

4.13. FIGURE CAPTIONS AND FIGURES

Figure 4.1 Schematic depositional model, Unit 2 (late Oxfordian to late Volgian age), South Viking Graben (after Stoker & Brown, 1987)

Figure 4.2 South Brae area top structure map showing location of wells studied and the location of the major faults.

Figure 4.3 Minus cement porosity data for concretions in wells 16/7a-A6, A11, A27 & 16/7b-A19, showing decreasing cement volumes and increasing compaction towards the concretion margins.

Figure 4.4a Cathodoluminescence photomicrograph of a rock fragment in a calcite cemented conglomeratic unit, microporosity shows up as a bottle green colour, 16/7a-A11, 13702'4" (T.V.D.)

Figure 4.4b Plane polarized photomicrograph of the same rock fragment with microporosity stained green, 16/7a-A11, 13702'4" (T.V.D.)

Figure 4.5 Cathodoluminescence photomicrograph of a recrystallized brachiopod, the cathodoluminescence colour of the clast and the cement are identical, 16/7a-A11, 13694' (T.V.D.).

Figure 4.6 Cathodoluminescence photomicrograph of the centre of a calcite cemented concretion, here the feldspar is preserved to a greater extent and has only suffered minor dissolution, 16/7a-A11, 13702'4" (T.V.D.).

Figure 4.7 Cathodoluminescence photomicrograph of a feldspar grain almost completely replaced by calcite cement, 16/7a-A11, 13707'9" (T.V.D.).

Figure 4.8 Cathodoluminescence photomicrograph of two large feldspar grains showing partial dissolution, whilst a smaller grain in the corner of the view is still fresh. This sample is from the lower rim of an 11ft concretion (see Fig.4.3.), 16/7a-A6, 13422'8" (T.V.D.).

Figure 4.9 Crossed polars photomicrograph of a calcite cemented concretion (near margin), notice that many of the quartz grains have large embayments, 16/7a-A6, 12996'6" (T.V.D.).

Figure 4.10 Crossed polars photomicrograph of a calcite cemented concretion with a mica grain being splayed and with embayed detrital quartz grains, 16/7b-A19, 13501' (T.V.D.).

Figure 4.11 Cathodoluminescence photomicrograph of a calcite cemented concretion where replacement of a feldspar grain or a rock fragment has left an obvious grain-sized pore. In this example it is impossible to determine the precursor grain mineralogy, 16/7a-A27, 13535' (T.V.D.).

Figure 4.12 Paragenetic sequence showing timing of major authigenic and dissolution events in the South Brae oilfield.

Figure 4.13 Crossed polars photomicrograph showing minor dissolution of a microcline grain. Throughout the reservoir plagioclase

and microcline grains are fresher in appearance than K-feldspar. 16/7b-A19, 13504' (T.V.D.).

Figure 4.14a,b Plane and crossed polarized light photomicrographs showing a large grain of feldspar undergoing dissolution, yet the plagioclase grain in the corner of view remains untouched. 16/7b-A19, 13415' (T.V.D.).

Figure 4.15 Scanning Electron Microscope back scatter image which highlights secondary porosity (black) development at the top edge of a calcite cemented concretion. The calcite cement is pale grey, 16/7b-A19, 13501' (T.V.D.).

Figure 4.16 Plane polarized light photomicrograph showing dissolution of concretionary calcite cement resulting in oversized pores. Remnants of calcite cement occur, and the lack of quartz overgrowth shows this to have been an 'early' calcite cement, 16/7b-A19, 13501' (T.V.D.).

Figure 4.17 Plane polarized light photomicrograph showing a quartz overgrowth protruding into a large secondary dissolution pore, which contains remnants of the original grain (possibly feldspar). The dark pore filling material is bitumen, 16/7a-A3, 12433'2" (T.V.D.).

Figure 4.18 Plane polarized light photomicrograph of well developed quartz overgrowths, in depositionally coarse sandstones they prevent further compaction of the sandstone and the large porespaces allow through movement of dissolving fluids, 16/7a-A27, 13554'4" (T.V.D.).

Figure 4.19 Crossed polars photomicrograph showing a fine-grained sandstone with mudstone laminae. 16/7a-A11, 13772'3" (T.V.D.).

Figure 4.20a-d Vertical porosity trends (primary plus secondary) for wells 16/7a-A3, A6, A11, A27 & 16/7b-A19 showing overall decline with depth-controlled mainly by facies. The porosity values are derived from an internal Marathon report, they are mean values for each subzone (The average values for each zone can be found in table 4.4.).

Figure 4.21 A plot of the % vertical porosity gradients against depth (T.V.D.) for the wells 16/7a- A3, A11, A27 & 16/7b-A19. The gradients vary between 8.2%.km^{-1} to 9.5%.km^{-1}. Each well shows a similar decline of porosity with depth, although A19 has an excess of 3.0% porosity (if the A3 gradient is projected to a similar depth). This is probably due to its distal position in the field ie. it is closest to the dispelled basinal fluids.

Figure 4.22 This diagram shows the average porosity value for each zone in wells 16/7a-A3, A11, A27 & 16/7b-A19. The values have been taken from Table 4.4. There is an obvious increase in porosity towards the top of the reservoir, particularly in zone A. The dissolving fluids were focused in this zone due to its excellent aquifer qualities. Large arrows indicate the main route taken by dissolving fluids. The star indicates the highest porosity of all 4 wells.

Figure 4.23 This diagram shows the porosity value (for each zone) calculated from the vertical porosity trends shown in Figure 4.20a-d. The porosity values have been contoured to show the possible pathway of the dissolving fluid. Porosities are lower in A27 (due to its conglomeratic nature) which makes the pathway slightly convoluted.

Figure 4.24 Burial curve for the Brae Formation (Oxfordian) in the South Brae field with rough estimates of precipitation and dissolution events. The reconstructed burial curve is based on well 16/7a-8 and uses present day rock thicknesses.The burial curve has been decompacted and backstripped.

Figure 4.25a,b Four diagrams which show the different zones of the South Brae reservoir. The varying amounts of carbonate in the numerous wells for each zone are illustrated. It is apparent that the lower zones (B &C) contain a greater amount of carbonate cement than zone A. This is due to preferential dissolution of calcite in the most porous and permeable layer.

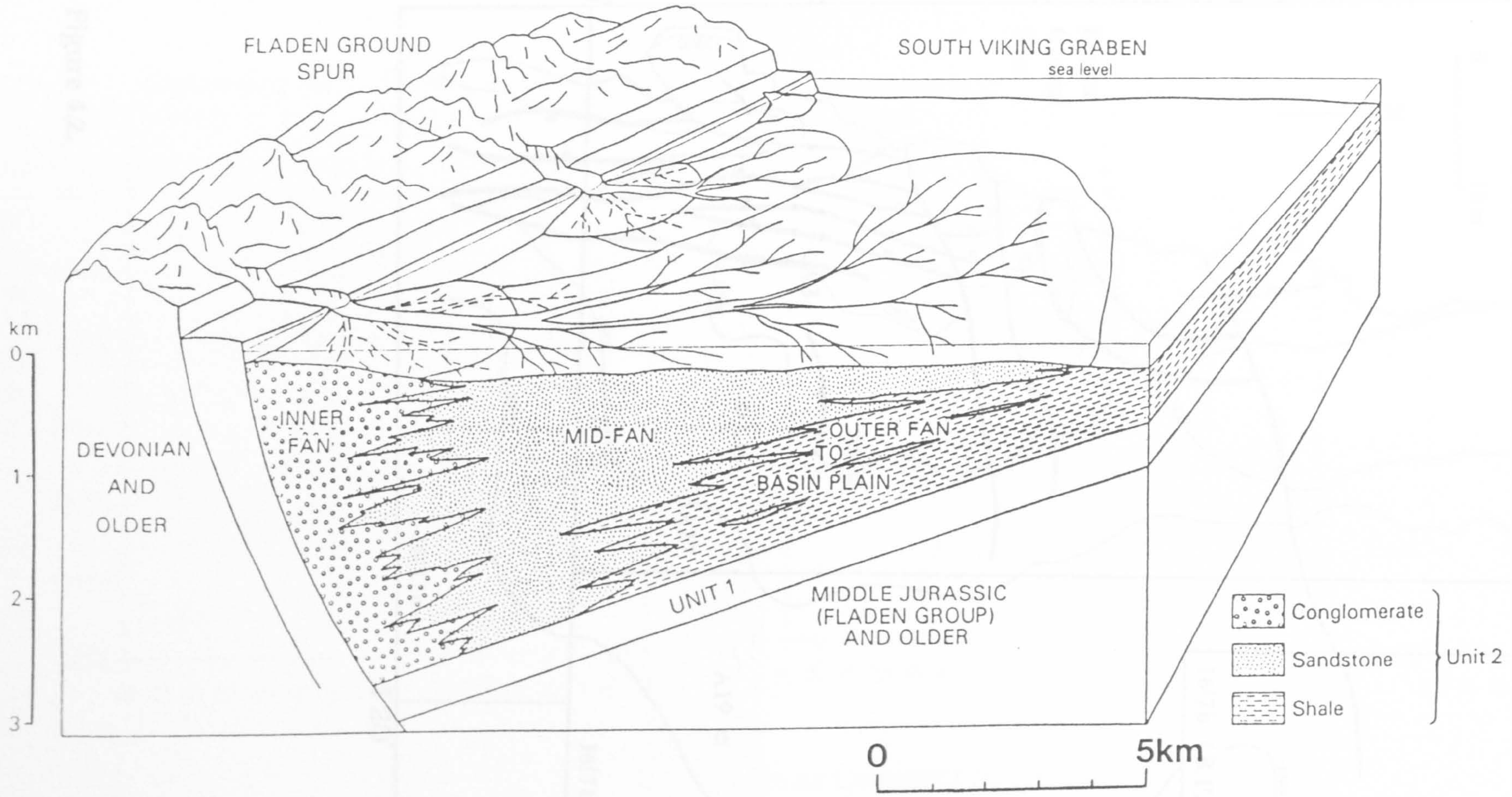
FLADEN GROUND
SPUR
SOUTH VIKING GRABEN
sea level
km
0
1
2
3
DEVONIAN
AND
OLDER
INNER
FAN
MID-FAN
OUTER FAN
TO
BASIN PLAIN
UNIT 1
MIDDLE JURASSIC
(FLADEN GROUP)
AND OLDER
Conglomerate
Sandstone
Shale
Unit 2
0
5km

Figure 4.1.

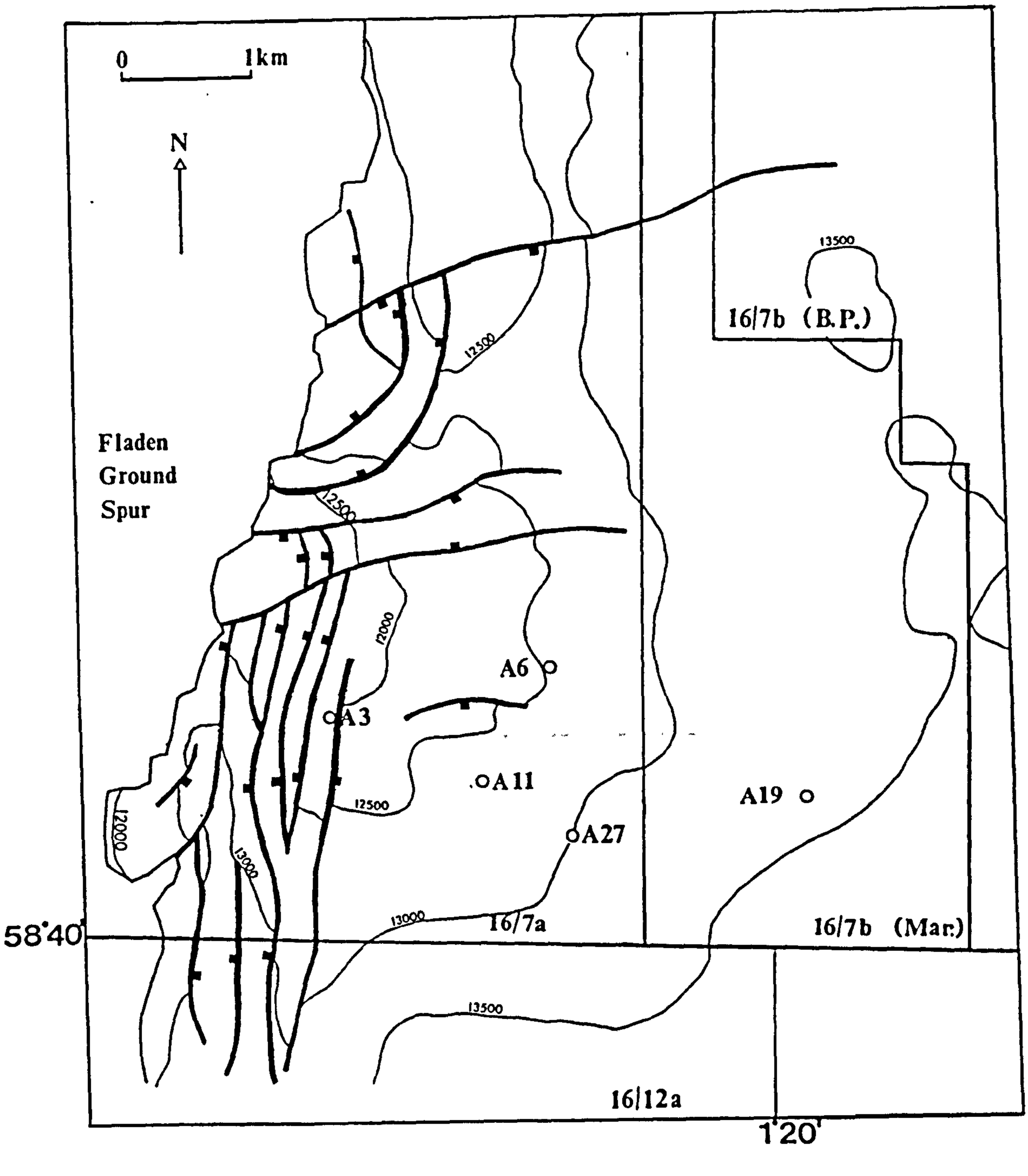
0
1km
N
Fladen
Ground
Spur
12500
12500
12000
12000
13000
13000
13500
16/7b (B.P.)
A6
A3
A11
A19
A27
16/7a
16/7b (Mar.)
16/12a
58°40'
1°20'

Figure 4.2.

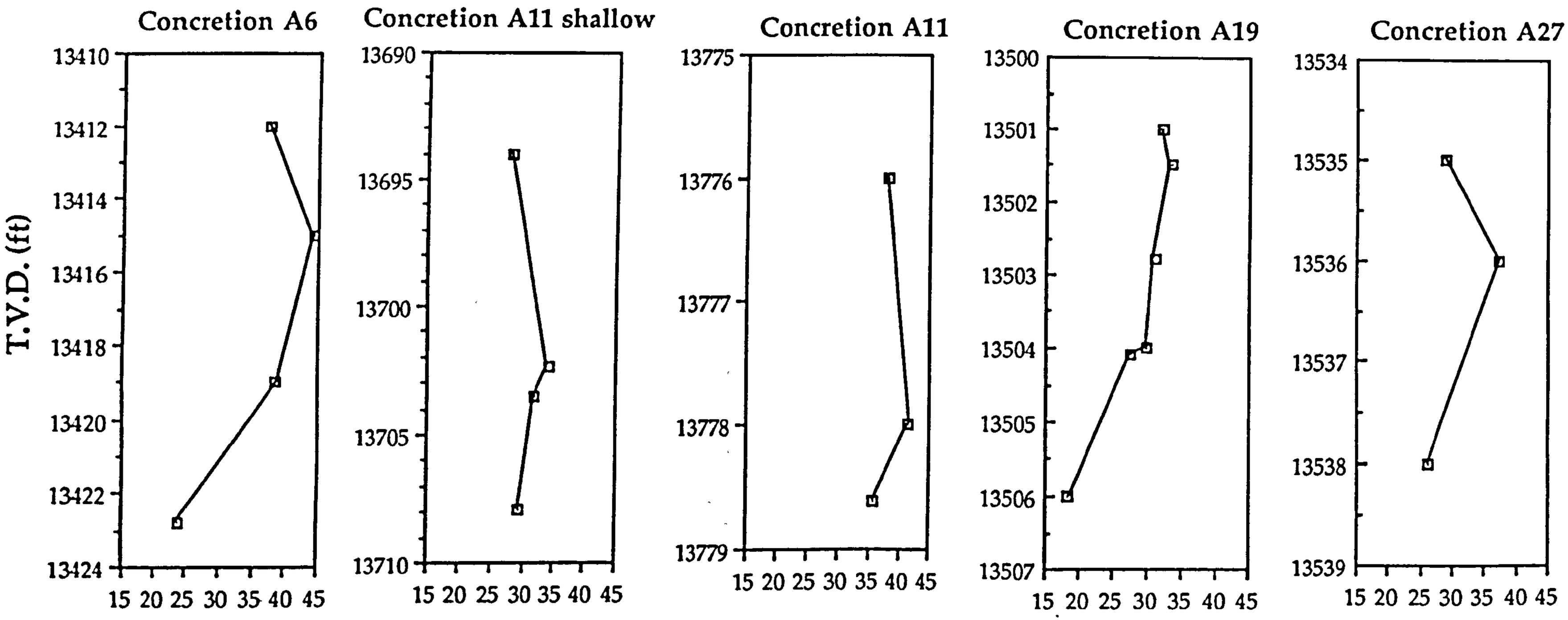
Concretion A6
Concretion A11 shallow
Concretion A11
Concretion A19
Concretion A27
T.V.D. (ft)
13410
13412
13414
13416
13418
13420
13422
13424
13690
13695
13700
13705
13710
13775
13776
13777
13778
13779
13500
13501
13502
13503
13504
13505
13506
13507
13534
13535
13536
13537
13538
13539
15 20 25 30 35 40 45
Minus Cement Porosity%

Figure 4.3.

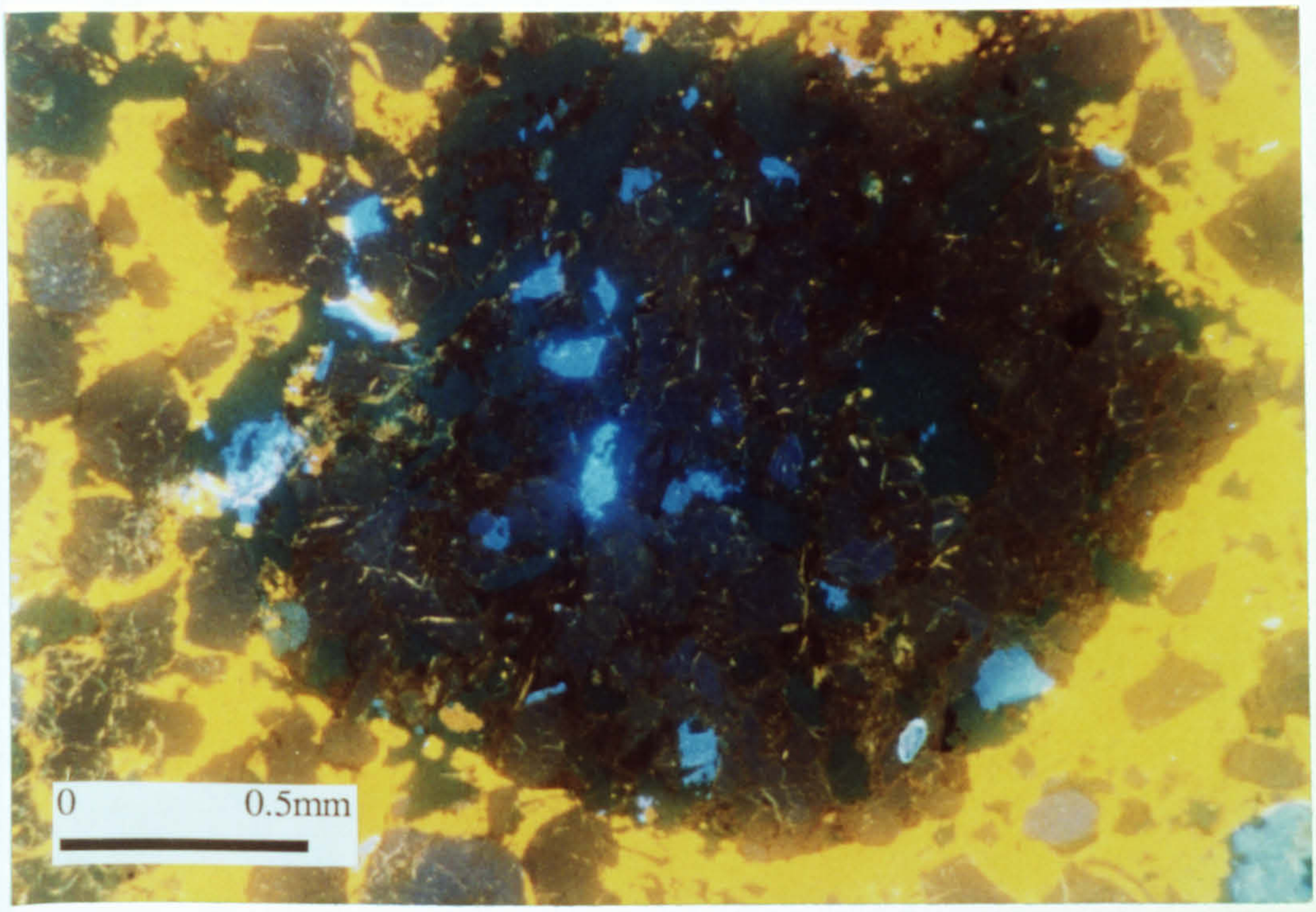

Figure 4.4a.

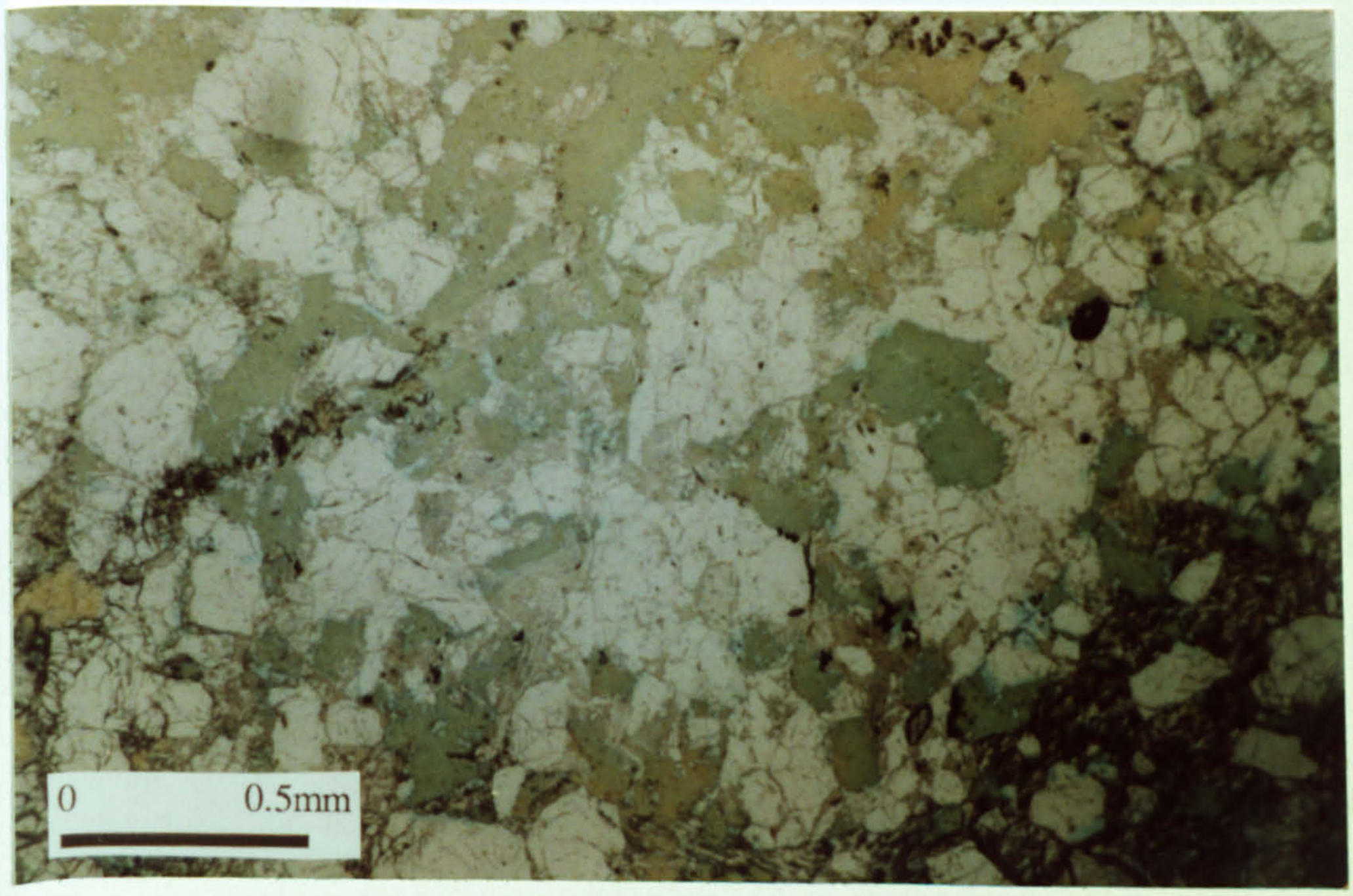

Figure 4.4b.

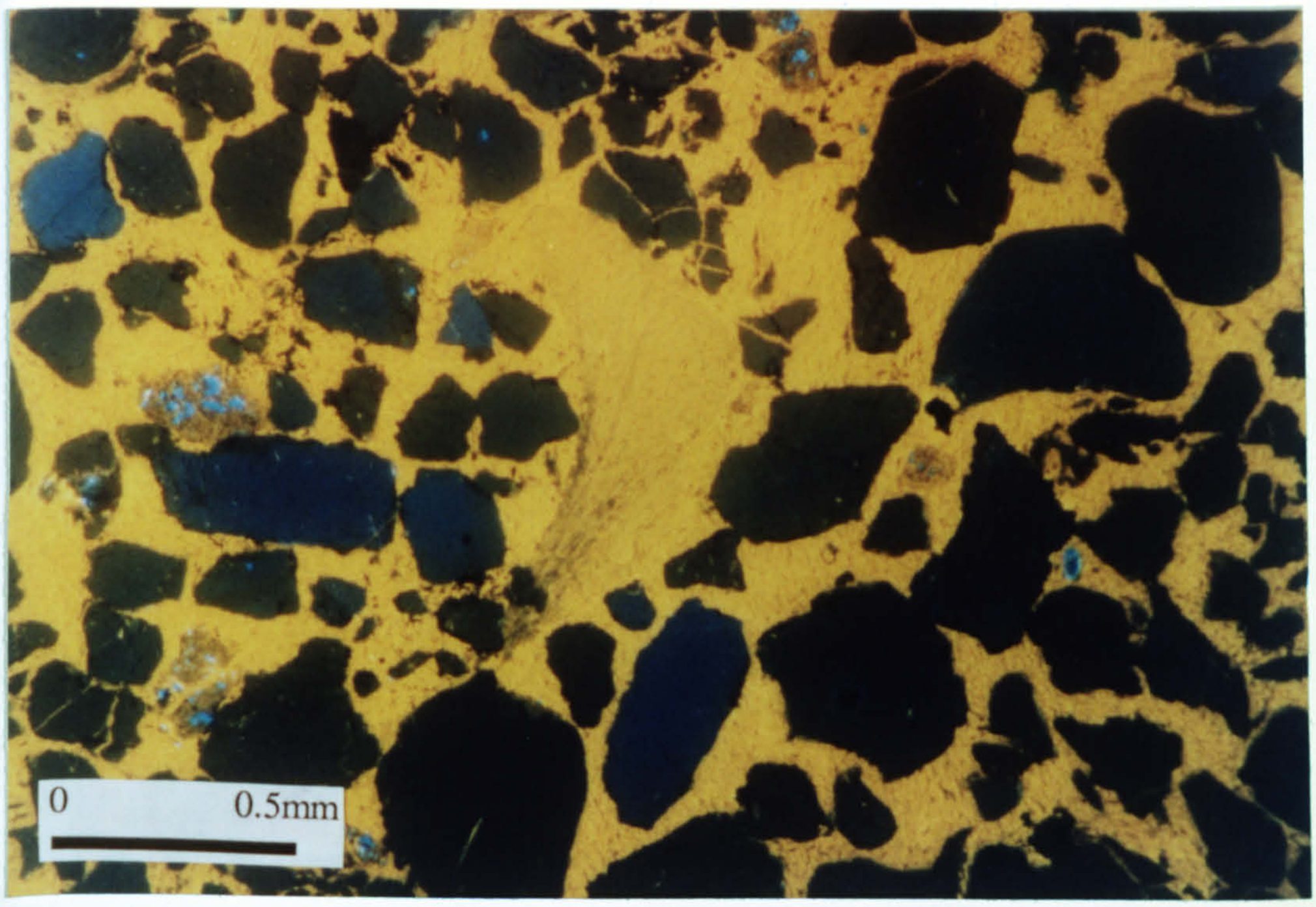

Figure 4.5.

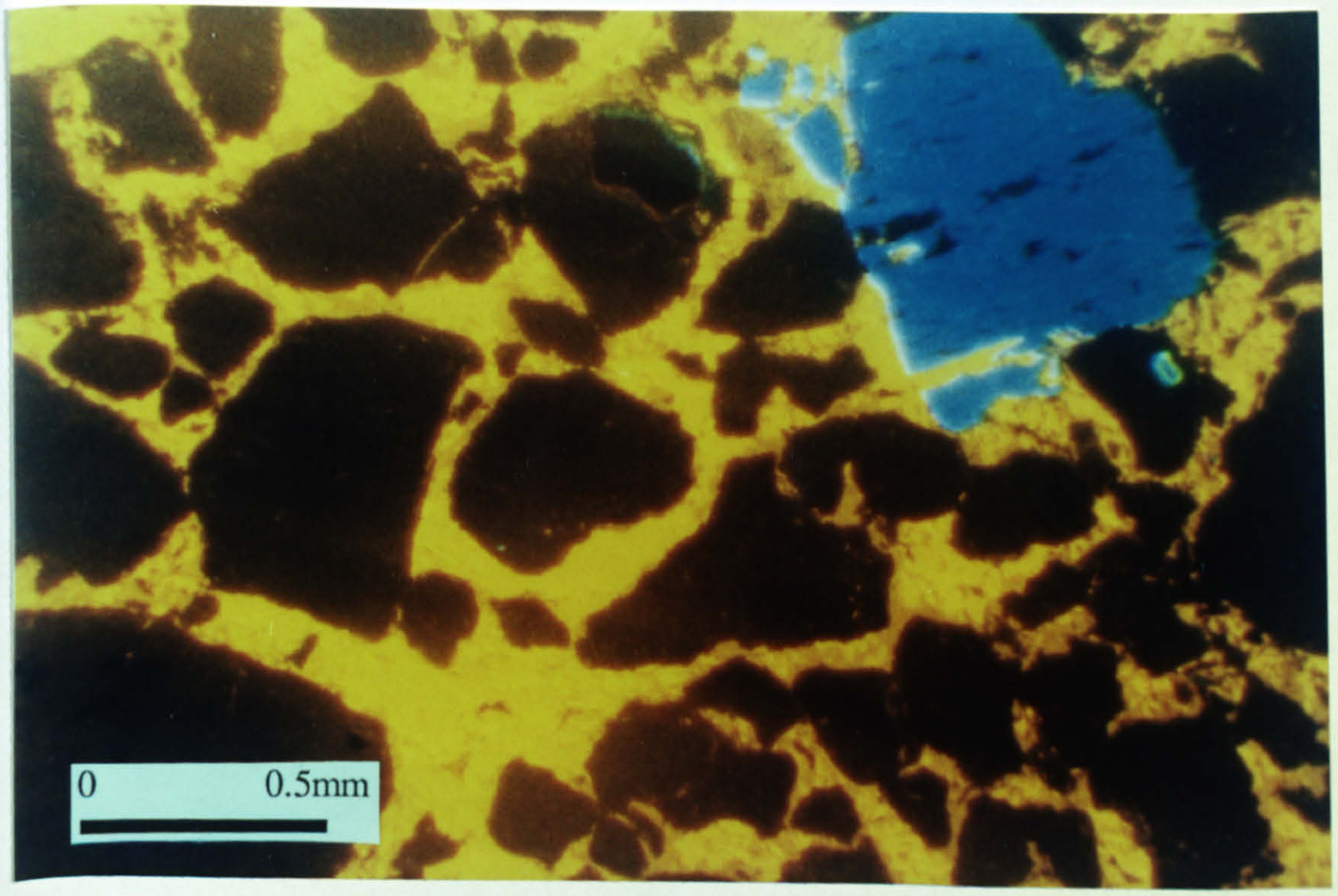

Figure 4.6.

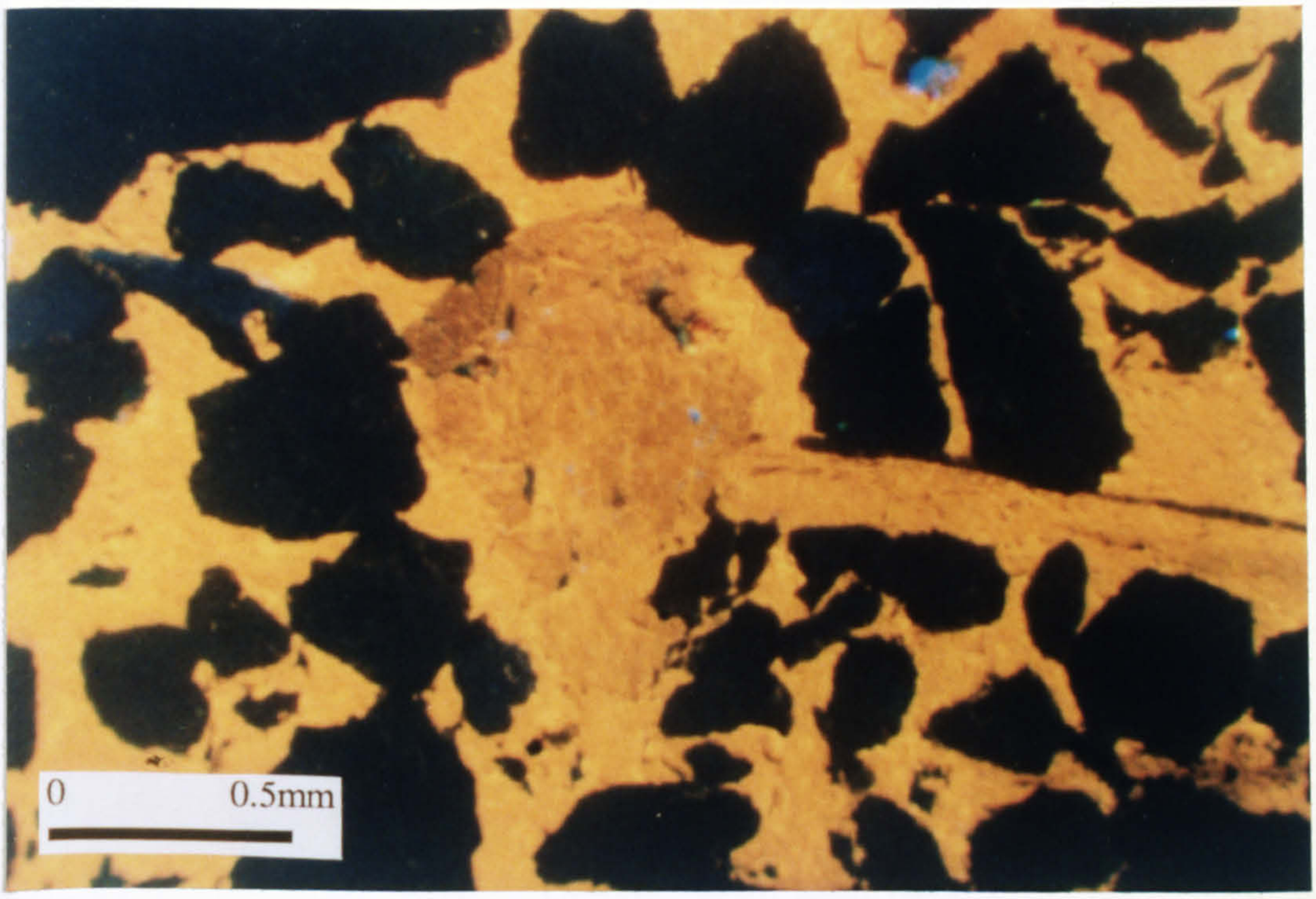

Figure 4.7.

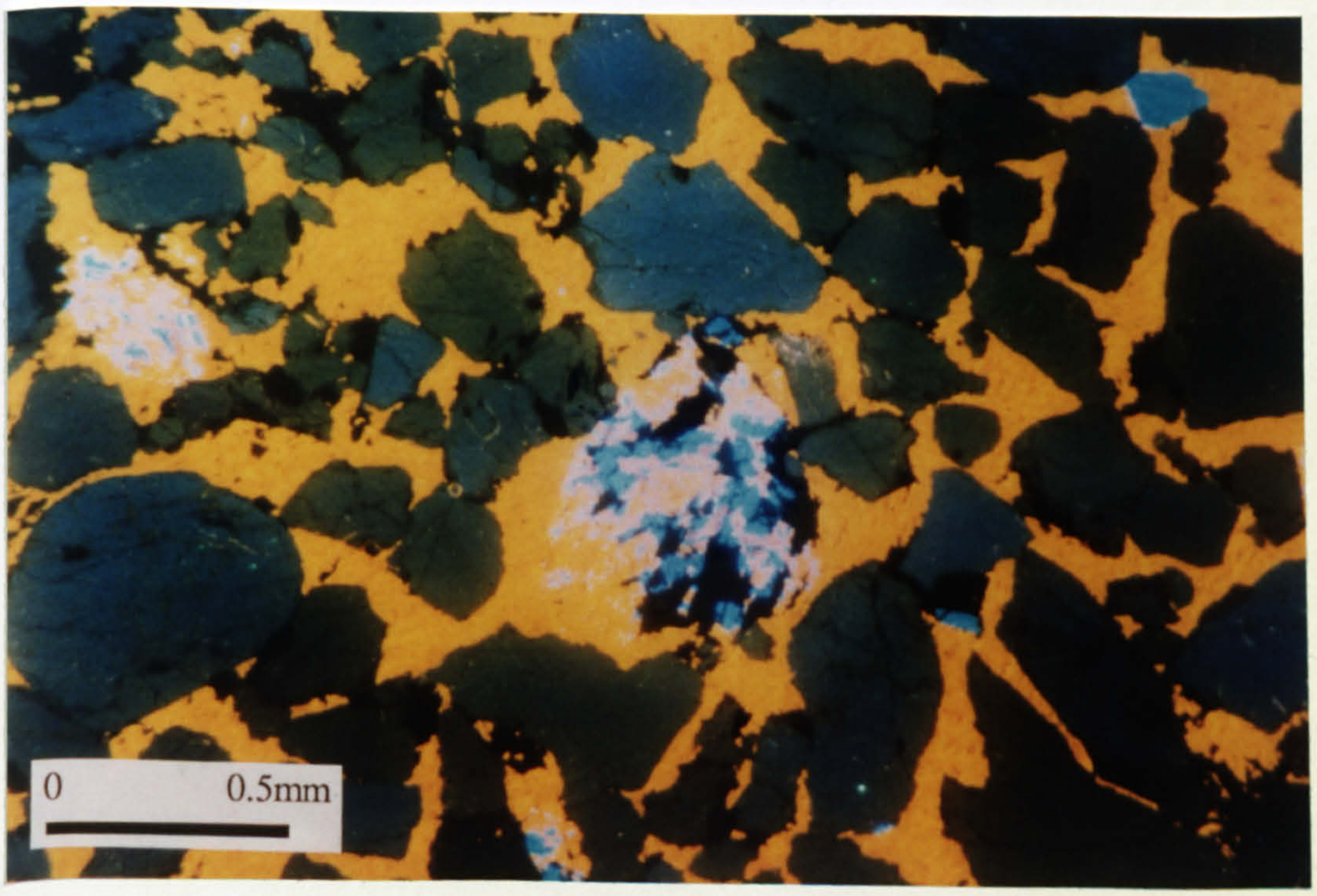

Figure 4.8.

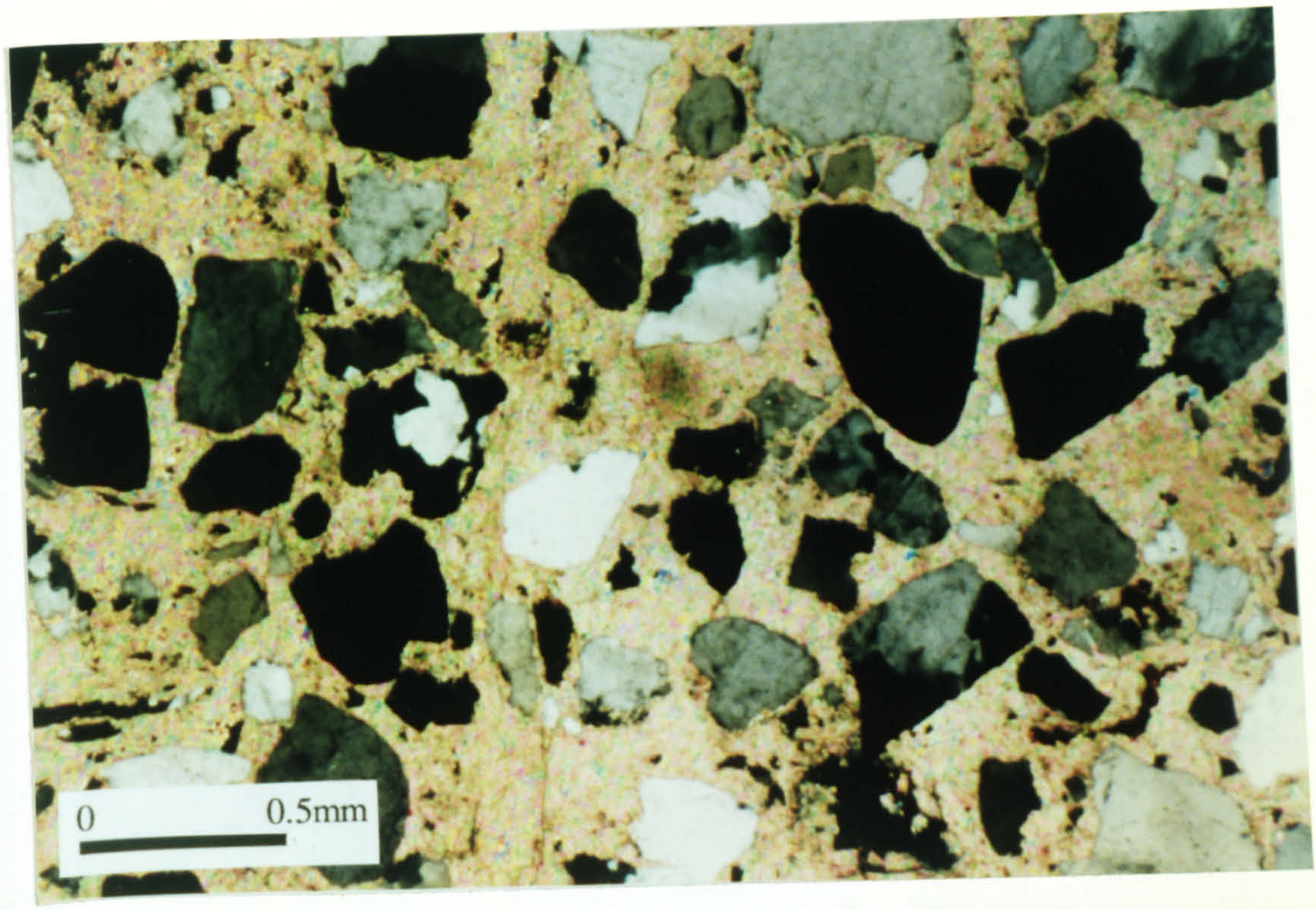

Figure 4.9.

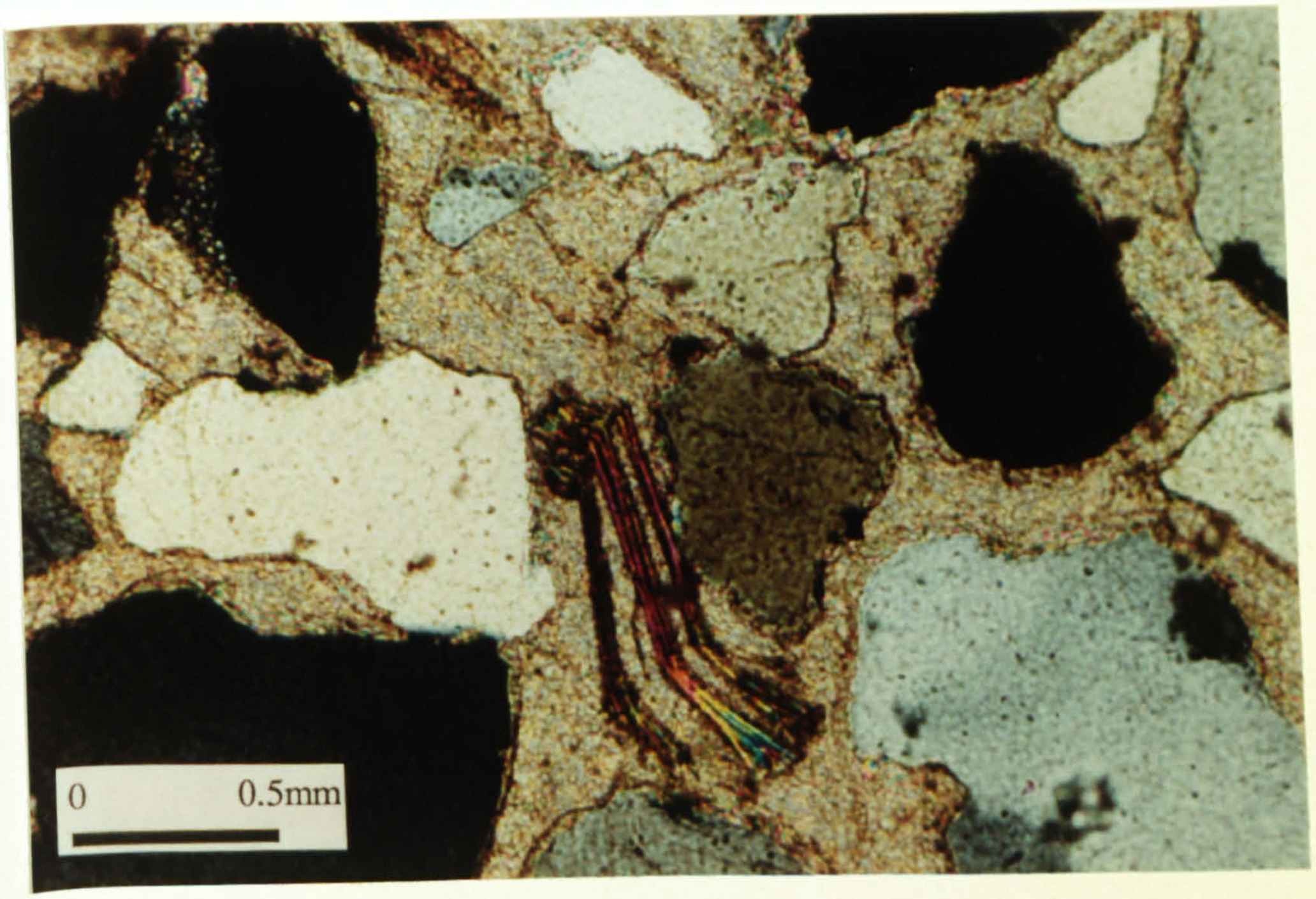

Figure 4.10.

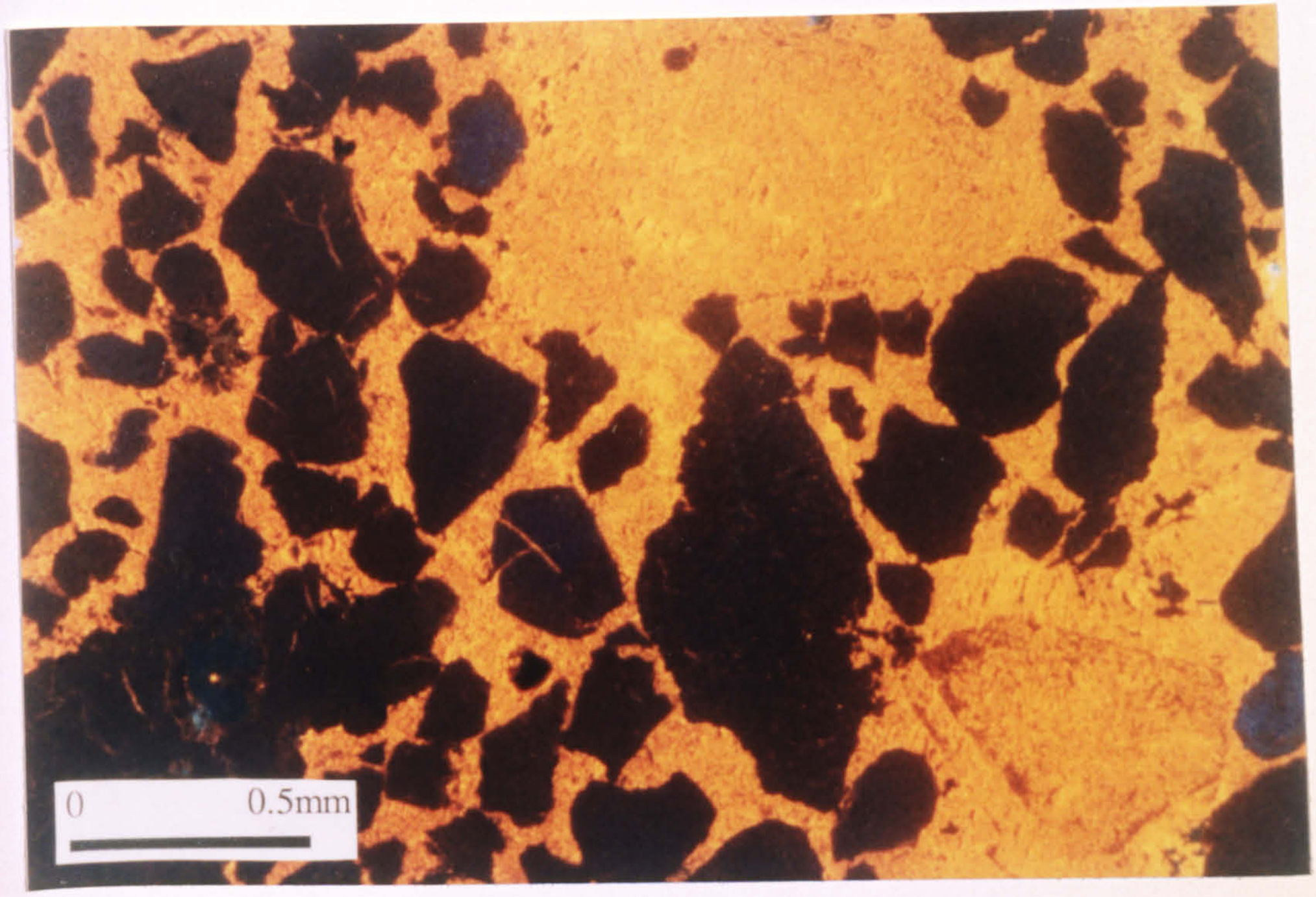

Figure 4.11.

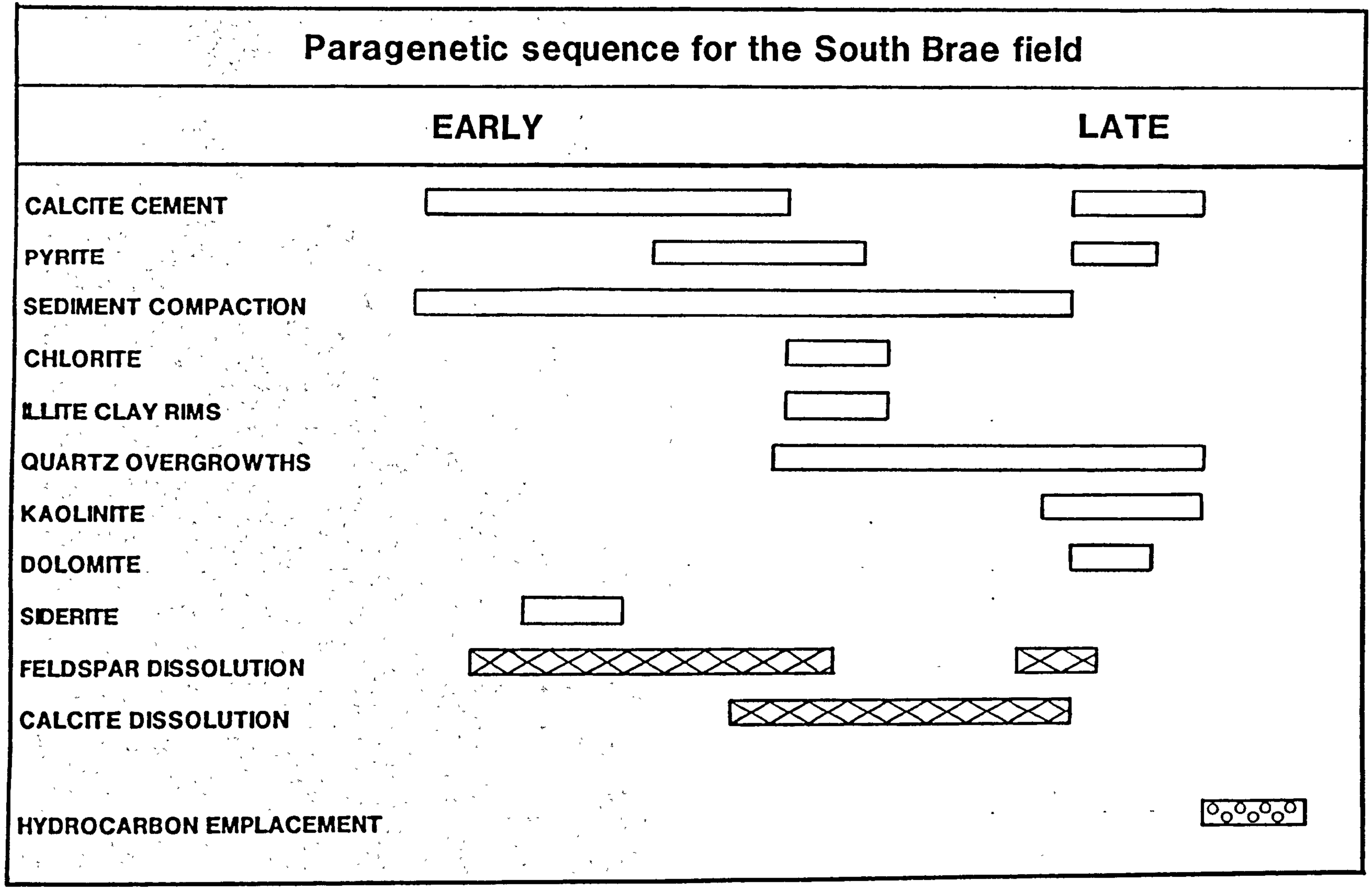
Paragenetic sequence for the South Brae field
EARLY
LATE
CALCITE CEMENT
PYRITE
SEDIMENT COMPACTION
CHLORITE
ILLITE CLAY RIMS
QUARTZ OVERGROWTHS
KAOLINITE
DOLOMITE
SIDERITE
FELDSPAR DISSOLUTION
CALCITE DISSOLUTION
HYDROCARBON EMPLACEMENT

Figure 4.12

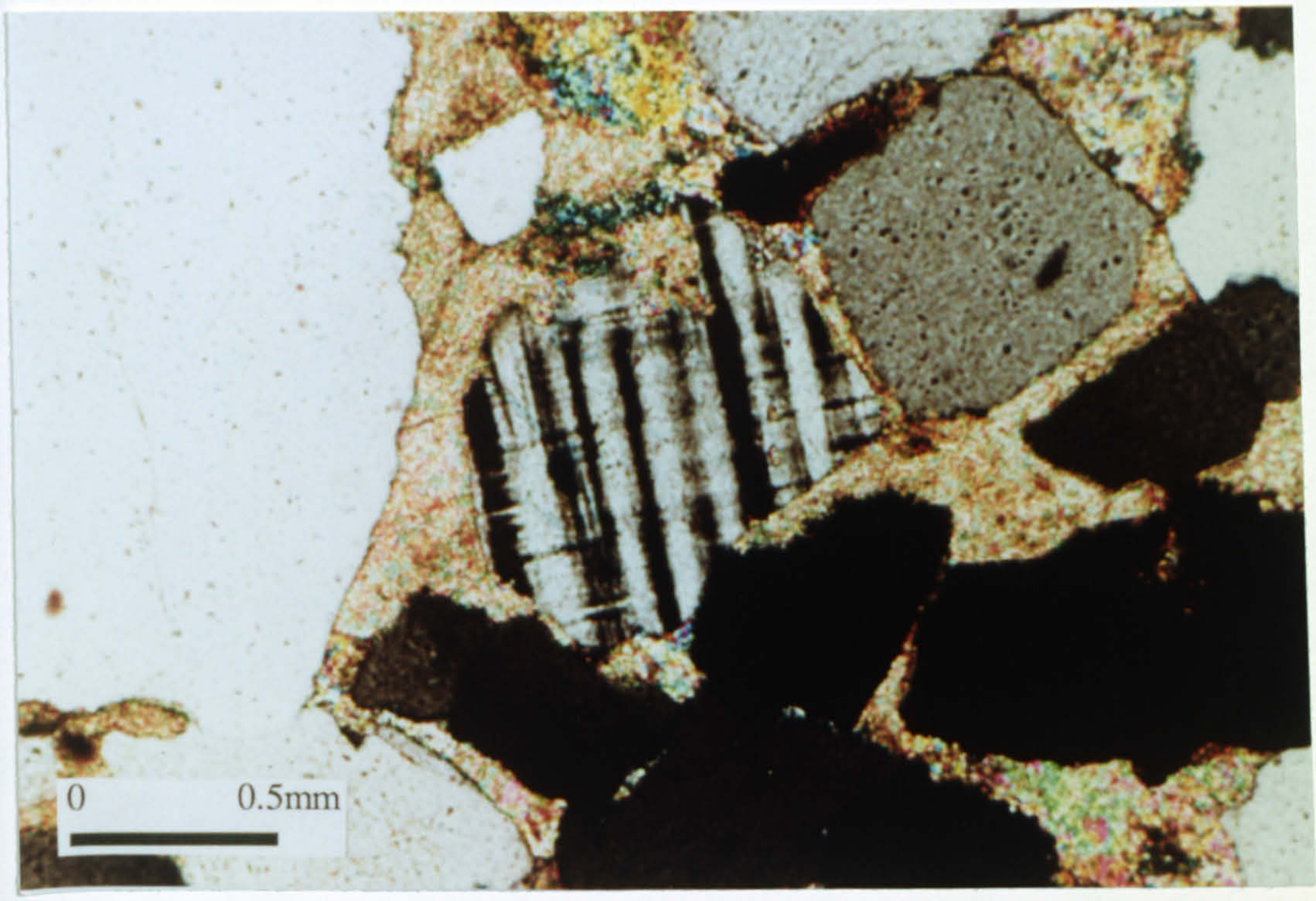

Figure 4.13.

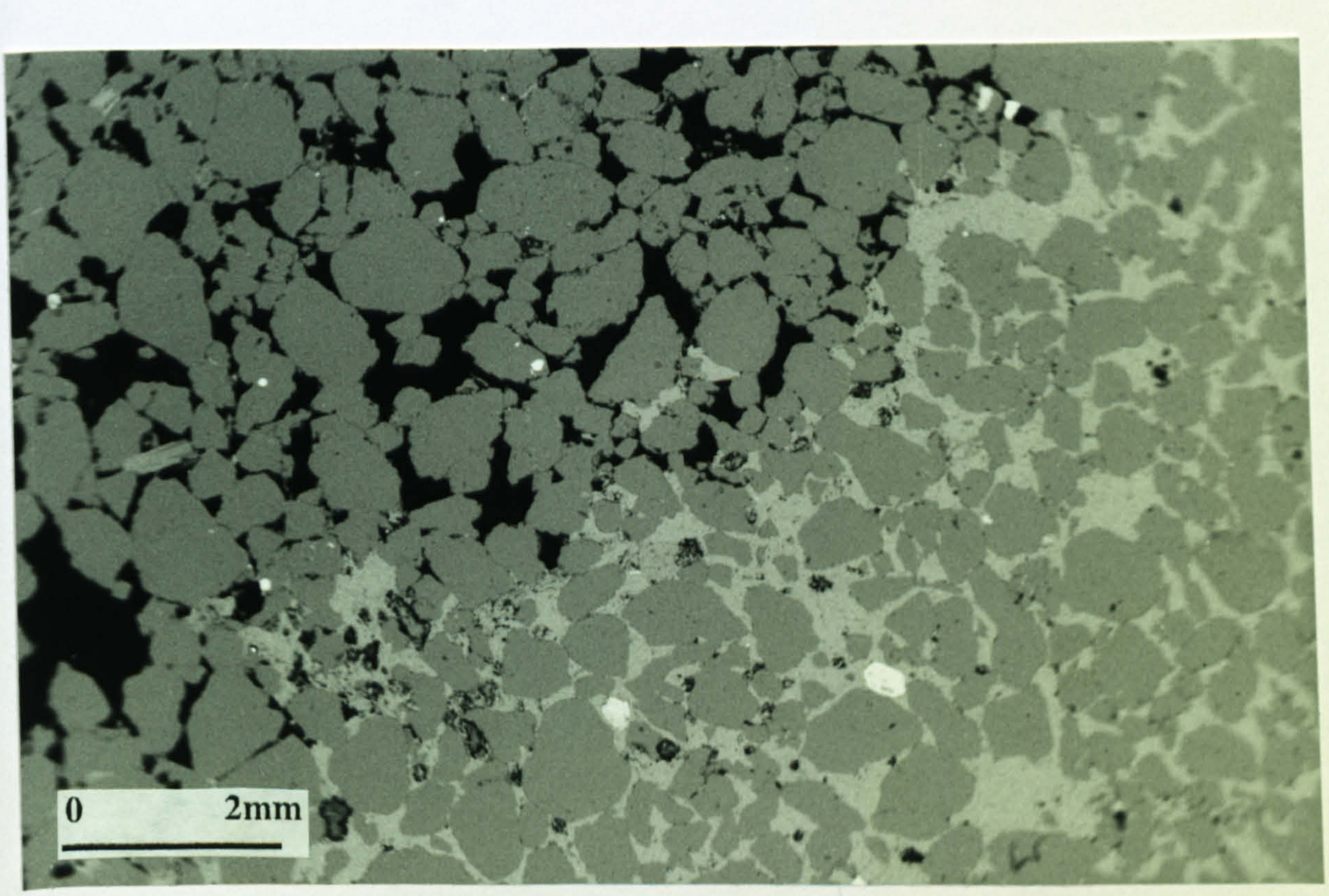

Figure 4.15 .

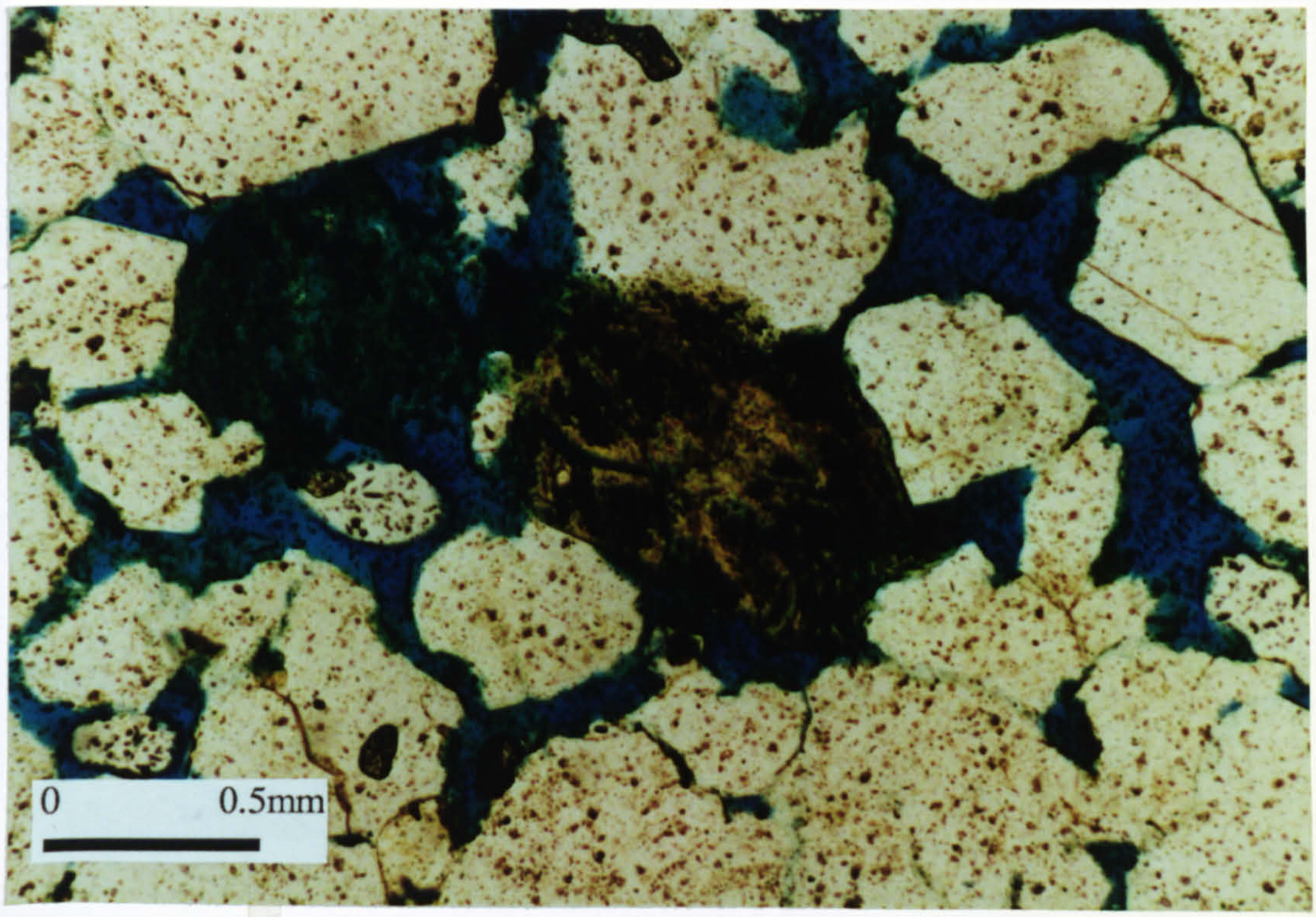

Figure 4.14a.

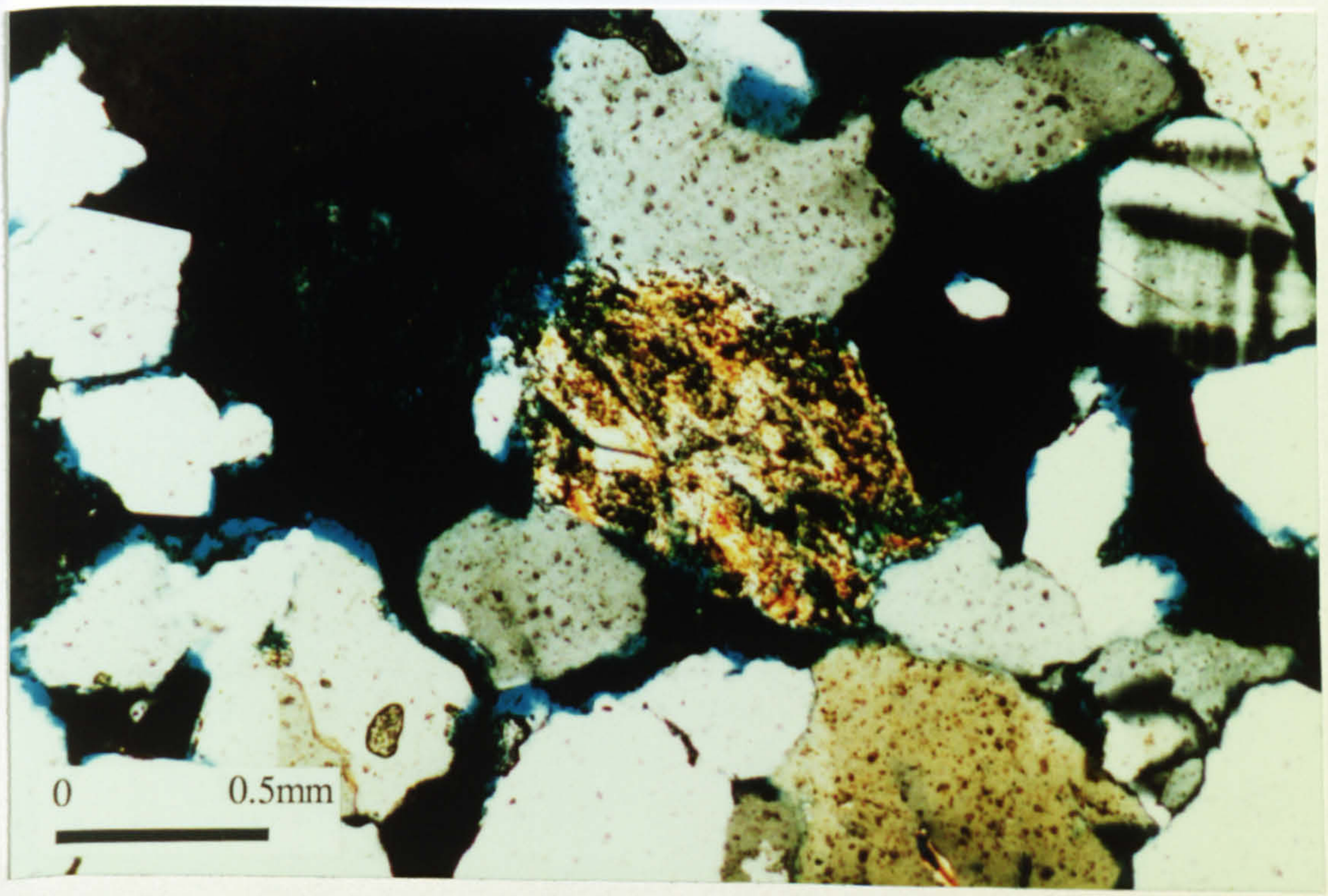

Figure 4.14b

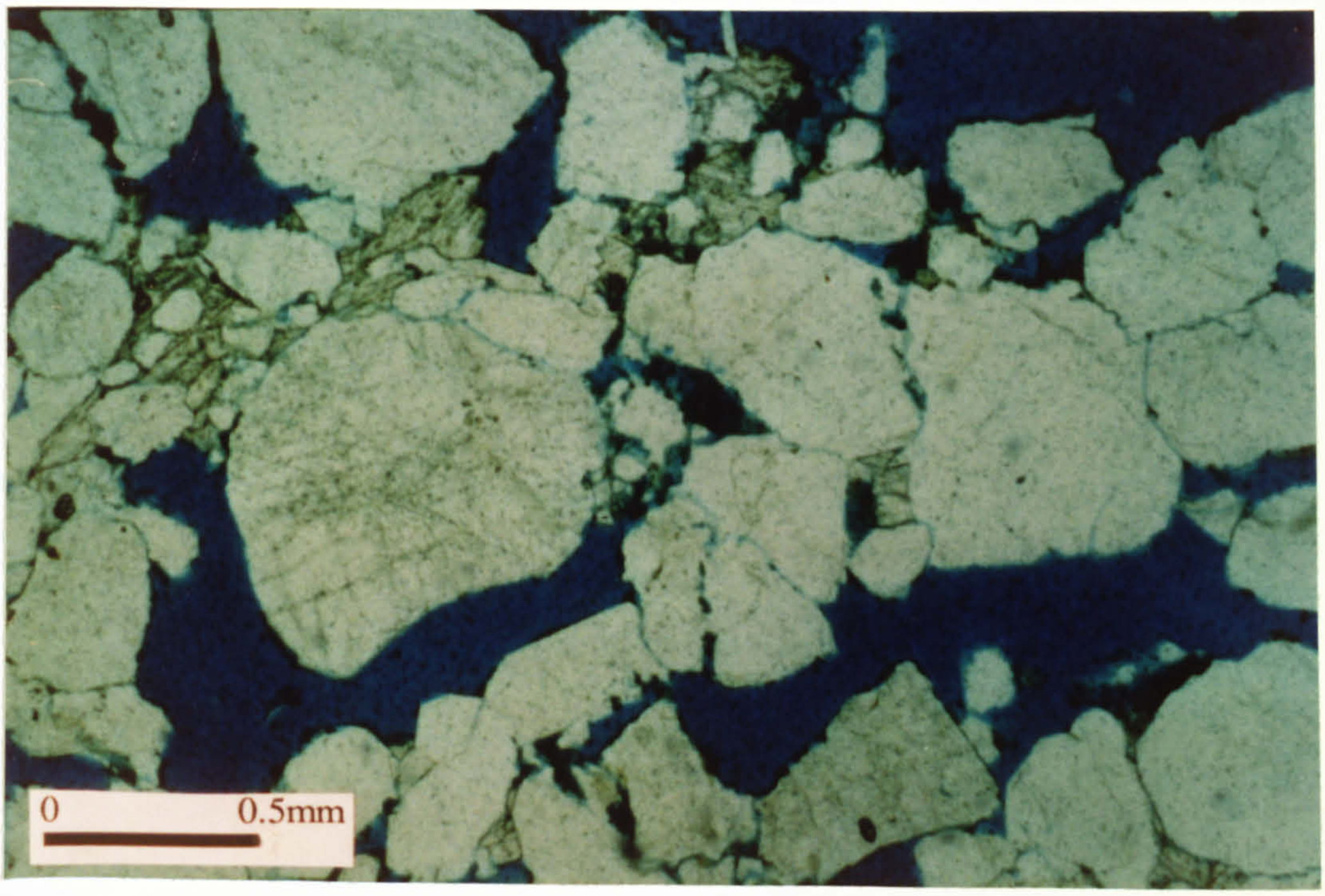

Figure 4.16.

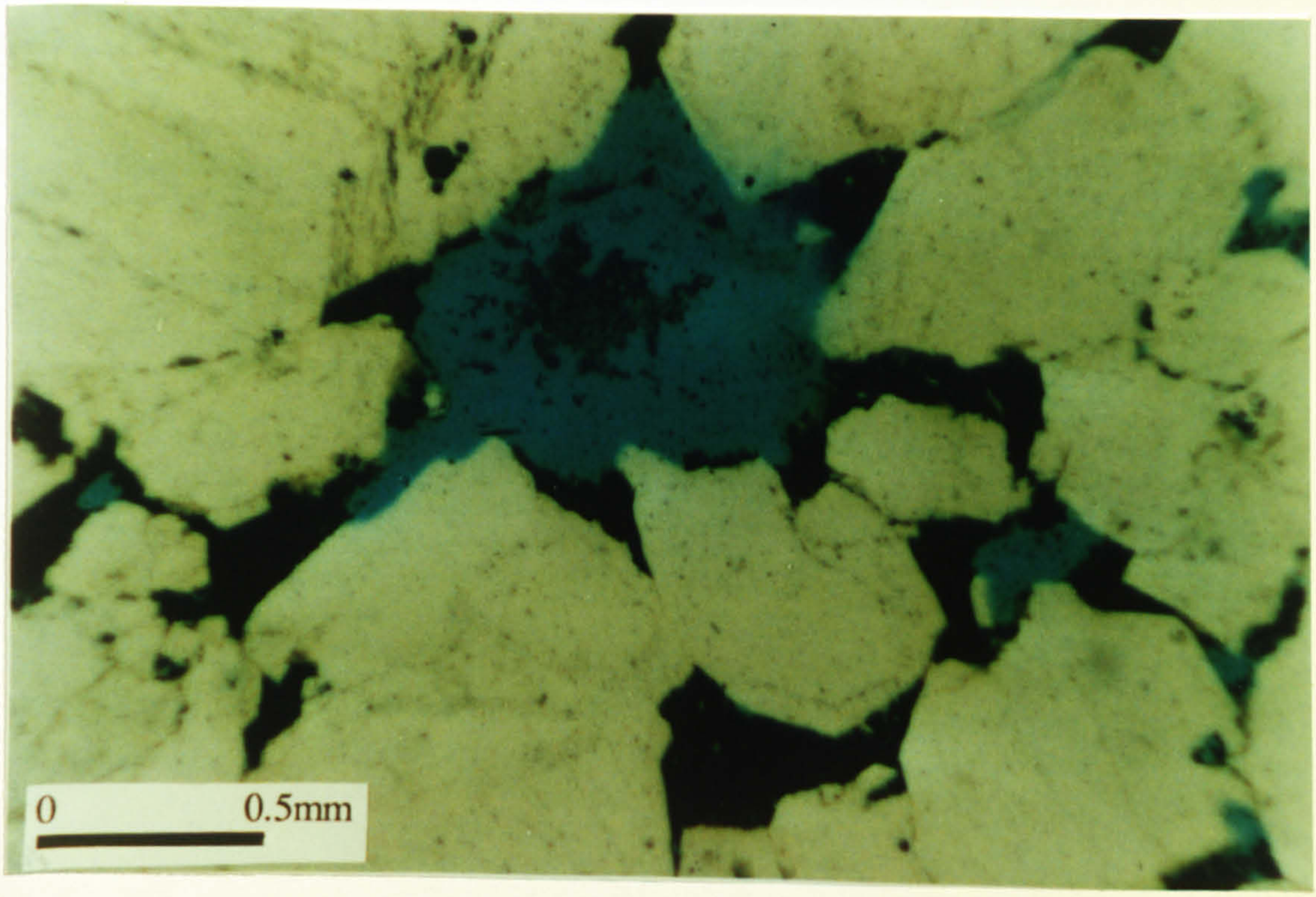

Figure 4.17.

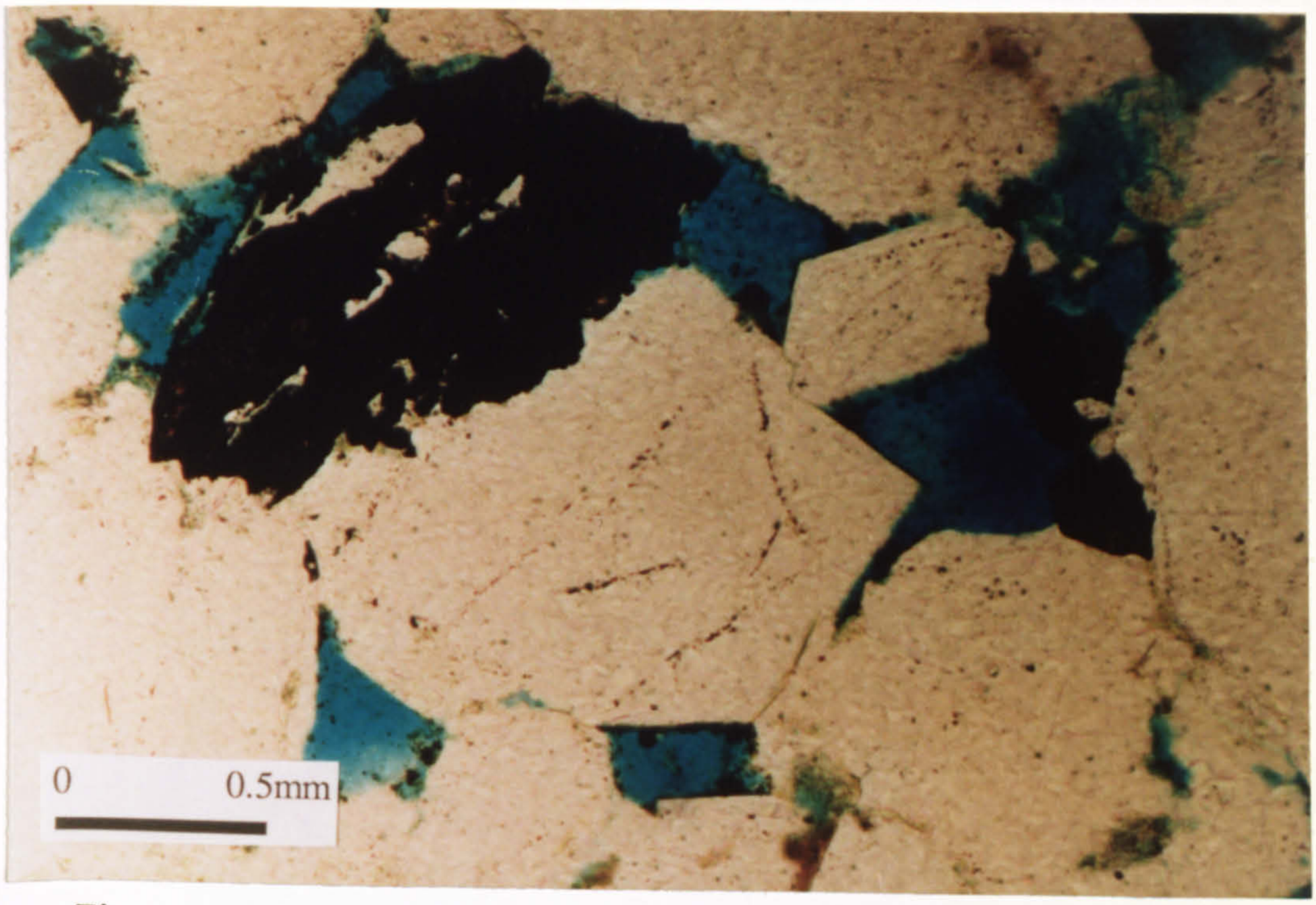

Figure 4.18.

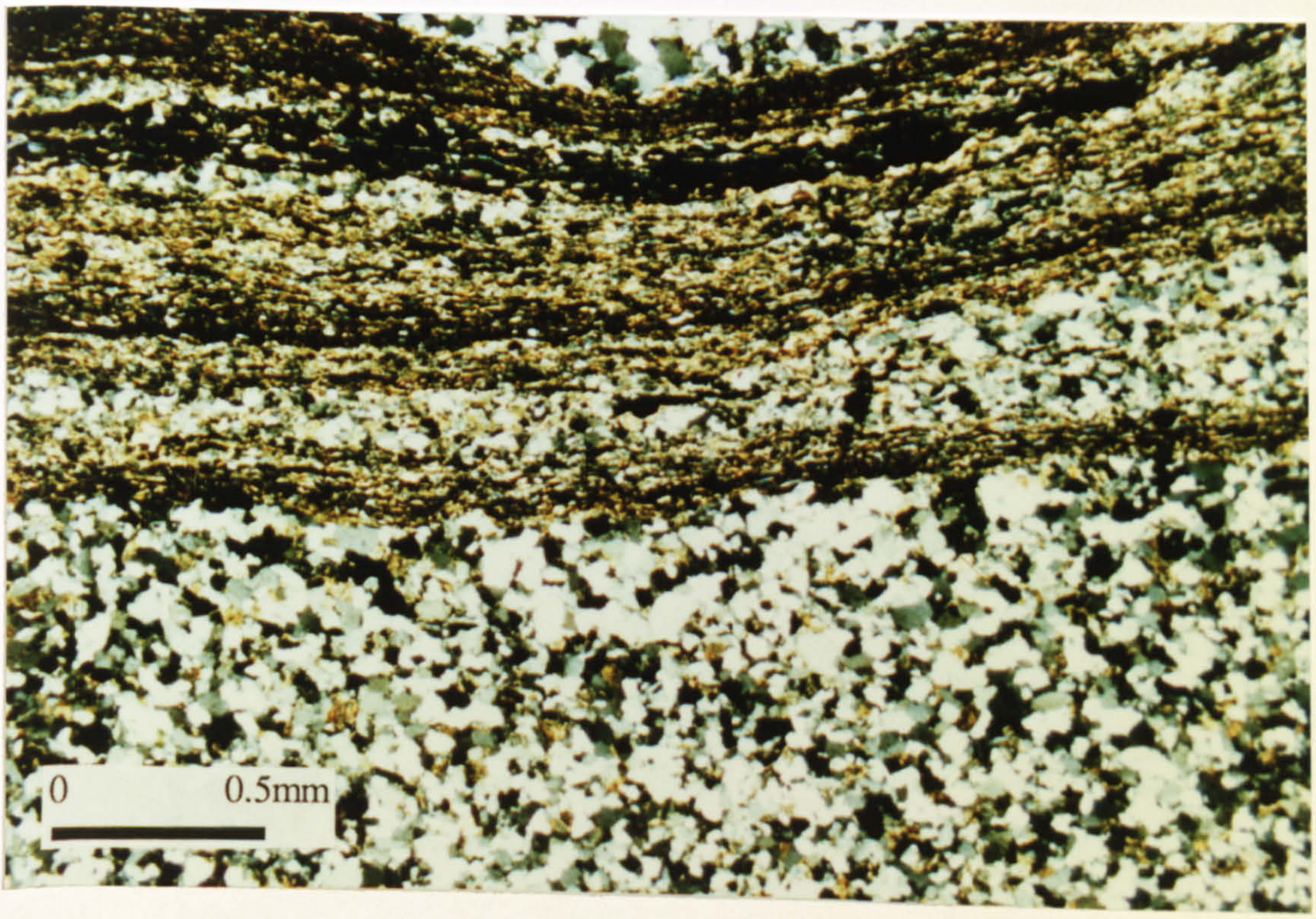

Figure 4.19.

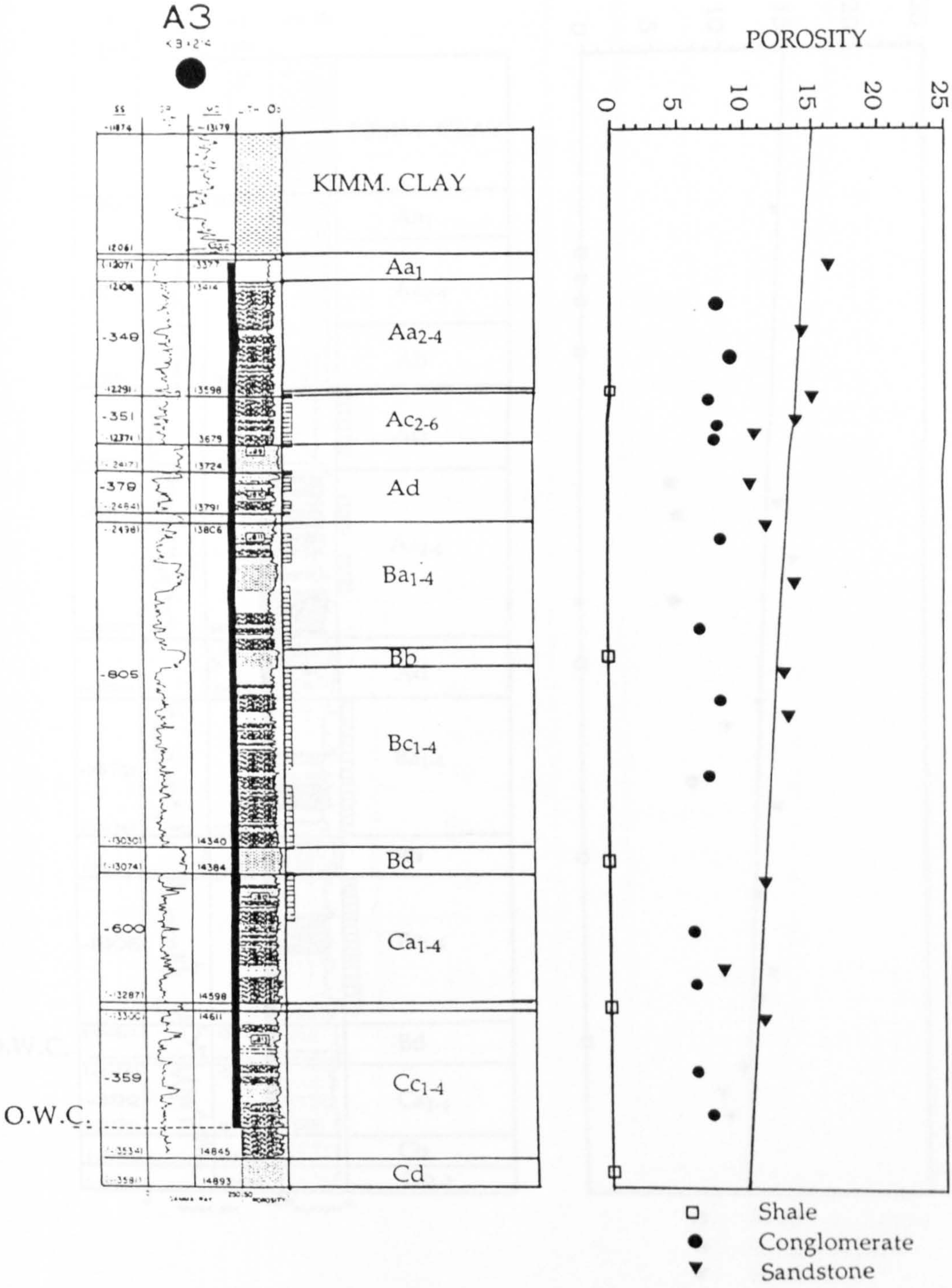
A3
POROSITY
0
5
10
15
20
25
KIMM. CLAY
Aa1
Aa2-4
Ac2-6
Ad
Ba1-4
Bb
Bc1-4
Bd
Ca1-4
Cc1-4
Cd
O.W.C.:
Shale
Conglomerate
Sandstone

Figure 4.20a.

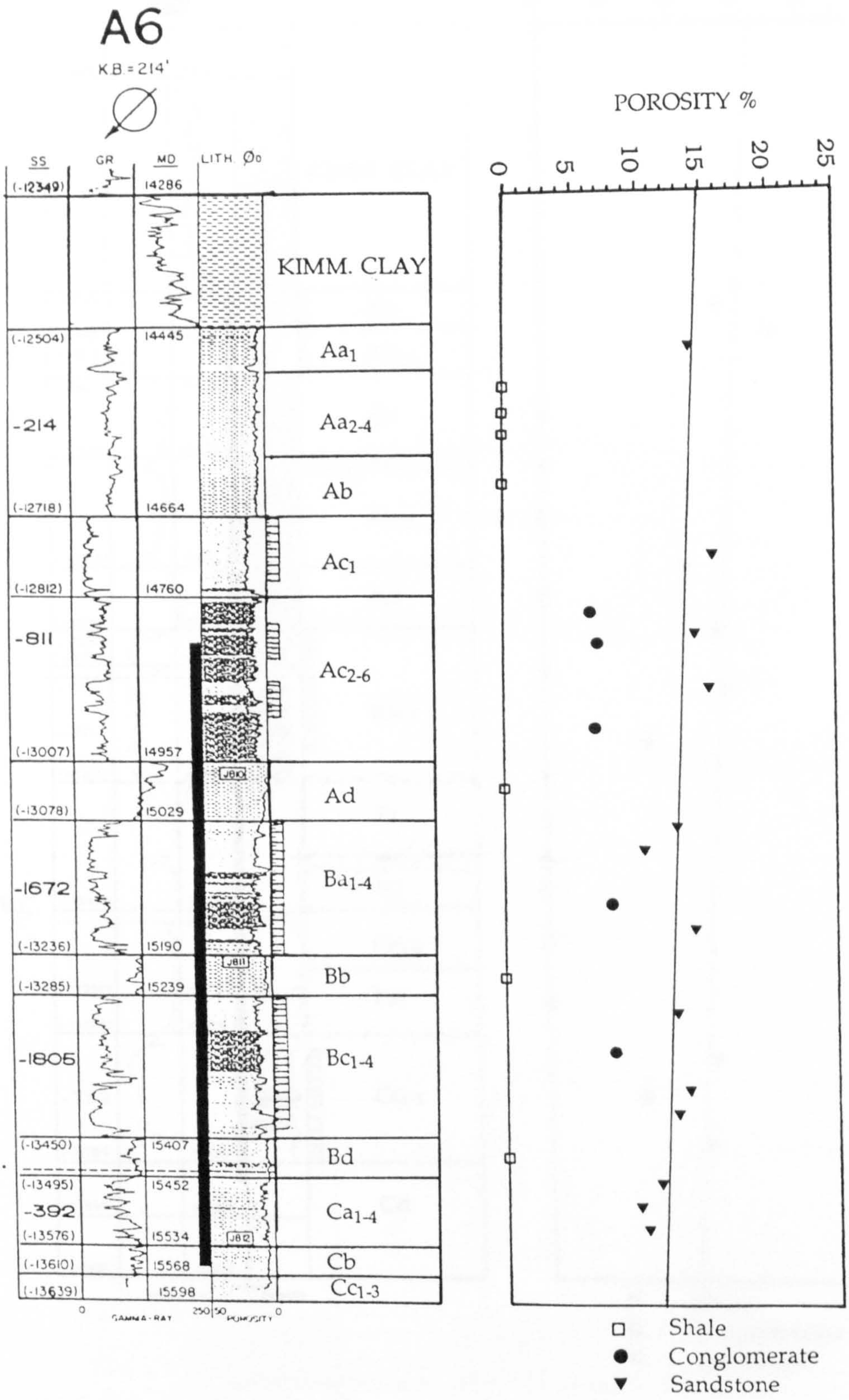
A6
K.B. = 214'
SS
GR
MD
LITH. Øo
(-12349)
14286
KIMM. CLAY
(-12504)
14445
Aa1
-214
Aa2-4
(-12718)
14664
Ab
(-12812)
14760
Ac1
-811
Ac2-6
(-13007)
14957
(-13078)
15029
Ad
-1672
Ba1-4
(-13236)
15190
(-13285)
15239
Bb
-1805
Bc1-4
O.W.C.
(-13450)
15407
Bd
(-13495)
15452
-392
Ca1-4
(-13576)
15534
(-13610)
15568
Cb
(-13639)
15598
Cc1-3
0
GAMMA-RAY
250
50
POROSITY
0
POROSITY %
0
5
10
15
20
25
Shale
Conglomerate
Sandstone

Figure 4.20b.

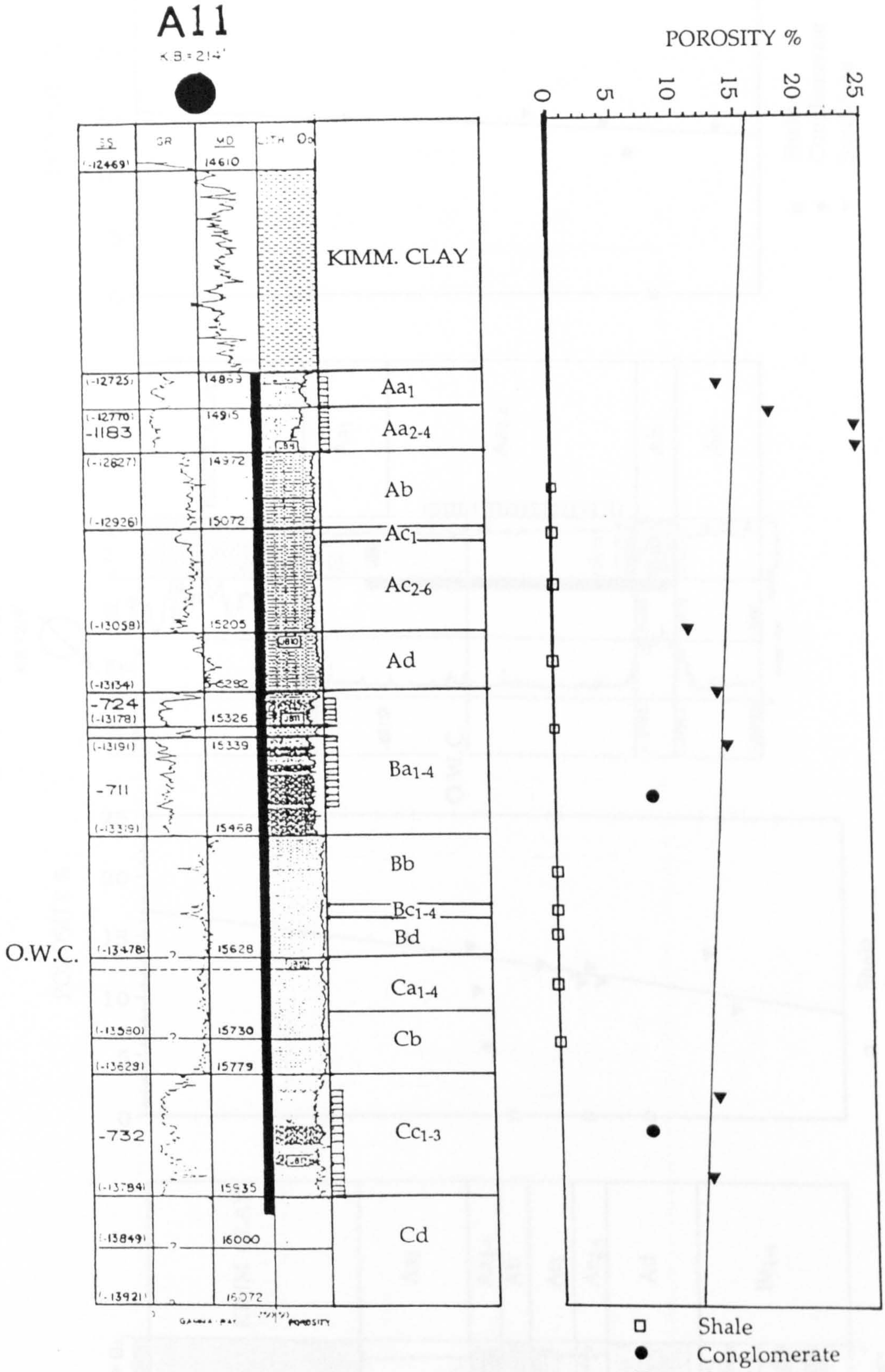
A11
K.B.=214'
ES
(-12469)
GR
MD
14610
LITH
Oc
KIMM. CLAY
(-12725)
14859
Aa1
(-12770)
-1183
14915
Aa2-4
(-12827)
14972
Ab
(-12926)
15072
Ac1
Ac2-6
(-13058)
15205
Ad
(-13134)
15282
-724
(-13178)
15326
(-13191)
15339
-711
(-13319)
15458
Ba1-4
Bb
Bc1-4
Bd
O.W.C.
(-13478)
15628
Ca1-4
(-13580)
15730
Cb
(-13629)
15779
-732
(-13784)
15935
Cc1-3
(-13849)
16000
Cd
(-13921)
16072
GAMMA RAY
POROSITY
POROSITY %
0
5
10
15
20
25
Shale
Conglomerate
Sandstone

Figure 4.20c.

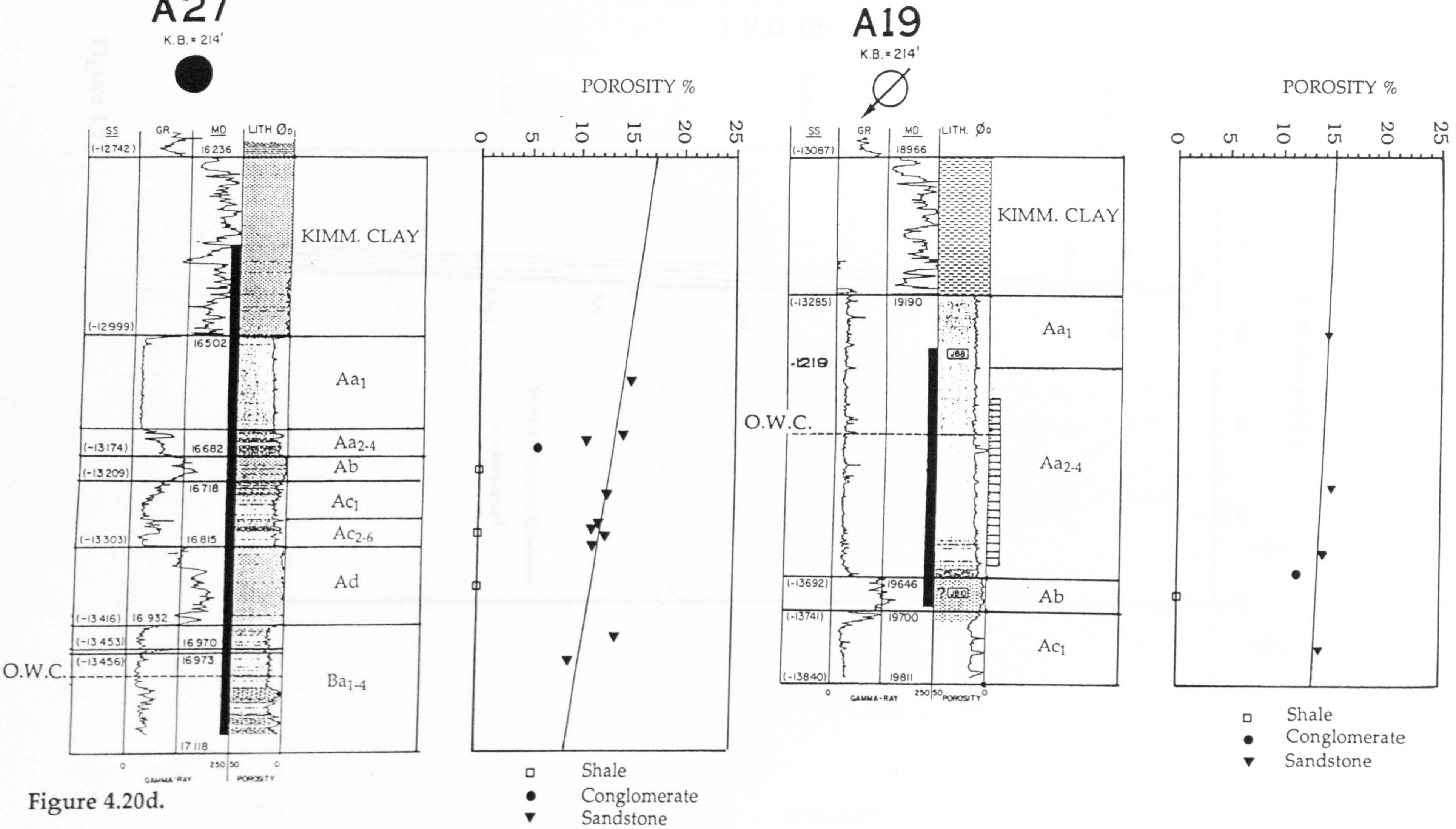
A27
K.B. = 214'
SS
GR
MD
LITH Ø
(-12742)
16236
KIMM. CLAY
(-12999)
16502
Aa1
(-13174)
16682
Aa2-4
(-13209)
Ab
16718
Ac1
(-13303)
16815
Ac2-6
Ad
(-13416)
16932
(-13453)
16970
(-13456)
16973
O.W.C.
Ba1-4
17118
0
250
50
0
GAMMA-RAY
POROSITY
POROSITY %
0
5
10
15
20
25
Shale
Conglomerate
Sandstone
A19
K.B. = 214'
SS
GR
MD
LITH. Ø
(-13087)
18966
KIMM. CLAY
(-13285)
19190
Aa1
-1219
J68
O.W.C.
Aa2-4
(-13692)
19646
? J80
Ab
(-13741)
19700
Ac1
(-13840)
19811
0
GAMMA-RAY
250
50
POROSITY
0
POROSITY %
0
5
10
15
20
25
Shale
Conglomerate
Sandstone

Figure 4.20d.

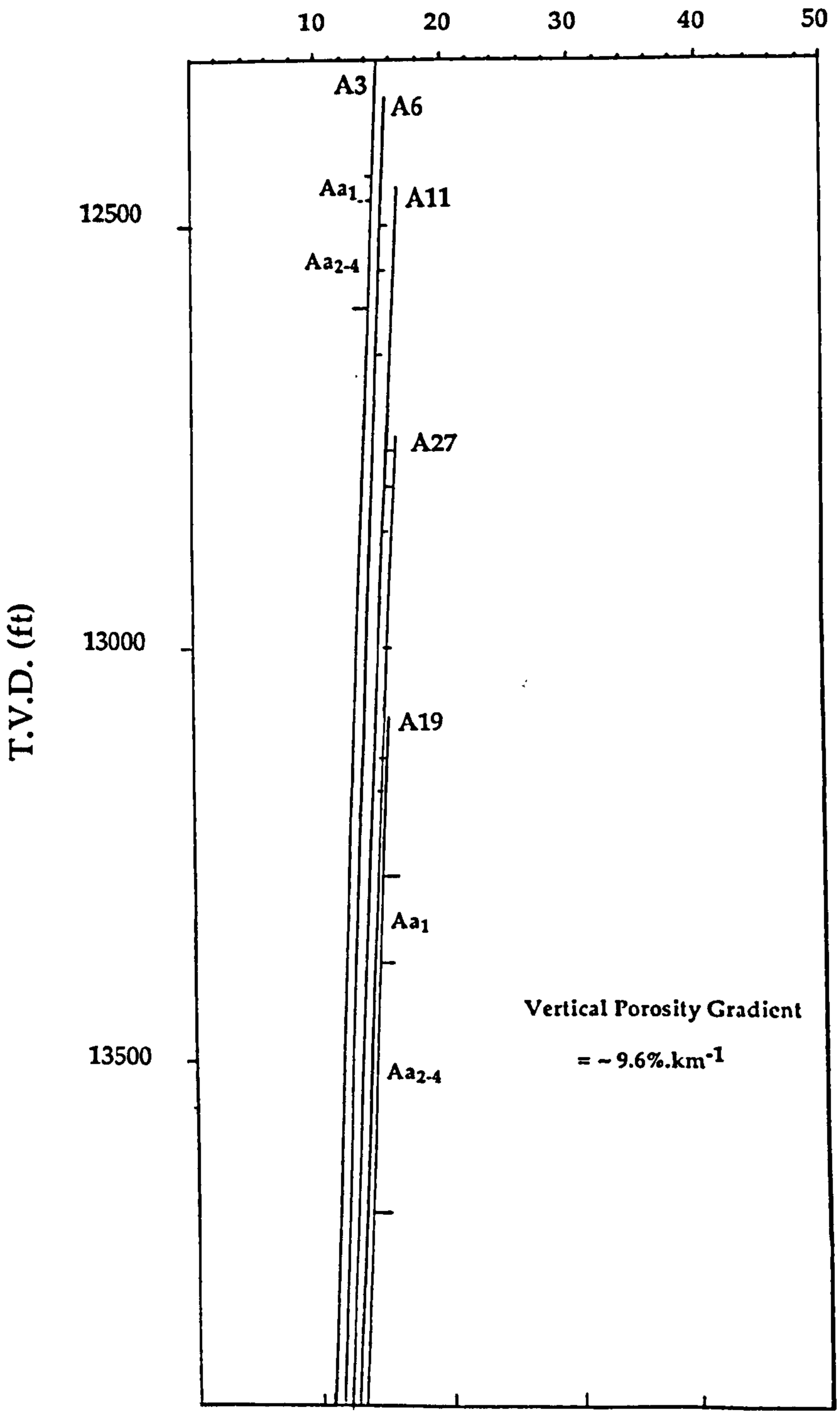
% POROSITY
10
20
30
40
50
T.V.D. (ft)
12500
13000
13500
A3
A6
Aa1-
A11
Aa2-4
A27
A19
Aa1
Aa2-4
Vertical Porosity Gradient
= ~ 9.6%.km-1

Figure 4.21.

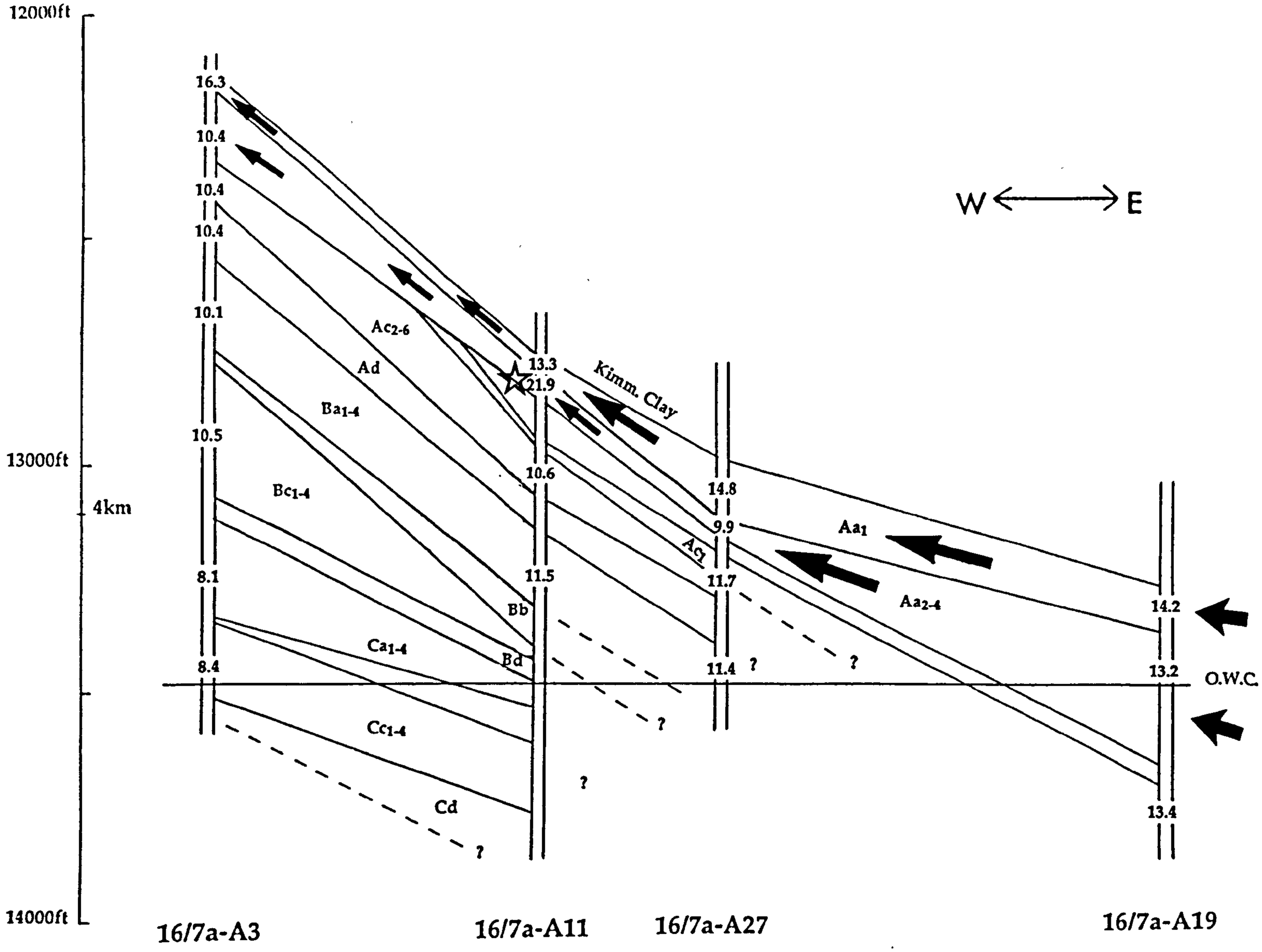
12000ft
13000ft
4km
14000ft
16.3
10.4
10.4
10.4
10.1
10.5
8.1
8.4
10.6
11.5
11.4
14.8
9.9
11.7
13.3
21.9
14.2
13.2
13.4
Ac2-6
Ad
Ba1-4
Bc1-4
Bb
Bd
Ca1-4
Cc1-4
Cd
Kimm. Clay
Aa1
Aa2-4
Ac1
O.W.C.
W
E
16/7a-A3
16/7a-A11
16/7a-A27
16/7a-A19

Figure 4.22.

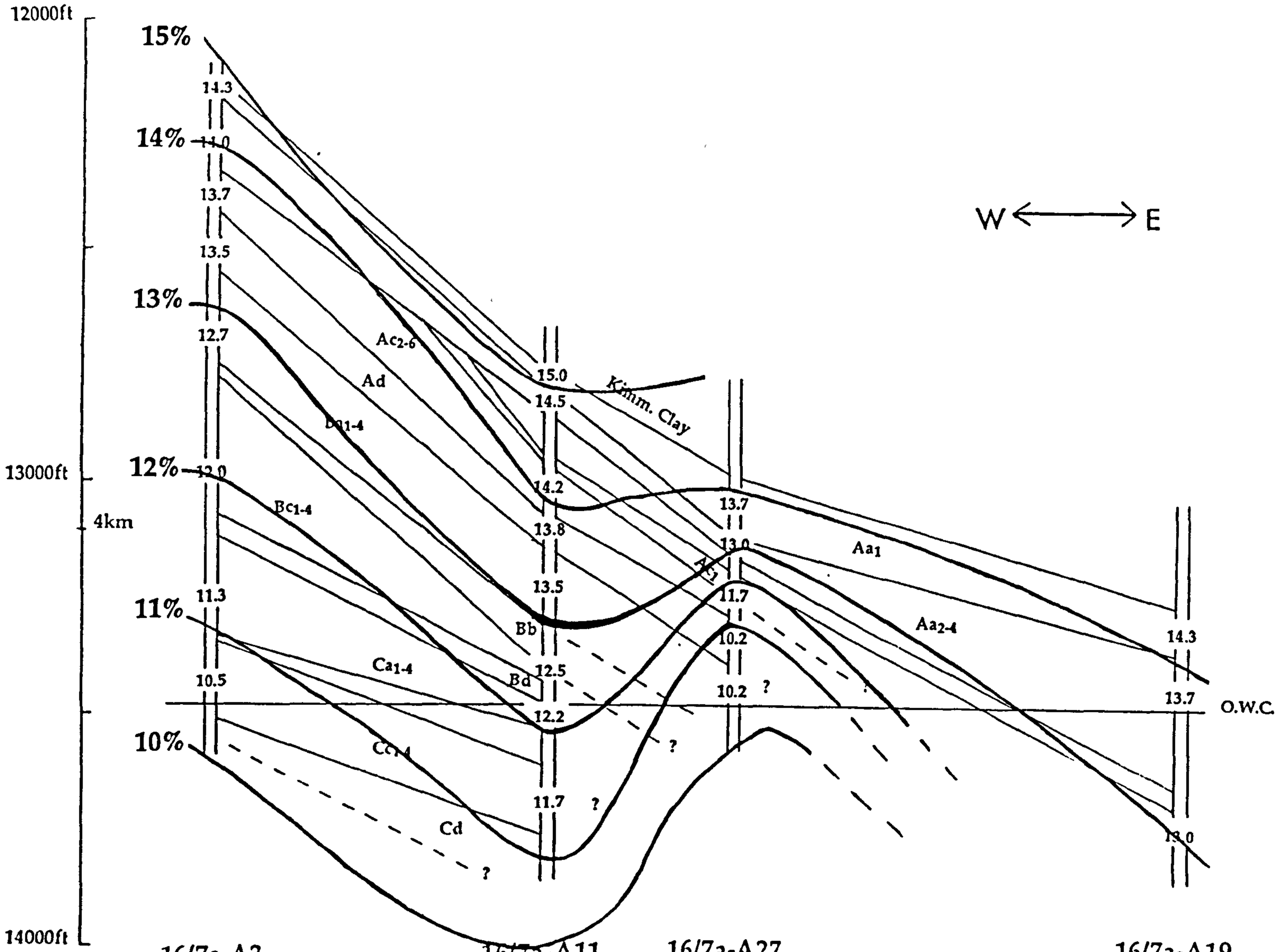
12000ft
13000ft
4km
14000ft
15%
14%
13%
12%
11%
10%
W
E
14.3
14.0
13.7
13.5
12.7
12.0
11.3
10.5
Ac2-6
Ad
Bd1-4
Bc1-4
Ca1-4
Cc1-4
Cd
Bb
Bd
15.0
Kimm. Clay
14.5
14.2
13.8
13.5
12.5
12.2
11.7
?
Aa1
Aa2-4
13.7
13.0
11.7
10.2
10.2
14.3
13.7
13.0
O.W.C.
16/7a-A3
16/7a-A11
16/7a-A27
16/7a-A19

Figure 4.23.

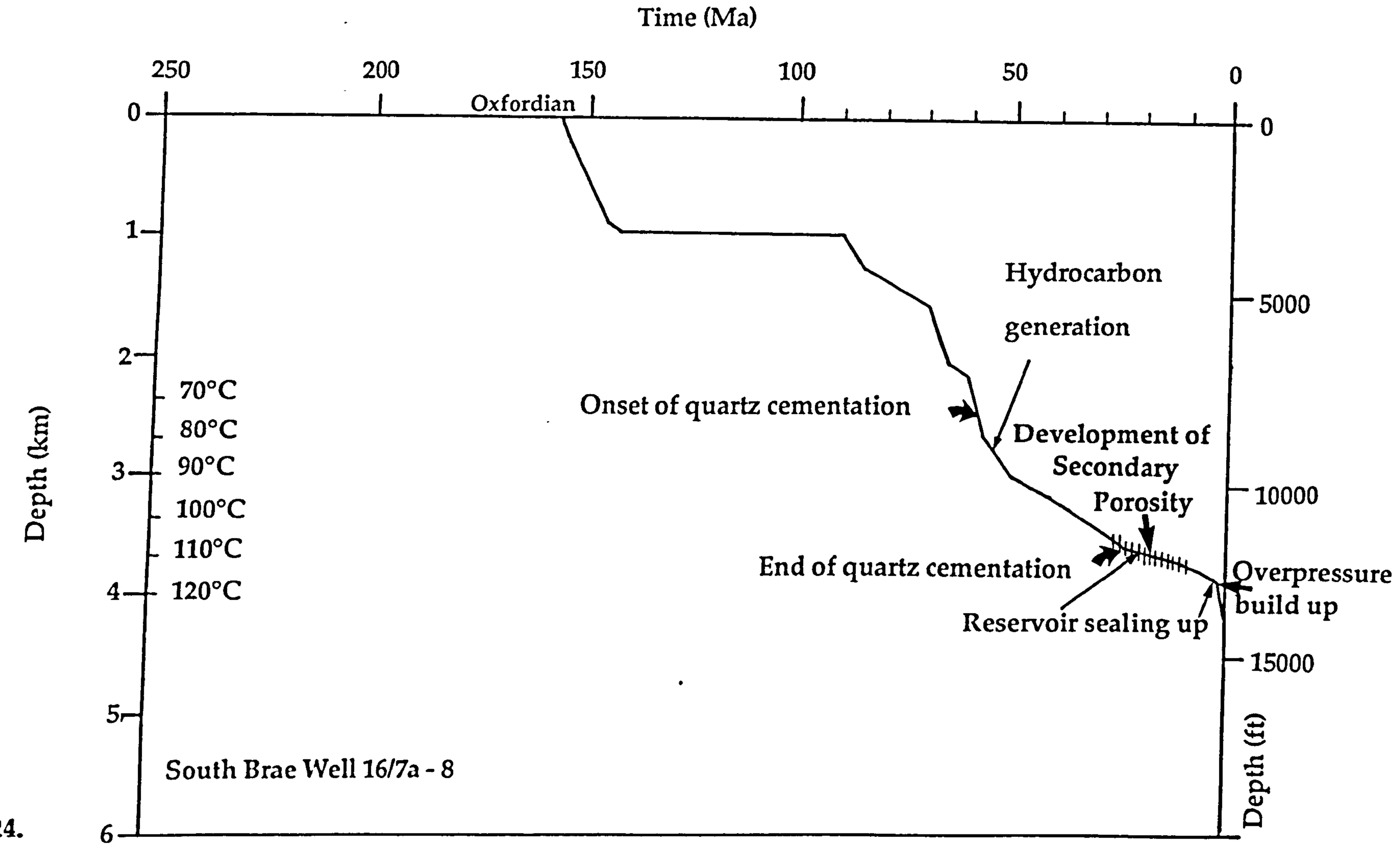
Time (Ma)
250
200
150
100
50
0
Oxfordian
0
1
2
3
4
5
6
Depth (km)
70°C
80°C
90°C
100°C
110°C
120°C
South Brae Well 16/7a - 8
Hydrocarbon
generation
Onset of quartz cementation
Development of
Secondary
Porosity
End of quartz cementation
Overpressure
build up
Reservoir sealing up
0
5000
10000
15000
Depth (ft)

Figure 4.24.

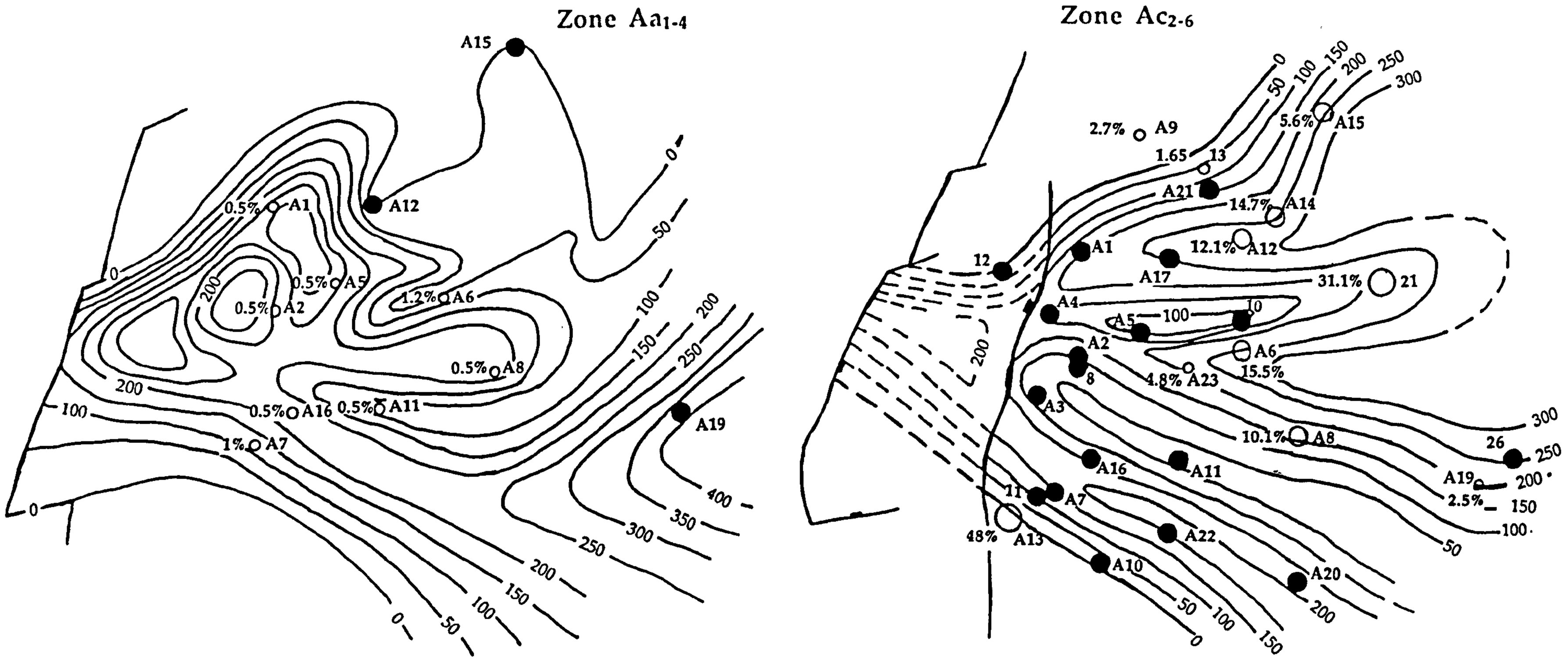

South Brae Field

Net Reservoir Maps

● No significant carbonate cements recorded

○ ○ ○ ○ ○

>50% 20.1-50% 10.1-20% 5.1-10% 0.1-5%

Contours in percent

Figure 4.25a.

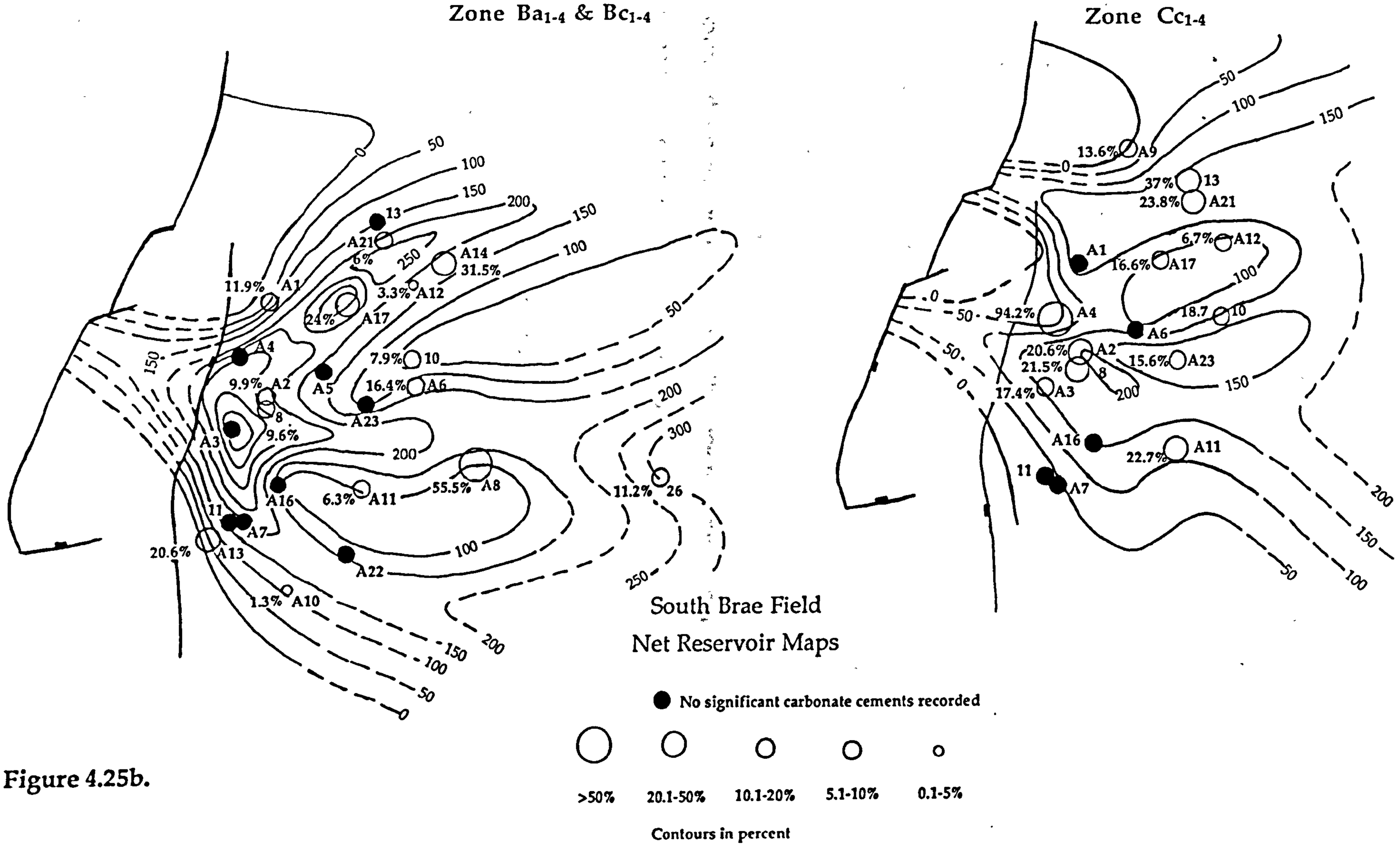
Zone Ba1-4 & Bc1-4
Zone Cc1-4
South Brae Field
Net Reservoir Maps
No significant carbonate cements recorded
>50%
20.1-50%
10.1-20%
5.1-10%
0.1-5%
Contours in percent

Figure 4.25b.

5.1 CONCLUSIONS

Many sedimentary basins contain two or more superimposed hydrological systems (Hunt 1990), so it is not surprising to find that reservoir rocks over 150My exhibit a similar phenomena. Except in this case, the hydrologies have been fossilised. We suggest that the paleo-hydrologies for the South Brae reservoir can be broadly reconstructed for the oilfields diagenetic history. In the late Jurassic the Fladen Ground Spur was a topographic high, so that meteoric recharge into the reservoir was driven by the head of the elevated ground water table (Fig.5.1.). The early calcite cements which started to grow during shallow burial were precipitated from oxidising meteoric waters. The meteoric waters flushed through the South Brae sediments in a water-dominated open flow system, which displaced and homogenized the original porewaters at the time. Concretion growth commenced during the late Jurassic and continued up to the end of the Paleocene. The formation of concretions appears to require that a supersaturation maximum is maintained for a long time (Wilkinson & Dampier, 1991) and is commonly associated with sequences deposited during periods of low sedimentation or a hiatus. In South Brae during the early Cretaceous such an hiatus occurred, as there was a pause in subsidence of 50My (Fig.5.2.).

The meteoric porewater was initially undersaturated with respect to carbonate phases resulting in dissolution of shell material and plagioclase. This fluid also became locally aggressive with respect to the silicate minerals, thus causing leaching of detrital quartz grains and K-feldspar.

Eventually the fluid became saturated with respect to carbonate resulting in the precipitation of calcite. Ions for the calcite cement were supplied

from within the sandstones, with Ca being supplied from dissolved shell material and plagioclase. Strontium was initially supplied from dissolved shell material, but as diagenesis proceeded the calcite cement incorporated a more radiogenic component (silicate dissolved Sr). Eventually Sr from mica and feldspar saturated the Sr supply, thus the margins of the concretions had high $^{87}Sr/^{86}Sr$ ratios and low Sr concentrations. CO_2 was initially supplied from the shelly debris and there was also an increasing input from the surrounding mudrocks. As burial and dewatering of the reservoir occurred, fluids rich in organic carbon due to decarboxylation of Brae Formation shales and muds were released. The mixture of meteoric water saturated with respect to marine carbonate ($\delta^{13}C$=0‰PDB) and CO_2 charged waters which had depleted $\delta^{13}C$ values (=-25‰PDB) resulted in calcite cements with intermediate values. The concretion cores were slightly enhanced in Fe, but generally the Fe, Mn and Mg chemistry of the calcite cements is typical of meteoric porewater precipitation (ie. low concentrations). The changing $\delta^{18}O$ mineral values reflect cements being precipitated from an evolving meteoric fluid at increasingly higher temperatures as burial proceeds (Fig.5.3.). Because the $\delta^{18}O$ of the porefluid evolved somewhat throughout calcite precipitation, the water and rock were never in equilibrium. This implies that although the reservoir may have been continually flushed by meteoric porewater, the $\delta^{18}O$ of the porefluid still evolved due to mixing with other fluids. This mixed fluid precipitated the calcite cements.

Diagenetic quartz grew in a distinctly different paleo-hydrological system (Fig.5.4.). Cementation occurred between 55-20Ma, Eocene to the mid Miocene (Fig.5.2.) From our $\delta^{18}O$ values for quartz overgrowths we have developed an ad hoc model for quartz cementation. The fluids which precipitated the quartz cement were possibly warm, compaction-driven, basinal waters ($\delta^{18}O$=+4‰SMOW). These fluids floated over the cooler,

possibly more saline and denser South Brae porewaters. This hot basinal water initially fingered into the topmost reservoir - the most porous and permeable layer (zone A), consequently these cementation temperatures were higher than those of the deeper zones (Fig.5.3.). As the fluid moved towards the western margin of the field, it became cooler and isotopically lighter as it mixed with the colder interstitial porefluids.

No differences in volumes or type of silica cement are seen between the layered basinal flow, and static meteoric connate water. Thus we consider that pressure solution between quartz grains and in mudrocks, and the leaching of feldspar were the main internal silica sources. They appear to have been sufficient to supply the total volume of authigenic quartz precipitated. Some type of ionic or diffusive transport allowed quartz cementation. Because the silica was locally and internally derived, and the basinal water was of external origin, it seems that silica transport was decoupled from fluid type and fluid flow.

From our constructed model the top reservoir zones behaved like an open system as water flushed through the aquifer and up the fault. The deeper zones possibly formed a more closed system, wherein the porefluid evolved to a more positive value, suggesting that the water/rock system was moving towards equilibrium. The quartz cementation event was possibly linked to a period of overpressure release permitting compactional drainage of excess pore fluid from the Kimmeridge Clay Formation basin.

This was followed by the development of secondary porosity which was due to the continuing movement of compaction driven fluids out of the basin (Fig.5.5.). These fluids were also focused in the uppermost aquifer (zone A). As the fluid moved upwards into the aquifer it may have

cooled and became undersaturated with respect to calcite and feldspar, causing late stage leaching and dissolution. The short time span of secondary porosity generation may be related to rapid basinal fluid expulsion due to a drop from overpressure to hydrostatic pressure. The low content of late kaolinite in South Brae suggests that Al from diagenetically late feldspar dissolution has been transported out of the reservoir and lost to the system. Once the reservoir became sealed and overpressured, only limited *fluid movement* would be possible. Hydrocarbon accumulation was allowed to occur and late diagenesis was halted. No differences in cementation are observed across the oil-water contact, making it feasible that this was established only 2Ma.

5.2. PROPOSED FUTURE WORK

As a result of the work carried out on this project, it is obvious that there are certain aspects of this work which could be further researched and developed.

1.) For the reservoir and production geologists, computer modelling of South Brae fluid pathways and movements could prove a useful and predictive tool for estimating extents of cementation and secondary porosity development. The quantities and three dimensional distribution of the different authigenic cements could be easily incorporated into such a model. Another project worthy of research time, is the detailed three dimensional mapping of cements. In South Brae it appears that calcite cement occurs most abundantly within the main channel axis, with reduced amounts of calcite cement found in similar facies on the margins of the channel. This phenomena has not been recorded for other oilfields, but may also be the case if the oilfields were mapped in a similar manner.

2.) A detailed fluid inclusion study of the authigenic quartz overgrowths in the various reservoir zones could prove useful in constraining the

quartz cementation model (temperatures & salinities) that we have outlined.

3.) In this thesis we have assumed a geothermal gradient of 30°C/km suitable for the South Brae reservoir. This gradient is slightly lower than the geothermal gradient generally used for the North Sea (35°C/km). There are possibly many excursions from the geothermal gradient we have used. A more accurate burial curve would be useful, to try and make estimates for possible variations in the geothermal gradient due to tectonic and diagenetic events (eg. periods of rifting, or meteoric/basinal flushes).

4.) As discussed previously in Chapter 4, there is a deficit in the Al budget in South Brae. To our knowledge there is even less late kaolinite to the east, in the Miller field. Obviously this Al must have been transported out of the graben, it would be interesting to investigate where it has been precipitated (ie. a reservoir with Al excess).

5.) It would also be interesting to compare and contrast the diagenetic histories of South and North Brae, in order to try and understand why one has trapped oil and the other, condensate. Is this due to release of overpressure at different times? or the effect of efficient sealing?

5.3 REFERENCES CITED

Hunt, J.M. (1990) Generation and migration of petroleum from abnormally pressured fluid compartments. American Association of Petroleum Geologists. v.74. pp.1-12.

Wilkinson, M. & Dampier, M.D. (1990) The rate of growth of sandstone hosted calcite concretions. Geochimica et Cosmochimica Acta. 54. pp.3391-3399.

5.4 FIGURE CAPTION & FIGURES

Figure 5.1 Cartoon illustrating the late Jurassic hydrological system. It was an open system with a rapid flow of deep penetrating meteoric water (wavy arrows) driven by a 100-200m subaerial topographic head (Fladen Ground Spur). Marine porewaters were flushed out of the reservoir, and the meteoric water ($\delta^{18}O$=-7‰SMOW) precipitated early calcite cements at increasing temperatures as burial proceeded.

Figure 5.2 Burial curve for the South Brae Oilfield showing times and temperatures of authigenic mineral precipitation and other major diagenetic events. The reconstructed burial curve is based on well log 16/7a-8, which has been decompacted and backstripped.

Figure 5.3 Idealized porewater evolution path ($\delta^{18}O$ porefluid vs temperature) for the South Brae Oilfield. Early calcite cements formed from open meteoric fluid, quartz formed from mixing of meteoric and a different basinal (+4‰SMOW) fluid and late calcite was precipitated from this mixed fluid also.

Figure 5.4 Cartoon illustrating quartz cementation in the south Brae reservoir, spanning the Eocene to Miocene. Hot compaction-driven, basinal fluids ($\delta^{18}O$=+4‰SMOW) fingered into the most porous zone A (wavy arrows) and precipitated quartz. The basinal fluid "floated" as it was less saline and hotter than the surrounding interstitial porefluids. As the fluid moved through the field it mixed with the interstitial meteoric porefluid, becoming cooler

and isotopically lighter. Consequently overgrowths in the shallow zones have been precipitated from a higher temperature fluid than the deeper overgrowths. The short arrows indicate no flow, they represent the diffusion of silica on a small scale.

Figure 5.5 Cartoon illustrating the development of secondary porosity in the Miocene. Secondary porosity formation was due to the continuing movement of compaction-driven basinal fluids which entered the most porous layer of the reservoir (zone A), as it moved to the west of the field it cooled and became undersaturated with respect to feldspar and calcite, causing dissolution.

Chapter 5. Conclusions.

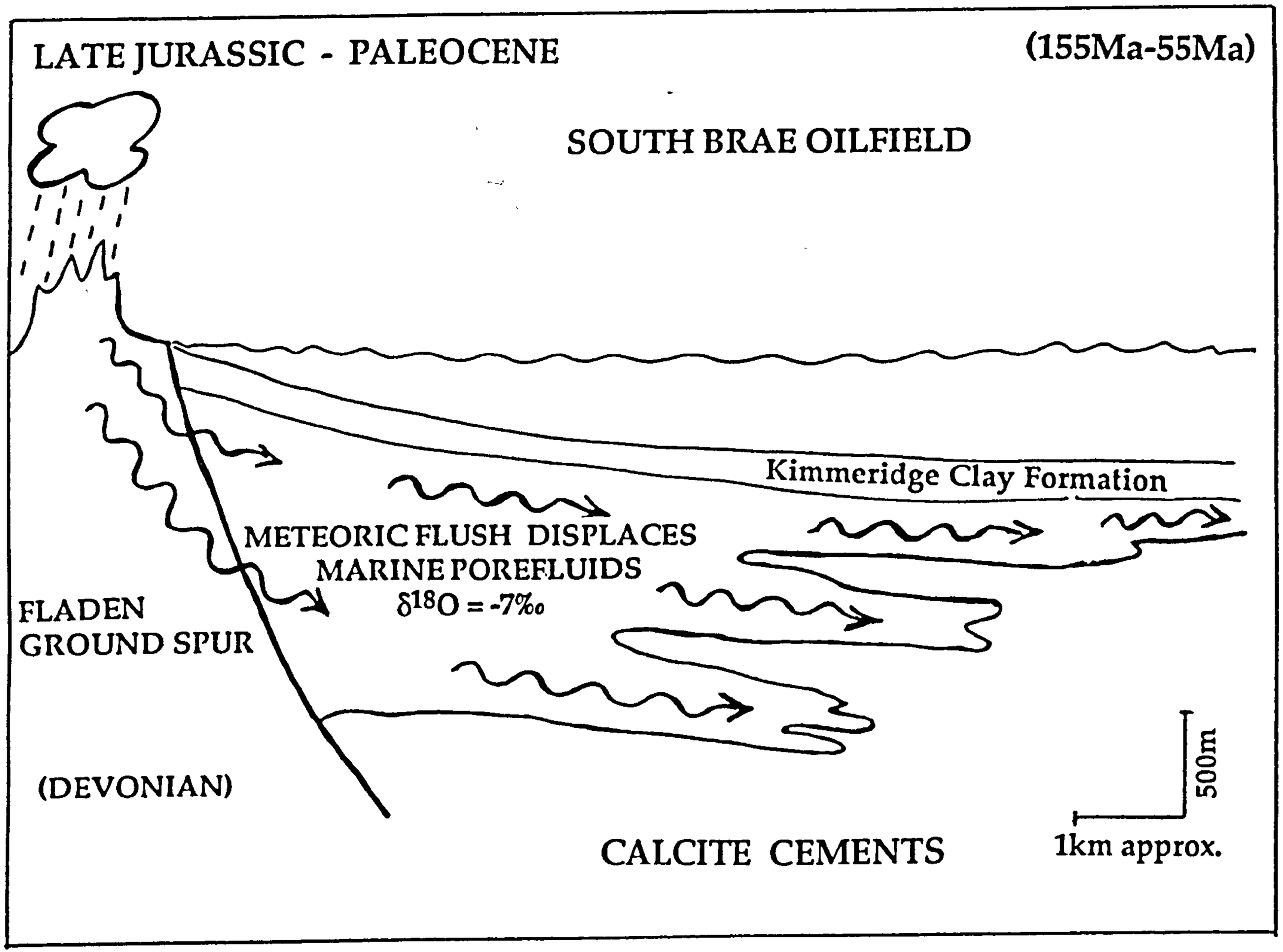
LATE JURASSIC - PALEOCENE
(155Ma-55Ma)
SOUTH BRAE OILFIELD
Kimmeridge Clay Formation
METEORIC FLUSH DISPLACES
MARINE POREFLUIDS
$\delta^{18}O = -7‰$
FLADEN
GROUND SPUR
(DEVONIAN)
500m
1km approx.
CALCITE CEMENTS

Figure 5.1.

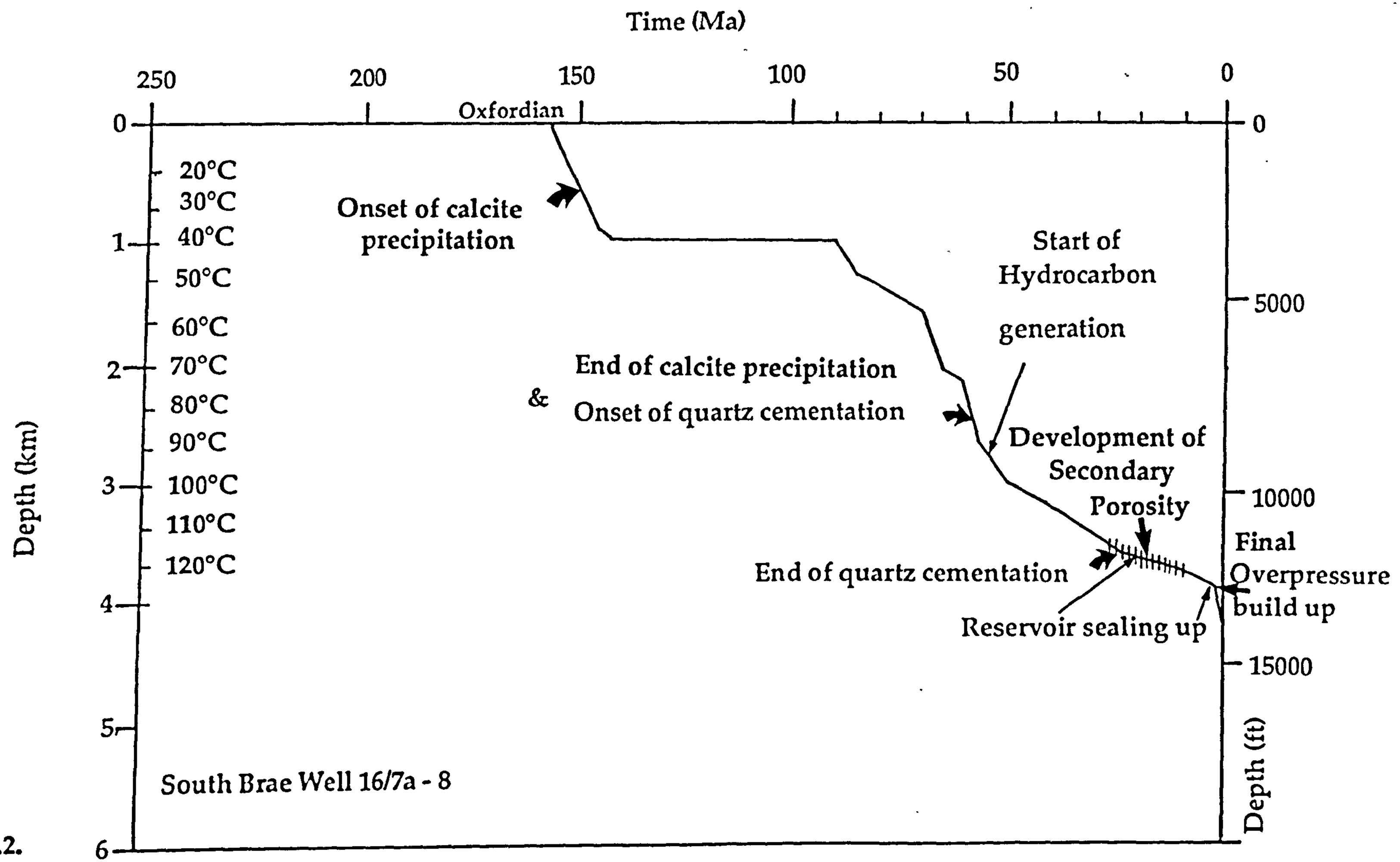
Time (Ma)
250
200
150
100
50
0
Oxfordian
0
20°C
30°C
1
40°C
50°C
60°C
2
70°C
80°C
90°C
3
100°C
110°C
120°C
4
5
6
Depth (km)
Onset of calcite precipitation
End of calcite precipitation
&
Onset of quartz cementation
Start of Hydrocarbon generation
Development of Secondary Porosity
End of quartz cementation
Reservoir sealing up
Final Overpressure build up
5000
10000
15000
Depth (ft)
South Brae Well 16/7a - 8

Figure 5.2.

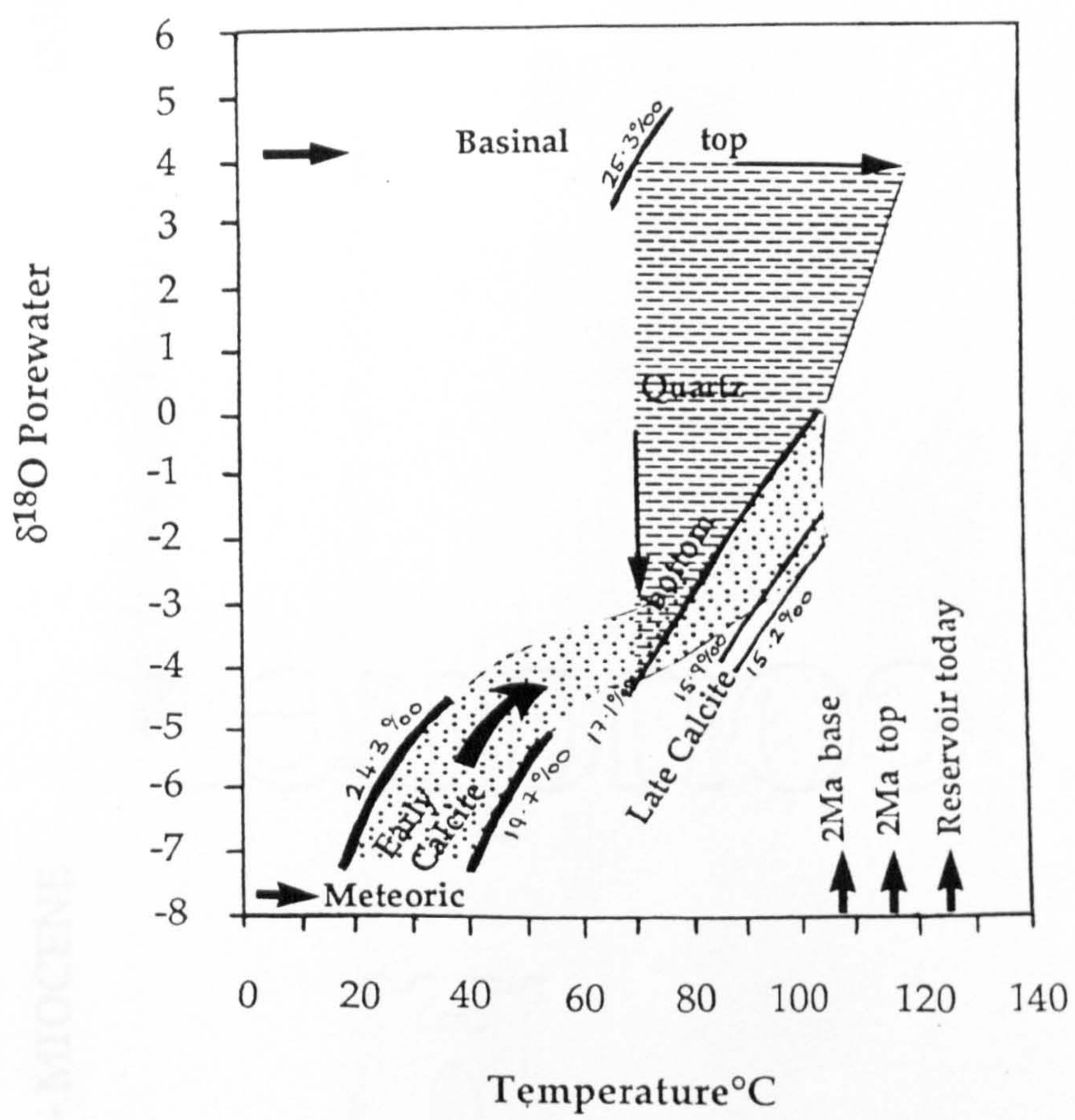
Basinal
top
25.3‰
Quartz
Early Calcite
24.3 ‰
19.2‰
19.1‰
15.9‰
15.2‰
Late Calcite
Meteoric
2Ma base
2Ma top
Reservoir today
δ18O Porewater
6
5
4
3
2
1
0
-1
-2
-3
-4
-5
-6
-7
-8
0
20
40
60
80
100
120
140
Temperature°C

Figure 5.3.

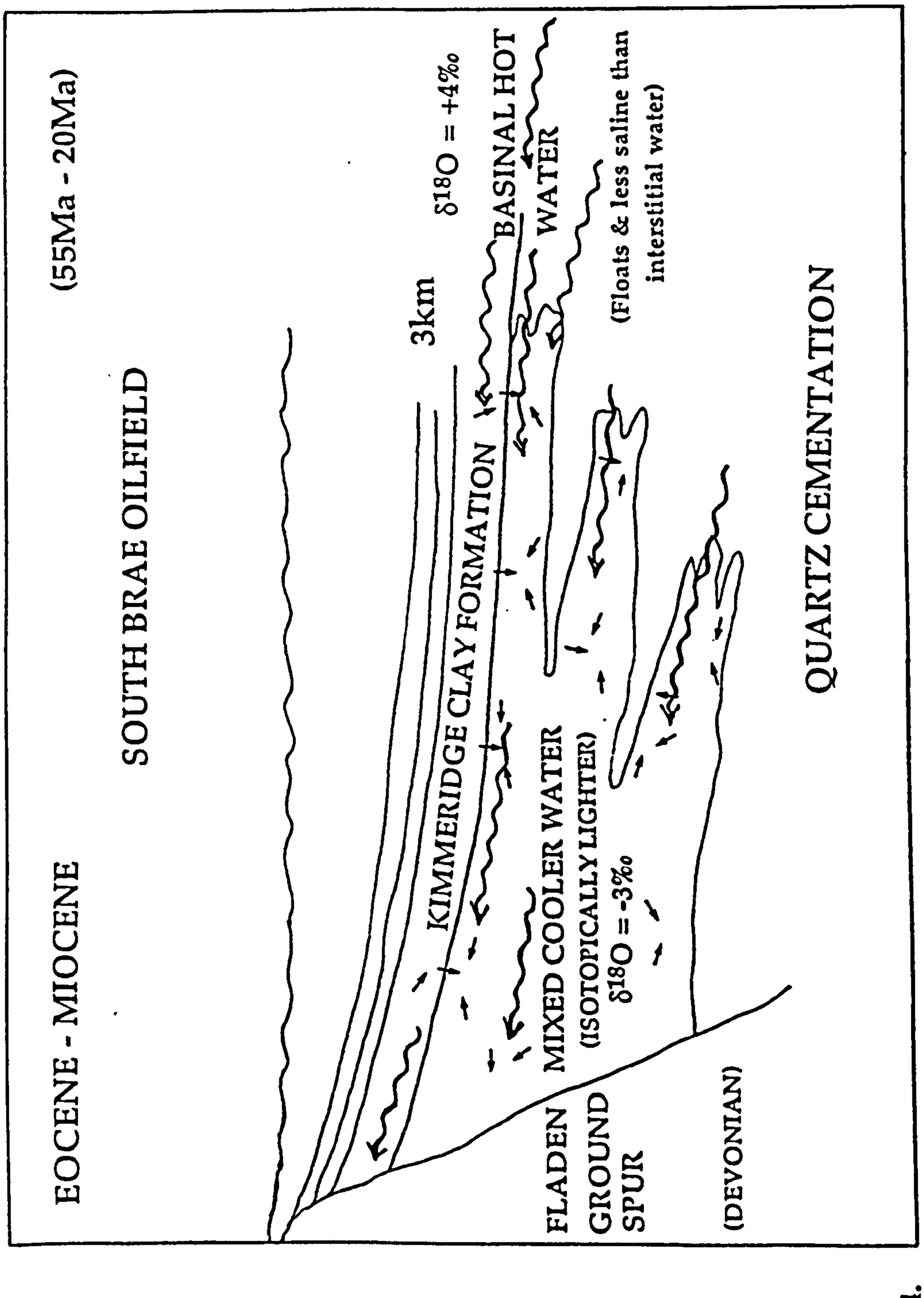
EOCENE - MIOCENE
SOUTH BRAE OILFIELD
(55Ma - 20Ma)
3km
KIMMERIDGE CLAY FORMATION
BASINAL HOT WATER
MIXED COOLER WATER
(ISOTOPICALLY LIGHTER)
δ18O = -3‰
δ18O = +4‰
(Floats & less saline than interstitial water)
FLADEN GROUND SPUR
(DEVONIAN)
QUARTZ CEMENTATION

Figure 5.4.

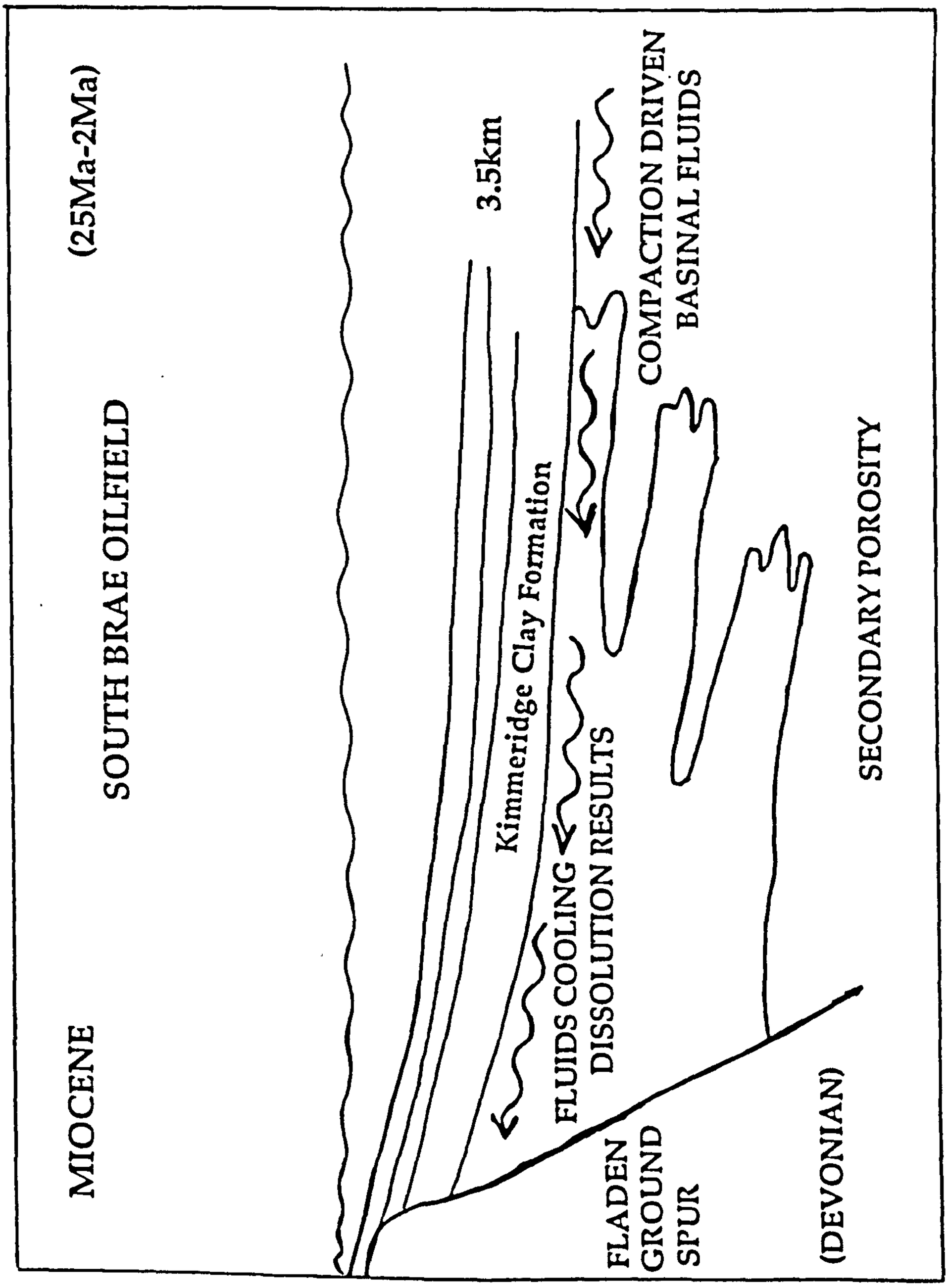

Figure 5.5.